MODELLING OF ANTIBIOTIC PRODUCTION BY *BACILLUS LICHENIFORMIS* USING A STRUCTURED/SEGREGATED APPROACH

APPROVED BY
DISSERTATION COMMITTEE:

Supervisor: ______________________________

____

____

____

____

This dissertation was prepared with the LaTeX document preparation system using additional macros written by John W. Eaton based on the thesis style written by Khe-Sing The for The University of Texas at Austin.

Printed in the United States of America.

10 9 8 7 6 5 4 3 2 1

To Diana.
You make it all worthwhile.

MODELLING OF ANTIBIOTIC PRODUCTION BY *BACILLUS LICHENIFORMIS* USING A STRUCTURED/SEGREGATED APPROACH

by

ANDREW PATRICK FORDYCE, B.S. Ch.E.

DISSERTATION
Presented to the Faculty of the Graduate School of
The University of Texas at Austin
in Partial Fulfillment
of the Requirements
for the Degree of

DOCTOR OF PHILOSOPHY

THE UNIVERSITY OF TEXAS AT AUSTIN
May1992

Acknowledgments

I have received an immense amount of help and support during my time at The University of Texas. I would like to acknowledge those people who were most instrumental in my success.

Special gratitude is owed to my research advisor, Professor James B. Rawlings. Through his advice I was able to gain many insights concerning my project. I learned a great deal from observing his approach to solving engineering problems.

I would like to thank my dissertation committee members: Professors Thomas Edgar, James Brock, George Georgiou, and Alan Schauer. Special thanks to Professor Georgiou, who graciously allowed me complete freedom in using his laboratory.

Someone once told me I would learn more in graduate school from the students than the professors. Someone was right. I would like to thank W. Witkowski, S. Miller, T. Mullins, K. Muske, and H. Matthews for sharing some of their intelligence with me. John Eaton deserves special acknowledgment for keeping my head above the computational backwaters.

I have been fortunate enough to meet some good friends in Austin. Thanks to Allen Hoffman, Bill Wagner, and John Knoblauh for the hilarious times. Tony and Jodee Mullins deserve my sincere gratitude. Their unselfish generosity made my last months in Austin tolerable. I would also like to thank the Bytnar family for making me feel welcome in their home.

These acknowledgments would not be complete without mention of my family. The love and support my parents and siblings have given me throughout my life have inspired me to be my best.

I would like to thank my wife, Diana. Her unfailing love and belief in me convinced me I could succeed.

Finally, I thank God for staying with me throughout the difficult times.

Andrew Patrick Fordyce

The University of Texas at Austin
May1992

MODELLING OF ANTIBIOTIC PRODUCTION BY *BACILLUS LICHENIFORMIS* USING A STRUCTURED/SEGREGATED APPROACH

Publication No. ______________

Andrew Patrick Fordyce, Ph.D.
The University of Texas at Austin, 1992

Supervisor: James B. Rawlings

This study evaluates the effectiveness of a segregated model for prediction of differentiation-related secondary metabolism in a bacterial system. Specifically, this work has examined the production of the peptide antibiotic bacitracin by *Bacillus licheniformis* in a submerged-culture fermentation system. A segregated model recognizing the three morphological stages of the *Bacillus* life cycle has been developed. The sporangium biomass has been characterized using an age-population model to reflect the age-dependent antibiotic kinetics. Constitutive relationships governing the rates of vegetative cell reproduction, spore germination, commitment to sporulation, and substrate consumption have been proposed. Based on this model framework, the dynamic cell growth, differentiation, and antibiotic production equations have been developed. Numerical solution techniques have been designed to provide solutions to the steady-state and dynamic fermentation equations.

As a means of comparison between the segregated modelling approach and more common fermentation models, a structured model has been adapted to the bacitracin system. The comparison model utilizes a two-compartment age model to describe cell growth, differentiation and bacitracin production.

Batch, steady state, and step-test fermentation data from a laboratory-scale fermentor have been incorporated into a maximum likelihood parameter estimation scheme for model identification. Confident estimates of the growth and differentiation parameters have been obtained for the segregated model using available measurements. However, the insensitivity of the bacitracin data to the production function only allowed for confident determination of a constant antibiotic production coefficient.

In contrast to the segregated model, the structure of the comparison model prevented complete utilization of the available measurements in the parameter estimation scheme. This created a situation in which the information provided by the applicable measurements was insufficient for confident determination of the model parameters. The two-compartment age model was also unable to adequately describe the delay between fermentor inoculation and the appearance of antibiotic.

Open-loop optimal control studies were utilized to compare the suggested control policies of the two models. The computed strategies were significantly different, with the segregated model suggesting a non-batch feeding policy that predicts improved antibiotic yield of 30% over the comparison model batch policy.

Table of Contents

List of Tables

List of Figures

Chapter 1

Introduction

Products derived from microbial sources have played an important role in the development of our society. A significant class of microbially-derived products are the secondary metabolites, also known as idiolite compounds. The secondary metabolites are considered to include all metabolic compounds that do not play a direct role in the normal activities of an organism. While the role of these compounds in the producing organisms is an interesting question that has stimulated much research, the secondary metabolites have achieved a higher level of importance due to fact that many of these compounds have found applications in human and animal medicine. An example of the significance of the secondary metabolites is the realization that most antibiotic compounds used in the treatment of bacterial infection are derived from compounds that are classified as idiolites.

The economic importance and increased demand for many secondary metabolites has stimulated the search for improved production strategies. Currently, these strategies have concentrated on screening for higher producing microorganisms, generation of more efficient microbial strains through mutagenesis, and improvement of growth and production media. An underutilized means by which bioprocesses can be improved is the application of process control strategies. In this context, the term control strategy is meant to imply manipulation of the available process operating variables such that some predetermined measure of process performance is improved. The basic reason that advanced control strategies are rarely utilized to improve bioprocess performance is because a high level of process understanding is essential to the success of the control scheme. Normally, process understanding is represented in the form of a mathematical model that a model-based control scheme can utilized to make decisions on how to manipulate operating variables to best achieve the desired operating goal. The complex nature of microorganisms makes them difficult systems to model. Nonlinear dynamic behavior, complex input interactions, and large time delays are common features of microbial systems.

Current efforts at developing advanced-control schemes for secondary metabolite systems have utilized simple unstructured microbial growth and product production models. These unstructured models assume microbes are a single component distributed continuously through the fermentation medium. This oversimplified picture of a fermentation system generally results in a poor characterization of observed secondary metabolite production behavior. This in turn degrades the ability of control algorithms to optimize process performance.

In actuality, microorganisms are individual entities consisting of a heterogeneous mixture of many different chemical species. Therefore, compared to the unstructured description, a more accurate picture of a fermentation system would be to recognize that a population of individual organisms exists, where the behavior of each individual cell contributes to the behavior of the population as a whole. Models that recognize the existence of individual cells and account for their effects on the cell populations are known as structured-segregated models.

Historically, the utility of population models has been limited due to several factors. A primary barrier is the lack of understanding of the mechanisms involved in cell growth and product production, making it difficult to formulate useful segregated model descriptions of fermentation systems. A second problem is the computationally-intensive nature of solution techniques required to solve the modelling equations resulting from the population balance. Further, the difficulty in obtaining measurements of cell population characteristics has been perceived as a limitation in the ability to identify segregated models. However, advances in molecular biology and the increased computation capabilities of digital computers have begun to remedy the basic problems with the segregated modelling approach.

Considering the desire to develop effective control strategies for secondary-metabolite fermentations, the goal of this work has been to develop a segregated model for secondary metabolite production and to analyze the advantages and disadvantages of the segregated approach compared to less sophisticated fermentation models. Due to the diverse nature of secondary metabolites and the organisms that produce them, it is difficult to make generalizations concerning the utility of a particular modelling approach for characterizing all secondary-metabolite fermentations. Therefore, to narrow the scope of this research to a manageable level, a specific fermentation system, representative of an industrially important subclass of secondary metabolites, will be the focus of the work presented in this thesis.

Specifically, this work develops a structured population model for the production of the peptide-antibiotic bacitracin from the bacterium *Bacillus licheniformis.* Included in this development is analysis of the issues involved in model identification, and an examination of the ability of the model to characterize fermentation behavior under a range of operating conditions. To provide a means of comparison between the proposed segregated model and the less sophisticated modelling approaches, a model from the fermentation literature has been adapted to the bacitracin system.

1.1 Review of Secondary Metabolite Production Models

Prior to a detailed development of the segregated growth and antibiotic production model, a review of the modelling approaches in the fermentation literature is helpful. Due to the economic importance of secondary metabolites, many researchers have attempted to model the growth and production characteristics of organisms that form secondary metabolites. Many different modelling approaches have been utilized to characterize secondary metabolite systems. The following discussion provides a review of the idiolite production models.

1.1.1 Unstructured Models

The simplest modelling approach, known as unstructured, is to approximate the microbial culture as a single chemical compound distributed evenly throughout the fermentation medium. Unstructured models do not recognize any measure of the culture viability, nor the fact that a population of individual microbes exists. The unstructured approach assumes that the system

Model Type	Product	Reference
Luedeking and Piret	penicillin	Constantinides et. al. 1970 [19]
Monod	griseofulvin	Calam et. al. 1971 [15]
Luedeking and Piret	penicillin	Calam and Russel 1973 [16]
substrate inhibition	penicillin	Hegewald and Rückbeil 1978 [49]
Monod multisubstrate	penicillin	Giona et. al. 1976 [40]
Monod	exotoxin	Holmberg et. al. 1980 [53]
Monod multisubstrate	penicillin	Bajpai and Reuß 1980 [5]
Monod multisubstrate	oxytetracycline	Shnaider and Biryukov 1985 [95]
catabolite repression	α-amylase	Yoo et. al. 1988 [113]

Table 1.1: Examples of unstructured idiolite production models.

behaves independently of its history, and the culture can be characterized using a measure of the quantity of biophase, such as biomass concentration or dry weight [48]. Implicit in the unstructured model is the assumption that balanced growth prevails at all times. A growth period is called balanced if every extensive variable of the system increases at the same rate. With this assumption, a single measure of the culture, e.g., biomass concentration, is sufficient to characterize all changes during the growth period [34].

The simplicity of the unstructured model has led to its historical dominance in the fermentation modelling literature. Table 1.1 provides a sampling of the unstructured models applied to idiolite producing systems. The first attempt at utilizing an unstructured model for a secondary metabolite fermentation has been attributed to Luedeking and Piret [64]. This classic model assumes that the rate of product formation is proportional to a combination of biomass concentration and the biomass growth rate:

$$\frac{dP}{dt} = a_1 X + a_2 \frac{dX}{dt} \tag{1.1}$$

where P is the product of interest, and X is the biomass concentration. This function takes into account growth-related production along with non-growth associated enzymatic activity. The Luedeking and Piret model has been utilized to model penicillin production by Constantinides et al. [19] and Calam and Russel [16]. A similar model was used by Holmberg et. al. [53] to describe exotoxin production by *B. thuringiensis.* One shortcoming of this modelling approach is its inability to predict a time delay between culture inoculation and the onset of product formation. The groups using this approach for penicillin production assumed a 20 hour delay between culture inoculation and penicillin production. Holmberg et. al. estimated that approximately 5 hours delay occurred before exotoxin appeared in batch culture. A second problem of modelling product formation based only on growth rate and biomass concentration is evident in fed-batch culture where the addition of easily metabolizable sugars can lead to unmodelled catabolite repression of product formation.

In an attempt to model the catabolite repression effect, and to explicitly recognize the dependence of idiolite production on substrate concentration, several groups have utilized unstructured kinetic models. In this approach, product formation is a function of the culture conditions:

$$\frac{dP}{dt} = f(\mathbf{s}, X) \tag{1.2}$$

where $\mathbf{s}$ is the substrate concentration vector, and $f(\mathbf{s}, X)$ is a general nonlinear function relating substrate and biomass concentration to the product formation rate. Calam et al. [16], Hegewald and Rückbeil [49], Yoo et. al. [113], and Shnaider and Biryukov [95] have considered a variety of limiting substrate kinetic models including Monod, catabolite repression, and substrate inhibition kinetics in attempting to model several different antibiotic and enzyme production fermentations. Bajpai and Reuß [5] and Giona et al. [40] both utilized models where the rate of penicillin formation depended on limiting sugar and dissolved oxygen concentration.

1.1.2 Structured Models

The structured modelling approaches have emerged as an attempt to provide a better measure of the culture state, thus allowing for dependence of current behavior on culture history, and allowing for situations where unbalanced growth prevails. Reviews of structured microbial growth models have been provided by Harder and Roels [48] and Shuler [98]. Structured models treat the culture not as a single entity, but as groups of distinguishable entities, which taken together represent the biotic phase. While these models can account for time-dependent changes in the makeup of the biotic phase, they cannot account for variation between individual organisms within the population. However, the structured models do provide a better approximation to the actual culture state then an unstructured approach. Chemical structure is the most common type of structured model. An example would be a model tracking the concentration of RNA and protein [87]. This two compartment chemical model is more complex than the unstructured model allowing for a measure of the biomass quality, rather than just a simple measurement of biomass quantity.

Several applications of structured models to secondary metabolite forma-

Model Structure	Product	Reference
age	antibiotics	Aiba and Hara 1965 [1]
morphological	antibiotics	Megee et. al. 1970 [72]
age	gramicidin-s	Blanch and Rogers 1971 [11]
age	streptomycin	Brown and Vass 1973 [13]
chemical	exoenzymes	Van Dedem et. al. 1973 [24]
age	antibiotics	Fishman and Biryukov 1974 [31]
age	macrolides	Martin and McDaniel 1975 [69]
morphological	cephalosporin C	Matsumura et. al. 1981 [71]
chemical	alkaloids	Patžoutova et. al. 1981 [80]
morphological	δ endotoxin	Schulz et. al. 1985 [93]
chemical	tetracycline	Běhal et. al. 1985 [14]
chemical	cycloheximide	Dykstra et. al. 1988 [27]

Table 1.2: Examples of structured secondary metabolite production models.

tion, shown in Table 1.2, have appeared in the literature to date. Examples of chemically structured models are common. One example is the production of alkaloids by *Claviceps purpurea.* Pažoutova et al. [80] utilized a chemically structured model that accounts for the intracellular phosphate concentration as an indicator of the product formation rate. Other researchers have used catabolite repression models to track the intracellular concentration of some critical product synthetase enzyme. Dykstra et al. [27] used this approach for cycloheximide production by *Streptomyces griseus*. Běhal et al. [14] modelled tetracycline production by predicting the activity of an oxygenase enzyme, considered limiting in the tetracycline fermentation. Van Dedem and Moo-Young [24] have compared induction and repression mechanisms in the formation of extracellular enzymes using a structured model.

A second form of structured model is the age-structured model. A number of natural aging phenomena have been observed in microbial systems. Growth in many mycelial organisms occurs in the apical region. Bud scars in yeast cells establish a physical age marker that affects the ability of the yeast cell to reproduce. Cell differentiation has been attributed to an aging process and has been linked to product formation [96]. In a general formulation, a model based on age would be considered segregated because age is a continuous variable providing a unique identity to each cell in the culture. Several authors have reduced the general age-segregated model to a structured conceptualization by assuming the continuous age distribution can be approximated by two or more age groups. Blanch and Rogers [11] used an age-structured model to predict gramicidin S formation by *Bacillus brevis*. They divided the cell culture into two groups, mature and immature cells. Mature cells were responsible for both antibiotic formation and reproduction. This model was able to simulate experimental fermentation responses for both batch and continuous culture, except at high dilution rates. The authors suggest several possible explanations for the poor performance at high dilution rate, including unmodelled growth lags, and chemostat instability. Brown and Vass [13] used a similar age-structured model for gramicidin S and streptomycin fermentations. Martin and McDaniel [69] also used the age grouping technique to model macrolide antibiotic production by a variety of *Streptomyces* species.

A minor variation of the age-structured model, introduced by Aiba and

Hara [1], correlates the culture's "cumulative age" to the specific antibiotic formation rate. The cumulative age is a crude measure of the average age of the cell population. The cumulative age, θ, was given by:

$$\theta = \frac{X_0\theta_0 + \int_{t_0}^{t} \tau X(\tau)\, d\tau}{X(t)} \tag{1.3}$$

where X_0 and θ_0 are the initial cell concentration and cumulative age, respectively. Fishman and Biryukov [31] used this approach fitting a quadratic function of cumulative age to the specific product formation rate and developed feeding strategies for maximizing product.

Models that can be considered structured, but do not use chemical or age grouping have also appeared in the literature. Megee et al. [72] designed an idiolite production model based on the different mold morphologies observed in submerged culture. This model takes advantage of the common observation that secondary metabolites appear concomitant with cellular differentiation processes. A similar approach was used by Matsumura et al. [71] to characterize the production of cephalosporin C by *Cephalosporium acremonium.* This group divided the biotic phase into three separate morphological groups: hyphae, swollen fragments, and arthrospores. From experimental observation it was noted that the swollen fragments were the highly productive fraction of the biomass. Using the morphologically-structured model they were able to closely approximate experimental antibiotic production data. A final morphologically-structured example is provided by Schulz et. al. [93] who used several morphological states to model the δ endotoxin formation in spores of *B. thuringiensis.*

1.1.3 Segregated Models

A more accurate portrait of a microbial system is a population of cells, each cell having its own distinguishing characteristics, each cell responding to its local environment. The segregated modelling approach attempts to characterize the fermentation based on the idea that the overall population behavior can be attributed to the behavior of the individual members of the population. This methodology can be used to account for phenomena such as cell-size dependent growth rates, age-dependent production rates, or any other activity which can be related to some characteristic that distinguishes members of the population. The segregated modelling approach, known as population modelling, has been reviewed by Ramkrishna [86, 85] and a general discussion is provided by Hulburt and Katz [54].

Very few population models have been applied to secondary metabolite fermentations. One possible reason for the dearth of population models for secondary metabolite systems is the difficulty in measuring distributions of population characteristics in fermentation systems [97, 5]. One exception is the model presented by Shu [96]. Shu used an age-segregated population balance to model product accumulation in batch and continuous fermentation systems. The specific product formation rate was fit using a set of exponential basis functions, given by:

$$\mu_p = \sum_i A_i \exp(-k_i \tau) \tag{1.4}$$

where τ is the cell age and A_i are experimentally fit parameters. This formulation is fairly versatile, and it can be used to model the transient behavior of many types of fermentations. Some drawbacks of this approach include difficulty in estimating the parameters of the production function and the fact that this model does little to explain the physical mechanisms involved in secondary metabolite formation [97].

1.2 Research Goals

At this time, there are few experimental studies concerning the application of a population balance model to a microbial system. It is the objective of this research to help fill this void by examining the feasibility and utility of using a segregated model to predict the dynamic behavior of a microbial secondary metabolite fermentation system. As a part of this project, the following research goals were identified:

- To identify a secondary metabolite system for which a segregated model could facilitate improved predictive capabilities.
- To develop a dynamic model describing the growth and product production using a segregated model.
- To construct a laboratory–scale fermentation apparatus to collect data for model identification.
- To examine the accuracy in different regions of the operating space.
- To compare the proposed model to a structured model existing in the fermentation literature.
- To analyze and compare open-loop optimal control strategies for maximization of bacitracin production based on each model.

1.3 Dissertation Organization

This dissertation is divided into six chapters. This chapter contains introductory material concerning the author's perception of the role of mathematical modelling in the realm of fermentation engineering. This includes a literature review of fermentation models for secondary metabolite production, and a discussion of the goals of this research project.

Chapter 2 proposes modelling of the production of the peptide antibiotic bacitracin by *Bacillus licheniformis* as a model system to explore the utility of the segregated modelling approach. Based on the biology and physics of the proposed model system, a dynamic, segregated model is developed, and solution techniques for the resulting model are described. To provide a comparison for the segregated approach, a structured model proposed by Blanch and Rogers [11], is modified to describe the bacitracin system.

The third chapter describes the experimental apparatus used for model identification and validation. A detailed description of the laboratory-scale fermentor is given, along with discussion of the experimental procedures for growth and analysis of the bacteria and the product assays.

Chapter 4 examines the issues of model identification and validation. Model parameters for growth, differentiation, and antibiotic production are estimated for both the segregated and comparison models, based on experimental fermentation data. Evolution of the models from their initial proposed forms to their final form is discussed. The resulting parameter estimates are examined.

In Chapter 5 comparisons of the two models are made. Included in the comparison are issues of model identification, effectiveness of model fit, and open-loop optimal control strategies suggested by each model.

The final chapter summarizes the conclusions of this research, and suggests directions for further study.

Chapter 2

Model Development and Solution

2.1 Model System

The basic goal of this research is to explore the effectiveness of the segregated modelling approach for the prediction of secondary metabolite production. In selecting a model system several criteria were considered important. First, to analyze the utility of a segregated model it was necessary that suitable non-segregated models existed in the literature to provide a yardstick for comparison purposes. Additionally, since experimental verification of a model is desirable, the growth of the model organism and metabolite production needed to be experimentally tractable. Finally, it was important that the chosen metabolite product be industrially relevant. With those considerations in mind, production of the peptide antibiotic bacitracin by the bacteria *Bacillus licheniformis* was chosen to explore the effectiveness of the segregated modelling approach.

Bacitracin production is a good choice as an experimental model for many

Product	Application
peptide antibiotics	feed additives, Topical Antibiotics
amino acids	nutritional supplements
exoenzymes	food, textiles, paper Industries
insect pathogens	biopesticides
biosurfactants	enhanced oil recovery

Table 2.1: Industrial applications of sporulation-associated products from *Bacilli* [23, 35].

reasons. First, many of the useful *Bacillus* products are associated with the differentiation process, and insight into strategies for production of bacitracin could be directly applicable to a wide variety of *Bacillus* derived metabolites, including the sporulation-related products shown in Table 2.1. Concerning experimental tractability, species from the *Bacillus* genus generally have simple nutritional needs and grow quickly. A large literature exists concerning growth conditions, and procedures for the assay of bacitracin are available. Also, the *Bacillus* unicellular morphology greatly simplifies the measurement of cell numbers. Finally, although no structured models have appeared for the production of bacitracin, an age-structured model, conceived by Blanch and Rogers [11], exists for the production of a closely related peptide antibiotic, gramicidin. This model is adaptable to the bacitracin system, and serves as a comparison model for the segregated approach.

The genus *Bacillus* includes the aerobic, unicellular endospore forming bacteria. These microorganisms are normally gram positive, but some species become gram negative upon differentiation. All species can utilize oxygen in

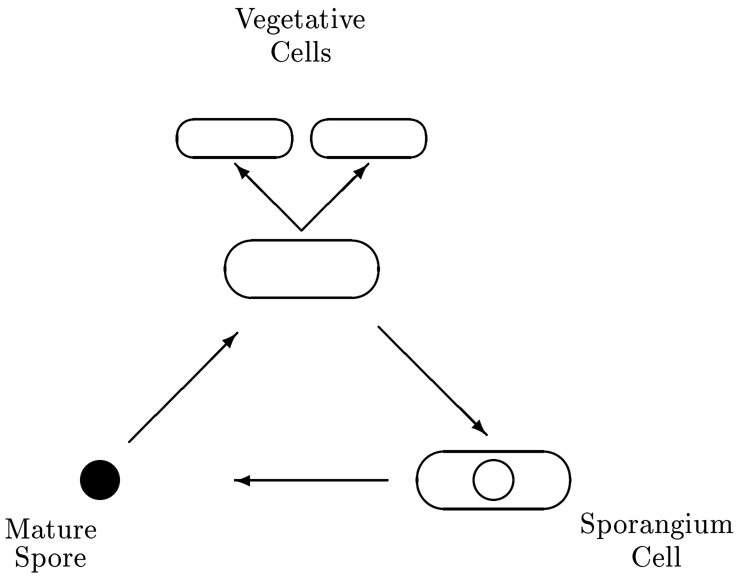

Figure 2.1: The *Bacillus* life cycle consists of three stages. The first is the vegetative stage, in which cell growth and fission occur. In nutrient depleted surroundings sporangium cells form, starting the cell differentiation process. A mature endospore is the final stage of the cycle.

aerobic respiration, while some species can also take advantage of anaerobic fermentative and denitrificative pathways [103]. The *Bacillus* life cycle, illustrated in Figure 2.1, begins with germination of an endospore cell when environmental conditions become favorable. The resulting vegetative cell reproduces via binary fission until the environment becomes adverse to normal growth. At such a time, the cell begins a differentiation process converting from a vegetative cell to a sporangium. In a sequence of well-timed steps a single endospore forms within the sporangium cell. Concurrent with the differentiation process many secondary metabolites, including several types of antibiotics and exocellular enzymes, are produced. When the endospore reaches maturity the sporangium cell lyses, releasing a mature spore. The spore remains in a state of cryptobiosis, with no detectable metabolic activity, until environmental conditions become favorable for growth again [103].

2.1.1 Review of Sporulation Models

Considering the connection between idiolite production and the differentiation process exhibited by *B. licheniformis*, a prerequisite of predicting antibiotic production is the ability to model the dynamics of growth and differentiation. At this time, only a few mathematical models for the *Bacillus* growth and differentiation processes have appeared. The first is attributable to Dawes and Thornley [22], who developed a segregated model to describe growth and sporulation of *B. subtilis* in continuous culture. More recently, sporulation models have been examined by Ollis [79] and Schulz et. al. [93]. Ollis modelled the production of exotoxin from *B. thuringiensis* using an age-structured model. The kinetics of exotoxin production were treated using the Luedeking-Piret equation (see Section 1.1.1), and spore formation was considered to be first order with respect to the delayed biomass concentration. Ollis' model results in 3 ordinary differential equations coupled to a delay differential equation for the spore concentration. The age-structured model was able to model batch data well. However, the simple spore initiation model used could lead to problems in continuous and fed batch fermentations, where the addition of easily metabolizable sugars leads to repression of sporulation commitment.

Similar to Ollis, Schulz et. al [93] modelled exotoxin production from *B. thuringiensis* using a morphologically-structured model with four distinguishable cell states. Transition between the vegetative phase to sporangium, and in turn, to endotoxin containing cells, and finally mature spores was modelled using delay differential equations. This model was used to characterize batch and continuous growth, and optimal operation was determined for one and two-stage continuous fermentations.

The development of highly-structured, single-cell models, popularized by the Cornell *E. coli* model of Shuler et al. [99], have recently been applied to *Bacillus* species in an attempt to model the differentiation process. Jeong et. al. [56] have proposed a structured single-cell model consisting of 39 nonlinear differential equations with almost 200 parameters. The goal of this model is to account for the principal interactions between the major metabolic networks in *B. subtilis*, with the goal of describing the biochemical patterns associated with the transition from vegetative growth to sporulation. A similar structured approach has been used by Starzak and Bajpai [104] to model the vegetative growth cycle and the transition to sporulation. Neither of the highly-structured models make a clear distinction between cells in the vegetative or sporangium stages of development, instead commitment to sporulation is treated as a continuous transition with no clear demarcation between growth and differentiation The inability of these models to predict simultaneous presence of vegetative and differentiated cells is an obvious shortcoming, but the basic structure of these models does allow for an in depth analysis of the intracellular dynamics of growth and the control system for sporulation initiation.

2.2 Segregated Model Development

In contrast to the goals of the single-cell models proposed by Jeong et. al. [56] and Starzak and Bajpai [104], the intended use of the model proposed in this research is as a tool for development of control strategies. Considering this, it was determined desirable properties of the model included a minimum of adjustable parameters and reasonable computational times, while still main-

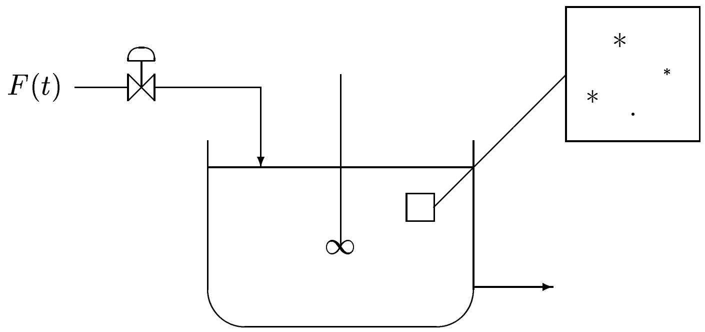

Figure 2.2: A well-mixed, stirred-tank fermentor depicting a microscopic view of a population of *Bacillus licheniformis*.

taining an accurate representation of the physical system.

2.2.1 Microscopic View

A typical *Bacillus* fermentation consists of a mixture of cells in an aqueous environment containing a variety of soluble nutrient components and metabolic byproducts. A view of a microscopic fluid packet, depicted in Figure 2.2, shows a collection of cells in various stages of growth and differentiation. Each cell consists of many different chemical components with a multitude of simultaneous reactions, allowing the cell to both affect and respond to its local environment. The situation is further complicated by a variety of mass transfer processes involved in the internalization, transformation, and incorporation of nutrients into existing and new biomass. Based on this description, it is easy to imagine how overwhelming a complete mechanistic model of all reactions and transport processes would be. Therefore, the task is to determine the essential elements of the fermentation, and to translate those processes into a mathematical description. In this way, the complexity of the problem is reduced, and the important aspects of the system are captured.

In an effort to develop a useful, yet tractable, model for production of bacitracin from *B. licheniformis*, inspiration is taken from the microscopic picture of a culture. An obvious characteristic of a *Bacillus* culture is the presence of three distinct cell types: vegetative, sporangium, and spore, as shown in Figure 2.1. A logical modelling approach is to structure the biomass according to its three distinct morphologies. Morphological structure is appealing because it provides an accurate representation of the actual microscopic picture. Also, since bacitracin production is localized in the differentiating portion of the biomass, it is important that a model recognize the existence of the different types of biomass. Dawes and Thornley [22] have utilized morphological structure to develop a steady-state model for *Bacillus subtilis* in continuous culture. In this work, a similar morphological structure has been utilized to develop a dynamic model for *Bacillus licheniformis* in batch and continuous culture modes.

2.2.2 Spore Biomass

Species from the *Bacillus* genus are ubiquitous in soil environments and exist primarily in a dormant state, known as a spore. The spore morphology is ellipsoidal and approximately 0.3–0.5 μm in diameter. This is distinctly different than the rod-shaped vegetative cell morphology. Using phase-contrast microscopy spores appear as phase-bright bodies. In comparison, the vegetative cell form appears as dark, elongated body, and thus the presence of spores is readily detectable using light microscopy.

In addition to the visible morphological differences, spores also exhibit significantly altered resilience with respect to harsh environmental conditions. This includes an abnormally high resistance to heat, desiccation, radiation, and chemicals. The unusual resistance properties of spores are attributable to several major differences between the outer layers of a spore and those of vegetative cells. Normal gram-positive vegetative cells are contained by a phospholipid bilayer enclosed by a rigid peptidoglycan cell wall. In addition to a cell wall and membrane, spores are enclosed by several extra layers, including the cortex, spore coat, and exosporangium. It appears that these additional layers, along with several stabilizing adaptations of the spore protoplast, are responsible for the acquisition and maintenance of resistance properties, allowing for sustained viability in unfavorable environmental conditions [38].

The spores remain protected in a dormant state, until environmental conditions change such that growth becomes favorable. At this time, the spore sheds its protective layers and returns to the vegetative state.

2.2.3 Vegetative Biomass

In a normal growth situation a *B. licheniformis* culture consists primarily of vegetative cells. These cells represent the portion of the biomass that is actively growing and dividing. Vegetative cells are gram positive and are rod shaped, measuring approximately 0.6 μm in diameter and 2.2 μm in length. The mode of reproduction is binary fission, resulting in the production of two daughter cells of approximately equal size. Vegetative cells can exist in short chains of 2–3 cells, however, in a well-mixed environment the majority of the cells exist as singlets. Most strains exhibit motility, particularly in nutrient depleted conditions [41].

B. licheniformis is a facultative aerobe, having a functional respiratory chain, allowing for growth using electron transport with oxygen as the terminal electron acceptor. In anaerobic conditions, *B. licheniformis* utilizes either an anaerobic respiratory pathway, with nitrate as the electron acceptor, or a fermentative pathway yielding a mixture of organic acids [59]. Vegetative growth is possible using a variety of carbon and nitrogen sources in defined and complex media, and typical doubling times range from 50–90 minutes, depending on the nutrient source and oxygen availability [59].

2.2.4 Sporangium Development

In addition to vegetative cells and spores, a third type of cell exists in a pure *B. licheniformis* culture. These cells, known as sporangia, represent the individuals in transition between the vegetative growth state and the dormant spore.

After commitment to the sporulation pathway, the cell goes through a tightly regulated differentiation process coded in the DNA. Historically, the progress of sporulation has been gauged based on morphological changes visible by microscopy. The morphological markers of sporulation are depicted in Figure 2.3. Stage 0 is the vegetative state, and therefore, represents a growing cell, prior to commitment. There exists controversy concerning the first morphological manifestation of sporulation. Prior to mutational studies, stage I was consider to be condensation of the chromosome in an axial filament. However, since no mutants have been found to be deficient in formation of the axial chromosomal filament, stage I has been generally discarded [63]. The first accepted morphological development, termed stage II is the appearance of an asymmetric membrane division, dividing the cell into two compartments of unequal size. Both the small compartment, known as the forespore, and the large compartment, the mother cell, contain intact copies of the chromosomal DNA. At this point, the sporulation sequence progresses to stage III, where the small compartment is engulfed by the mother cell, producing a free protoplast within the mother cell's cytoplasm. The protoplast has a double-walled membrane created during engulfment. During stage IV a thick layer of modified-peptidoglycan wall material is deposited between the two forespore membranes, creating the spore cortex. Stage V brings enclosure of the outer membrane layer in a covering of polypeptides, called the spore coat. At this time, the spore develops its characteristic refractility, and becomes visible using phase-contrast light microscopy. Following the development of refractility, the prespore develops into a mature spore, gaining the resistance properties against heat, chemicals, desiccation and radiation. The stage of spore maturity is termed stage VI. The final development, stage VII is lysis of the mother cell releasing a mature spore. The entire sporulation process, from commitment to appearance of mature free spores takes approximately 8–10 hours [76, 63].

Along with the characteristic morphological changes observed during differentiation, a variety of biochemical markers are also recognized in association with stages of spore formation. Production of extracellular macromolecular degradation enzymes including α–amylase, proteases, and nucleases are all associated with early sporulation (i.e. stages 0–II). Antibiotics, including bacitracin in *B. licheniformis*, are also expressed early in the differentiation sequence [76]. Mid-sporulation biochemical markers include alkaline phosphatase at stage II and glucose dehydrogenase between stages III and IV. A pronounced late-sporulation marker is the expression of dipocolinic acid, which is unique to spores [83].

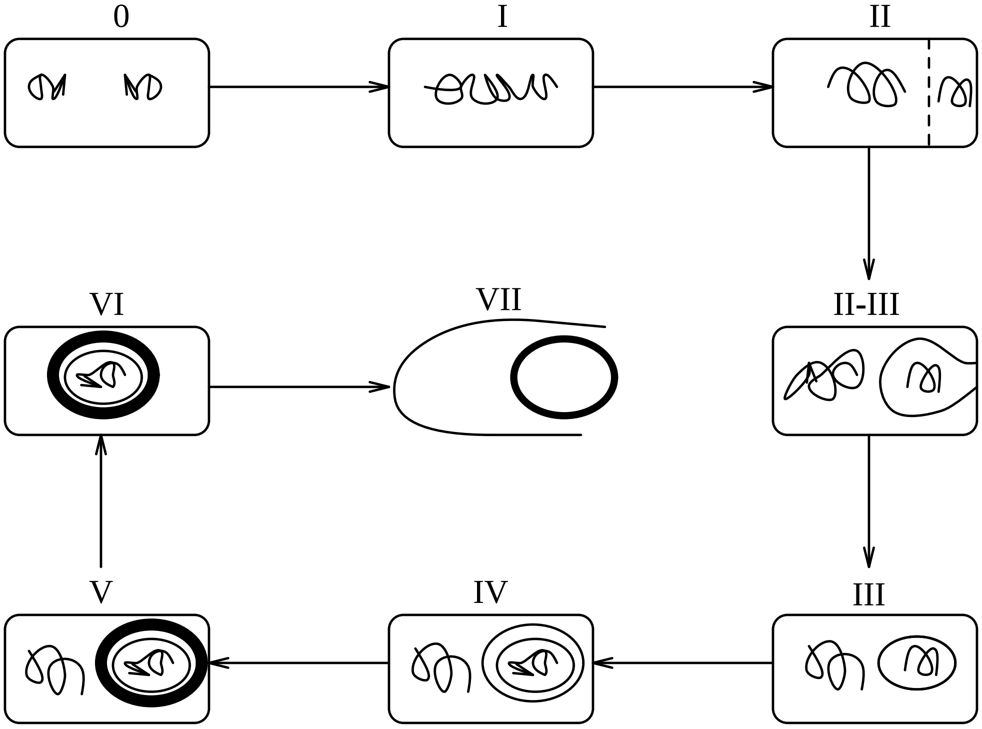

Figure 2.3: The morphological markers of spore formation.

2.2.5 Model Structure

By deciding to structure the *B. licheniformis*-bacitracin system based on cell morphology, a foundation for the proposed model has been established. In addition to the model structure, it is necessary to characterize the level of sophistication required to model each portion of the biophase. Finally, to complete the model, it is essential that the mechanisms by which the cell groups interact with each other and their environment are identified and characterized.

The interconnect cycles of growth and differentiation exhibited by *B. licheniformis* are diagrammed in Figure 2.4. Processes including spore germination,

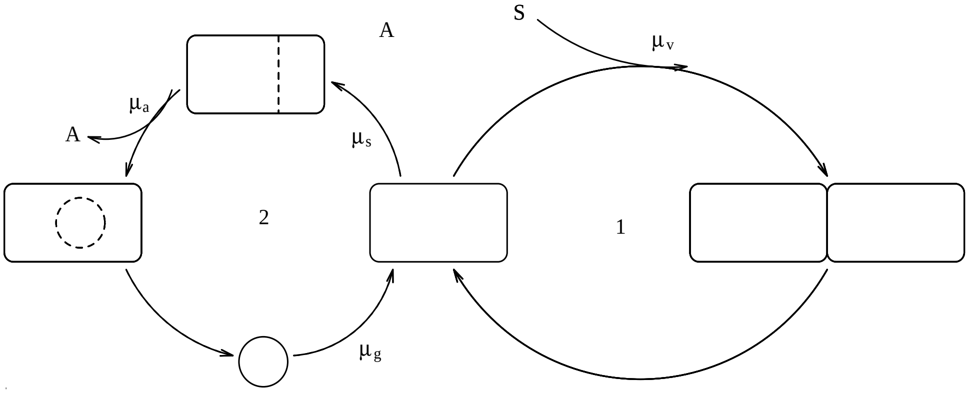

Figure 2.4: The interconnected cycles of growth and differentiation in *B. licheniformis*. Cycle 1 depicts the process of vegetative reproduction and its connection to the consumption of substrate, s. Cycle 2 represents the differentiation cycle, and its connection to the production of antibiotic, A. The rates of spore germination, vegetative growth, sporulation commitment, and antibiotic production are represented by μ_g, μ_v, μ_s, and μ_a, respectively.

vegetative growth, substrate consumption, and sporulation commitment are all involved in the relationships relating cell morphologies, and therefore must be described by the model. Further, the relationship between the process of differentiation and production of bacitracin is essential in attaining the desired goal of modelling bacitracin production.

In the following sections, a model for each of the three portions of the biomass is developed. Also, mathematical representations for the growth and differentiation rate processes are examined. The combination of the rate expressions and the structure of the biophase comprise the kinetic portion of the segregated mathematical model for the *B. licheniformis* fermentation system.

2.2.6 Vegetative Biomass Model

In its original formulation the Dawes and Thornley model [22] was primarily for description of steady-state growth and sporulation kinetics found in the chemostat fermentor. Therefore, a Monod type vegetative growth law was used to represent the balanced growth conditions of the chemostat. Assuming growth of vegetative cells, X_v, is limited by a single substrate, of concentration s, then the Monod growth law is of the form:

$$\frac{dX_v}{dt} = \mu_v X_v \tag{2.1}$$

$$\mu_v = \frac{\alpha_v s}{K_v + s} \tag{2.2}$$

The Monod growth function, illustrated in Figure 2.5, models the specific rate of vegetative cell production using two parameters. The parameter α_v represents the maximum attainable growth rate, and K_v is the substrate concentration that will support a growth rate of half the maximum. The structure of the Monod model is based on the assumption that growth is limited by a single biochemical pathway that exhibits Michaelis-Menten saturation kinetics. In most cases, this is an oversimplification of the actual situation, so it is not possible to link any phenomenological meaning to the growth parameters. However, the Monod expression has been successfully applied in many growth situations [4]. Utilization of Monod growth kinetics implicitly assumes vegetative cells are indistinguishable from each other, and the growth properties of the culture are based on an average cell. Further, balanced growth is a basic assumption of this approach. Based on the assumptions of indistinguishability and the lack of structure in the vegetative biomass, the Dawes and Thornley vegetative model is both nonsegregated and unstructured.

While this unstructured model of vegetative cells proved adequate under the steady-state conditions presented by Dawes and Thornley, batch growth

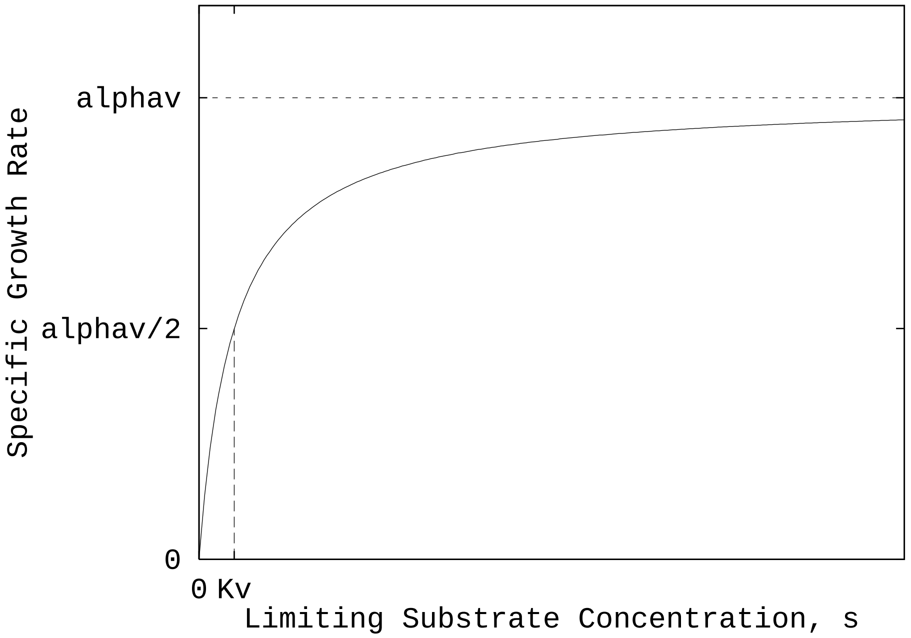

Figure 2.5: Monod saturation kinetics. The parameter α_v represents the maximum growth rate, and K_v is the Michaelis constant representing the substrate concentration needed to sustain a growth rate of $\alpha_v/2$.

experiments carried out in this study showed the unstructured growth model was unable to describe many characteristics of transient batch growth. A detailed discussion of the experimental work used for parameter estimation is provided in Chapter 4. However, to provide a basis for the model development discussion, dimensionless cell number and substrate concentration data from a typical *Bacillus licheniformis* batch fermentation are shown in Figure 2.6. An obvious oversight of the pure Monod growth law is it inability to predict a decline in nonspore biomass associated with cell death. The batch data show a rapid decrease in the nonspore biomass without an associated increase in the spore count, thus implying not all vegetative cells form spores. This

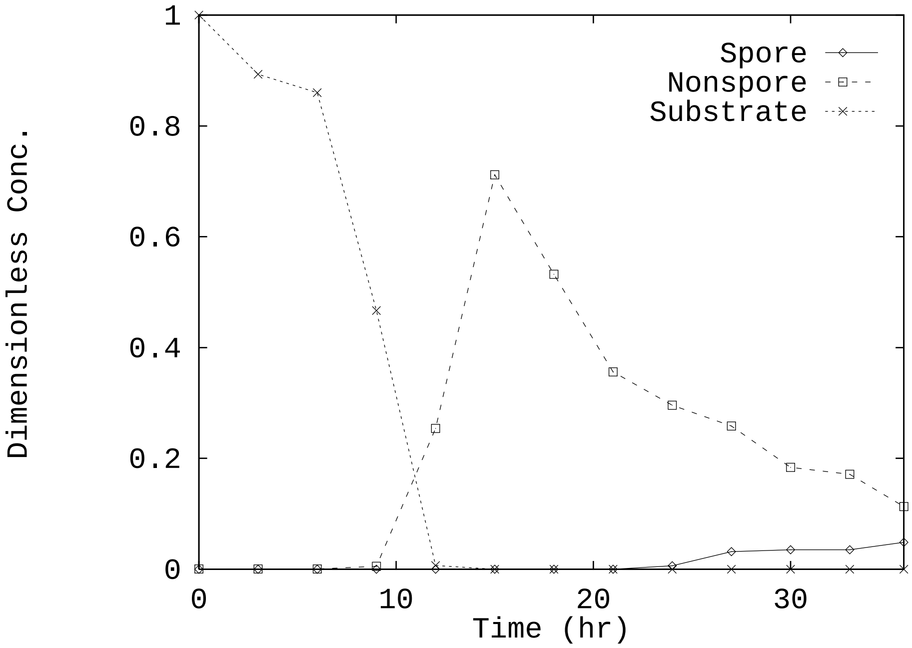

Figure 2.6: Batch growth and sporulation data for *Bacillus licheniformis* showing transient growth phenomenon unexplained by a Monod growth law.

phenomenon is unaccounted for using Monod kinetics. A second more subtle inconsistency between the batch data and the unstructured growth law is the continued growth of the non-spore biomass after the limiting substrate has been exhausted. Finally, the initial phase of the fermentation, where little or no growth is apparent even though substrate is consumed, is also unexplained by an unstructured growth model.

Structured Vegetative Growth. While the morphological structure of the Dawes and Thornley model is still considered appealing, a more sophisticated vegetative growth model is necessary to adequately describe the transient

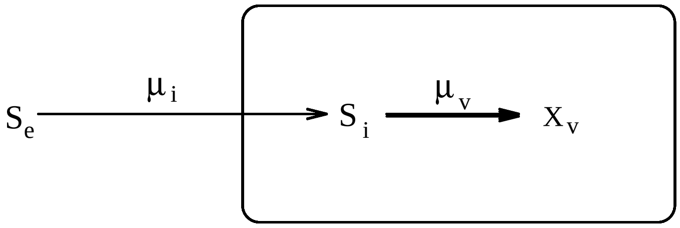

Figure 2.7: Structured vegetative cell model. First, external substrate, s_e, is internalized at a rate μ_i, and converted to readily utilizable biosynthetic precursors, s_i. Second, cell precursor, s_i, is converted into new biomass, X_v, at a rate μ_v.

growth phenomenon observed in the batch experiments. A two-compartment chemical model, diagrammed in Figure 2.7, has been proposed to describe the transient growth kinetics. The structured growth model makes a distinction between the ability of a cell to take up a limiting nutrient, and the capacity to convert that nutrient into biomass. The hypothesis of competitive rates of nutrient transport and biomass production was first proposed by von Bertalanffy (see [106] pg. 195). Similar two-compartment models have also been proposed by Williams [111] and Ramkrishna et. al. [87].

Using the structured vegetative model, growth is considered to be a two-stage process. First, the limiting nutrient is taken up by the existing biomass at a rate given by μ_i. This nutrient exists internally in the cell as readily available precursors for biosynthesis and energy production. In the second stage, the internalized nutrient pool is utilized at a rate given by μ_v, to produce biomass and energy necessary for growth and maintenance. The buildup of internal substrate, s_i, can be interpreted as an increase in average cell mass, and conversely a decrease in the internal metabolite pool occurs when the rate of cell division exceeds the rate of replenishment of biosynthetic capacity leading to a decrease in average cell mass. This concept is supported by the observation that cells growing in nutrient rich environments are large and become smaller when the surroundings become nutrient depleted.

The two-stage growth process provides a possible explanation for the transient growth phenomenon observed in the batch fermentation experiments. According to the structured vegetative model, the initial growth lag results because the newly inoculated cells must build biosynthetic capacity to utilize the available substrate. During the lag phase, the process of substrate internalization is the growth limiting step. A transition between the slow-growth lag period and the logarithmic growth phase occurs when enough substrate has been internalized to promote rapid growth. At that time, the rate limiting process shifts from substrate internalization to biosynthesis. The logarithmic phase continues until nutrient depletion forces a decline in the growth rate.

The two-compartment growth model also provides a possible explanation for post-nutrient exhaustion cell division observed in the batch fermentations. According to an unstructured vegetative growth model, cell growth rate immediately responds to changes in the external environment. This would suggest that cell growth would cease immediately upon exhaustion of the limiting substrate in the surrounding environment. Observation of batch fermentations shows that production of colony forming units continues for a short time after the limiting carbon source has been depleted in the growth medium. With the structured model, growth is dependent on the internal substrate concentration, thus allowing for situations where growth can continue in lieu of completely nutrient deficient surroundings. After the initial lag phase, the batch growth is limited by biosynthetic capacity. When the limiting substrate becomes exhausted in the growth medium, the internal biosynthetic capacity begins to decline. Thus, the rate-limiting process reverts back to the substrate internalization step, and growth slows until finally ceasing with the exhaustion of the internal nutrient supply. Therefore, the process of vegetative reproduction continues for a short period after the external limiting substrate is gone.

The death-associated decline in nonspore biomass can be modelled by including an death rate constant, m_v in the biosynthetic grow rate function, μ_v.

$$\mu_v(s_i) = \mu_t(s_i) - m_v \tag{2.3}$$

The explanation for this is that the total biosythetic rate, μ_t, is a combination of growth and maintenance activity. Utilization of substrate for growth activity results in an increase in biomass. However, substrate is also consumed for energy and precursor generation necessary to retain viability. Therefore, substrate consumption resulting in increased biomass is only part of the total substrate consumption. Typically, the maintenance activity is considered to be constant, and thus results in a downward shift of the substrate dependent specific growth rate. The Monod growth law including a death term is shown in Figure 2.8. As the plot shows there exists a critical substrate concentration, below which the growth rate is negative. The negative growth rate represents loss of colony forming units resulting from cell death [4].

Utilizing the structured growth kinetics including death kinetics, the substrate internalization and cell growth rate expressions are given by:

$$\begin{aligned} \mu_i &= \frac{\alpha_i s_e}{K_i + s_e} && (2.4) \\ \mu_v &= \frac{\alpha_v s_i}{K_v + s_i} - m_v && (2.5) \end{aligned}$$

The resulting equations utilize five adjustable parameters. Again, α_v and α_i represent the maximum rates of the respective processes and K_v and K_i are affinity constants representing the concentration needed for half the maximum rate. Cell death is accounted for by the endogenous metabolism term, m_v.

An additional consideration in modelling cell growth is the effect of the

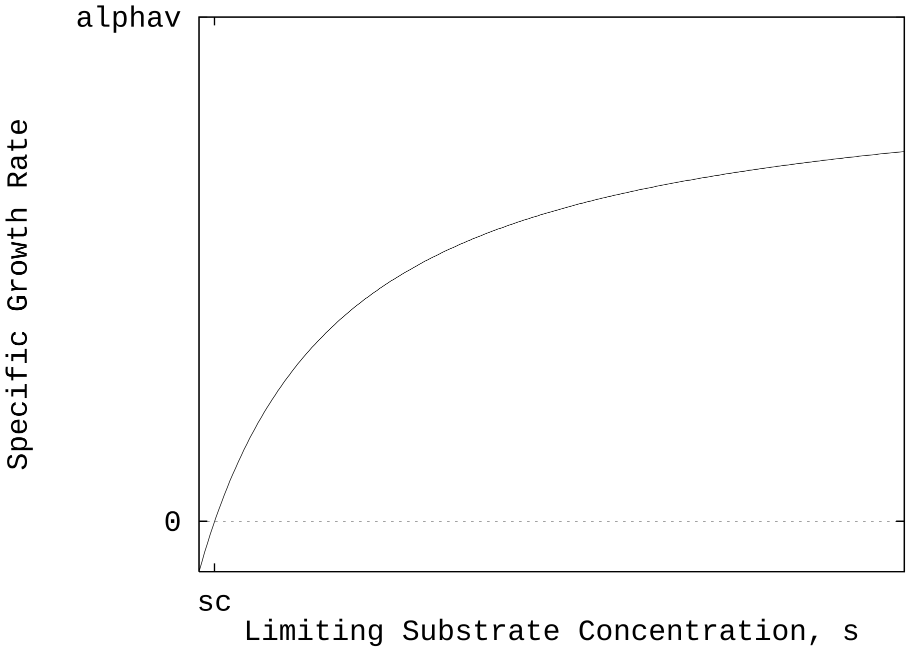

Figure 2.8: Monod growth rate including death kinetics. The substrate concentration, s_c, is the critical substrate concentration below which cell death occurs.

antimicrobial product on the producing organism. In the case of *B. licheniformis*, Haavik [45] observed a minimal effect of bacitracin on growth rate for bacitracin concentrations up to 30 (IU/ml). In this study, maximal bacitracin titers reached approximately 3.0 (IU/ml), and therefore, the effect of bacitracin on growth rate was assumed to be negligible.

2.2.7 Spore Biomass Model

The spore biomass is a source for vegetative cells through the process of germination. Therefore, to provide a complete characterization of the *Bacil-*

lus licheniformis system, it is necessary to develop a rate expression relating germination to the fermentor conditions. The approach taken in this research is to treat the spores as indistinguishable and unstructured. In line with this simple conceptualization for the spore biophase, a Monod growth expression has been used to relate the specific rate of germination to the current limiting-substrate concentration:

$$\mu_g = \frac{\alpha_g s_e}{K_g + s_e} \tag{2.6}$$

As in the case of vegetative growth, α_g and K_g represent the maximum germination rate and the germination Michaelis constant, respectively. Again, the biochemical significance of parameters α_g and K_g is not obvious and this relationship is considered empirical. However, for most industrial fermentations, spore germination does not contribute significantly to vegetative cell concentrations after the initial inoculant is prepared [22]. Also, spore germination experiments, described in Section 4.3.1, indicate that germination is subject to a significant time delay. This observation is consistent with the findings of other groups. In particular, Maraheil et. al. [68] found that outgrowth in *B. brevis* occurred after a 8–10 hour lag period. Also, Dawes and Thornley [22] considered the number of germinating spores to be insignificant in continuous culture experiments with *B. subtilis.* These results indicate that germination is a relatively slow process compared to growth and sporulation in normal batch and continuous culture. Therefore, since the spores generally appear at the end of batch runs, when nutrient depletion has occurred, and there is a significant lag time during germination, it seems likely that spores contribute an insignificant number of cells to the vegetative phase. For this reason, little emphasis has been placed on the spore germination model.

2.2.8 Sporangium Model

As was discussed Section 2.2.4 on sporangium development, there are many morphological and biochemical differences between sporangia at different stages of development. Significantly, bacitracin is produced during sporulation, and the rate of bacitracin production for an individual sporangium is thought to depend on its progress through the sporulation pathway. Therefore, not only are the sporangia distinguishable based on their progress toward creating a spore, but it is logical that the model should recognize the differences in sporangia if the goal is to predict production of a sporulation dependent product, i.e. bacitracin. This implies the need for a segregated model, which recognizes the differences in sporangia, and allows for incorporation of the distinguishing characteristics of the sporangium population into the antibiotic production model.

Population Balance. Translation of the notion of distinguishability between individuals into a mathematical description involves development of the population balance. The basis of the mathematical description for a population is the definition of the particle density function, $f(\mathbf{z}, t)$. This scalar valued function is defined as the number of individuals per unit volume. The particle density expression is a function of $\mathbf{z}$ and t, where $\mathbf{z}$ defines a vector of distinguishing characteristics, and t represents time. It is convenient to break the coordinate vector, $\mathbf{z}$, into two vectors, $\mathbf{x}$, representing the external or spatial coordinates, and $\mathbf{y}$, representing internal or descriptive coordinates. The need to include spatial coordinates comes from the fact that an individual could behave differently than others and is distinguishable due simply to its location in space. The internal coordinates represent the characteristics of an individual which make it distinguishable regardless of position. Examples of internal coordinates are size, age, and chemical composition. The choice of the internal coordinates allows the modeller infinite flexibility, but with increased coordinates comes increased complexity. Therefore, internal coordinates are chosen such that they reflect the most important characteristics of the system of interest.

After selection of suitable descriptive coordinates, the derivation of the population balance equations is simply an accounting of individuals with respect to the coordinate system of choice. General derivations of the microscopic population balance are provided by several researchers including Randolph and Larson [88], Rawlings [89], and Hulburt and Katz [54].

The population balance resulting from microscopic continuity is given by:

$$\frac{\partial f}{\partial t} + \nabla \cdot (f \frac{d\mathbf{z}}{dt}) = B - D \tag{2.7}$$

This equation describes the changes in the particle density function due to the changes in the coordinates, $\mathbf{z}$, and due to particles entering and leaving the population through birth and death mechanisms, B and D respectively.

Age Population Model. With the purported connection between differentiation and expression of bacitracin, a logical characterization of the sporangia population is some measure of progress through the differentiation process. As research into the sporulation process has progressed, it is becoming clear that differentiation in *Bacillus* is a precise sequence of temporally, spatially, and morphologically regulated events [62]. It appears that the steps of the differentiation process are controlled at the transcriptional level, with each set of genes in the sequence being activated at a specific time in the process [61]. This strict regulatory pattern forces a close correlation between the biochemical and morphological markers of sporulation and time since commitment to differentiation [63, 114, 91]. Therefore, a convenient means to characterize the sporangium population, based on stage of spore development, is the sporangium age, or time since commitment to sporulation.

Let τ represent the internal coordinate of sporangium age. Defining $X_s(\mathbf{x}, \tau, t)$ as the sporangium age density function allows for a segregated description of the sporangium population. Now, the remaining tasks to complete the population balance description is elucidation of birth and death mechanisms, by which cells enter and leave the population, and a description of how the population changes due to the fact that the internal coordinate, age, changes in time. Selection of cell age as an internal coordinate makes the latter of these two tasks a trivial matter. Cell age is directly correlated with time since birth, therefore, the rate that cells age, $d\tau/dt$, is a constant of one.

The choice of cell age as the descriptive coordinate in the population balance provides a convenient simplification to the modelling of sporangium birth. Since by definition, cells are of age zero at birth, all entries to the population resulting from birth mechanisms are localized at the zero age boundary. Therefore, an understanding of the rate that vegetative cells sporulate is sufficient information to describe the effect of birth on the sporangium population.

Sporulation Commitment. The mechanism by which vegetative cells begin differentiation and enter the sporangia age distribution is through sporulation commitment. Due to the utilization of bacterial sporulation as a paradigm for cellular differentiation mechanisms, great progress in the understanding of the genetics and biochemistry of sporulation has been made. A majority of the sporulation research to date has been done using a *Bacillus subtilis* experimental model. Assuming that *B. subtilis* and *B. licheniformis* have similar regulatory mechanisms for sporulation, a brief discussion of the current knowledge concerning sporulation is provided to help motivate the formulation of sporangium birth and maturation models.

In response to nutrient depletion the *Bacillus* have evolved several regulatory responses to attempt to adapt to the changes in the environment. These include the stringent response, induction of transport systems for alternative nutrient sources, expression of chemotaxis and motility mechanisms, secretion of macromolecular degrading enzymes, and induction of competence for transformation [102, 100]. These regulatory adaptations all represent ways the cell could possibly obtain an alternative nutrient source to replace the current dwindling supply. In the event that all efforts fail, the cell has a final avenue to preserve itself, that being activation of the sporulation pathway. By proceeding through a set of genetically predetermined steps, the vegetative cell transforms itself into a highly resistant storage vessel, containing the bacterial DNA and dormant metabolic machinery. Thus, by transforming into a spore, the cell effectively saves itself for a better day.

Although many aspects of sporulation remain a mystery, the basic regulatory mechanism for *Bacillus* sporulation initiation is becoming clear, and a summary of the current speculative regulatory pathways are shown in Figure 2.9.

The decision to sporulate begins with a two-stage signal transduction mechanism. In the first stage, a transmitter protein, which in some way recognizes nutrient depletion, passes an activation signal to a receiver protein. At this time, the identity of the transmitter and the mechanism by which the transmitter senses the environment have not been substantiated, however, evidence indicates a potential role for GTP as the environmental stress signal [102, 77]. At any rate, when the differentiation signal is recognized, it is believed auto-

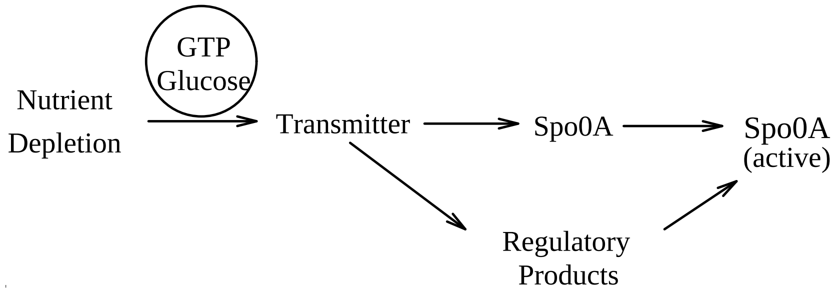

Figure 2.9: Regulatory pathway for sporulation initiation. Arrows indicate flow of the initiation signal. Circles indicate down-regulation. Adapted from Smith [100].

phosphorylation of the transmitter protein occurs. The phosphorylated transmitter transfers the activation signal to a receiver protein through a subsequent phosphorylation of the receiver protein. Currently, the identity of the receiver protein has been attributed to the *spo*0A gene product. Evidence pointing to Spo0A as the receiver protein includes the sequence homology exhibited between Spo0A and known signal receiver proteins in other bacterial systems [100], and to the fact that the Spo0A protein is recognized as a master regulator of late growth processes and early sporulation events [81].

Once the receiver has been activated, a combination of events ensues, triggering the cascade of morphological and biochemical events associated with differentiation. The receiver protein, Spo0A, is a DNA binding protein that interacts with the promoter of at least one gene, *abrB*. The gene product of *abrB* plays a major role in the sporulation cascade as a repressor of many sporulation related genes [100]. The AbrB protein is expressed during exponential growth and is able to bind to a set of similar promoter regions, rendering them untranscribable. The interaction of Spo0A with the promoter region of *abrB* interferes with the expression of AbrB and allows for transcription of the previously repressed sporulation genes [115].

A particularly important product, expressed only after inhibition of AbrB, is the sigma factor, σ^H. This product of the *spo0H* gene is a protein that in combination with the "core" RNA polymerase enzyme, is able to transcribe a specific set of sporulation-associated genes. The altered selectivity of the RNA polymerase holoenzyme complex, Eσ^H, is due to a selective association between the sigma factor and the promoter region of the differentiation genes. Utilization of different sigma factors is a major regulatory mechanism in the response of *Bacillus* to adverse environmental conditions [18]. In the case of σ^H, mutational analysis has shown that this sigma factor must be functional for sporulation initiation, due to the fact that the spore development pathway depends on products whose transcription is directed by the Eσ^H complex [62, 102]. The cascade of sporulation related events continues with the sequential expression of products involved in formation of the endospore, along with additional sigma factors, needed to direct sporulation.

Although the regulatory mechanism for control of sporulation initiation is becoming clear, it is difficult to translate the detailed regulatory information into a useful mechanistic model due to the lack of kinetic understanding for the various developmental steps. As was mentioned previously, some researchers are utilizing highly-structured models to describe sporulation [104, 56]. However, the large number of parameters, and the lack of measurable states brings into question the feasibility of model identification for these single cell models. Prior to the single-cell models, work concerning sporulation modelling has depended on empirical approaches to describe sporulation initiation.

Researchers have shown that several *Bacillus* species form spores during exponential growth in a chemostat [21, 92]. It has also been shown that sporulation initiation decreases with increased growth rate. The observation that spore production did occur at steady state in an exponentially-growing continuous culture contradicted the commonly held belief that sporulation was a threshold event, in which vegetative cells committed to spore formation in mass when the culture environment could no longer support a basal growth rate. In light of the knowledge concerning the sporulation regulatory mechanism, it seems likely that the inverse relationship between sporulation and growth rate at steady state is a result of interactions between the nutrient-limitation signal molecule (GTP) and the nutrient-sensing transmitter protein. This can be described using an equilibrium relationship:

$$SP \rightleftharpoons S + P^* \rightarrow \text{sporulation} \tag{2.8}$$

where SP represents the inactive nutrient-protein complex and P^* is the activated transmitter protein initiating sporulation. Lower growth rate implies lower nutrient concentration, which would shift the equilibrium relationship toward activated transmitter. The belief that mass sporulation was attributed to a threshold event could be of a sudden shift in the equilibrium relationship due to rapid exhaustion of limiting substrate in batch culture. This theory is consistent with the low, but non-zero sporulation rate observed in high dilution rate continuous cultures, as well as the mass sporulation seen at low dilution rate and in batch growth.

In an attempt to model the apparent dependence of sporulation on growth rate, Dawes and Thornley [22] defined the specific rate of sporulation to represent the rate of loss of vegetative cells, X_v due to sporulation:

$$\mu_s = -\frac{1}{X_v}\frac{dX_v}{dt} \tag{2.9}$$

Based on observation of steady-state sporulation in *B. subtilis*, they postulated a linear relationship between the vegetative growth rate, μ_v, and μ_s:

$$\mu_s = \alpha_s - \beta_s \mu_v \tag{2.10}$$

The parameter α_s represents the maximum rate of sporulation and β_s modulates the inhibitory effect of vegetative growth on the rate of sporulation. This relationship shows the decrease in sporulation observed when growth rate is high. The dependence of μ_s on μ_v provides an implicit dependence of sporulation on limiting substrate concentration through Equation 2.2.

Dawes and Thornley were able to accurately represent steady-state sporulation data for *B. subtilis* using the linear relationship in Equation 2.10. However, batch experimental data in combination with dilution-rate step tests, indicate that the linear relationship does not hold when limiting substrate concentration reaches zero. Therefore, instead of assuming a linear relationship between growth and sporulation, an experimentally-fit polynomial expression has been utilized to model the dependence of sporulation commitment, μ_s on limiting substrate concentration. In a general formulation, the empirical sporulation function can be represented by:

$$\mu_s = \sum_{j=0}^{n} \gamma_j \phi_j(s_i) \tag{2.11}$$

where ϕ_j represents the jth basis function and γ_j is the experimentally determined basis function weight. Utilization of a general polynomial approximation has proved effective in describing sporulation commitment during both steady state and transient growth, and avoids the assumption of linear dependence of sporulation on growth rate, which was made by Dawes and Thornley. A detailed discussion of the estimation of the sporulation function is given in Section 4.3.2.

Spore Maturation. Along with the description of the sporangium birth through sporulation initiation, an understanding of the mechanisms by which cells leave the population is required to complete the population description. For this study, it is assumed that there is no significant loss of cells resulting from death of sporangia. There is, however, a mechanism by which sporangia leave the population. At the conclusion of the sporulation process, cells have been completely transformed from the vegetative state to dormant spores. Therefore, by definition, the maturation time represents a division between the sporangium population and the unstructured spore state. Even though maturation does not represent the "death" of a sporangium, it is a mechanism by which sporangia leave the population, and therefore, it is convenient to treat it as a death term in the population balance equation.

After the completion of the differentiation process, sporangium cells are considered to be mature spores, capable of renewing the vegetative growth process through germination. While the point where a sporangium cell has truly reached maturity is somewhat arbitrary, for the purposes of this research it is defined to be the stage of development where sporangia acquire heat resistance. Based on the assumption that spore development occurs in a fixed amount of time, the age of spore maturation is defined as τ_m. The period required for *B. subtilis* to achieve maturity has been estimated by several researchers to be in the range of 8–10 hours [76, 63]. Recognizing that the true time of spore maturation is vague, and to account for any species related differences between *B. licheniformis* and *B. subtilis*, τ_m has been treated as an adjustable parameter. It is also assumed that the maturation time is relatively insensitive to changes in culture conditions.

The rates of sporulation commitment and spore maturation are tied into the population balance equation by definition of the birth and death terms in

Equation 2.7.

$$\frac{\partial X_s}{\partial t} + \frac{\partial X_s}{\partial \tau} = \delta(\tau)\mu_s X_v - \delta(\tau - \tau_m) X_s \tag{2.12}$$

The Dirac delta functions associated with birth and death account for the fact that the processes of sporulation commitment and maturation act as a point source and sink, respectively.

Antibiotic Formation Model. The observation that secondary metabolites are most commonly found in organisms that utilize sporulation mechanisms has led to considerable speculation about the role of secondary metabolites in the process of cellular differentiation [70, 57, 10]. The role played by secondary metabolism in the differentiation process is still a matter of controversy, and although the sporulation regulatory mechanism is becoming clear, the exact connection of the late growth products to sporulation is still unknown [102].

Initially, speculation that antibiotic compounds were essential to sporulation was based on several experimental observations. First, it was noted that the production of most peptide antibiotics, including bacitracin, coincided with sporulation initiation [9, 10]. Growth studies examining the connection of spore formation to antibiotic production noted that catabolite repression affected both antibiotic expression and sporulation similarly [65, 47, 9]. Majumdar and Bose [66] were able to show simultaneous derepression of production of the peptide mycolinic acid and sporulation in *B. subtilis* using cyclic dibutryl GMP. Further, genetic studies showed mutants that were blocked early in the sporulation sequence were also antibiotic negative [91]. These observations from genetic and biochemical experiments lead Hodgson [52] to speculate that peptide antibiotics were required for normal sporulation.

Although much evidence points to a connection between sporulation and antibiotics, Katz and Demain [57] conclude that none of the evidence discussed above conclusively prove that the antibiotics are required for successful spore formation. Nakano and Zuber [75] point out that the evidence that Hodgson's speculation is based on could be explained by the presence of parallel regulatory pathways for spore formation and antibiotic expression starting at a common origin. This scenario would explain spo$^-$ and antibiotic$^-$ phenotypes of early blocked mutants, and the production of antibiotics in sporulation late-blocked mutants. Schaeffer [91] explains that a causal relationship between antibiotics and spore formation is difficult to prove, but easy to disprove. To disprove the necessity of a particular compound in sporulation, a mutant must be isolated whose phenotype is antibiotic$^-$, and yet, is able to sporulate normally. Antibiotic-negative mutants that sporulate normally have been discovered in several cases [84, 67]. In particular for bacitracin, Haavik and Thomassen [46] were able to isolate a sporulating mutant that was bacitracin deficient.

Although it is likely that bacitracin is not essential to sporulation in *B. licheniformis*, the evidence indicates that the regulatory pathways for spore formation and antibiotic production overlap in some fashion [57]. Before attempting to describe a model for antibiotic formation, it is helpful to access the experiences of previous researcher involved in bacitracin production. Reviews of the early fermentation studies are provided by Hickey [51] and Weinberg [110]. A more recent review of bacitracin production is given by Frøyshov [35].

In one of the first studies of fermentation conditions promoting bacitracin production, Hendlin [50] studied growth and antibiotic production of a strain of *B. subtilis* in shake flasks using various synthetic media. He reported simultaneous growth and antibiotic production. No attempt was made to analyze any connection between sporulation and secondary metabolism. However, the effect of aeration on bacitracin production was examined by varying medium volume in shake flasks. Hendlin observed increased rate of bacitracin production in the low-volume flasks, and based on these results he concluded increased aeration improved production.

Bernlohr and Novelli [9] studied bacitracin production during batch growth on minimal medium in shake flasks. They noted that bacitracin production was inhibited by high concentrations of glucose ($\approx$ 40 g/l), and they attributed the inhibition to lowering of pH due to organic acid production. The level of inhibition was related to the agitation rate of the shake flasks. Fast-shake agitation lead to significant inhibition of bacitracin production, slow-shake agitation and stagnant conditions allowed for production of bacitracin after approximately 48 hours. By limiting the glucose concentration ($\approx$ 5 g/l), Bernlohr and Novelli were able to stimulate bacitracin production at approximately 10 hours, and the dependence of antibiotic production on aeration rate was eliminated. These researchers observed that bacitracin was only produced in cultural conditions that eventually supported spore formation. Their explanation was that bacitracin regulation was connected to spore formation. However, Bernlohr and Novelli note that they did not find a direct proportionality between the quantity of spores produced and the bacitracin titer.

Haavik [43] observed bacitracin production concomitant with growth in a synthetic medium that lacked glucose. In similar experiments with glucose added to the medium, bacitracin production was retarded, appearing after a delay proportional to the concentration of glucose added. However, the maximum bacitracin titer was positively affected by the addition of glucose, and this was attributed to reduction of the high pH observed during the late growth in medium without glucose. Haavik suggests that bacitracin is not inhibited by glucose, but rather, the low pH induced by organic acid production resulting from glucose metabolism. To test this theory, Haavik used $CaCO_3$ buffered growth medium to show that the repression effect could be eliminated in the presence of glucose.

After more experimental work, Haavik [44] modified his theory of pH dependent inhibition of bacitracin production. It was discovered that pH alone was not responsible for reduced bacitracin titers. Cultures acidified with inorganic acids did not exhibit inhibition of bacitracin production. The repression effect was only observed when pyruvate and acetate where used for acidification. Additionally, the inhibitory effect of these organic acids, which result from metabolism of glucose, was only observed when the pH of the culture was allowed to drop. Haavik concluded that repression of bacitracin results when undissociated organic acids penetrate the cell, creating a lower internal cell pH. The conclusion that it is possible to produce bacitracin during growth is also asserted, and that previous studies have not seen this phenomenon because of repression due undissociated organic acids. However, it is important to note that Haavik did not examine the relationship between organic acid addition and sporulation. Therefore, it is difficult to rule out the possibility that sporulation was occurring at the same time as growth, resulting in bacitracin production.

Flickinger and Perlman [32] attempted to analyze the effects of oxygen-enriched aeration on the production of bacitracin by *B. licheniformis* in complex media. Oxygen enrichment had wide-ranging effects on growth and antibiotic production. The maximum growth rate declined and sporulated sooner than in normal air-sparged control cultures. Also observed was a reduced rate of carbohydrate utilization as oxygen transport was improved. In contrast to the reduced growth rate, increased aeration increased the final antibiotic yield, and significantly increased the rate of bacitracin synthesis. Flickinger and Perlman suggest that the oxygen enrichment simulates conditions of slow carbohydrate feeding, and thus, reduce any catabolite repression of antibiotic production created during growth on carbohydrates.

The question of whether bacitracin production was possible during active growth lead Hanlon and Hodges [47] to look into the relationship between bacitracin production and growth rate. These researchers grew *B. licheniformis* on a minimal-salts medium, while altering the defined carbon, or nitrogen source. Five carbon sources were analyzed, ranging from glucose, which was an excellent growth source, to lactate, which promoted growth at about 1/4 the rate of glucose. It was observed that the carbon sources that allowed rapid growth did not promote bacitracin synthesis, and slow growth on poor carbon sources yielded bacitracin production. The propensity to produce bacitracin during exponential growth was correlated with the maximal growth rate supported by the carbon source. It was also observed that the quantity of spores produced corresponded to the growth rate in the same manner as bacitracin production. Based on these observations, Hanlon and Hodges claim it is obvious that bacitracin can be produced during exponential growth. However, they are careful to point out that this does not mean that bacitracin production is unassociated with sporulation.

From the review of experimental studies of bacitracin production, it is clear that the regulatory mechanisms for bacitracin production and sporulation are not completely coupled. Bernlohr and Novelli [9] indicate that cultural conditions requiring sporulation were required for bacitracin expression, however they were not able to directly correlate the bacitracin titer to the extent of spore production. Haavik [43, 44] claims bacitracin can be produced during exponential growth, implying that differentiation is not required for antibiotic production, even though the rate of sporulation was not monitored. The results of Hendlin [50] and Flickinger and Perlman [32] suggest a connection between the increased aeration and increased bacitracin production. This observation conflicts with the observations of Bernlohr and Novelli [9], who claim increased mixing, implying improved oxygen transfer, leads to inhibition of antibiotic production.

The conflicting experimental results indicate a complex regulatory mechanism for bacitracin production. In spite of the assertions of Haavik [43] that bacitracin production is not necessarily sporulation dependent, the remaining experimental evidence indicating a link between differentiation and antibiotic production are impossible to ignore. The consensus seems to be that antibiotics and other *Bacillus* secondary metabolites are coupled to the differentiation mechanism at the point of initiation. Smith [100] proposes that expression of secondary metabolites that are associated with sporulation, but are not essential to the differentiation process, is controlled by a regulatory pathway that is distinct from sporulation regulation, but shares a common origin. A possible regulatory structure is shown in Figure 2.10. A branched regulatory mechanism could explain the seeming dependence of bacitracin on sporulation, while still allowing for independent regulation of antibiotic production.

For fermentation experiments carried out in this study, detailed in Chapter 4, a dependence of bacitracin production on aeration was observed, indicating some effect of dissolved oxygen concentration on bacitracin synthesis. Two aeration levels were utilized during bacitracin fermentations. At high aeration, growth and sporulation were observed, however, bacitracin synthesis was highly repressed, with no measurable bacitracin produced. Utilizing the

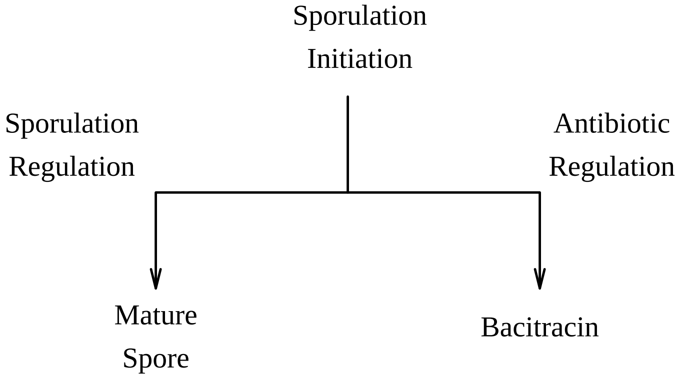

Figure 2.10: Possible connection between the regulatory pathways for sporulation and antibiotic production.

same growth medium with reduced air flowrate and slower agitation speed, growth and differentiation were observed, along with production of bacitracin shortly after the onset of stationary phase. The observation of repressed antibiotic synthesis with increased aeration agrees with results obtained by Bernlohr and Novelli [9] and conflicts with the observations of Flickinger and Perlman [32] and Hendlin [50]. Possible explanations for the discrepancy could be differences attributable to strain variations, media composition, or shear sensitivity.

In light of the fact that the sporulation pattern and the connection of antibiotic production to that pattern are not well understood, an empirical model for the rate of bacitracin synthesis is appropriate. To capture the dependence of bacitracin production on sporangium cell age, a polynomial expression in sporangium age has been used to describe the specific bacitracin formation rate:

$$\mu_a = \sum_{j=0}^{m} \alpha_j L_j(\tau) \tag{2.13}$$

The antibiotic production coefficients, $\alpha_1, \cdots, \alpha_m$, are experimentally fit, allowing for an empirical age-based idiolite formation expression. This approach is similar to that of Shu [96], except that the age-dependence of product formation is isolated in the sporangium population, rather than the entire cell population.

For the fermentation experiments in this study, the dissolved oxygen concentration was not measured. Therefore, it is difficult to account for the dependence of bacitracin production on dissolved oxygen in the age-based model. Since dissolved oxygen is not considered, the bacitracin production parameters are based on the aeration operating conditions used for their estimation.

2.2.9 Segregated Fermentation Model

Dynamic Equations. The dynamic segregated fermentation model is developed by coupling the kinetic expressions for the various rate processes to the fluid dynamics model for the fermentation apparatus of interest. In this study, a stirred tank fermentation reactor has been utilized, and in the development of the segregated model equations the following assumptions have been made:

1. The fermentation broth is a dilute solution of constant density.
2. The stirred tank fermentation vessel is perfectly mixed.
3. The fermentor is maintained at constant temperature.
4. All rate process are limited by a single substrate.
5. Feed to the fermentor is sterile, and is fed at a flowrate F_i, with a limiting substrate concentration, s_f.

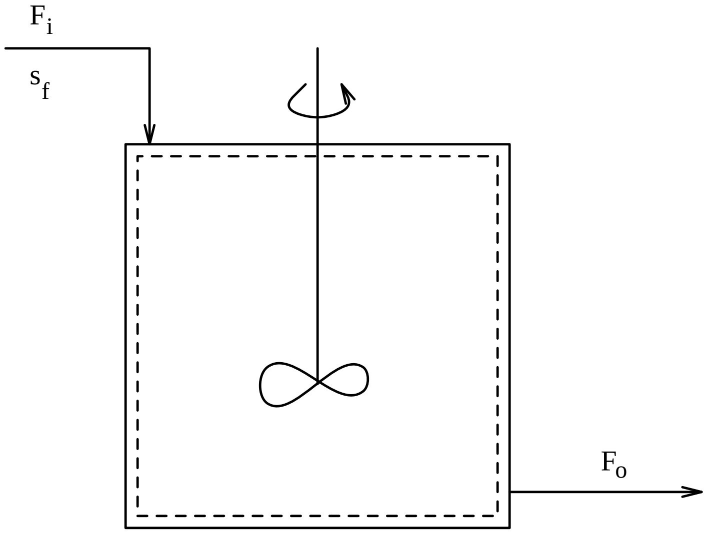

Figure 2.11: Continuous stirred tank fermentor with a material-balance control volume defined by the dotted line.

Based on a continuous stirred tank fermentor of liquid volume V_r, with a control volume as indicated in Figure 2.11, the modelling equations are formed by performing material balances on spore and vegetative cell concentrations, limiting substrate concentration, antibiotic concentration, fermentor volume, and sporangium cell number density. The resulting coupled integro-differential equations compromise the dynamic segregated fermentor model. With ˆ over a variable representing a dimensionless state, the model is presented in dimensionless form:

$$\underline{\text{Spore Biomass}}$$

$$\frac{d(\hat{X}_e\hat{V}_r)}{d\hat{t}} = \delta(\hat{\tau}-1)\hat{X}_s(\hat{t},\hat{\tau})\hat{V}_r - \mu_g\hat{X}_e\hat{V}_r - \frac{F_o}{V_o}\hat{X}_e \qquad (2.14)$$

$$\underline{\text{Vegetative Biomass}}$$

$$\frac{d(\hat{X}_v\hat{V}_r)}{d\hat{t}} = (\hat{\mu}_v - \hat{\mu}_s)\hat{X}_v\hat{V}_r + \hat{\mu}_g\hat{X}_e\hat{V}_r - \frac{F_o}{V_{r0}}\hat{X}_v \qquad (2.15)$$

Bacitracin

$$\frac{d(\hat{A}\hat{V}_r)}{d\hat{t}} = \int_0^1 \hat{\mu}_a \hat{X}_s \hat{V}_r \, d\hat{\tau} - \frac{F_o}{V_{r0}}\hat{A} \tag{2.16}$$

External Substrate

$$\frac{d(\hat{s}_e\hat{V}_r)}{d\hat{t}} = \frac{F_i}{V_{r0}}\hat{s}_f - \hat{\mu}_i \hat{X}_v \hat{V}_r - \frac{F_o}{V_{r0}}\hat{s}_e \tag{2.17}$$

Internal Substrate

$$\begin{aligned}\frac{d(\hat{s}_i\hat{V}_r)}{d\hat{t}} &= \hat{\mu}_i \hat{X}_v \hat{V}_r - \frac{y_v}{y_g}\hat{\mu}_g \hat{X}_e \hat{V}_r - \left(\hat{\mu}_v + \frac{y_v}{y_s}\hat{\mu}_s\right)\hat{X}_v\hat{V}_r \\ &\quad - \left(\frac{y_v}{y_a}\int_0^1 \hat{\mu}_a \hat{X}_s \hat{V}_r \, d\hat{\tau}\right) - \frac{F_o}{V_{r0}}\hat{s}_i \end{aligned} \tag{2.18}$$

Culture Volume

$$\frac{d\hat{V}_r}{dt} = \frac{F_i}{V_{r0}} - \frac{F_o}{V_{r0}} \tag{2.19}$$

Sporangium Number

$$\begin{aligned}\frac{\partial(\hat{X}_s\hat{V}_r)}{\partial\hat{t}} &= -\frac{\partial\hat{X}_s}{\partial\hat{\tau}}\hat{V}_r + \delta(\hat{\tau})\hat{\mu}_s\hat{X}_v\hat{V}_r \\ &\quad -\delta(\hat{\tau}-\hat{\tau}_m)\hat{X}_s\hat{V}_r - \frac{F_o}{V_{r0}}\hat{X}_s \end{aligned} \tag{2.20}$$

Definitions of the variables are provided in the nomenclature section. For convenience, the state and independent variables, with their dimensionless definitions, are summarized in Table 2.2. The specific kinetic rate functions are described in Table 2.3. For convenience, the dimensionless notation, $\hat{}$ will be dropped, and all equations are presented in dimensionless form unless otherwise noted.

Equations 2.14–2.19 represent the dynamic ordinary differential equations (ODE) modelling the non-segregated vegetative and endospore cell populations along with the substrate, culture volume, and antibiotic material balances. Equation 2.20 is a balance on the sporangium cell number, resulting in a hyperbolic partial differential equation representing the change in number of sporangium cells of age, τ, at time t. The sporangium cell balance is

Variable	Dimensionless Definition	Description
t	t/τ_m	Time (hr)
τ	τ/τ_m	Sporangium age (hr)
X_e	$\frac{X_e}{y_v s_{e0}}$	Endospore concentration (1/l)
X_v	$\frac{X_V}{y_v s_{e0}}$	Vegetative cell concentration (1/l)
A	$\frac{A}{s_{e0}}$	Antibiotic concentration (g/l)
s_e	$\frac{s_e}{s_{e0}}$	External substrate concentration (g/l)
s_i	$\frac{s_i}{s_{e0}}$	Internal substrate concentration (g/l)
$X_s(t,\tau)$	$\frac{X_s \tau_m}{y_v s_{e0}}$	Sporangium number density $(1/(\mathrm{l} \cdot \mathrm{hr}))$
V_r	$\frac{V_r}{V_{r0}}$	Working reactor volume (l)

Table 2.2: Definitions of the state and independent variables for the age-segregated antibiotic production model.

Function	Description
μ_a	Antibiotic production rate (1/hr)
μ_g	Endospore germination rate (1/hr)
μ_i	Substrate internalization rate (1/hr)
μ_s	Sporulation rate (1/hr)
μ_v	Vegetative growth rate (1/hr)

Table 2.3: Specific rate processes for the age-segregated antibiotic production model.

coupled to the vegetative cell balance through sporulation initiation, which is treated as a point birth source in Equation 2.20. Maturation of sporangia couples the sporangium population balance to the endospore balance, appearing as the input term, $X_s(t, 1)$, in Equation 2.14. Finally, integral terms in Equations 2.16 and 2.18 represent the cumulative age-dependent antibiotic formation and substrate consumption rates, coupling the population balance to the antibiotic and substrate balances.

Defining $\mathbf{x} = [X_e V_r, X_v V_r, A V_r, s_e V_r, s_i V_r, V_r, X_s V_r]^T$, $\mathbf{u} = [F_i, F_o, s_f]^T$, and θ as a vector of model parameters, along with specification initial conditions allows the segregated modelling problem to be conveniently represented by:

$$\dot{\mathbf{x}} = \mathbf{f}(\mathbf{x}, \frac{\partial \mathbf{x}}{\partial \tau}, \mathbf{u}; \theta) \tag{2.21}$$

$$\mathbf{x}(0, \tau) = \mathbf{x}_0(\tau) \tag{2.22}$$

Solution of these model equations constitutes the segregated model predictions of the dynamic growth, differentiation and antibiotic production of *B. licheniformis* in perfectly mixed stirred tank fermentor.

Steady-State Equations. Steady-state operation of a continuous stirred tank fermentor involves continuous feed of nutrient medium, accompanied by continuous removal of fermentation broth. Continuous operation of a fermentor, known as chemostat operating mode [4], is a useful technique for accessing organism behavior in constant environmental conditions. In this study, steady-state experiments have been utilized to gain information for estimation of model parameters. Therefore, a steady-state formulation of the segregated model is required to predict the steady-state behavior of the *B. licheniformis* system.

The steady-state behavior of the segregated fermentation model is represented by the fixed points of the dynamic equations. For a stable system, it is possible to find fixed-point solutions by integrating the dynamic model from a known initial point in time until all dynamics have damped out. A more direct approach is to form the steady-state model by substituting zero for all time dependent terms in the dynamic model. Since the reactor volume is constant, along with the flow into and out of the fermentor, it is convenient to define the operating parameter, $D = F/V_r$, known as the dilution rate. Substitution of $\mathbf{0}$ for the time dependent terms, and introduction of D into the dynamic modelling equations gives the steady-state model:

$$
\begin{aligned}
0 &= \delta(\tau - 1)X_s(t,\tau) - \mu_g X_e - DX_e && (2.23)\\
0 &= (\mu_v - \mu_s)X_v + \mu_g X_e - DX_v && (2.24)\\
0 &= \int_0^1 \mu_a X_s \, d\tau - DA && (2.25)\\
0 &= D\,(s_f - s_e) - \mu_i(s_e)X_v && (2.26)\\
0 &= -\frac{1}{y_g}\mu_g X_e - \left(\mu_v + \frac{1}{y_s}\mu_s\right) X_v \\
&\quad - \left(\frac{1}{y_a}\int_0^1 \mu_a X_s \, d\tau\right) - Ds_i && (2.27)\\
0 &= -\frac{dX_s}{d\tau} + \delta(\tau)\mu_s X_v - \delta(\tau - \tau_m)X_s - DX_s && (2.28)
\end{aligned}
$$

Cast in vector form, the steady-state model is represented by:

$$\mathbf{0} = \mathbf{f}(\mathbf{x}, \frac{d\mathbf{x}}{d\tau}, \mathbf{u}; \theta) \tag{2.29}$$

At steady-state, the fermentor conditions are time invariant, and the dynamic modelling equations are reduced from a set of coupled ordinary differential and partial differential equations to a set of algebraic equations coupled to a differential equation representing the population balance. Solution of these equations for a given set of operating conditions results in the steady-state bacitracin production model.

2.2.10 Solution of the Segregated Fermentation Model

Dynamic Model Solution. Complete analytical solutions of the resulting segregated dynamic modelling equations are generally not possible due to the nonlinear nature of the problem. Therefore, development of a numerical solution technique is necessary for solution of the fermentor model. Fortunately, efficient computer codes exist for the solution of nonlinear ODEs [12]. The population balance, which is a PDE, adds a degree of complexity to the problem. In fact, efficient solution of the PDE and the integral terms in Equations 2.16 and 2.18 is the crux of the numerical solution task.

While a variety of numerical techniques exist for solution of PDEs, the hyperbolic nature of the population balance leads to propagation of discontinuities along characteristic lines in the domain, creating difficulties when using standard finite-difference and method of weighted residuals techniques [60]. However, the linear structure of the age-population balance allows for a semi-analytical solution of Equation 2.20:

$$X_s(t,\tau)V_r(t) = X_s(t-\tau,0)V_r(t-\tau)\exp\left[-\int_{t-\tau}^{t}\frac{F_o(s)}{V_r(s)}\,ds\right] \tag{2.30}$$

The semi-analytical solution shows the propagation of the boundary condition down the characteristic lines defined by $t-\tau=c$. These characteristic lines of unit slope, represent the fact that time and age progress at an identical rate. An illustration of the age-time domain, and the relative roles of the initial and boundary conditions are shown in Figure 2.12.

To utilize the semi-analytical solution, $X_s(t,\tau)$ is approximated by a linear combination of polynomial basis functions in τ with time-varying coefficients:

$$X_s(t,\tau) \approx \sum_{i=0}^{n}\gamma_i(t)L_i(\tau) \tag{2.31}$$

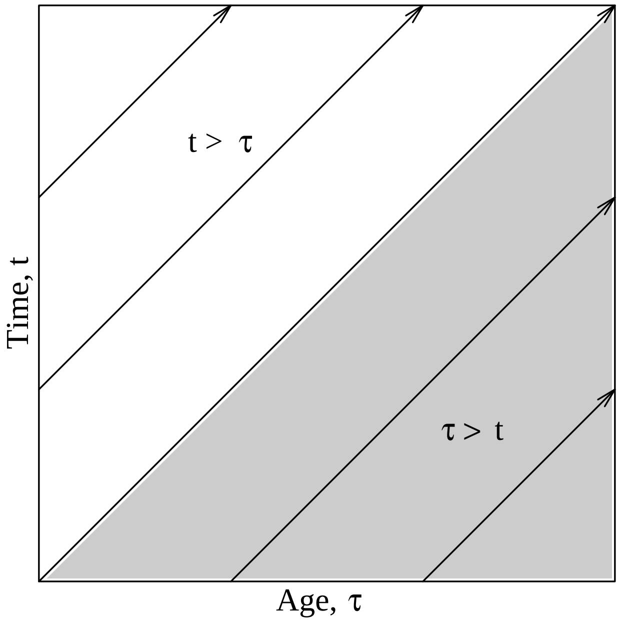

Figure 2.12: Age-time characteristic lines for the age-segregated population balance. The PDE initial condition provides the initial data for characteristics in the shaded region where $\tau > t$, and the PDE boundary condition provides the initial data for characteristics where $t > \tau$.

The function can be represented equivalently, and more conveniently, in terms of its values $X_{s_i}(\tau_i)$ at n points, $(\tau_i, \cdots, \tau_n)$, in the domain, known as collocation points [30]. The $L_i(\tau)$ polynomials are chosen such that they are orthogonal to each other on the problem domain, and the collocation points are chosen to be the $n+1$ roots of the $L_{n+1}(\tau)$ polynomial.

Expansion of the sporangium number density in orthogonal polynomials offers the advantage of an efficient means by which the substrate consumption and antibiotic production integrals, present in Equations 2.16 and 2.18, can be evaluated. The integral terms are approximated using an optimal Gaussian quadrature rule:

$$\int_a^b g(\tau)\, d\tau \approx \sum_{i=0}^{n} w_i g(\tau_i) \tag{2.32}$$

The w_i are integration weights based on the type of orthogonal polynomials basis functions chosen, and $g(\tau_i)$ is the integrand evaluated at the ith collocation point. The quadrature rule is exact for any polynomial integrand of order $2n + 1$ or less. This approach offers the advantages of high accuracy and low computational load over other quadrature techniques, such as Simpson's rule and the trapezoidal rule [109].

As mentioned previously, the hyperbolic nature of the population balance allows propagation of discontinuities down characteristic lines. The semi-analytical solution provides a convenient means by which the deformation of a point on the sporangium number density function can be tracked from its entry at the population boundary to its maturation. Since it is most convenient to follow a point as it travels through the age-time domain, the nature of the problem suggests an adaptive solution grid is needed to avoid storage of the boundary condition, and re-solution of the population balance for each point in a fixed grid. Additionally, since the characteristic lines are of constant slope, the structure of the quadrature grid is preserved during adaptation, and therefore, the optimal quadrature rule applies regardless of grid adaptation.

One problem encountered with the adaptive characteristics scheme is the fact that the grid moves away from $\tau = 0$, creating a poor approximation of the sporangium age distribution near $\tau = 0$. The approximation becomes progressively worse as the characteristics move farther away from the boundary. To improve the approximation an elemental grid is appropriate, allowing for addition of new elements to the quadrature grid as space becomes available. The adaptive elemental grid is illustrated in Figure 2.13. At the initial time,

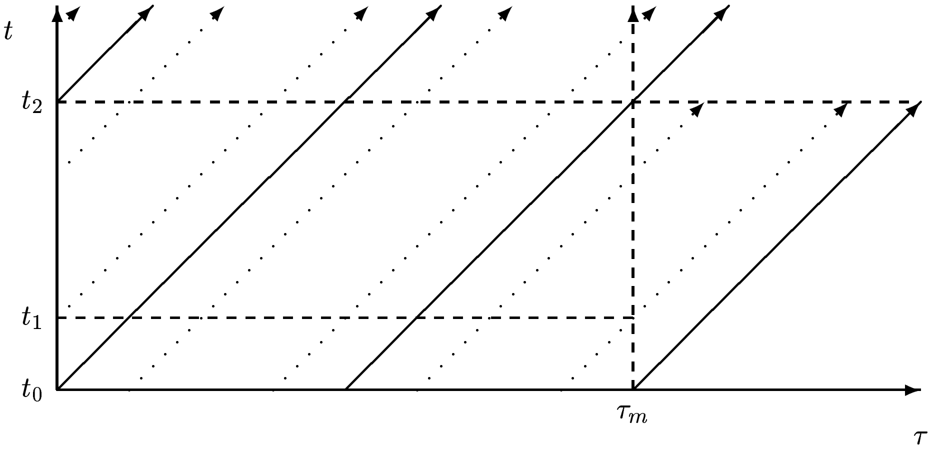

Figure 2.13: The adaptive characteristics grid. Solid lines represent element boundaries, and dotted lines are internal collocation points. At $t = t_1$ the first new characteristic is initiated. At $t = t_2$ an entire new element has been added and the oldest element is deactivated.

the domain of interest is discretized by an elemental grid of the desired accuracy. As time increases, the grid moves away from the boundary. When time has increased a period that is equal to the distance from the elemental boundary to the next collocation point, a new characteristic is introduced, with an initial value determined by the boundary condition:

$$X_s(t,0) = \mu_s X_v \tag{2.33}$$

Initiation of a new characteristic line is depicted at time t_1. As time progresses further, new characteristics are initiated as each collocation point crosses into the right half plane of the time-age domain. Adaption continues until an entire element has been added to the grid, illustrated at t_2. At the same time as the new element moves into the age domain, the oldest element has moved out of the region of interest. The oldest element becomes inactive and is dropped. By constantly repeating elemental addition and deactivation, the age domain of interest is accurately approximated without accumulating unneeded characteristics.

Substitution of the approximate integral terms into the dynamic differential equations for the lumped fermentor states, and coupling of the discretized population balance equations reduces the dynamic fermentation model to a set of nonlinear, ordinary differential equations coupled to the semi-analytical solution to the population balance. While it is currently not possible to solve general nonlinear differential equations analytically, a variety of numerical integration packages exist for solution of coupled nonlinear ODEs. Therefore, the dynamic fermentation model has been reduced to a numerically tractable form.

2.2.11 Steady-State Segregated Model Solution

Similar to the dynamic model solution, the nonlinear nature of the fermentation model precludes a general analytical solution for the steady-state case. However, at steady-state there is a simple semi-analytical solution to the sporangium age distribution equation. Integration of Equation 2.28 with respect to sporangium age and substitution of the steady-state sporulation initiation expression gives the semi-analytical, steady-state sporangium age density:

$$X_{s_{ss}}(\tau) = \mu_s(s_{i_{ss}}) X_{v_{ss}} \exp\left[-D\tau\right] \tag{2.34}$$

This equations reflects the fact that the sporangium age distribution falls off exponentially at steady state due to the increased probability that a cell will wash out of the fermentor as it ages.

As with the dynamic model, the analytical solution to the population balance is utilized by discretizing the age-dependent sporangium density, and expanding the steady-state number density as orthogonal polynomials in τ. Representing the steady-state distribution in terms of its value at the collocation points reduces the state state sporangium distribution to a set of algebraic equations:

$$X_{s_i}(\tau_i) = \mu_s(s_{i_{ss}}) X_{v_{ss}} \exp\left[-D\tau_i\right] \tag{2.35}$$

With this representation of the sporangium density function, the antibiotic production and substrate consumption integrals can be approximated using Gaussian quadrature. This reduces the steady-state model to a set of nonlinear algebraic equations. Similar to the dynamic case, general analytical solutions to the steady-state model are not possible, however, a variety of algorithms exist to solve sets of nonlinear algebraic equations.

Segregated Model Solution Code: SEGMOD. To obtain solutions for the dynamic and steady-state segregated fermentation models, the adaptive grid algorithm discussed in Section 2.2.10 was implemented as a FORTRAN-77 subroutine. The solution routine, called SEGMOD, was constructed in modular fashion, allowing easy portage to a variety of driver applications requiring model solutions.

SEGMOD was designed to handle both the steady state or the dynamic model solution, based on the user's request. To solve both problems, the solution routine needs the capability to generate numerical solutions to nonlinear algebraic equations for the steady-state problem, and to numerically integrate nonlinear ordinary differential equations for the dynamic model. To reduce the burden of software development, two public domain routines were utilized to handle the bulk of the computations. The subroutine HYBRD1, from the MINPACK subroutine library [74], uses a modified Powell-hybrid method to find a zero of a system of nonlinear algebraic equations. HYBRD1 was utilized to find the steady-state solutions of the segregated fermentation model, through the solution to Equations 2.23–2.28. The dynamic model differential equations were integrated using the the FORTRAN subroutine DDASSL [82]. DDASSL is designed to solve first-order differential algebraic systems using a variable stepsize, variable order, backward differentiation algorithm.

Since the primary numerical tasks are handled by DDASSL and HYBRD1, the routine SEGMOD serves as a management routine for the model solution task. However, coupling the adaptive grid algorithm to the normally self-contained integration routine, DDASSL, requires tight coordination between the processes of grid adaptation and the integration. A general flowchart for the SEGMOD model solution routine is shown in Figure 2.14. The model solution begins by obtaining the initial conditions for the dynamic model, or an initial guess for the steady-state solution. Then the user determined fermentor operating conditions are loaded. At this point, depending whether a steady-state, or dynamic simulation is desired, the routine directs the initial conditions and operating parameters to the appropriate canned software. In the steady-state case, the program flow is straightforward, with HYBRD1 solving the steady-state algebraic equations, returning to the calling routine after convergence to the fix-point solution. Program flow in the dynamic simulations is more complex, due to coupling of the adaptive sporangium grid to the DDASSL integration software. DDASSL integrates dynamic problems in a step-wise manner. In the SEGMOD routine, DDASSL is put in intermediate step mode, forcing the integration to stop at each successful integration step. At the stopping point, the progress of the integration is checked. If the integration has progressed to a characteristics addition point or elemental falloff, as shown in Figure 2.13, the sporangium grid is adapted appropriately. After the grid is adapted, control is returned to the integrator for continued progression of the solution. This process continuous until the final integration time is reached, at which point, the model solution is returned to the calling

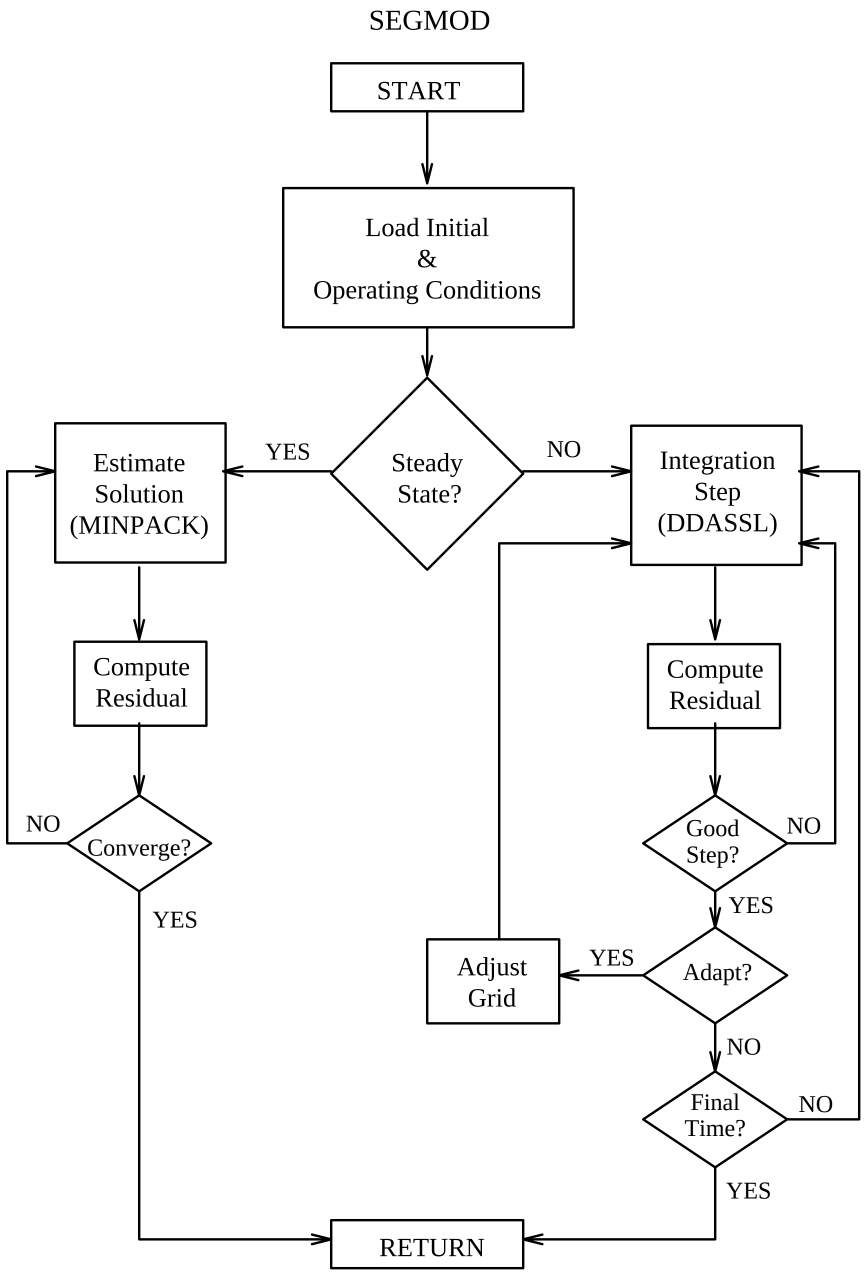

Figure 2.14: Flowchart for the segregated model solution subroutine SEGMOD.

routine.

It is important to access the ability of the numerical solution scheme to accurately represent the dynamics of the fermentation model. In the case of the segregated model, the accuracy of the solution hinges on the ability of the adaptive grid to track the sporangium age distribution. Since the solution scheme utilizes an adaptive elemental grid, it is important to determine what level of grid refinement is necessary to accurately model the population dynamics. However, since additional grid elements increase the size and computational overhead of the problem, it is imprudent to overload the solution grid with more elements than necessary.

For computational convenience, the adaptive grid has been designed such that the elements are equally spaced, and the polynomial basis functions are identical on each element. Therefore, the accuracy of the solution is controlled by varying the number of elements making up the grid. To access the accuracy of the solution scheme, the effect of grid refinement on solution to the population balance has been analyzed. Batch fermentations of *B. licheniformis* are typified by a burst in sporulation initiation when substrate levels fall to critical levels. Since sporulation bursts lead to the introduction of steep fronts in the sporangium age distribution, the solution of the batch fermentation model poses a tough test for the numerical solution scheme. A simple way to visualize the effect of grid refinement on the population balance solution is to examine the variation in the age-distribution at constant time, as the number of elements increases.

Figures 2.15–2.17 show the predicted batch sporangium number density versus cell age at a given time, with varying numbers of quadratic elements. The three plot sequence compares the solution at early, medium, and late times in the batch simulation. In each case, as the number of elements increases the sporangium age density curve converges and eventually the addition of elements has an insignificant effect on the approximate solution. The increased accuracy at the high-element approximations is evident in the early and medium-time plots, due to the existence of a peak in the distribution. With a ten-element grid, the basic shape of the curve has been captured, and additional elements add little to the description. In the late-time case, the lack of a peak allows for a accurate low-element approximation to the distribution. Since it is necessary that the solution be accurate throughout the simulation, the grid was set to ten quadratic elements, allowing for a good approximation at all times.

After testing of the model solution routine, and analysis of the required grid spacing, solutions of the segregated model are available for simulation of fermentor operation. A simulation of a batch fermentation with nominal model parameters is shown in Figures 2.18 and 2.19. The lumped parameter states show the typical batch behavior, with rapid increase in the vegetative cell biomass until limiting substrate is exhausted. At the point of substrate depletion, vegetative cell death and sporulation phenomenon become active. Bacitracin is produced during the mass sporulation, and spores appear after the sporangia begin to mature.

The sporangium number density is a distributed parameter state, and complete representation of $X_s(t, \tau)$ requires a surface plot. The surface plot shown in Figure 2.19 shows the sporangium age distribution as it deforms in time for the batch fermentation. At the initial condition, there are few sporangia, however, as the nutrient is depleted, sporulation initiation creates a burst of newly born sporangia. After a short period of mass sporulation, the rate of spore initiation decreases and the peak in sporangium moves through the age-time

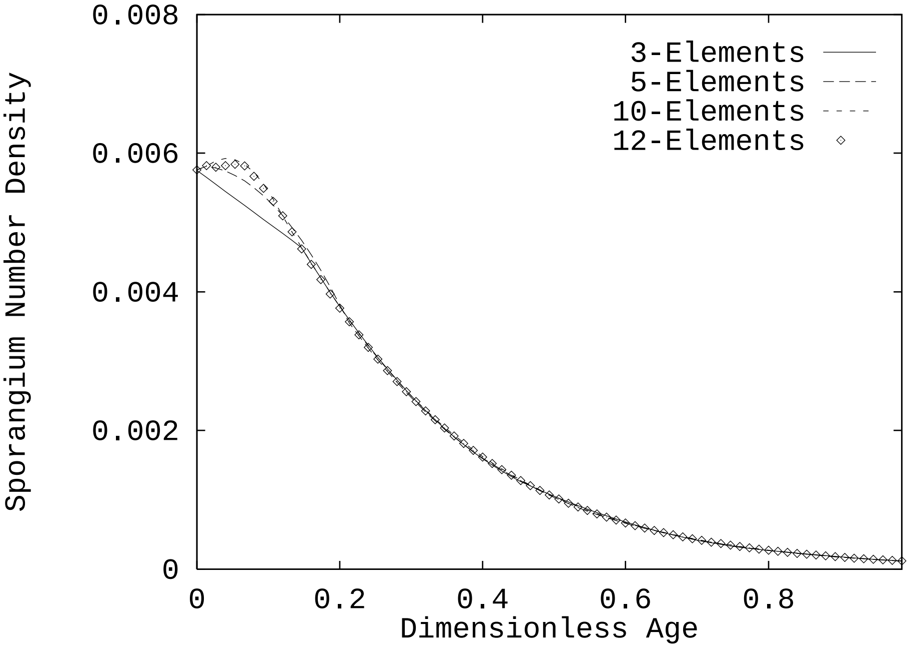

Figure 2.15: The effect of grid refinement on the sporangium number density solution early in a batch fermentation.

domain as the sporangia develop into mature spores.

2.2.12 Segregated Model Parameters

To finalize the segregated model, the parameters describing fermentation kinetics, stoichiometry, and sporulation maturation time must be determined. For the kinetic processes the parameters include:

- Maximum germination rate and substrate affinity: α_g and K_g.
- Maximum substrate internalization rate and external substrate affinity: α_i and K_i.

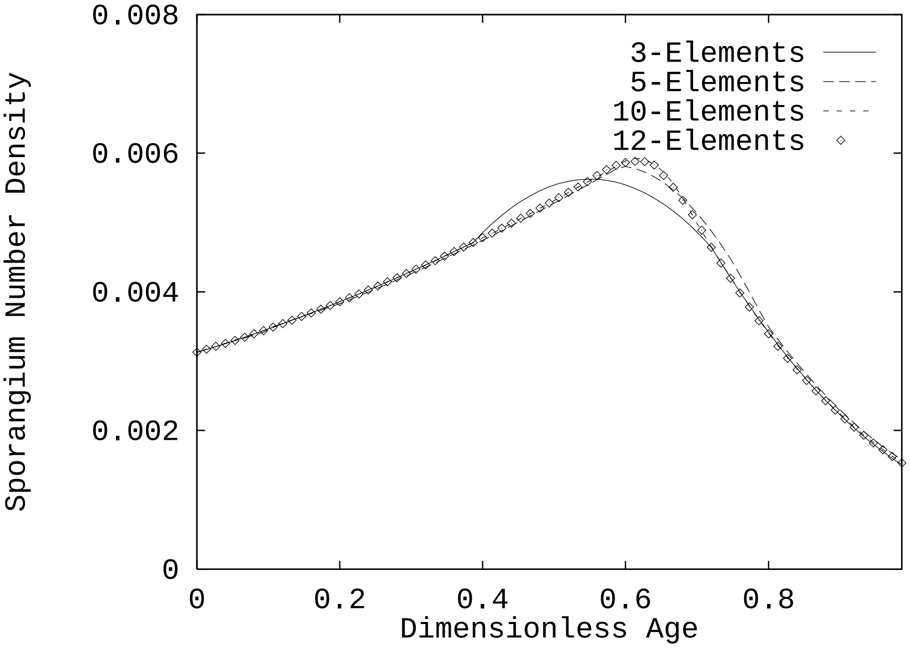

Figure 2.16: The effect of grid refinement on the sporangium number density solution midway through a batch fermentation.

- Maximum vegetative growth rate and internal substrate affinity: α_v and K_v.
- Cell death rate, m_v.
- Sporulation initiation coefficients: $\gamma_i,\ i = 1, n$.
- Antibiotic production coefficients: $\alpha_j,\ j = 1, m$.

For the growth and differentiation processes, the parameters relate the process rates to the limiting substrate concentration. Substrate consumption is related to growth, differentiation, and bacitracin production through stoichiometric

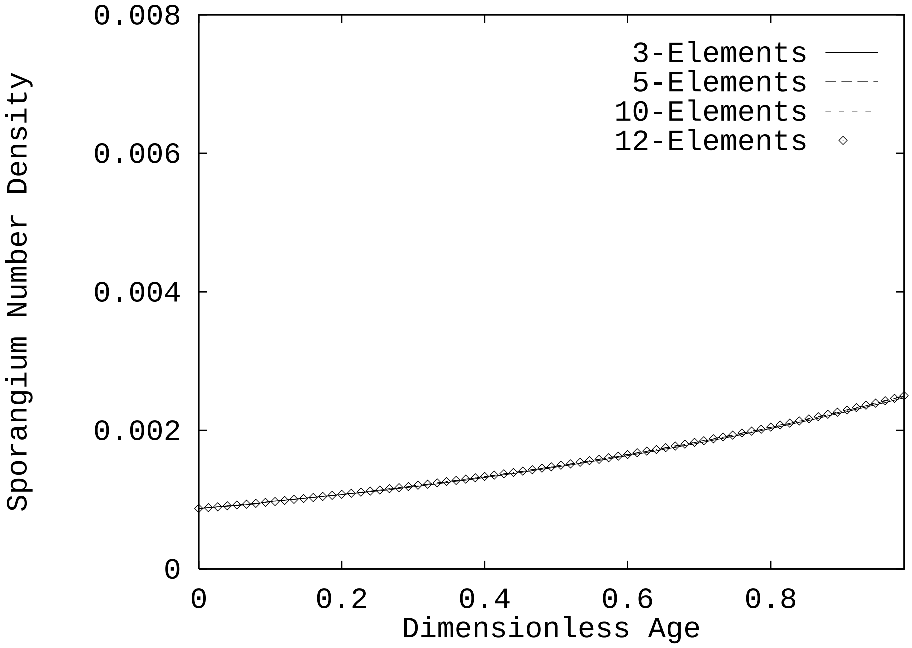

Figure 2.17: The effect of grid refinement on the sporangium number density solution late in a batch fermentation.

constants, y_v, y_g, y_s, and y_a. The final parameter is the spore maturation time, τ_m, marking the time from sporulation initiation to maturation.

The lack of relevant literature data for the *B. licheniformis* system precludes the possibility of determining all model parameters from existing models or data. Therefore, it is necessary to estimate the parameters from experimental data generated for this study. Fortunately, sensitivity analysis indicates the model is insensitive to some parameters, allowing those parameters to be fixed at reasonable values. Then parameter estimation can concentrate on estimating the high sensitivity parameters. These topic are discussed in detail in Chapter 4.

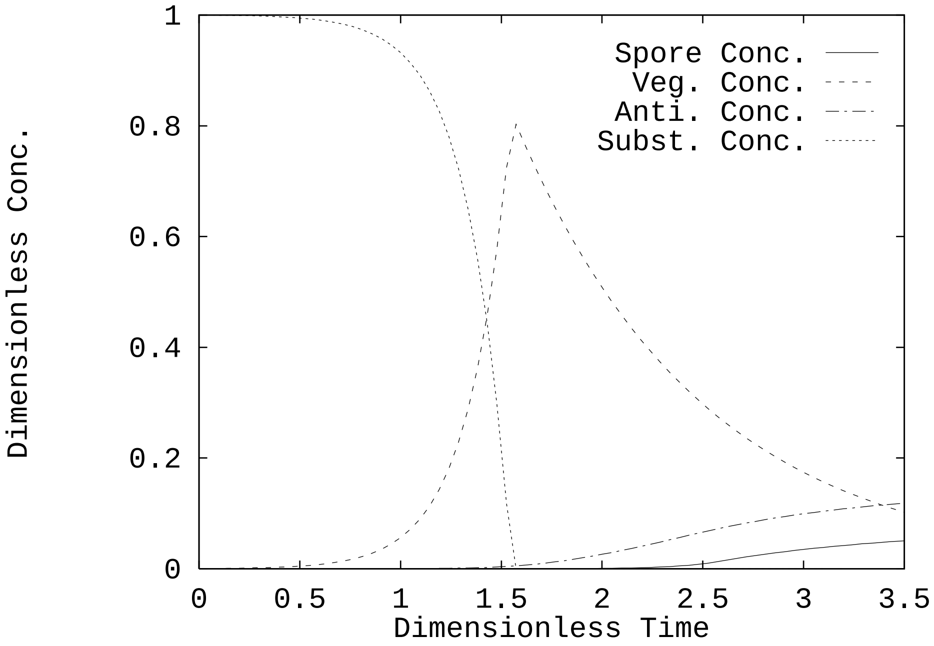

Figure 2.18: Dynamic profiles of the lumped parameter segregated fermentation model states.

2.3 Development of the Structured Comparison Model

A useful tool for evaluating a model is comparison to other modelling approaches. In the case of antibiotic production by *Bacillus* an age-structured model exists in the fermentation literature. This model was developed by Blanch and Rogers to describe production of gramicidin S by *B. brevis* [11]. This model has been selected as a model suitable for comparison to the structured/segregated model developed in this research. Since the Blanch and Rogers (BR) model lacks segregation but includes structure, it was decided it would provide a valid test of the advantages and disadvantages of the segre-

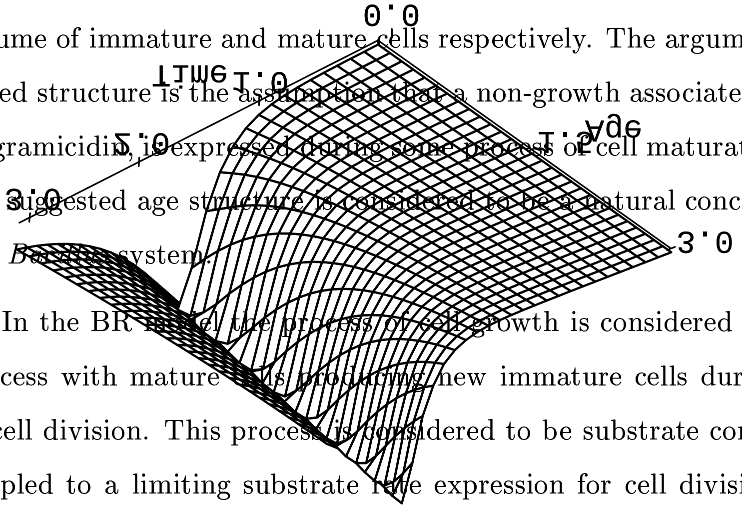

Figure 2.19: The dimensionless sporangium number density versus dimensionless time and dimensionless cell age for a batch fermentation simulation.

gated modelling approach.

The model structure and kinetic relationships for the Blanch and Rogers model are illustrated in Figure 2.20. Blanch and Rogers treat the culture as a mixture of two cell groups: N_i and N_m representing the number per unit volume of immature and mature cells respectively. The argument for the age-based structure is the assumption that a non-growth associated product, such as gramicidin, is expressed during some process of cell maturation. Therefore, the suggested age structure is considered to be a natural conceptualization of the *Bacillus* system.

In the BR model the process of cell growth is considered to be a cyclical process with mature cells producing new immature cells during the process of cell division. This process is considered to be substrate consuming, and is coupled to a limiting substrate rate expression for cell division, a_{21}, by us-

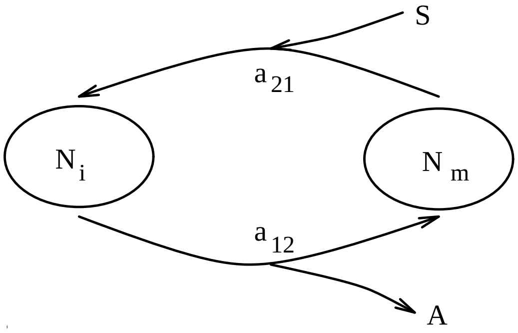

Figure 2.20: The structure of the Blanch and Rogers model for production of gramicidin from *B. brevis*.

ing the ubiquitous Monod growth law (see Section 2.2.6). The newly created immature biomass immediately begins the process of maturation at a rate, a_{12}, independent of substrate concentration. As Figure 2.20 shows, it is proposed that antibiotic is produced during the transition between immature and mature biomass.

The concept of a cyclical developmental path from immature cell to mature cell and back to immature through cell division is reminiscent of the cell growth cycle, where maturation is the process of increasing cell mass until replication of the chromosomal DNA signals cell division. Since antibiotic production is linked directly to the maturation process, the BR model suggests production of gramicidin S in *Bacillus brevis* is coupled to the normal growth process, rather than some differentiation process.

In actuality, gramicidin S is a peptide antibiotic that is regulated in a fashion similar to bacitracin. That is, normally gramicidin production is a late growth process associated with sporulation initiation. Regardless of this fact, the model structure suggested by Blanch and Rogers describes their gramicidin

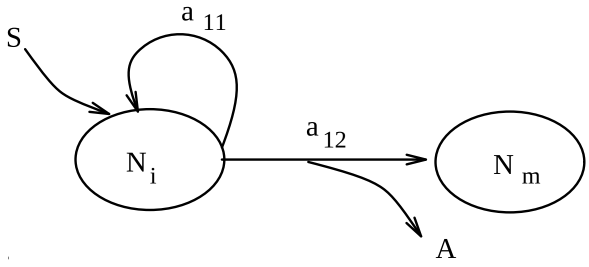

Figure 2.21: The modified age-structured model reflecting differentiation associated production of bacitracin.

production data quite well. However, the original model structure does not lend itself to describing gramicidin production data presented by Vandamme et. al. [108] where the antibiotic does not appear simultaneously with growth, but rather appears toward the end of the growth phase in batch culture. Similarly, bacitracin appears toward the end of the growth phase in batch culture, and the utilization of the BR model, with the direct association of bacitracin production to the cell growth cycle, does a poor job of describing the data. For this reason, it was necessary to modify the structure of the comparison model, such that it was able to more accurately represent the *B. licheniformis* system.

The most basic change made to the BR model is the decoupling of the growth cycle from antibiotic production. This is accomplished by assuming that growth occurs in the "immature" portion of the biomass, and antibiotic production is related to maturation. The modified model structure is illustrated in Figure 2.21. This adaptation of the model preserves the basic structure, still assuming a two-compartment age-structured model, but with the adaptation, the role of the age groups is more in tune with the true nature of *Bacillus* physiology. In this case, the "immature" cells represent the actively growing, or vegetative, portion of the biophase, and the "mature" cells reflect the portion of the biomass which is involved in differentiation and bacitracin production. The delayed appearance of bacitracin is accounted for by assuming that the maturation process is linked to substrate concentration. The inhibition of maturation by substrate has been modelled using the original Dawes and Thornley model of linear dependence of maturation on growth rate, which is discussed in Section 2.2.8:

$$a_{12} = \alpha_{12} - \beta_{12} a_{11} \tag{2.36}$$

A second modification to the BR model is the utilization of a structured vegetative biomass model. To obtain a fair comparison between the segregated model and the modified Blanch and Rogers (MBR) model, it was necessary to incorporate a similar vegetative growth law in both modelling approaches. The same problems outlined in Section 2.2.6, including a batch lag phase and post-nutrient exhaustion growth, associated with the unstructured vegetative model used in the segregated approach exist with the unstructured BR biomass growth law. Therefore, to overcome the inability of the BR model to describe transient batch-growth phenomena, the same structured vegetative growth model, shown in Figure 2.7, has been incorporated into the MBR model. This results in two Monod rate expressions describing substrate internalization and immature cell growth, respectively:

$$\begin{aligned} a_{1i} &= \frac{\alpha_{1i} s_e}{K_{1i} + s_e} && (2.37) \\ a_{11} &= \frac{\alpha_{11} s_i}{K_{11} + s_i} - m_{i1} && (2.38) \end{aligned}$$

2.3.1 Comparison Model Equations

Based on the control volume defined in Figure 2.11 and the assumptions outlined in Section 2.2.9, the dynamic comparison model equations are formulated by performing material balances for immature and mature cells, internal and external substrate, bacitracin, and reactor volume. Based on the material balances, the dynamic comparison model is represented in dimensionless form by the following equations:

Immature Biomass

$$\frac{d(\hat{N}_i\hat{V}_r)}{d\hat{t}} = (\hat{a}_{11} - \hat{a}_{12})\hat{N}_i\hat{V}_r - \frac{F_o}{\alpha_{11}V_{r_0}}\hat{N}_i \tag{2.39}$$

Mature Biomass

$$\frac{d(\hat{N}_m\hat{V}_r)}{d\hat{t}} = \hat{a}_{12}\hat{N}_i\hat{V}_r - \frac{F_o}{\alpha_{11}V_{r_0}}\hat{N}_m \tag{2.40}$$

External Substrate

$$\frac{d(\hat{s}_e\hat{V}_r)}{d\hat{t}} = \frac{F_i}{\alpha_{11}V_{r_0}}\hat{s}_{e_f} - \frac{F_o}{\alpha_{11}V_{r_0}}\hat{s}_e - \hat{a}_i\hat{N}_i\hat{V}_r \tag{2.41}$$

Internal Substrate

$$\frac{d(\hat{s}_i\hat{V}_r)}{d\hat{t}} = \hat{a}_i\hat{N}_i\hat{V}_r - \hat{a}_{11}\hat{N}_i\hat{V}_r - \frac{F_o}{\alpha_{11}V_{r_0}}\hat{s}_i \tag{2.42}$$

Bacitracin

$$\frac{d(\hat{A}\hat{V}_r)}{d\hat{t}} = ky_v\hat{a}_{12}\hat{N}_i\hat{V}_r - \frac{F_o}{\alpha_{11}V_{r0}}\hat{A} \tag{2.43}$$

Culture Volume

$$\frac{d\hat{V}_r}{d\hat{t}} = \frac{F_i}{\alpha_{11}V_{r_0}} - \frac{F_o}{\alpha_{11}V_{r_0}} \tag{2.44}$$

(2.45)

The variables and parameters are defined in the nomenclature section, however for convenience the comparison model variables, with their dimensionless definitions, are shown in Table 2.4. To fully specify the model, a set of initial conditions for each differential equation is required. The fully specified com-

Variable	Dimensionless Definition	Description
t	$t\alpha_{11}$	Time (hr)
N_i	$\frac{N_i}{y_i s_{e0}}$	Immature Cell Conc. (1/l)
N_m	$\frac{N_m}{y_i s_{e0}}$	Mature Cell Conc. (1/l)
s_e	$\frac{s_e}{s_{e0}}$	Ext. Substrate Conc. (g/l)
s_i	$\frac{s_i}{s_{e0}}$	Int. Substrate Conc. (g/l)
A	$\frac{A}{s_{e0}}$	Antibiotic Conc. (g/l)
V_r	$\frac{V_r}{V_{r0}}$	Fermentor Volume (l)

Table 2.4: Definitions of the state and independent variables for the modified Blanch and Rogers model.

parison model consists of six ordinary differential equations. The nonlinear nature of the coupled equations necessitates a numerical solution technique. As with the segregated model, the DDASSL [82] differential-algebraic equation solver has been used to obtain solutions to the dynamic comparison model.

The steady-state comparison model is formed by equating the differential terms in the dynamic model to zero. Solutions to the resulting nonlinear-algebraic equations comprises the steady-state points in the comparison fermentation model. Again, the numerical algebraic equation solver, HYBRD1, from the MINPACK software package [74] has been utilized to obtain steady-state solutions.

Parameter	Description
α_{1i}	Maximum rate of substrate internalization (1/hr)
K_{1i}	Michaelis constant-substrate internalization (g/l)
s_{i0}	Initial internal substrate concentration (g/l)
α_{11}	Maximum rate of immature cell reproduction (1/hr)
K_{11}	Michaelis constant-immature cell reproduction (g/l)
m_{i1}	Specific rate of immature cell death (1/hr)
y_i	Immature reproduction yield coefficient (1/g)
α_{12}	Maximum rate of immature cell maturation (1/hr)
β_{12}	Maturation inhibition coefficient
k	Bacitracin production coefficient (g)

Table 2.5: The comparison model parameters.

2.3.2 Comparison model parameters

The comparison model contains a parameter set, listed in Table 2.5, that must be determined for the *B. licheniformis* system. Blanch and Rogers estimated parameters for their original model based on the production of gramicidin S from *B. brevis*. Unfortunately, the differences between *B. brevis* and *B. licheniformis* preclude any correspondence between the parameter values obtained by Blanch and Rogers and those needed to represent the bacitracin producing system used in this study. Therefore, the parameters for the comparison model need to be determined from data generated in this study.

The parameters of interest include the kinetic rate parameters relating the growth and differentiation process to the substrate concentration, the stoichiometric coefficients coupling growth to substrate consumption, and the proportionality constant for bacitracin production. The kinetic expression describing vegetative growth, including substrate internalization and biomass production, are identical between the MBR model and the segregated description. Therefore, the two maximum rate constants, α_{1i} for substrate internalization and α_{11} for biomass production, exist in the MBR model. The parameters representing substrate affinity for the growth rate processes, the Michaelis constants K_{1i} and K_{11}, are also identical between the segregated and comparison modelling approaches. Thus, including the death rate constant, the growth rate expressions require five parameters.

The differentiation expression in the MBR model is represented by the linear maturation model, shown in Equation 2.36. This introduces two parameters, α_{12} and β_{12}, representing the maximum rate of maturation and the growth attenuation coefficient, respectively. The antibiotic production expression adds a single parameter to the model, because the rate of bacitracin production is assumed to be directly linked to differentiation. Therefore, the parameter k is the proportionality constant between the maturation rate and the bacitracin production rate.

Finally, a stoichiometric constant is required to couple the growth process to substrate consumption. For the MBR model the parameter y_i represents the number yield of immature cells per gram of limiting substrate consumed.

Similar to the segregated model, there is limited sensitivity of the comparison model to several of the parameters. Therefore, to facilitate estimation of the significant parameters, sensitivity analysis has been utilized to determine which parameters have a large effect on the model solution. Those parameters that have a relatively small effect are set to reasonable values and considered fixed during parameter estimation. A detailed discussion of the comparison model sensitivity analysis and parameter estimation are provided in Chapter 4.

2.4 Chapter Summary

In this chapter production of bacitracin by *Bacillus licheniformis* has been proposed as a good system to explore the effectiveness of a segregated modelling approach. A morphologically-structured model, including descriptions of the vegetative, sporangium, and spore morphologies, has been developed. The coupling of bacitracin production to the sporulation process is treated by including an age-segregated population model of the sporangium biomass.

A numerical solution technique for the segregated model, based on a semi-analytical solution to the sporangium population balance, has been implemented to solve the dynamic fermentation model. Grid refinement studies indicate an adaptive finite element grid is effective at tracking solutions for sporangium age density throughout batch and continuous fermentation simulations.

To provide a comparison to the segregated model, a structured model from the literature has been adapted to the bacitracin system. The modified Blanch and Rogers model uses an age-structured approach, assuming bacitracin production is related to the maturation of vegetative cells into differentiated biomass.

In the following chapters, the laboratory fermentation system is described, and estimation of the adjustable model parameters for the segregated and comparison models is discussed.

Chapter 3

Laboratory Fermentor and Assay Procedures

Due to the dearth of suitable experimental data, it was necessary to construct a laboratory scale fermentation apparatus for use in model identification and validation. It was also necessary to develop media for single substrate limited growth, and to find assay techniques suitable for the quantification of substrate, biomass, and antibiotic. This chapter discusses the apparatus and methods used in the experimental portion of this project.

3.1 Fermentor

The fermentor used for both batch and continuous fermentation studies was the New Brunswick Multigen Model F–2000 Convertible Fermentor. The apparatus, detailed in Figure 3.1, is essentially a stand enclosing temperature control hardware, an agitation motor, and an air pump for vessel aeration. A variable sized clamping system allows for various fermentor vessel sizes, rang-

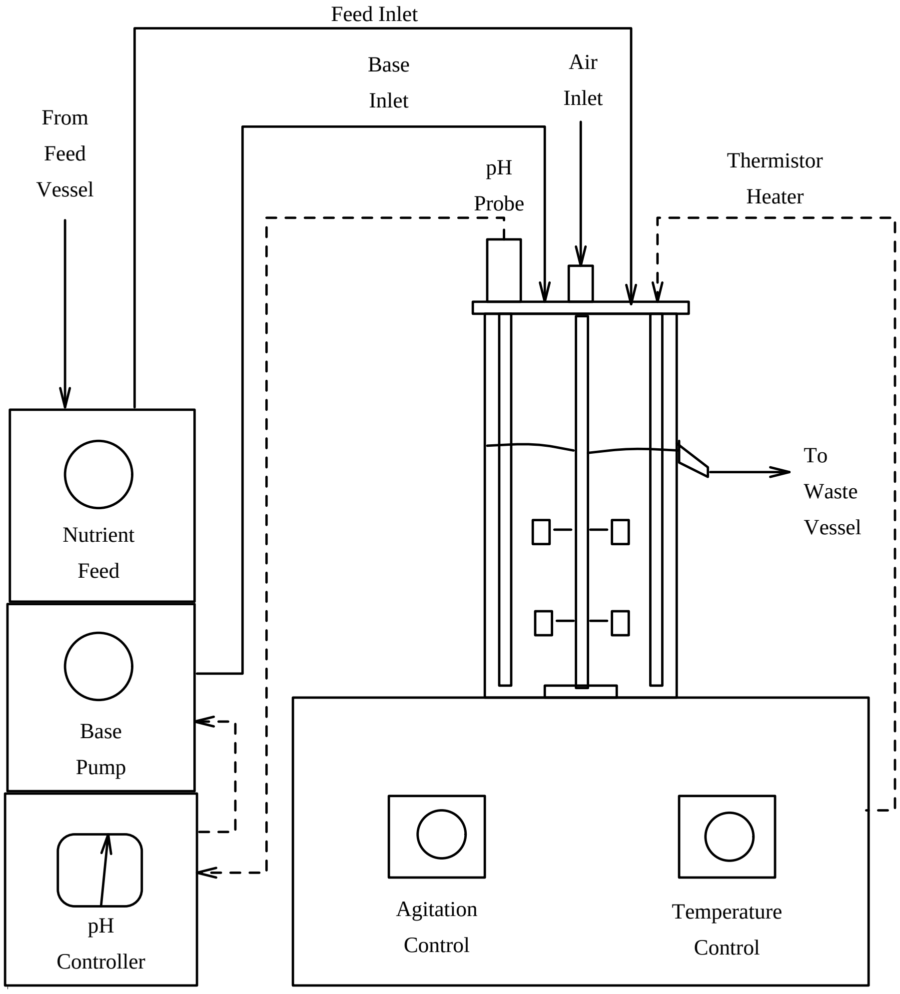

Figure 3.1: Multigen fermentation apparatus.

ing from 1.0 to 2.0 liters. The stand serves as a base for the fermentation vessel allowing for coupling of the temperature, agitation and aeration hardware to the fermentation vessel.

3.1.1 Vessel and Headplate Assembly

In this study, a 2.0 liter borosilicate glass fermentation vessel was used. The vessel is cylindrical in shape and is constructed with a side–draw arm to allow for medium overflow during continuous operation. The vessel is diagrammed in Figure 3.2.

A stainless steel headplate clamps to the vessel top with a rubber o-ring system, effectively sealing the vessel from the outside environment. The headplate, shown in a top view in Figure 3.3, is equipped with several baffles projecting into the vessel to promote mixing. Along with the baffles, several stainless steel wells protrude into the vessel, allowing for indirect contact between external instrumentation and the culture medium. Two openings exist for direct contact between measurement devices and the culture medium. In this study, one opening was used for a pH probe, and the other was unused, and was therefore sealed. The headplate contains several medium sampling and addition ports. These ports are used for acid/base addition in pH control, medium feed for continuous operation, culture sampling, and inoculation. Finally, two ports are used for aeration, and off gas removal. The aeration port feeds directly into the center of the headplate, where it is coupled to the fermentor stirring mechanism. The off-gas port allows the sparged air out of the vessel.

3.1.2 Agitation, Aeration and Temperature Control

As mentioned previously, the Multigen fermentation apparatus is equipped with agitation and temperature control hardware. The fermentation medium is agitated using two 3-blade impellers mounted on a rotating shaft. The agitation shaft fits over a glass guide at the bottom of the vessel. The agitation

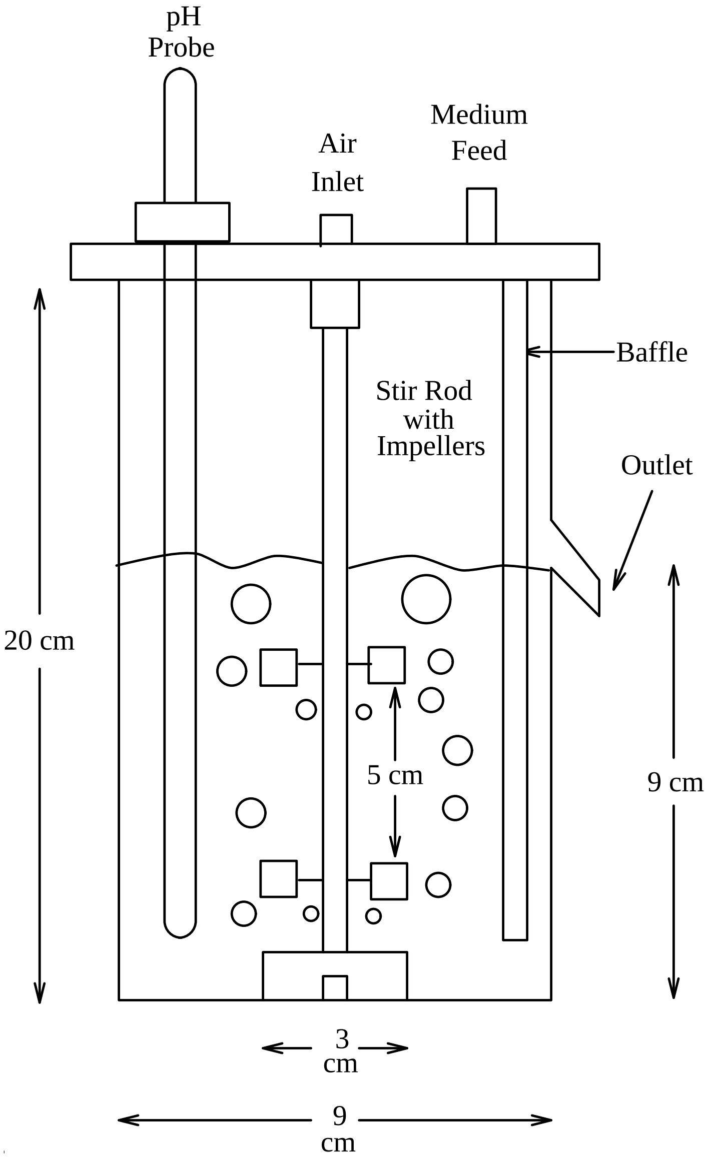

Figure 3.2: Diagram of the Multigen 2.0 liter fermentation vessel.

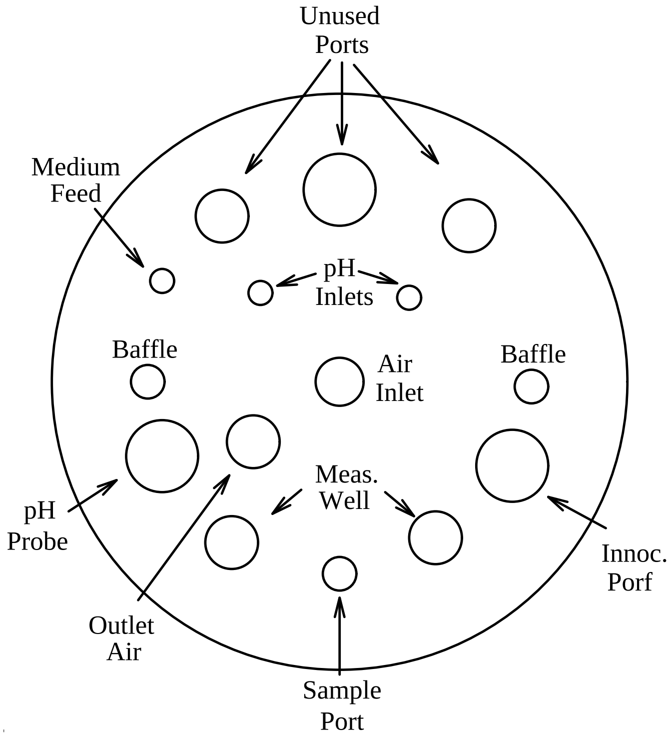

Figure 3.3: Fermentor headplate assembly.

shaft is magnetically coupled to a variable speed motor housed in the Multigen fermentor base. Agitation speeds can be varied between 50–1000 rpm. The magnetic coupling avoids any contamination problems associated with a direct drive agitation system.

Aeration was achieved by connecting the laboratory bench airline, through a sterilization filter (cellulose filter 0.45μm poresize) to the headplate agitation/sparge port. The air flow was measured on-line using a precalibrated air rotameter, and this measurement was used to control the aeration rate by manually adjusting the bench air valve at the beginning of a run.

Off gas was vented from the fermentation vessel through the side arm during continuous fermentations. For batch operation, the off-gas port was equipped with a sterilization filter (cellulose filter 0.45μm poresize) to allow escape of the gas from the vessel, while preventing outside contaminants from entering.

The temperature control hardware consists of a thermistor temperature sensor fed through an on-off control circuit to a Tempco 30 watt heating element. Both the sensor and the heater are placed in thermowells through the headplate, thus they are not in physical contact with the culture broth. The on-board control system is able to maintain temperatures up to 60±0.2° C. For all fermentations carried out in this work the temperature was maintained at 37° C.

3.1.3 pH Control Hardware

Previous studies have shown the major metabolic products of *B. licheniformis*, in both aerobic and anaerobic growth conditions, are short chain organic acids [59, 101, 112]. Therefore, it was necessary to implement a pH control system. The fermentor headplate was fitted with a double-reference reservoir, steam-sterilizable pH electrode (Phoenix Electrode Co.). The electrode signal was feed to a bench-model pH amplification and control system (Cole-Parmer Co.). Culture pH is maintained using an on–off control scheme, through the activation of peristaltic pump for acid or base addition. Since the *B. licheniformis* primarily produces acidic metabolites, the pH controller was only supplied with alkaline feed solution consisting of 1.0 M KOH. Using this setup, the culture pH was maintained at 7.0 ± 0.1.

3.1.4 Nutrient Feed

Continuous feed fermentations were utilized for parameter estimation experiments. Therefore, a nutrient medium supply and pumping system was needed for continuous medium feed. A nutrient feed reservoir was constructed out of a 13 liter Pyrex carboy, fitted with a rubber cap containing two separate ports, one for feed supply and the other acted as a vent for pressure equalization. The vent port was connected to a 20 ml plastic syringe packed with glass wool. This allowed air to pass into the reservoir while excluding microbial contaminates. A piece of autoclavable silicon tubing was attached to the feed port of the medium reservoir. Medium was pumped out of the reservoir using a low-speed valveless metering pump (Flow Metering, Inc.). Accurate flow was obtained for flowrates varying between 50 (ml/hr) to 800 (ml/hr). The pump-head was fully autoclavable, therefore contamination of the feed medium by the pump was avoided. Nutrient medium was pumped through the feed line into a medium break tube, and through the headplate, allowing a continuous drip of medium into the vessel.

During the continuous runs a constant culture volume was maintained by liquid overflow at the fermentation vessel side–draw arm. The overflow traveled through outlet tubing into a 50 liter polypropylene vessel. When filled, the used culture liquid was autoclaved and emptied.

3.2 Medium Preparation

The single limiting substrate assumption was used for the segregated and the modified Blanch and Rogers model. This necessitated the development of a chemically-defined, minimal growth medium, designed such that all nec-

Component	Molar Concentration
Glucose	variable
NH_4Cl	0.01
$Na_2HPO_4 \circ 12H_2O$	0.04
KH_2PO_4	0.026
$MgSO_4 \circ 7H_2O$	5.0×10^{-4}
$CaCl_2 \circ 6H_2O$	1.0×10^{-4}
$FeSO_4 \circ 7H_2O$	1.0×10^{-5}
$MnCl_2 \circ 4H_2O$	1.0×10^{-5}

Table 3.1: Fermentation medium composition.

essary nutrients, except for the limiting substrate, were provided in excess. Previous studies have successfully grown several *Bacillus* species in minimal medium [47]. From these studies it was found that normal sporulation behavior required the presence of the divalent cations Ca^{2+} and Mn^{2+} in the growth medium. Commensurate with these observations, a basic growth medium recipe was obtained from Hanlon and Hodges [47]. The medium composition is listed in Table 3.1. For this study, all components were provided in excess, except for glucose, the limiting substrate. Glucose was chosen as the limiting substrate due to the fact that this experimentally relevant concentrations of this sugar were readily measured using available experimental equipment.

The medium was prepared in two stages. First, the phosphate buffering components and the nitrogen source were dissolved in distilled-deionized water to the specified concentration. This mixture was steam-sterilized (121°C,

$1.2\ \mathrm{kg/cm^2}$) for an exposure period dependent on volume (15 minutes for 1.0 liter or less, 90 minutes for the 10 liter feed bottles). The remaining components, including the metal salts and glucose were dissolved in concentrated form in distilled-deionized water, and filter sterilized using sterile cellulose acetate filters (0.22μm poresize). The concentrated nutrient solution was added aseptically to the cooled buffered ammonium solution. This medium was utilized in inoculum preparation, and for batch and continuous fermentations.

3.3 Fermentation Conditions

3.3.1 Inoculum Preparation

Vegetative Cell Inoculum. The inoculum for fermentation experiments was prepared by seeding of *B. licheniformis* (ATCC 10716) from a master culture to test tubes containing 5.0 ml of minimal growth medium. The master culture was stored at −70°C in 2.0% glycerin–water solution. The inoculum tubes were incubated in 37°C water shaker bath. After approximately twelve hours the inoculum tubes had visibly dense growth in the solution. At this time, 1.0 ml of inoculum broth was used to seed 50 ml of growth medium in a 250 ml Erlenmeyer flask. These flasks were incubated at 37°C in the shaker bath. After sufficient growth had occurred in the shake flask inoculums (approximately 12 hours), 10 ml of the 50 ml shake flask was used to inoculate the fermentation vessel for either batch or continuous experiments.

Spore Inoculum Preparation. Following the water-washing spore purification technique of Nicholson and Setlow [76], spore inoculum were prepared for spore germination experiments. Shake flasks were utilized to grow *B. licheniformis* to high optical density and allowed to sporulate. After 48 hours of incubations at 37°C the cells were harvested and centrifuged ($10,000 \times$ g, 10 min.). The pellet was washed with cold, sterile deionized water three times, with subsequent centrifugations steps in between each washing. The resuspended pellet was stored at 4°C. The water washing was repeated daily until a single consistent pellet was obtained upon centrifugation. These free spores were suspended in cold deionized water and used as spore inoculum.

3.4 Model Assumption Validation

In developing the segregated and comparison models, several assumptions were made. Before attempting to identify the model, it is important to consider the validity of the assumptions. The assumptions are as follows:

1. Constant density
2. Perfect mixing
3. Single substrate limited growth

All fermentations carried out in this study involved dilute aqueous suspensions. Since cells are primarily water, and growth never achieved densities higher than 1.0 mg/ml, it is likely that the fermentation broth density never varied significantly from the density of water. Since the fermentation broth can be considered an incompressible liquid for the experimental conditions dealt with in this study, any volume effects related to medium composition, and microbial growth were negligible and hence were ignored.

The completed fermentor model involves coupling of the constitutive kinetic relationships, which describe process rates, to a hydraulic description of the reactor, which describes flow and mixing characteristics. The reactor used for the fermentation experiments was assumed to be an ideal stirred tank vessel, as implied by the assumption of perfect mixing. The laboratory fermentation vessel is equipped with a double impeller agitation system and four vertical baffles, as discussed in Section 3.1.2. An indication of the validity of the perfect mixing assumption is the impeller Reynolds number for the laboratory fermentation vessel. For typical operating conditions used in the fermentation experiments $N_{\mathrm{Re}} \approx 1.0 \times 10^5$, well above the critical Reynolds number of 1.0×10^4 for turbulent mixing [37, 78]. This suggests adequate mixing was provided to approximate the ideal stirred tank vessel.

The kinetic rate processes developed in this study are based on the assumption that a single chemical species is rate limiting. The growth medium used for the fermentation experiments was designed with the intent that the carbon source, glucose, would be the single limiting nutrient. Therefore, all nutrients except glucose were provided in excess. To evaluate the range of limiting glucose concentrations, *B. licheniformis* was grown in minimal medium of varying glucose concentration. The flasks were harvested after batch growth was completed, and dry weight concentration measurements were made for each glucose concentration. A plot of dry weight versus initial glucose concentration is shown in Figure 3.4. The resulting experiments showed that for the base medium composition described in Table 3.1, glucose was limiting up to concentrations of at least 0.2 wt%. Based on these results, glucose composition was kept within the glucose-limiting range, and all rate expressions were based on glucose as the limiting nutrient.

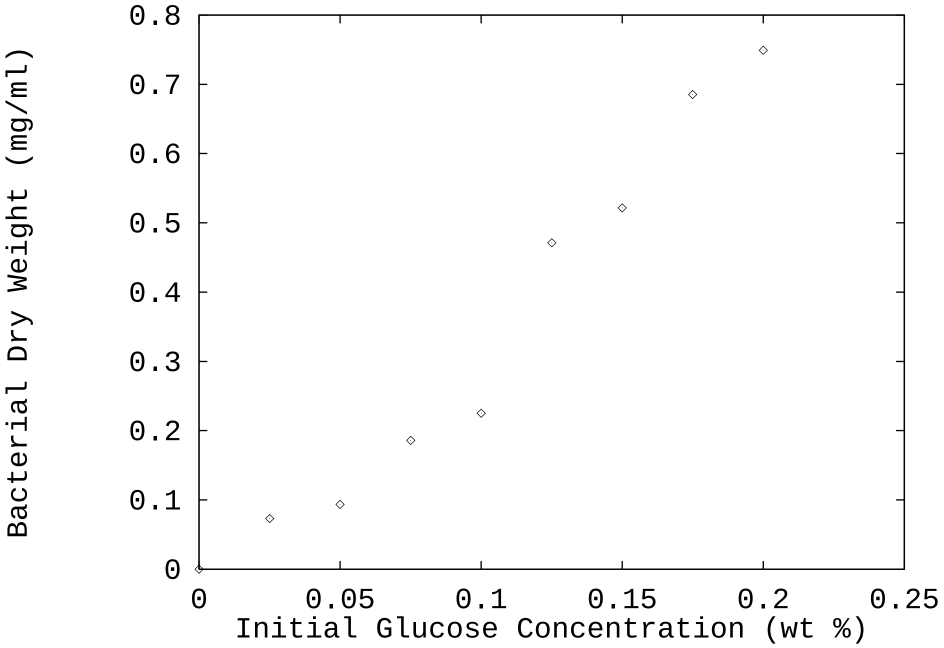

Figure 3.4: Bacterial dry weight at termination of batch growth vs. initial glucose concentration.

3.5 Assay Procedures

3.5.1 Biomass Measurements

To access the levels of spore and nonspore biomass, measurements of the number densities of fermentation broth were obtained. Although three distinct types of biomass were assumed to exist in *B. licheniformis* fermentation samples, measurement capabilities limited the available biomass concentration information to two independent measurements: total biomass number density, and spore number density. The spores were distinguished from nonspores using the heat-tolerance characteristics of spores.

The biomass assay procedure was as follows. Growth samples approximately 5 ml in volume were obtained aseptically from the fermentation vessel. The sample was split into two volumes, and retained in heat-sterilized test tubes. The sample used for the spore biomass assay was placed in a water bath at 80°C for 10 minutes. This heat treatment was assumed to kill all cells except for mature spores [76]. At this point, both the heated and unheated tubes were serially diluted using sterile deionized water to obtain approximately 20–200 colony forming units per milliliter. The diluted samples were plated into cooled LB soft agar (Luria-Bertani broth 2% (Difco), Gum Agar 0.5% (Sigma)), and incubated at 37 °C for 12 hours. After the incubation period, plate counts were obtained. Plate counts were made on two replicate plates for a given dilution factor. The resulting replicated counts show standard deviations of approximately 20%.

3.5.2 Glucose Assay

Fermentation samples of approximately 1.0 ml obtained aseptically from the fermentation vessel were centrifuged (5000×g, 6 minutes) and subsequently frozen for assay at a later date. The glucose concentration measurements were obtained upon the thawed samples using a Model 23A immobilized-enzyme glucose analyzer (Yellow Springs Instruments).

3.5.3 Bacitracin Assay

The activity of bacitracin was assayed using the cylinder-plate diffusion method as given in the United States Pharmacopeial Convention (USPC) [107]. The basis of the assay is the concentration-dependent inhibitory capability of the antibiotic upon the growth of a test organism. Descriptions of the assay procedure are provided in the following discussion. Recipes for the various media and buffers used in this assay are given in USPC manual [107].

Test Organism Preparation. The recommend test organism for bacitracin is *Micrococcus luteus* American Type Culture Collection number 10240. The test organism was transferred weekly to fresh USPC agar medium # 1 slants and stored at 25 $^\circ C$. Test organism inoculum for the bacitracin assay was prepared by inoculating the surface of 250 ml of USPC agar medium # 1 in a roux bottle with a 5.0 ml of a 12 hour liquid inoculum of *M. luteus.* After 24 hours of incubation at 32 $^\circ C$, the surface growth was collected in 50 ml of sterile phosphate buffered saline. To promote consistency between assay runs, the concentration of the *M. luteus* stock solution was standardized such that a 30:1 dilution of the stock gave 25% light transmittance at 580 nm. The test organism stock solution was stored at 4 $^\circ C$, and was used for a period of 1 week before making new solution. The bacitracin assay test agar, USP agar medium #1 was seeded with standardized *M. luteus* stock solution at a ratio of 0.3 ml per 100 ml test agar.

Antibiotic Stock Preparation. The cylinder-plate assay requires a standard antibiotic sample for comparison with the unknown samples. Standardized zinc bacitracin A of 58.5 IU/mg was obtained for the assay procedure from the United States Pharmacopeial Convention in Rockville, Maryland. Bacitracin stock solution of 50 IU/ml was prepared by dissolving an accurately weighed and previously dried quantity of zinc bacitracin powder in 0.01 N HCl. The stock solution was diluted to the desired test concentrations using phosphate buffer #1.

Cylinder Plate Diffusion Assay. Disposable petri dishes of dimensions 20×100 mm (Falcon-Optilux) were used to assay for bacitracin. A double agar layer was poured into each dish, the base layer consisting of 20 ml of sterile USP agar #2, followed by 7 ml of USP #1 agar, seeded with M. luteus. After solidification, 6 stainless steel penicylinders were dropped onto the plates using a mechanical cylinder dropper (Arthur Farmer Inc., Trenton, New Jersey). The cylinders were dropped from a height of 12 mm in a symmetrical circular pattern of radius 2.8 cm. Three cylinders were filled with bacitracin test solution of 1.0 IU/ml and the remaining three cylinders were filled with the supernatant from a centrifuged sample of the fermentation broth. The plates were covered to prevent contamination and refrigerated at 4 $^{\circ}C$ for a period of 4 hours, to allow diffusion of the antibiotic solutions into the agar. After refrigeration, the plates were incubated for 24 hours at 32 $^{\circ}C$. After the incubation, the plates consisted of yellow lawns of *M. luteus* except in clearly defined circular zones around the antibiotic containing cylinders. The size of the inhibition zone for each cylinder was determined to the closet 0.1 mm using a Fisher-Lilly zone reader (Fisher Scientific). The average inhibition zone for the test solution and the unknown sample were calculated for each plate, and this was used to determine bacitracin concentration in the unknown by comparison of the averaged difference between the unknown and the test solution to a bacitracin standard curve.

Bacitracin Standard Curve. A bacitracin inhibition standard curve was developed by conducting the bacitracin assay with known dilutions of USP bacitracin standard. The test dilution of 1.0 IU/ml was compared to known dilutions ranging from 0.2 IU/ml to 3.7 IU/ml. The resulting average inhibition zones are shown in Table 3.2.

Test Dilution (IU/ml)	Ave. Test Zone (mm)	Ave Stand. Zone (MM)
0.2	17.6 ± 0.3	22.9 ± 0.7
0.5	20.3 ± 0.7	22.2 ± 0.2
0.8	21.0 ± 0.5	21.6 ± 0.3
1.1	22.4 ± 0.3	22.3 ± 0.1
1.4	22.5 ± 0.6	22.2 ± 0.5
1.7	23.0 ± 0.2	21.9 ± 0.1
2.0	24.1 ± 0.2	22.4 ± 0.3
2.3	24.2 ± 0.8	22.2 ± 0.3
2.6	24.8 ± 0.5	21.7 ± 0.2
2.9	24.8 ± 0.2	21.8 ± 0.4
3.2	24.8 ± 0.3	21.7 ± 0.2
3.5	24.8 ± 0.6	21.5 ± 0.5

Table 3.2: Inhibition zones for standard bacitracin dilutions.

Based on the inhibition zone data for the standard bacitracin solutions a inhibition zone standard curve was calculated, according to Darker et. al. [20]. The diffusional based mechanism of zone inhibition should show a power law dependence of inhibition size on bacitracin concentration:

$$\log y_{anti} = md + \log b \tag{3.1}$$

where y_{anti} is the antibiotic concentration, d is the diameter of the inhibition

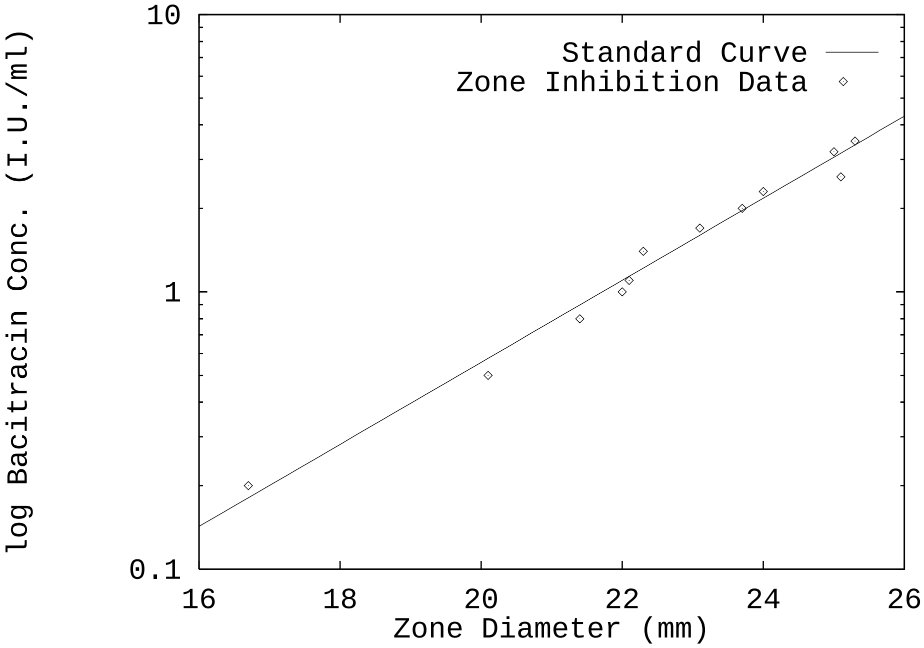

Figure 3.5: Standard curve for determining bacitracin concentration from agar diffusion inhibition zone.

zone, m and b are experimentally fit assay parameters. The fit of Equation 3.1 to the standard inhibition data are shown on semi-log axes in Figure 3.5. The resulting standard curve, referenced to 22 mm for 1.0 (IU/ml), is given by:

$$y_{anti} = (6.119 \times 10^{-4})10^{0.148d} \tag{3.2}$$

As Figure 3.5 shows, this correlation provides an effective bacitracin measurement for concentrations ranging from 0.2–3.5 (IU/ml).

Chapter 4

Model Identification and Validation

In most modelling studies, the lack of sufficient *a priori* knowledge necessitates the use of parameter estimation techniques to determine the unknown model parameters. It is often the case, that this is looked upon as simply the process of choosing parameters such that the proposed model fits a set of experimental results. Since it is desirable that the model reflects the system in as wide a range of operating conditions as possible, a more satisfying approach is that of model identification. The goal of model identification is to determine a set of adjustable model parameters, that not only fit the data well, but also give an estimate that on average closely approximates the "true" value of the parameters. By taking this approach, it is hoped the model will accurately predict the system behavior in a large region of the operating space. This contrasts the situation usually obtained when the model is merely "fit" to a given set of experimental results, resulting in poor model performance when system operation moves away from the conditions used for estimation.

4.1 Preliminaries

4.1.1 Stochastic Model Formulation

Prior to discussing parameter estimation, it is necessary to define a few terms relating to the structure of the models analyzed in this study. The class of models dealt with in this work can be expressed in a general form as:

$$\dot{\mathbf{x}} = \mathbf{f}(\mathbf{x}, \mathbf{x}', \mathbf{u}, \theta) \tag{4.1}$$

$$\mathbf{y} = \mathbf{g}(\mathbf{x}, \theta) \tag{4.2}$$

The l-dimensional vector, $\mathbf{x}$, represents the model states, and the m-dimensional vector, $\mathbf{y}$, contains the model outputs, or measured variables. The r-dimensional vector $\mathbf{u}$ represent the independent, or manipulated variables, and $\boldsymbol{\theta}$, a p-dimensional vector, represents the model parameters. The term $\mathbf{x}'$ represents state derivatives with respect to cell age, reflecting segregation of the sporangium state. If the independent variables are known precisely, (at least in a relative sense), solving the differential equations given in (4.1) converts the model to standard reduced form:

$$\mathbf{x} = \mathbf{h}(\mathbf{u}, \theta, t, \tau) \tag{4.3}$$

$$\mathbf{y} = \mathbf{g}(\mathbf{h}(\mathbf{u}, \theta, t, \tau), \theta) \tag{4.4}$$

Equations 4.3–4.4 relate the system outputs to the manipulated variables, parameters, time, and sporangium age. This formulation is deterministic, meaning for a set of precisely known manipulated variables and parameters, the state variables are assumed to be known exactly. Since the presence of measurement noise and structural model error makes the deterministic formulation unrealistic, it is useful to recast the model into a stochastic framework. This can be achieved by including a random error term, accounting for both model and measurement error:

$$\tilde{\mathbf{y}} = \mathbf{g}(\mathbf{h}(\mathbf{u}, \theta, t, \tau), \theta) + \epsilon \tag{4.5}$$

In the absence of model error, the "true" values of the outputs are represented by $\mathbf{y}$, and the observed values are given by $\tilde{\mathbf{y}}$. The stochastic form is known as the likelihood–standard reduced model, and with the model in this form it is possible to define the residuals:

$$\mathbf{e}_i(\theta) = \tilde{\mathbf{y}}_i - \mathbf{y}_i(\theta) \tag{4.6}$$

The residuals represent the difference between the observed values of the outputs and those predicted by the model. While the ideal situation would be to estimate the parameters such that the model fits the "actual" values of the outputs as closely as possible, the presence of measurement noise makes the true value of the outputs unknown. Therefore, it is assumed the model is structurally correct and the residuals reflect measurement error when the estimated parameters are close to their "true" values.

4.1.2 Estimation Methods

Now that the model has been placed in a stochastic context, it is appropriate to discuss the process of parameter estimation. In essence, the parameter estimation task can be posed as an optimization problem, where the goal is to adjust the parameters, such that some measure of the model fit is optimized. The main consideration in development of a parameter estimation scheme is the choice of how to measure the model fit to the data. In other words, what optimization objective function is appropriate for the given problem? In the next section, a brief discussion of the most common approaches is given. In reviewing parameter estimation theory, it is hoped the motivations for the choice of the estimation objective function used in this study are made clear.

Weighted Least Squares. A common choice for an estimation objective function is weighted least squares:

$$\min_{\theta} \Phi = \sum_{i=1}^{n} \mathbf{e}_i^T \mathbf{B}_i \, \mathbf{e}_i \tag{4.7}$$

In this equation, $\mathbf{B}_i$ represents a positive semi-definite weighting matrix. The $\mathbf{e}_i$ represents the vector of residuals for the ith experiment. Using least squares estimation, the goal is to minimize some weighted measure of the residuals. It is tempting to choose this form of objective function because it is straightforward, and the weighting matrix can be used as a tuning device such that the estimation converges to a set of realistic parameters. However, using weighted least squares with an arbitrary weighting matrix can be erroneous, because the choice for the weighting matrix makes assumptions concerning the statistical nature of the data. In the case of a model linear in the parameters with measurement error distributed normally with zero mean, the minimum variance estimates of θ are obtained when $\mathbf{B}$ is set to the inverse measurement error covariance matrix $\tilde{\mathbf{V}}_i^{-1}$ [6]. Therefore, use of the weighting matrix to achieve parameter convergence alters the assumptions concerning the statistical structure of the data, and can lead to erroneous parameter estimates.

Maximum Likelihood Estimation. A different approach to the estimation task is maximum likelihood estimation (MLE). The likelihood function of the sample is defined as the joint probability distribution of the residuals, $\mathbf{e}$, as a function of the unknown parameters. In this case, the unknown parameters include the adjustable model parameters, θ, and the distribution parameters for the observations, $\boldsymbol{\psi}$. If the model is structurally accurate, and the parameter vector is close to the true parameters, then the residuals should be representative of the measurement errors for a given set of experimental data.

Given a probability distribution function (pdf) for the measurement error, the likelihood function is formed by replacing the measurement errors, ϵ, with the residuals, $\mathbf{e}$, in the measurement error pdf:

$$L(\theta, \psi) = p(\mathbf{e}(\theta) \mid \psi) \tag{4.8}$$

Accepting the assumption that the residuals reflect measurement error, the likelihood function describes the probability of realizing a set of residuals for a given set of probability distribution parameters. For a given set of data, the residuals are purely functions of the model parameters. Therefore, the likelihood function is a function only of the model and distribution parameters. Maximization of the likelihood function with respect to the model and distribution parameters, subject to the model equation constraints, yields the maximum likelihood parameter estimates. Put simply, the MLE is the most probable set of parameters that would have led to the given set of measurement errors distributed as $p(\mathbf{e} \mid \boldsymbol{\psi})$.

Maximum likelihood estimation is appealing for many reasons. First, the very nature of the method forces the user to define a probability distribution for measurement errors. This is because MLE explicitly acknowledges the statistical structure of the data in the estimation objective function. This is in direct contrast to weighted least squares estimation, where the objective function does not necessarily have a basis in statistics. By forcing a choice for the pdf, MLE creates a situation where the user must consider the statistical nature of the data, and thus must consider what assumptions are appropriate for the given system. Are the errors normally distributed, or are there reasons to expect different distributions? Are the errors independent, or are correlations expected? Is it appropriate to assume that all the errors come from the same distribution, or are the errors of different experiments distributed differently? While the answer to these questions may not be clear, it is important to consider them. In the situation where there is little insight into the statistical structure of the data, a common assumption is that the errors are distributed normally with zero mean. The validity of the normality assumption is based on the central limit theorem, which states the distribution of the sum of random variables becomes normal as the number of terms in the summation becomes large, regardless of the individual distributions of the random variables [73]. Since measurement errors probably result from a combination of factors, it is common that they appear normally distributed. Although the central limit theorem is commonly invoked, the beauty of the MLE method is that if a different distribution is more appropriate, MLE allows for direct utilization of the error distribution information.

A second advantage of MLE arises from the dependence of the likelihood function on the measurement error distribution parameters, $\boldsymbol{\psi}$. If the structure of the error distribution function is decided upon, but the distribution parameters are unknown, MLE allows for treatment of the distribution parameters as optimization variables. The distribution parameters can then be estimated along with the model parameters using the experimental data. Therefore, given the functional form of the measurement error distribution, it is possible to estimate the distribution parameters that most likely resulted in the given experimental data. Estimation of the distribution parameters allows one to avoid the common assumption that the data are identically distributed. If the measurement errors are normally distributed, then Bard [6] points out that maximum likelihood estimation is equivalent to solving the weighted least squares problem with unknown weights.

4.2 Maximum Likelihood Estimator

Considering the advantages offered by the maximum likelihood method, the model parameters for both the segregated and comparison models have been estimated using the MLE approach. Detailed reviews of the maximum likelihood estimator are provided by Seber and Wild [94], Gallant [36], and Bard [6]. In this section, development of the maximum likelihood is summarized, and the nonlinear parameter estimation program used to estimate the model and distribution parameters is formulated.

To facilitate development of the objective function, a few definitions must be made. Define n to be the number of experiments included in a given estimation run. In this context, an experiment is defined as the set of measurements resulting from a single sampling period. If m is defined to be the number of individual measurements taken during an experiment, then $n \times m$ individual data measurements are incorporated into the estimation objective function.

The MLE objective function is based on the joint error distribution function for the experimental data. Therefore, to use MLE, it is essential that a form for the measurement error distributions be established. In this study, there are three types of measurements: biomass, substrate, and antibiotic. The nature of each type of measurement, and the measurement techniques used to obtain them, differ significantly between each other. This implies that the measurement error distributions could vary significantly between measurement types. For this work, several assumptions were made concerning the measurement error distributions:

1. The measurement error, ϵ_{ij}, for the jth measurement of the ith experiment was assumed to be normally distributed with zero mean: $\epsilon_{ij} \sim$

$N(0, \nu_{ij})$.

2. The error distribution for a given measurement, j, is constant between experiments: $\nu_{ij} = \nu_j$.
3. All measurements are independent, thus the measurement error covariance matrix, $\tilde{\mathbf{V}}$, is diagonal:

$$\tilde{\mathbf{V}} = \begin{pmatrix} \nu_1 & & 0 \\ & \ddots & \\ 0 & & \nu_m \end{pmatrix} \tag{4.9}$$

The assumption of normally distributed errors is based on the central limit theorem, implying that the summation of errors generated by each step in the measurement process leads to normally distributed errors, regardless of the forms of the individuals error distributions [73]. Further, the measurement procedure involves processing of an independently obtained sample for each measurement. This implies that the result of one measurement is independent of all other measurements, and justifies the assumption of statistically independent measurements, which leads to a diagonal covariance matrix, $\tilde{\mathbf{V}}$.

Using the above assumptions, the measurement error probability distribution for the ith experiment is given by the multivariate normal distribution:

$$p(\epsilon_i, \tilde{\mathbf{V}}) = (2\pi)^{-m/2} \det{}^{-1/2}\tilde{\mathbf{V}} \times \exp\left[-\frac{1}{2}\left(\epsilon_i^T \tilde{\mathbf{V}}^{-1}\epsilon_i\right)\right] \tag{4.10}$$

This provides the probability distribution for one experiment. However, to build the likelihood function, the joint probability distribution for all experiments is required. Using the assumption of statistically independent experiments, the combined probability distribution is the product of the individual distributions:

$$p(\epsilon, \psi_1, \ldots, \psi_n) = \prod_{i=1}^{n} p(\epsilon_i, \psi_i) \tag{4.11}$$

Substitution of Equation 4.10 into Equation 4.11 with the residuals, $\mathbf{e}$, substituted for the measurement errors, ϵ, results in the following likelihood function:

$$L(\theta, \tilde{\mathbf{V}}) = (2\pi)^{-\frac{nm}{2}} n \left(\det{}^{-1/2}\tilde{\mathbf{V}}\right) \times \exp\left[-\frac{1}{2}\sum_{i=1}^{n}\left(\mathbf{e}_i^T(\theta)\tilde{\mathbf{V}}^{-1}\mathbf{e}_i(\theta)\right)\right] \tag{4.12}$$

The definition of the likelihood function provides a measure by which sets of model parameters can be compared to determine which set allows the model to best describe the data. In this case, the best fit is recognized as the set of parameters, θ^*, that maximizes Equation 4.12, and is therefore the most "probable" set of parameters explaining the data. By using the likelihood function as a basis for model identification the effect of the data's statistical structure upon the estimates of the optimal model parameters has been explicitly acknowledged. Also, as Equation 4.12 shows, the likelihood equation is a function of the unknown measurement error covariance matrix, $\tilde{\mathbf{V}}$, which allows for estimation of the error distributions parameters along with the model parameters.

Objective Function Simplification. A convenient manipulation of the likelihood equation is realized by defining the concentrated likelihood function, $\mathcal{L}(\theta, \tilde{\mathbf{V}}) = \log L(\theta, \tilde{\mathbf{V}})$. Since the logarithm is a monotonic function, maximization of $\mathcal{L}$ is equivalent to maximizing L, but it allows for significant simplification of the estimation objective function. The logarithm of Equation 4.12 gives:

$$\mathcal{L} = -(nm/2)\log(2\pi) - (n/2)\sum_{j=1}^{m}\log \tilde{V}_{jj} - \frac{1}{2}\sum_{i=1}^{n}\mathbf{e}_i^T\,\tilde{\mathbf{V}}^{-1}\mathbf{e}_i \tag{4.13}$$

Now, it is obvious from Equation 4.13 that maximization of $\mathcal{L}$ in terms of $\mathbf{e}$, and $\tilde{\mathbf{V}}$, is equivalent to minimizing the negative terms of Equation 4.13 that are functions of $\mathbf{e}_i$ and $\tilde{\mathbf{V}}$. Based on this, the estimation problem can be defined as the following nonlinear program:

$$\min_{\theta,\tilde{\mathbf{V}}} \tilde{\Phi} = (n/2)\sum_{j=1}^{m} \log \tilde{V}_{jj} + \frac{1}{2}\sum_{i=1}^{n} \mathbf{e}_i^T \tilde{\mathbf{V}}^{-1} \mathbf{e}_i \qquad \text{(NLP1)}$$

subject to:

$$\begin{aligned} \dot{\mathbf{x}} &= \mathbf{f}(\mathbf{x}, \mathbf{x}', \mathbf{u}, \theta) && (4.14) \\ \mathbf{y} &= \mathbf{g}(\mathbf{x}, \theta) && (4.15) \end{aligned}$$

Based on the objective function defined in Equation NLP1, the maximum likelihood estimates of the model and distribution parameters could be realized using any appropriate optimization technique. However, a useful technique for simplifying the optimization problem is known as stagewise maximization [58]. In using the stagewise maximization technique, the optimization problem is tackled in two stages, as the name implies. First, the optimal estimates of the measurement error distribution parameters are found. In the case of constant, diagonal measurement error covariance, the optimal error variances can be found analytically, resulting in measurement variance estimates in terms of the model parameters:

$$\nu_j^* = \nu_j^*(\theta) \qquad (4.16)$$

By substituting the optimal variance functions into Equation NLP1, the optimization problem is reduced to finding the optimal model parameter estimates alone. Once the optimal model parameters, θ^*, are found, they can then be used to obtain the optimal variances, ν^*, through Equation 4.16.

The optimal estimate of the measurement error variances is found by differentiating the objective function in Equation NLP1 with respect to ν_j. At the minimum, the slope of the objective function is zero. Therefore, the derivative is set equal to zero, and then solved for ν_j^* in terms of θ.

$$\frac{\partial \Phi}{\partial \nu_j} = \frac{n}{2\nu_j} - \frac{1}{2\nu_j^2} \sum_{i=1}^{n} e_{ij}^2 = 0 \tag{4.17}$$

Solving for ν_j gives the measurement error variance that minimizes the likelihood equation for the current estimate of the model parameters.

$$\nu_j^* = \frac{1}{n} \sum_{i=1}^{n} e_{ij}^2 \tag{4.18}$$

Substitution and of the optimal estimates for the measurement error variances into Equation NLP1 yields a new objective function in terms of the model parameters only.

$$\Phi = \frac{n}{2} \sum_{j=1}^{m} \log \left(\sum_{i=1}^{n} e_{ij}^2 \right) \tag{4.19}$$

By using stagewise maximization the estimation problem has been reduced from the simultaneous estimation of both model and distribution parameters to a optimization problem in the model parameters alone.

The parameter estimation problem can be formally stated as:

$$\min_{\theta} \Phi = \frac{n}{2} \sum_{j=1}^{m} \log \left(\sum_{i=1}^{n} e_{ij}^2 \right) \tag{NLP2}$$

subject to:

$$\begin{aligned} \dot{\mathbf{x}} &= \mathbf{f}(\mathbf{x}, \mathbf{u}, \theta) && (4.20) \\ \mathbf{y} &= \mathbf{g}(\mathbf{x}, \theta) && (4.21) \\ \mathbf{c}(\theta) &\geq \mathbf{0} && (4.22) \end{aligned}$$

Where the optimization is constrained by the solution of the model outputs, $\mathbf{y}$ and any constraints on the parameters themselves, $\mathbf{c}(\theta)$. The solution to this nonlinear programming problem gives the maximum likelihood parameter estimates. These parameters are then used to obtain an estimate of the measurement error variances through Equation 4.18.

4.2.1 Parameter Confidence Region

In light of the desire to "identify" a model, rather than simply fitting it to data, it is important to gauge the certainty of the model and the confidence that the parameter estimates are approximately equal to the "true" parameters. An important issue in parameter estimation is the confidence that is placed in the parameter estimates. The model parameters obtained through the maximization of the likelihood equation represent point estimates of the model parameters. A measure of the confidence in the point estimates is obtained by quantifying a region of the parameter space that contains the "true" with some level of statistical certainty. This space is known as the parameter confidence region, and it represents a generalization of statistical confidence intervals from 1 dimension to the p dimensions of the parameter space.

High parameter confidence implies that insignificant changes in the data used for estimation do not cause large changes in the optimal parameter estimates. This implies that the model parameters are sensitive to the data, that is, the estimation objective function has a well-defined optimum, and thus, changes in the parameter vector have a significant effect on the objective function value. In the opposite case, when seeming large changes of the parameter vector around the optimum have little effect on the objective function, it is said that there is little confidence in the parameters for the given set of data. This translates into a large parameter confidence region, reflecting the lack of certainty about the location of the "true" parameter vector.

The importance of the confidence region is two-fold. First, it provides a measure of how effective the data are giving information concerning the parameters of interest. This is useful, when the goal of the experimental investigation is to determine a set of parameters. From a model identification viewpoint, the parameter confidence region is needed to provide some indication of how well the model is expected to perform from a predictive standpoint. A small confidence region implies that the model should be a reasonably accurate predictive tool, at least in the region of the operating space near to where data for estimation were obtained. In this sense, estimation of parameter confidence is essential in the model identification process.

Confidence Region Estimation. The goal is to define for any data set, W, a closed subset, $S(W)$, in the p-dimensional parameter space that contains the "true" parameters, $\hat{\theta}$, some defined fraction, γ, of the time for all data sets. This can be stated concisely as:

$$\Pr[\hat{\theta} \in S(W)] = \gamma \tag{4.23}$$

An approach to quantifying the size of the confidence region is to choose constant magnitude contours of estimation objective function and determine the parameter deviations that move the objective function onto the limiting contour. An understanding of the measurement error distribution, and the model transformation of that distribution to the parameter sampling distribution can be used to determine a statistical confidence level for a given objective contour.

To simplify the confidence analysis, a common approach is to utilize a quadratic approximation to the objective function so that contours of constant objective function are ellipsoidal. The objective function is expanded in a Taylor series in terms of a small change in the parameters, $\delta\theta$, around the optimum, θ^*. Truncation of the series at the quadratic term gives:

$$\Phi(\theta) \approx \Phi(\theta^*) + \left(\frac{\partial\Phi(\theta^*)}{\partial\theta}\right)\delta\theta \; + \frac{1}{2}\delta\theta^{\;T}\left(\frac{\partial^2\Phi(\theta^*)}{\partial\theta^2}\right)\delta\theta \tag{4.24}$$

If the Hessian matrix, $\mathbf{H}$, is defined to be the second order derivative matrix of Φ with respect to θ, then by recognizing that the gradient of the unconstrained objective function is zero at θ^*, the change of the objective function due to a change in the parameters can be approximated by:

$$\Phi(\theta) - \Phi(\theta^*) \approx \frac{1}{2}\delta\theta^{\,T}\mathbf{H}^*\delta\theta \tag{4.25}$$

Using Equation 4.25, the magnitude of a change in the parameter vector causing a significant change in the objective function can be quantified. Assuming that a definition of significant change for the objective function can be established, then a parameter confidence region can be formed by assuming that parameter changes that do not result in a significant change of the objective function are indistinguishable from the optimal parameters. If a significant change in Φ is defined as the positive constant $c/2$, then the confidence region can be defined by:

$$\mid \delta\theta^{\,T}\mathbf{H}^*\delta\theta \mid \leq c \tag{4.26}$$

The region in the parameter space implied by Equation 4.26 is a p-dimensional hyperellipsoid whose boundary is defined by treating Equation 4.26 as an equality. For a two dimensional system, the confidence region is easily illustrated, and an example is shown in Figure 4.1. However, to quantify the degree of confidence imparted by a particular choice for c, an understanding of how random changes in the data translate into changes in the objective function is necessary. In other words it is desired to know what value of c to choose such that $\Pr\left[\mid \delta\theta^{\,T}\mathbf{H}\,\delta\theta \mid \leq c\right] = \gamma$, where γ is some predetermined level of confidence.

Establishing a value for c is difficult for arbitrarily distributed measurement errors and models that are nonlinear in the parameters. Problems arise due to the nonlinear transformation of the measurement error distribution into an unknown distribution of the parameter vector random variable in the parameter space. For rare cases, it may be possible to analytically derive the

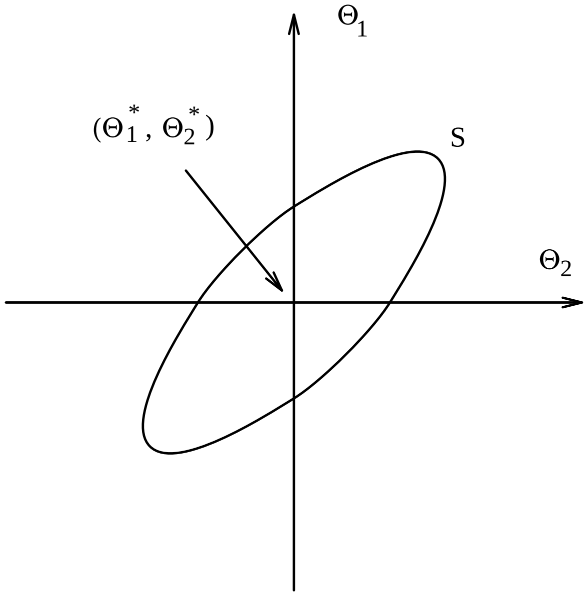

Figure 4.1: A possible parameter confidence region in two-dimensional space. The region S is defined as the parameter region which contains the true parameter vector, $\hat{\theta}$, for a certain fraction of all data samples.

parameter sampling distribution based on the model and the measurement error distribution. However, in the more common situation where a nonlinear transformation of the measurement error distribution prevents use of analytical techniques, approximate methods must be used to ascertain the parameter sampling distribution. In situations where an accurate representation of the nonlinear parameter confidence region is required, Bard suggests utilization of the Monte Carlo method. In this technique, numerically generated data sets with pseudorandom measurement errors are utilized to generate multiple estimates of the model parameters. The resulting distribution of parameter estimates is analyzed to determine suitable bounds for the nonlinear confidence region [6].

In most cases, where an accurate confidence region is not essential, approximations can be used to obtain a tractable representation of the confidence region. In the case of the maximum likelihood equation with a known, constant measurement error covariance matrix, $\tilde{\mathbf{V}}$, an approximation of the Hessian is given by the inverse parameter covariance matrix, $\mathbf{V}_\theta^{-1}$ [6]. Now, by linearizing the deviation of the output equations, $\mathbf{\Delta y}_i = \mathbf{y}_i - \mathbf{y}_i(\theta^*)$, in terms of the deviation of the model parameters, $\mathbf{\Delta}\theta = \theta - \theta^*$, the model is recast as a multiple linear regression problem:

$$\begin{aligned} \mathbf{\Delta y}_i &= \mathbf{W}_i \mathbf{\Delta}\theta && (4.27) \\ W_i(j,k) &= \frac{\partial y_j(t_i,\theta^*)}{\partial \theta_k} && (4.28) \end{aligned}$$

Now, defining Y to be the adjoined vector of output deviations for experiments 1 to n and then using the linear approximation given in Equations 4.27 and 4.28 the linearized model can be cast in matrix form:

$$\begin{aligned} \mathbf{Y}^T &= \left[\begin{array}{cccc} \mathbf{\Delta y}_1^T & \mathbf{\Delta y}_2^T & \cdots & \mathbf{\Delta y}_n^T \end{array} \right] && (4.29) \\ \mathbf{W}^T &= \left[\begin{array}{cccc} \mathbf{W}_1^T & \mathbf{W}_2^T & \cdots & \mathbf{W}_n^T \end{array} \right] && (4.30) \\ \mathbf{Y} &= \mathbf{W}\mathbf{\Delta}\theta && (4.31) \end{aligned}$$

Therefore, the deviation in the model outputs is approximated as the product of the output sensitivity matrix times the deviation in the parameter vector. If the measurement error covariance matrix is known, the parameter covariance matrix, $\mathbf{V}_\theta$, is directly obtainable from the linear representation of the model. Remembering that the measurement error covariance matrix is constant for each experiment, then parameter covariance matrix is formed by:

$$\mathbf{V}_\theta \approx \left(\sum_{i=1}^{n} \mathbf{W}_i^T \tilde{\mathbf{V}}^{-1} \mathbf{W}_i \right)^{-1} \qquad (4.32)$$

Since the data are distributed as $N(0, \tilde{\mathbf{V}})$, the parameters are also distributed normally, that is $(\theta - \theta^*) \sim N(0, \mathbf{V}_\theta)$. This implies that $\boldsymbol{\Delta}\theta^T \mathbf{V}_\theta^{-1} \boldsymbol{\Delta}\theta$ is distributed as a χ^2 random variable with p degrees of freedom. Therefore, the bound of the ellipsoidal confidence region can be determined by setting c to the upper bound of the χ^2 distribution with p degrees of freedom such that the fraction, γ, of the χ^2 distribution is enclosed.

Development of the linear confidence region from the nonlinear model included a quadratic approximation to the estimation objective function, and linearization of the model around the optimal parameters. It must be emphasized that the degree to which the linearized region reflects the true nonlinear confidence region is heavily dependent on the accuracy of these approximations. It is pointed out by Bates and Watts [7] that for many nonlinear problems the linearized confidence regions can be "woefully inadequate". In situations where an accurate representation of the confidence region is essential, Bates and Watts suggest analyzing the adequacy of the linear approximation using curvature measures of the model nonlinearity. If the nonlinearities are deemed significant, improved methods of confidence region generation are available as discussed by Bates and Watts [7] and Seber and Wild [94].

A geometric interpretation of the confidence region is that if the estimation objective function is steep around the optimum, then the norm of Hessian matrix is large, and small changes in the parameter vector lead to large changes in the objective function. In this case, the confidence region is small, and the parameter are considered to be well determined. A relatively flat objective function is the opposite situation, with large parameter changes having little effect on the objective function, and the resulting confidence region is large, indicating ill-determined parameters.

For this study, the 95% linearized confidence regions have been utilized merely as a guide concerning the level of parameter reliability. Therefore, it is not essential that the confidence region be exact, and the linear approximation is considered adequate.

The p-dimensional hyperellipsoid representing the parameter confidence region is difficult to report in its full form for more than 2 parameters. Therefore, to facilitate representation of the confidence information, the region has been reduced to confidence intervals on each of the parameters. The principal axes of the confidence ellipsoid are given by the eigenvectors of the parameter covariance matrix, $\mathbf{V}_\theta$, with the length of the axes proportional to the respective eigenvalues. The shortest and longest principal axes correspond to the best and worst determined combinations of the parameters. A conservative representation of the approximate confidence interval can be generated by projecting the bound of the confidence ellipsoid at the most ill-determined terminus for a given parameter onto the parameter coordinate axis. The confidence interval for the ith parameter is given by:

$$\Delta\theta_i = \max_j (\chi^2_{p,\gamma}\lambda_j)^{\frac{1}{2}} \, |\, \mathbf{v}_j \,| \cdot \mathbf{i} \tag{4.33}$$

where $\chi^2_{p,\gamma}$ represents a chi-square variable for p degrees of freedom and γ confidence, λ_j and $\mathbf{v}_j$ are the jth eigenvalue and eigenvector of the parameter covariance matrix, and $\mathbf{i}$ is a unit vector in the ith parameter direction. The resulting projection of the confidence region onto the parameter coordinate axis is easily visualized in two dimensions, and is illustrated in Figure 4.2. Confidence intervals reported for this work were computed using Equation 4.33.

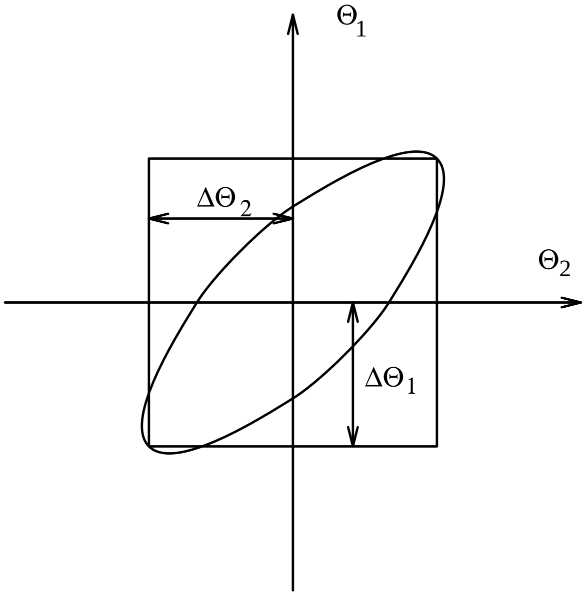

Figure 4.2: Projection of the ellipsoidal confidence region onto the parameter coordinates for presentation as confidence intervals.

4.2.2 Parameter Estimation Code: PAREST

The nonlinear nature of the parameter estimation problem requires a numerical solution to obtain the maximum likelihood estimates. There exist several types of numerical algorithms for the solution of nonlinear programming problems of the type shown in NLP2. This research has made use of the nonlinear programming package, NPSOL, developed by Gill et. al. [39]. This optimization package, coded in FORTRAN-77, utilizes a sequential quadratic programming (SQP) algorithm to repeatedly solve a quadratic approximation to the nonlinear objective function. NPSOL is able to handle constraints on the decision variables in the form of simple bounds and general linear and nonlinear constraints.

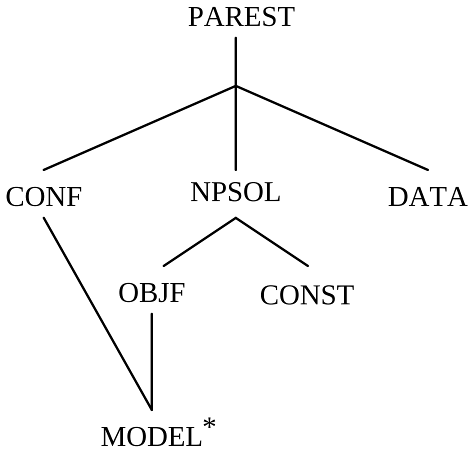

Figure 4.3: Calling hierarchy for the parameter estimation code PAREST. The symbol * indicates a problem-dependent subroutine that is replaced with the appropriate software depending on whether the segregated or comparison model is being identified.

Based on the optimization package NPSOL, the code PAREST was developed to solve the parameter estimation problem. A calling hierarchy for PAREST is shown in Figure 4.3. PAREST acts as a driver routine, controlling the activity of the various subroutines. The experimental data are read in using the DATA routine, and then control is switched to the optimization package, NPSOL. NPSOL utilizes the OBJF and CONST subroutines to evaluate the objective function, and the constraint equations, respectively. The optimization is carried out in a sequential manner, meaning that a model solution is required for each evaluation of the objective function. Therefore, the model solution subroutine MODEL is called from OBJF to provide the steady state, or dynamic model solution, based on the experimental operating conditions used to obtain the data.

Once NPSOL determines the optimal solution, the parameter estimates are used by the subroutine CONF to generate the confidence interval estimates. Generation of the confidence region requires output parameter sensitivities, therefore, CONF calls model to obtain dynamic sensitivity information through the canned routine DDASAC [17]. Upon conclusion of generation of the parameter vector covariance matrix, the information is written to an output file for further use.

Computational Considerations. Successful estimation of optimal parameter estimates depends on many computational issues. Based on experience for the estimation phase of this project, a key to convergence to the optimal parameter estimates using NPSOL is the accuracy of the objective function gradient. Although an analytical gradient for the maximum likelihood objective function is available, the nonlinear nature of the model forces the use of numerical integration techniques to obtain the predicted outputs and the parameter sensitivity coefficients. Because of this careful consideration must be given to the tolerance limits used during the integration of the model and sensitivity equations. Tolerances that are too loose can lead to convergence failure during optimization, due to inaccurate gradient information. Overly tight tolerances lead to unreasonably long computational times. Therefore, it is important that the tolerances a selected carefully, yielding an accurate gradient, and tolerable computational times.

A second concern is the issue of parameter constraints. Scientifically meaningful parameters are often constrained to lie in a particular region of the parameter space. For example, the maximum vegetative growth rate and Michaelis constant parameter used in this work are only meaningful if they are positive. When utilizing unconstrained optimization techniques to estimate physically constrained parameters, there is no guarantee that the optimal estimate will lie within the constraint region. Further, when using numerical solution techniques for solutions of the model, the ability of the solver routine to successfully generate a solution can be drastically affected by parameter guesses lying outside the physical meaningful parameter region. In extreme cases, certain parameter guesses can lead to computer overflow and model solution failure. For these reasons, it is usually necessary to take steps to ensure the optimization routine does not move out of the realistic parameter region.

In the segregated and comparison models, all of the parameters must be positive to be physically realistic. Estimation attempts using NPSOL without constraining the parameter guesses to be positive lead to failure of the integration package DDASAC, and the steady-state algebraic equations solver, HYBRD1. Since NPSOL handles constraints on the optimization decision variables, simple bounds were added to prevent negative estimates, and this alleviated most of the numerical solution failures. However, an additional problem arises in the Dawes and Thornley linear sporulation law:

$$\mu_s = \alpha_s - \beta_s \frac{\alpha_v s}{K_v + s} \tag{4.34}$$

Since the sporulation rate must be positive, the parameter constraint region for the sporulation initiation parameters cannot be handled using simple bounds, but rather, must account for the interdependence of the constraint on the combination of parameters. Fortunately, NPSOL has the capacity to handle nonlinear constraints, and therefore a constraint to ensure positive sporulation is included when using the linear sporulation law. The constraint is given by:

$$\alpha_s - \beta_s \alpha_v > 0 \tag{4.35}$$

Utilization of simple bounds and the nonlinear constraint from Equation 4.35 allowed for successful parameter estimation.

As an alternative to the introduction of explicit parameter constraints, Bates and Watts [7] suggest recasting the estimation problem in terms of transformed parameters. Using appropriate transformations, the new parameters can be mathematically constrained to avoid proscribed regions of the parameter space, thus allowing for utilization of unconstrained optimization algorithms.

4.3 Segregated Model Identification

After the primary model development stage is complete, it is necessary to obtain data to estimate adjustable model parameters, and evaluate the validity of the proposed model structure. Due to the dearth of suitable experimental data for the production of bacitracin from *B. licheniformis*, it was necessary to initiate an experimental phase of this project to identify and validate the proposed segregated model. In the follow discussion, a detailed examination of the experimental results and parameter estimation process is undertaken. Since it is often the case that modifications of the model are required once actual data have been obtained, included in this discussion is an examination of the evolution of the segregated model from its initially proposed form to its final form.

Like many fermentation applications, not all model states are readily measurable. The segregated model structures the biomass into three morphological phases, vegetative, sporangia, and spore, each having distinct physical characteristics. However, using available measurement techniques, it was not possible to measure the distribution of the biomass in the three phases. Further, the age-distribution characteristics of the sporangium population were also not measured. The only readily available technique to characterize the biomass is to utilize the heat resistant properties of the spores to distinguish between spore and nonspore biomass. In addition to the biomass measurements, the limiting substrate concentration was measured, as was the bacitracin concentration. The resulting outputs for the segregated model are given by:

$$y_{\mathrm{spo}} = X_e \tag{4.36}$$

$$y_{\mathrm{nspo}} = X_v + \int_0^{\tau_m} X_s \, d\tau \tag{4.37}$$

$$y_{\mathrm{anti}} = A \tag{4.38}$$

$$y_{\mathrm{sub}} = s_e \tag{4.39}$$

As the output equations show, the biomass outputs are the spore concentration and a combination of the vegetative and total sporangium cell concentrations.

In the model development, it is assumed that antibiotic production depends on the processes of growth and sporulation, but this dependence is one-way, with the antibiotic having no effect on the growth and differentiation processes. This suggests that the antibiotic concentration measurement is not required to estimate the growth and differentiation parameters. Based on the one-way coupling of the parameters, the estimation problem has been divided into two separate tasks. First, the growth and differentiation parameters are estimated using the biomass and substrate measurements. Once these parameters have been estimated, the antibiotic production parameters are estimated based on the dynamic antibiotic concentration measurements.

4.3.1 Spore Germination

One of the main differentiation pathways of the *Bacillus* is the production of a viable, actively growing vegetative cell from the once dormant spore. This process is the germination pathway, and an accurate description of the *Bacillus* life cycle must account for this renewal process. The germination model for the segregated approach is assumed to depend on limiting substrate through the Monod law:

$$\mu_g = \frac{\alpha_g s_e}{K_g + s_e} \tag{4.40}$$

with α_g representing the maximum sporulation rate, and K_g representing the effectiveness of the limiting substrate at stimulating germination. To evaluate the significance of spore germination kinetics, batch fermentations, seeded with pure spore inoculum, were carried out. During the fermentation, spore and substrate samples were taken at periodic time intervals. The goal of the experiment was to track the decrease in spore concentration that would be expected as the spores began to germinate. The resulting dynamic spore concentration data for the spore germination experiments B-Spo-1 and B-Spo-2 are listed in Appendix A. The change in spore concentration with time for spore fermentations B-Spo-1 and B-Spo-2 are shown in Figure 4.4. The spore concentration profiles indicate that a significant time delay exists for spore germination. After a period of 15 hours, there was little indication of germination, with a large portion of the original spore inoculum still existing as heat resistant spores. The germination time delay could be an artifact resulting from the spore purification process, which is detailed in Section 3.3.1, or it could result when spores are introduced to fresh medium. However, the presence of a germination time delay has been observed in at least one other *Bacillus* system. Marahiel et. al. [68], found that outgrowth in *B. brevis* spores occurs after an 8–10 hour delay.

In another study of germination kinetics, Dawes and Thornley [22] observed varying germination rates for *B. subtilis* spores suspended in steady-state culture filtrate, with spores in nonlytic cells germinating at a maximum rate of 0.092 (1/hr), and free spores at a maximum rate of 0.024 (1/hr). Al-

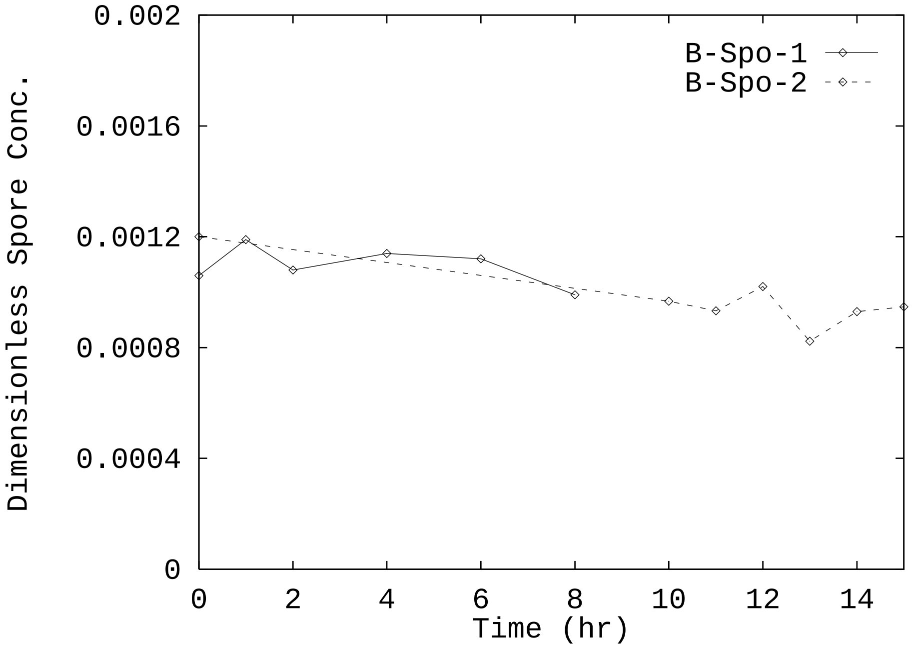

Figure 4.4: Spore concentration vs. time for batch spore germination fermentations B-Spo-1 and B-Spo-2.

though Dawes and Thornley did not observe a delay prior to germination, they comment that the relatively slow rate of germination suggests germination is insignificant during high dilution rate continuous experiments.

For this study, the combination of low spore concentration, germination delay, and low germination rate found by Dawes and Thornley, leads to the assumption that spore germination plays an insignificant role in normal fermentations, contributing little to the vegetative cell concentration once active vegetative growth begins. For this reason, the germination kinetic parameters have been set to reasonable values, based on the results of Dawes and Thornley, and considered fixed.

	High Aeration	Low Aeration
Stir Rate	400 rpm	150 rpm
Air Flow	$1.5\ \mathrm{v/(v \cdot min)}$	$0.5\ \mathrm{v/(v \cdot min)}$

Table 4.1: Air flow and stirring speed for high and low aeration conditions.

4.3.2 Growth and Sporulation Parameters

As an initial step toward identification of the segregated model parameters, batch fermentations have been utilized to track biomass development and antibiotic production. As mentioned previously, the propensity of the *B. licheniformis* system to produce measurable quantities of bacitracin was found to depend on the aeration conditions in the fermentor. For this reason, two different aeration conditions were utilized in fermentation experiments. The fermentor aeration level was adjusted using both air flowrate and impeller stirring speed. The two different operating conditions used in this study, termed high and low aeration, are show in Table 4.1. Under low aeration conditions, bacitracin was produced at measurable levels. However, at higher aeration conditions bacitracin production was completely repressed. Since dissolved oxygen was not measured, establishing a relationship between bacitracin production and dissolved oxygen concentration was not possible using these data. However, fermentations at the two different aeration conditions serve to compare the differences in growth characteristic between producing and non-producing fermentations.

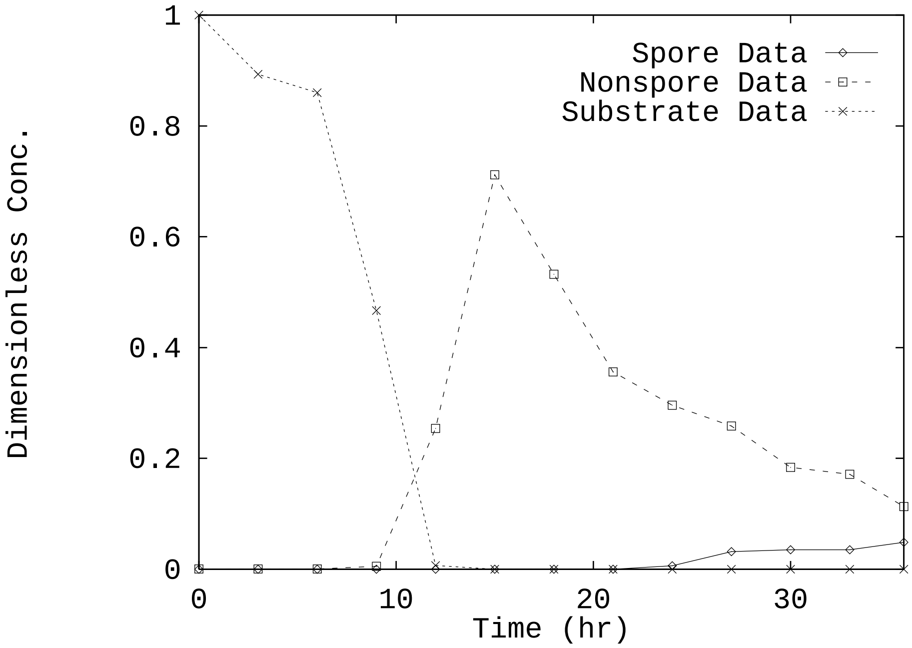

Figure 4.5: Batch growth and sporulation data from batch B-6-14.

High Aeration Fermentations. As an initial step toward estimation of the growth and sporulation parameters, biomass number concentration, and substrate concentration were tracked during batch fermentation under high aeration. The fermentor was charged with sterile minimal medium, and then inoculated with vegetative cells of *B. licheniformis.* Biomass counts and substrate concentration measurements from a typical batch fermentation, B-6-14, are shown in Figure 4.5. Dynamic batch fermentation data are listed in Appendix B.

The batch fermentation is typified by a slight delay between inoculation and rapid growth of vegetative cells. Concomitant to the growth phase, substrate is consumed, and becomes completely depleted at about 12 hours into the run. After substrate is depleted the nonspore biomass begins to fall. Also associated with substrate exhaustion, is the appearance of spores approximately 10 hours after the nonspore biomass peaks.

Unstructured Growth Parameter Estimates. In its initial form, the segregated model vegetative growth and sporulation model are based on the Dawes and Thornley continuous culture sporulation model [22]. The structure of the Dawes and Thornley model is discussed in detail in Section 2.2.6. Vegetative growth is modelled using an unstructured Monod growth law, and the rate of sporulation depends linearly upon growth rate:

$$\mu_v = \frac{\alpha_v s}{K_v + s} \tag{4.41}$$

$$\mu_s = \alpha_s - \beta_s \mu_v \tag{4.42}$$

The unknown model parameters needed to identify the segregated model are summarized in Table 4.2. They include the Monod parameters for vegetative growth, the sporulation parameters, the substrate yield parameter, y_v, and the spore maturation time, τ_m. It was assumed that the processes of germination, sporulation, and antibiotic production consumed negligible quantities of substrate, and therefore, the yield coefficients for these processesd were set to infinity. The model fit to the batch data B-6-14, using the optimal parameter estimates, is shown in Figure 4.6.

In its initially proposed form, it is obvious from Figure 4.6 that the segregated model does not explain the transient batch growth data. Bard [6] notes that the presence of large residuals that cannot be explained by measurement noise indicates some type of structural deficiency in the model.

The reason for the model's poor performance can be attributed to the fact

Parameter	Description
α_v	Maximum rate of growth (1/hr)
K_v	Michaelis constant - vegetative growth (g/l)
y_v	Vegetative yield coefficient (1/g)
α_s	Maximum rate of sporulation (1/hr)
β_s	Sporulation attenuation parameter
τ_m	Sporulation maturation time (hr)

Table 4.2: Adjustable Parameters of the structured vegetative growth and differentiation model.

that the initial model formulation does not account for several growth characteristics that are significant during batch growth. During the first 10 hours of the fermentation there is little increase in the number of colony forming units of the bacteria, even though there is substantial consumption of substrate. Following this lag period, there is a stage of rapid growth, accompanied by continued consumption of the limiting substrate. An important transient growth characteristic becomes clear during the rapid growth phase, which begins approximately 12 hours after inoculation. As Figure 4.5 illustrates, the rapid growth period begins when the substrate concentration approaches exhaustion. Soon after the onset of exponential growth, the substrate is completely consumed, however, the number of nonspore colony forming units continues to increase, peaking approximately 3 hours after substrate depletion.

The initial growth lag period, and the ability of the bacteria to continue reproducing after substrate has been exhausted are not accounted for by the un-

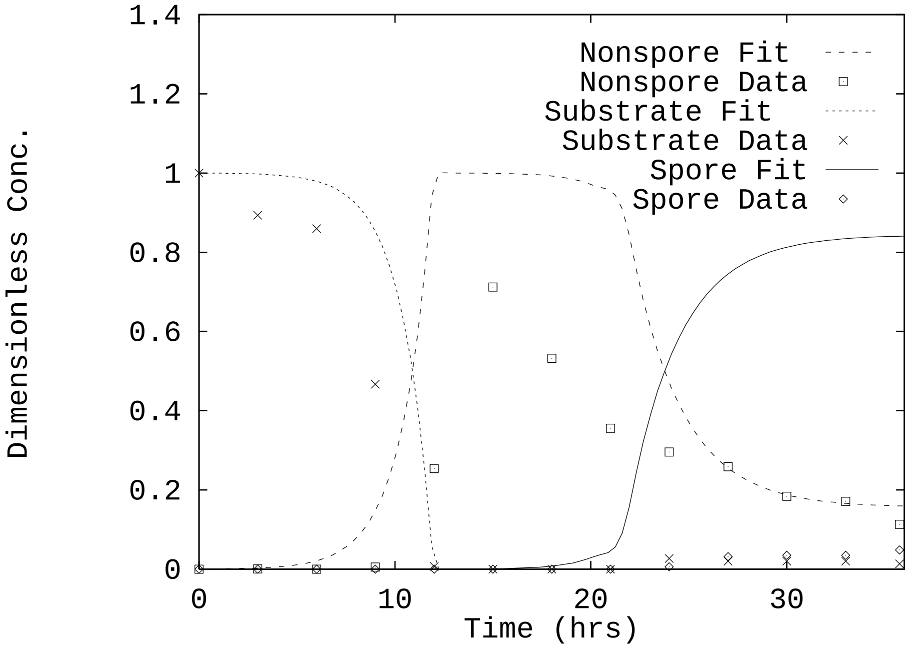

Figure 4.6: Fit of the initially proposed segregated model to batch fermentation B-6-14 using an unstructured vegetative growth law.

structured Monod growth model. The Monod model, shown in Equation 4.41, assumes that vegetative growth responds instantly to the local substrate concentration, remaining in a state of exponential balanced growth, until the limiting substrate is consumed. Obviously, this is not the case in reality, and the data show a substantial lag before the cells respond to the new environment, and they also exhibit continued growth after substrate is exhausted.

In addition to the unexplained growth phenomenon, another obvious shortcoming of the initially proposed segregated model is its inability to describe the rapid decline in nonspore biomass without an associated rise in spore count. The reason the model is unable to explain this observation is because the unstructured growth model assumes sporulation is an effective mechanism to prevent cell death, and therefore cell death is not taken into account. The data make it clear that cell death is a significant factor during batch growth on minimal medium.

The inadequacies of the initial segregated model formulation lead to poor comparisons between the model predications and the observed data, as shown in Figure 4.6. Because the vegetative growth model was unstructured, the predicted nonspore biomass concentration leads the data by about 2 hours. To compensate for the post-nutrient exhaustion growth, the model forces the predicted substrate concentration out in time, suggesting that substrate could not have been exhausted until nonspore biomass levels had peaked. Finally, since cell death is assumed by the model to be negligible, the model substantially overpredicts the rate of spore production to compensate for the decline in nonspore biomass.

Structured Growth Parameter Estimation. The poor performance of the segregated model necessitates modifications in the model structure to address the shortcomings discussed above. A detailed development of the model modification is provided in Chapter 2. The basic change is the reformulation of the vegetative growth law to a structured two-compartment conceptualization of growth with separate processes of substrate internalization and subsequent utilization for growth. With the two-compartment model a new model state, s_i, is formed, reflecting the concentration of internalized substrate. The concept of the internal substrate is not based on a specific chemical species that exists inside of the bacterial cell. Rather it is a conceptualized model state that is meant to reflect the internal biosynthetic capacity of the cells. Therefore, the internal substrate is considered to be an unmeasured state, and since

Parameter	Description
α_i	Maximum rate of substrate internalization (1/hr)
K_i	Michaelis constant - substrate internalization (g/l)
s_{i0}	Initial internal substrate concentration (g/l)
m_v	Maximum rate of cell death (1/hr)

Table 4.3: Additional adjustable parameters introduced by modification of the vegetative growth law to include an internal substrate state.

an initial condition is required for the dynamic model, the initial internal substrate concentration, s_{i0}, is treated as an additional adjustable parameter. In addition to the structured vegetative growth model, a death rate term has been added to the growth law to recognize death of vegetative cells when substrate falls below a critical level. The specific rate of substrate internalization, μ_i, and the modified vegetative growth relationship are given by:

$$\mu_i = \frac{\alpha_i s_e}{K_i + s_e} \tag{4.43}$$

$$\mu_v = \frac{\alpha_v s_i}{K_v + s_i} - m_v \tag{4.44}$$

With the reformulated model, the set of adjustable growth and differentiation parameters has expanded, now including the substrate internalization parameters, and a cell death parameter. The new parameters are summarized in Table 4.3.

To test the effectiveness of the reformulated model in describing the batch data, PAREST was used to get the maximum likelihood estimates of the parameters using the data from batch fermentation B-6-14. The corresponding

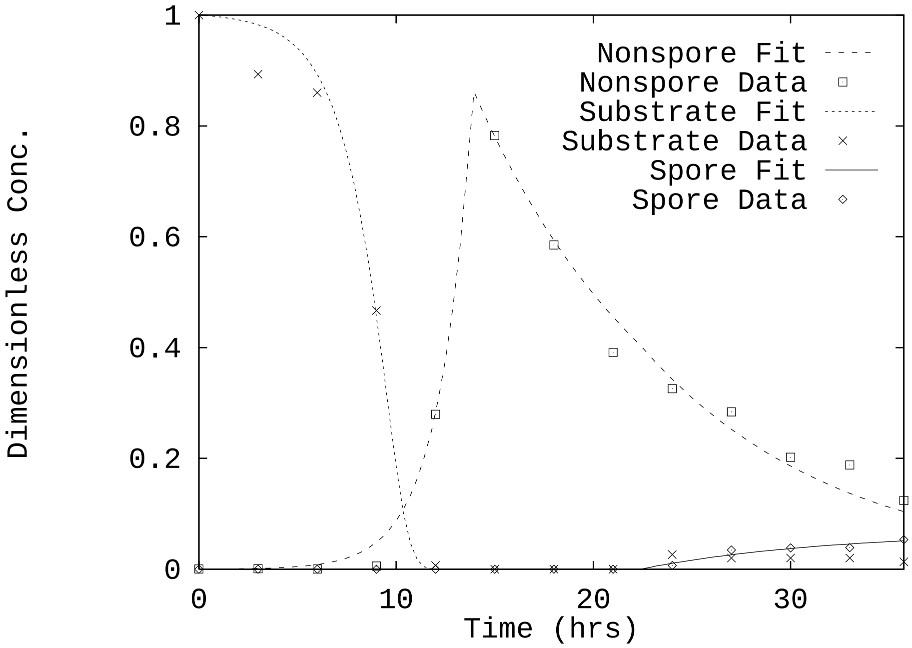

Figure 4.7: Reformulated segregated model fit to batch data B-6-14. Parameter estimates are given in Table 4.4.

fit of the model to the data are shown in Figure 4.7. The addition of structured growth and cell death expressions to the segregated model allow for significant improvement in the fit to the batch data, as shown in Figure 4.7. The model successfully predicts a lag period, and also allows for the peak nonspore biomass levels to be reached after external substrate is exhausted. The structured vegetative growth model allows for an accurate description of the nonspore biomass, while also successfully tracking the rapid decline in the external substrate. In addition, by providing a mechanism to account for cell death, the model tracks the rapid decline in nonspore biomass, without a large rise in spore biomass. The model is able to account for the delayed spore appearance by explicitly accounting for the delay between sporulation initiation, and production of a mature spore.

The adaptations incorporated into the segregated model give it enough flexibility to adequately describe the batch data. However, since the ultimate goal is to identify the model such that it accurately describes the fermentation system in as large an operating region as possible, one cannot be satisfied by a model fit to a single batch experiment. The repeatability of the system for a given experiment must be accessed, along with the ability of the model to simultaneously describe data from different regions of the operating space.

Prior to testing the model with more data, it is prudent to evaluate the sensitivity of the model to the parameters. Sensitivity analysis indicates which parameters have a significant effect on the model solution. This information can be used to reduce the size of the parameter estimation problem, by including only the sensitive parameters in the set of estimated adjustable parameters. Insensitive parameters are set to reasonable values, and then considered fixed, since relatively large changes in these parameters have little effect on the model solution. However, in using sensitivity analysis to eliminate parameters from the adjustable set, it must be kept in mind that the relative sensitivity of the model with respect to a parameter can be a function of the operating conditions. Therefore, as experimental conditions vary, parameters that had little effect on the model for prior experiments can become significant in the new region of the operating space. Therefore, the assumption of insensitivity for the non-adjustable parameters must be reevaluated as operating conditions change.

For the batch experiment, the significant parameters have been determined by perturbing the nominal parameter set and evaluating the change in the solution based on the perturbation. If a parameter perturbation causes a significant change in the model solution it is consider a significant parameter, and it is kept in the set of adjustable parameters. Those parameters that result in an insignificant change when perturbed are considered insensitive, and are removed from the adjustable set.

The sensitivity of the segregated model to the nominal parameters has been determined by perturbing each parameter by ±10%. The perturbation analysis shows that the segregated model is insensitive to several parameters during batch operation. The insensitive parameters include, α_i, K_i, K_v, and β_s. The insensitivity of the batch model to these parameters is typified by the insignificant change in the model solution in response to perturbations in the maximum rate of substrate uptake, α_i, shown in Figure 4.8. In contrast, the batch model solution exhibits sensitivity to the remaining growth and differentiation parameters, α_v, m_v, α_s, and τ_m. The effect of a perturbation in a sensitive parameter is typified by the change in the batch model solution for changes in α_v, shown in Figure 4.9.

Based on the sensitivity analysis the model parameters are divided into two groups: adjustable and fixed. Included in the adjustable parameter group are those parameters that have a significant impact on the model solution. The fixed parameters are those to which the model is insensitive. To ease the parameter estimation task, the insensitive parameters are considered fixed at their nominal values, and further estimation runs allow adjustment of the adjustable parameters only.

Based on batch fermentation B-6-14, the maximum likelihood estimates of the fixed and adjustable parameters, and the measurement error variances are given in Table 4.4. The batch experiment provides reasonable sensitiv-

Fixed Parameters		
Vegetative growth Michaelis constant	K_v	0.019 (g/l)
Maximum substrate internalization	α_i	10.27(1/hr)
Internalization Michaelis constant	K_i	1.01(g/l)
Sporulation inhibition coefficient	β_s	0.006
Maximum rate of germination	α_g	0.05(1/hr)
Germination Michaelis constant	K_g	0.10(g/l)

Adjustable Parameters		
Maximum vegetative growth	α_v	0.695 ± 0.054 (1/hr)
Maximum cell death	m_v	0.092 ± 0.012 (1/hr)
Vegetative yield coefficient	$y_v \times 10^{-12}$	0.900 ± 0.550 (1/g)
Maximum sporulation	α_s	0.007 ± 0.002 (1/hr)
Spore maturation time	τ_m	9.44 ± 2.05 (hr)
Initial Substrate Conc.	s_{i0}	0.17 (g/l)

Measurement Error Variances †		
Spore biomass	ν_{spo}	4.11×10^{-5}
Nonspore biomass	ν_{nspo}	9.34×10^{-4}
Substrate	ν_{sub}	8.88×10^{-4}

Table 4.4: Maximum likelihood growth and differentiation parameter estimates, and measurement error variance estimates based on batch fermentation B-6-14. † Error variances are in dimensionless form.

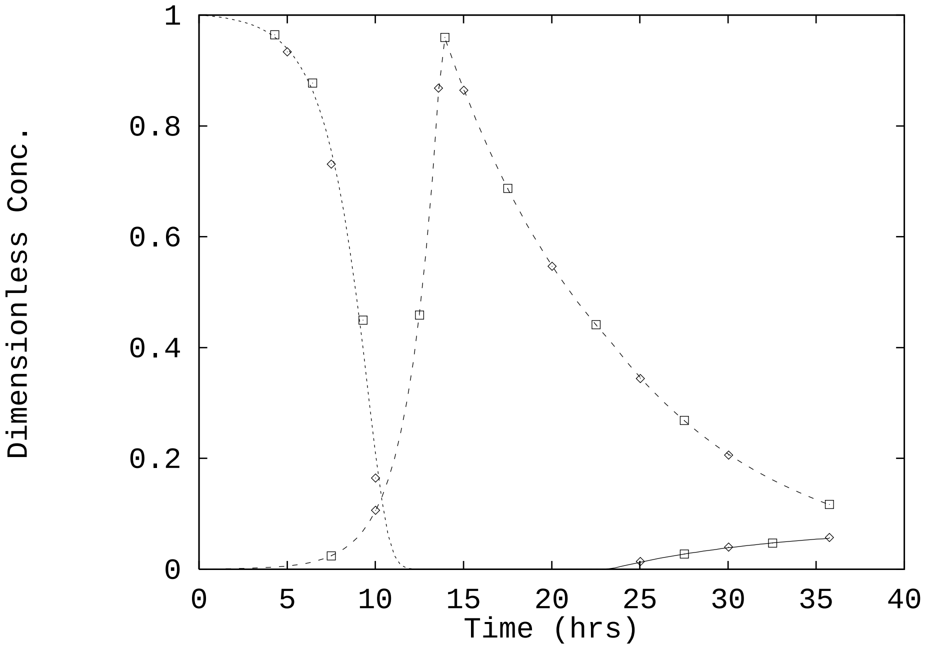

Figure 4.8: Insensitivity of the segregated model to 10% perturbations in the maximum rate of substrate internalization, α_i. The nominal spore, nonspore, and substrate profiles are given by the solid, dashed, and dotted lines, respectively. The symbol $\triangle$ represents solution with 10% increase in α_i, and $\square$ is the model solution with a 10% decrease in α_i.

ity to the maximum rate of vegetative growth, α_v, yielding an estimate with confidence intervals of less than 10% of the parameter magnitude. The estimated maximum growth rate of 0.695 (1/hr) corresponds to a doubling time of 60 minutes, which matches well with previously reported doubling times ranging from 50–90 minutes for *B. licheniformis* grown aerobically in glucose medium [25, 59].

A comparison of the estimated maximum vegetative growth rate to the maximum rate of substrate internalization indicates that once sufficient biosyn-

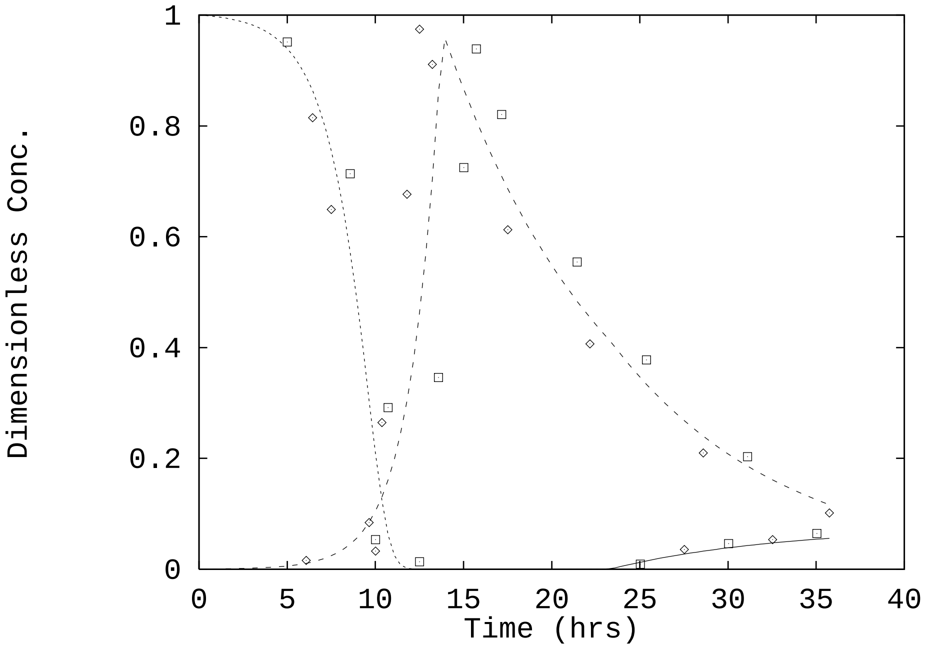

Figure 4.9: Response of the batch model to 10% perturbations in the maximum rate of vegetative growth, α_v. The nominal spore, nonspore, and substrate profiles are given by the solid, dashed, and dotted lines, respectively. The symbol $\diamond$ represents the model solution with 10% increase in α_i, and $\square$ is the model solution with a 10% decrease in α_i.

thetic capacity is built up, the vegetative growth capacity is limiting compared to the rate of substrate internalization. Because of the addition of the internal substrate state, the model is able to describe the growth lag, and post-external nutrient exhaustion growth. However, since this structured growth formulation is empirical, phenomenological conclusions concerning the relative rates of bacterial metabolic processes are not justified.

Similar to vegetative growth, the batch experiment provides sensitivity to the cell death rate parameter, m_v. Based on the modified Monod growth law, shown in Equation 4.44, the critical internal substrate concentration needed to prevent cell death can be derived:

$$s_{i_{crit}} = \frac{m_v K_v}{\alpha_v - m_v} \tag{4.45}$$

For a death rate of 0.092 (1/hr), the critical internal substrate concentration is 0.003 (g/l). Therefore, according to the parameters obtained through the batch experiment, the vegetative biomass is able to maintain viability down to low concentrations of the limiting substrate, indicating the effectiveness of glucose as a carbon and energy source.

The relative 95% confidence intervals for vegetative yield, maximum rate of sporulation, and spore maturation time are not as tight as the growth and death intervals, ranging from approximately 20% of the parameter magnitude for the maximum rate of sporulation, α_s, to 60% for the vegetative yield coefficient, y_v. This indicates that the batch fermentation provides less sensitivity for the estimation of these parameters, and this is reflected in the larger confidence intervals.

To gauge whether the sporulation parameters estimated using batch fermentation B-6-14 are reasonable, it is useful to compare these estimates to previously reported parameters. Based on steady-state *B. subtilis* experiments, Dawes and Thornley [22] report a maximum sporulation rate of $\alpha_s =$ 0.091 (1/hr), sporulation attenuation of $\beta_s = 0.143$, and spore maturation time of 4.0 hours. The Dawes and Thornley values for the sporulation initiation parameters are an order of magnitude higher than those found from the *B. licheniformis* batch data. It is not clear if this discrepancy results from differences between the species studied, differing operating conditions, or if sporulation kinetics differ significantly between batch and steady-state operation. A further discrepancy between the batch results and previously reported data, is the estimate of the spore maturation time, with the maturation time of 9.44 hours found from the batch data being more than double the value of 4.0 hours reported by Dawes and Thornley. A potential explanation of the differences between the two estimated maturation times is that Dawes and Thornley used cell refractility as an indication of maturation compared to heat resistance as the maturation marker in this study. Other possible explanations could be related to differences in species and cultural conditions.

It is important to access the repeatability of experimental data, and to evaluate the effects of replicate data on the estimated parameters. Therefore, data from a replicate high-aeration batch experiment, B-6-19 have been utilized to reestimate the adjustable batch parameters based on the replicated experimental data alone, and in combination with the batch fermentation B-6-14. The resulting maximum likelihood parameter estimates, with 2σ confidence intervals, are shown in Table 4.5. For convenience, the original parameter estimates from batch B-6-14 are also listed to provide a means of comparison of the variability of the parameters between replicates. Estimates for the adjustable parameters are reasonably close between runs. Also, the confidence intervals reflect the overlap between replicate runs, indicating a reasonable degree of repeatability.

Although the replicated batch data show a degree of variability between runs, the model does an adequate job of describing the data. Estimation of the parameters that are sensitive to the batch experiment leads to reasonable confidence limits for the current set of adjustable parameters. However, it is important to realize that repeatability for given operating conditions does not guarantee the model can represent the system for a wide region of the operating space. It must also be pointed out that the model parameters that have been considered "fixed" merely reflect the fact that the batch fermentations

Batch Run	Growth Parameter Estimates		
	α_v	m_v	y_v
B-6-14	0.695 ± 0.054	0.092 ± 0.012	0.900 ± 0.550
B-6-19	$0.772 \pm .114$	0.119 ± 0.034	0.918 ± 0.755
Combined	0.7250 ± 0.023	0.114 ± 0.019	0.933 ± 0.163

Batch Run	Sporulation Parameter Estimates	
	α_s	τ_m
B-6-14	0.007 ± 0.002	9.44 ± 2.05
B-6-19	0.014 ± 0.006	9.53 ± 0.50
Combined	0.012 ± 0.002	9.22 ± 0.49

Batch Run	Measurement Error Variances †		
	ν_{spo}	ν_{nspo}	ν_{sub}
B-6-14	4.11×10^{-5}	9.34×10^{-4}	8.88×10^{-4}
B-6-19	3.55×10^{-4}	4.63×10^{-3}	1.29×10^{-3}
Combined	1.82×10^{-4}	5.89×110^{-3}	9.42×10^{-4}

Table 4.5: Maximum likelihood parameter estimates and measurement error variance estimates based on individual replicate batch experiments: B-6-14, and B-6-19 and based on combined results. † Variances are reported in dimensionless form.

are not sensitive to those parameters. This does not mean that there do not exist operating conditions through which the previously insensitive parameters become significant. Of particular concern is the limited confidence the batch experiments provide about the dependence of sporulation initiation on substrate concentration. Estimation of the sporulation parameters based on the batch data provides adequate confidence in the maximum sporulation rate, α_s, however, there is little information concerning attenuation of the sporulation rate as growth rate increases. For the linear sporulation model, given in Equation 4.34, the effect of growth rate on sporulation is measured through the sporulation attenuation coefficient, β_s. Since the batch experiments were insensitive to this parameter, it was fixed at its nominal value. Since sporulation phenomenon are considered significant with respect to antibiotic production, it is important that the model's ability to explain sporulation phenomenon is tested.

In an effort to better explore the sporulation kinetics exhibited by *B. licheniformis*, experimental data that are more sensitive to the rate of sporulation at non-zero substrate concentration are needed. In an attempt to characterize sporulation, Dawes and Thornley [22] used continuous feed step-test experiments to evaluate the spore maturation time for *B. subtilis.* In a similar fashion, step-test experiments have been carried out in this study in an effort to gain information concerning the sporulation dynamics of *B. licheniformis.*

The step-test experimental data were obtained by running the fermentor as a chemostat, with continuous feed of sterile nutrient medium, accompanied by continuous removal of fermentation broth. After achieving steady-state at a high feed flowrate and high aeration, a step-down in the dilution rate was made at time zero, and then the response of the spore concentration to the step-down in dilution rate was monitored by periodic sampling of the

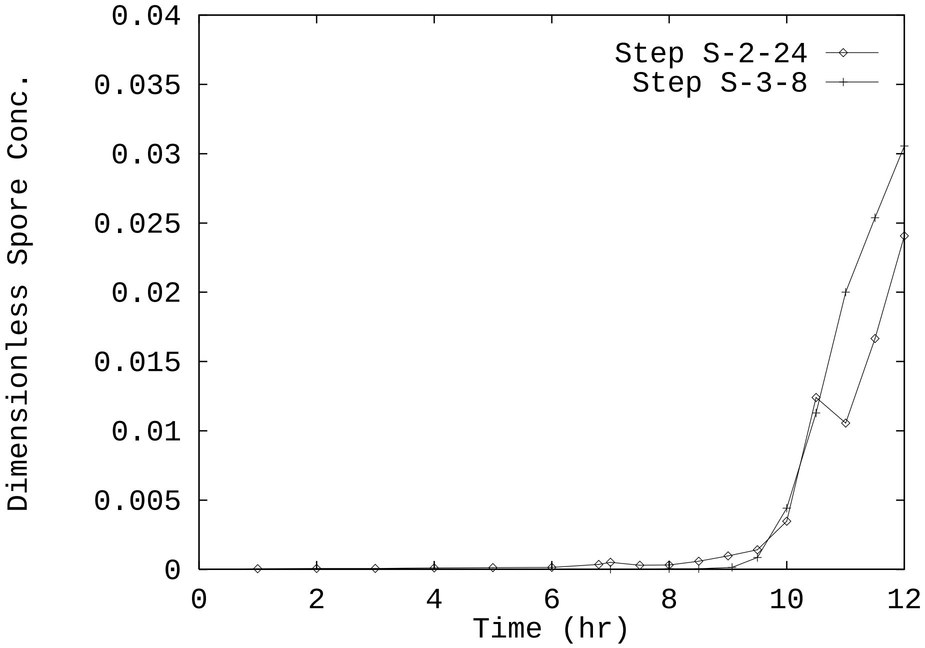

Figure 4.10: Dimensionless spore concentration profiles in response to a step down in dilution rate from steady state at $D = 0.5$ (1/hr) to $D = 0.1$ (1/hr).

continuous fermentor. The resulting dynamic spore concentration profiles for replicate step experiments at high aeration are shown in Figure 4.10. The data are listed in Appendix C. For these experiments steady-state was achieved for $D = 0.5$ (1/hr) and at time zero, the flowrate was stepped down to $D = 0.1$ (1/hr).

Prior to making the step down in dilution rate, the fermentor has achieved a non-trivial steady state. Assuming that germination is negligible, steady state is achieved when the apparent vegetative growth rate is equal to the dilution rate:

$$\mu_{\text{app}} = \mu_v - \mu_s = D \tag{4.46}$$

For non-inhibitory substrates, as the dilution rate increases, the steady-state substrate concentration increases, allowing for an increase in the apparent growth rate to match the dilution rate. Activation of the sporulation pathway becomes more likely as substrate limitations slow growth. Using this logic, the higher the dilution rate, the higher the substrate concentration, and therefore, the lower the rate of sporulation initiation. This analysis implies the steady-state spore concentration is low at high dilution rates, and would be expected to rise as dilution rate is lowered. The dynamic spore profiles, shown in Figure 4.10, exhibit the expected behavior. At time zero, the system is at steady state, and due to the high dilution rate, the spore concentration is very low. The system responds to the step down in dilution rate with a gradually increasing spore concentration, until approximately 9 hours, when a sudden increase in the spore count occurs. The delay prior to the appearance of increased spore counts can be attributed to two effects. Immediately after the step change, a period of time passes where the major system dynamics are the adjustment of the substrate concentration to the reduced feed rate. After substrate concentration falls, the biomass responds with a reduced growth rate, and a significant increase in the rate of sporulation. At that point, the delay of the spore appearance is the maturation lag, τ_m, resulting from the time required for a vegetative cell to differentiate into a spore.

Compared to the batch experiments, the operating conditions used for the step-test experiment create a situation in which the substrate dependence of the sporulation initiation dynamics are more apparent, as is the maturation time. To take advantage of the additional experimental information yielded from the dilution-step experiment, the data from step-test S-2-24 were added to the parameter estimation routine, and the growth and sporulation parameters were reestimated using both the batch and step-test data. Since the

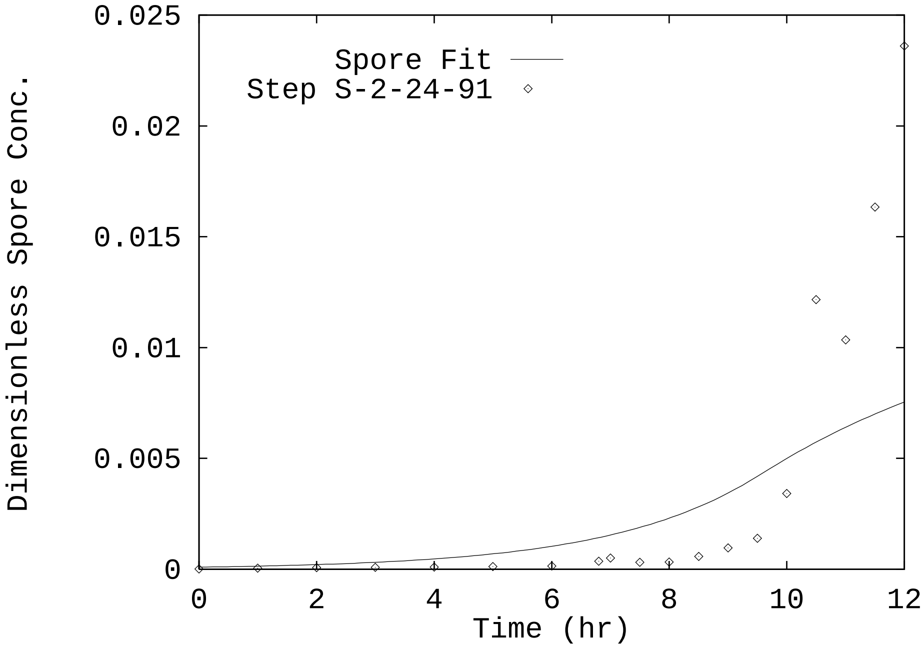

Figure 4.11: Optimal model fit to the dilution rate step test using a linear relationship between sporulation rate and growth.

primary reason for the additional experiment was to examine sporulation dynamics, the sporulation attenuation coefficient, β_s was considered to be part of the adjustable parameter group, and was estimated along with other adjustable parameters shown in Table 4.4. The model, using the optimal parameters estimates for both the batch and step-test data, are able to effectively fit the batch data, however, as Figure 4.11 shows, the model does a poor job of describing the system response to the step down in dilution rate. The batch data, in combination with the step-test experiment, make it clear that the linear relationship between sporulation rate and growth rate is not able to effectively describe both situations. The Dawes and Thornley model was intended to describe steady-state growth and sporulation, and it appears that the extension of the linear model to dynamic phenomenon is not effective for a wide range of operating conditions in the *B. licheniformis* system.

The Dawes and Thornley sporulation model is based on an observed linear relationship between growth and sporulation rates. Currently, there is no obvious theoretical basis for a linear connection between sporulation and growth. Since the batch and step test data indicate the linear sporulation law is inadequate for describing both the batch and step data, a more flexible empirical approach to describe the connection between sporulation and substrate concentration has been utilized in the segregated model. As detailed in Section 2.2.8, a linear combination of polynomial basis functions, with estimated coefficients, has been utilized to represent the substrate dependent sporulation rate:

$$\mu_s \approx \sum_{j=1}^{r} \gamma_j \phi_j(s_i) \tag{4.47}$$

For convenience, the basis function polynomials are chosen to be the Lagrange interpolating polynomials. These basis functions are constructed based on a set of interpolation points, such that the jth basis function has the value 1.0 at the jth interpolation point, and all other basis functions are zero at that point. This can be achieved using the following formula:

$$\phi_j = \prod_{k=1}^{r} \frac{s_i - s_{i_k}}{s_{i_j} - s_{i_k}},\ k \neq j \tag{4.48}$$

Using this methodology, the basis function coefficients become the sporulation initiation rate at the interpolation points.

$$\mu_s(s_i) \approx \sum_{j=1}^{r} \mu_{s_{i_j}} \bar{\phi}_j(s_i) \tag{4.49}$$

This is a more convenient formulation because it allows the actual sporulation rate at the interpolation points to be treated as the adjustable parameters, rather than basis function coefficients, whose physical meaning is less clear [8].

In the first attempts at developing a basis function approximation to μ_s, global polynomial basis functions were utilized. This leads to computational difficulties during parameter estimation because the estimation routine generated basis function coefficients leading to negative sporulation rates between interpolation points. To overcome this problem, the basis functions, ϕ_j, were chosen to be piecewise linear over subregions of the substrate concentration domain [8]. By using linear elemental basis functions, the problem of negative sporulation rate could be avoided by placing a lower bound of zero on the sporulation initiation rate at the interpolation points. Since the basis functions were linear, it was not possible to generate negative sporulation rates between interpolation points, and the computational problems associated with negative rates was avoided.

The ability of the linear-elemental sporulation function to effectively predict the batch and step-test data simultaneously is dependent on the number and placement of the interpolation points, because with each interpolation points comes an adjustable parameter adding more flexibility to the shape of the initiation function. Due to the lack of information concerning the number and placement of the interpolation points needed to describe the data, many grid designs were tested in the parameter estimation routine. The upper limit of the grid was chosen to be 1.0 (g/l) of internal substrate, thus assuring that the rate of sporulation was effectively zero, at the upper grid limit. Initial grid designs were based on even placement of interpolation points between the upper and lower grid points. For a 5 point grid, the resulting estimated sporulation function compared to the Dawes and Thornley linear growth sporulation function is shown in Figure 4.12. The optimal model fit for the 5 element sporulation function compared to the step-test data is shown in Figure 4.13. It

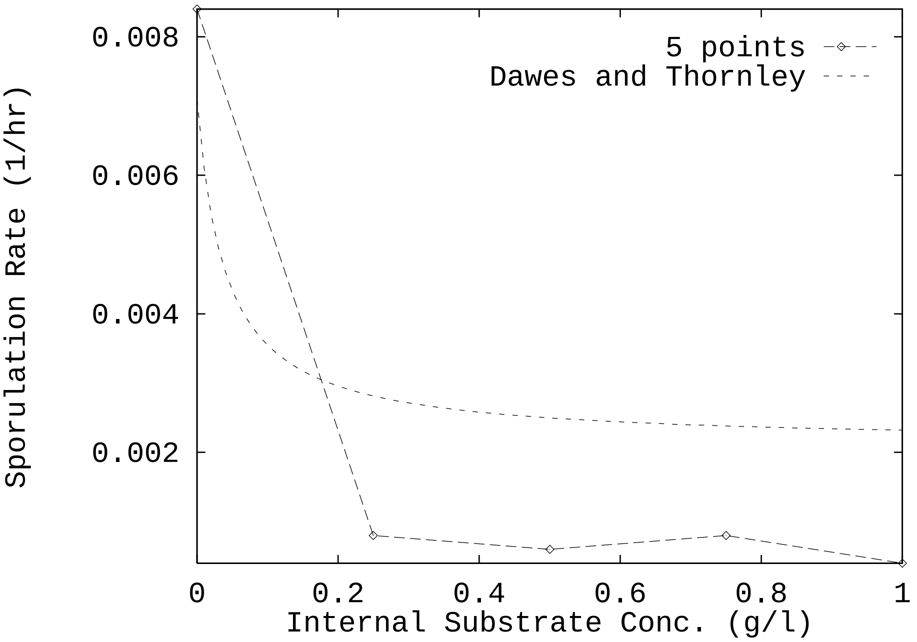

Figure 4.12: Comparison of the sporulation initiation function estimated using 5 linear elements compared to the Dawes and Thornley sporulation function.

is obvious that the evenly spaced grid does a poor job of correcting the sporulation model, with little improvement over the Dawes and Thornley sporulation model. The poor model fit resulting from evenly space sporulation interpolation points over a wide range of substrate concentrations is due to the fact that the bacteria have a very high affinity for glucose. The Michaelis constant, K_v, represents the internal substrate concentration required to support half the maximum growth rate. In this study, the Michaelis constant for *B. licheniformis* growing on glucose has been estimated to be approximately 0.02 (g/l). This means the growth rate saturates at low substrate concentration, and at steady-state, small changes in the substrate concentration result in relatively

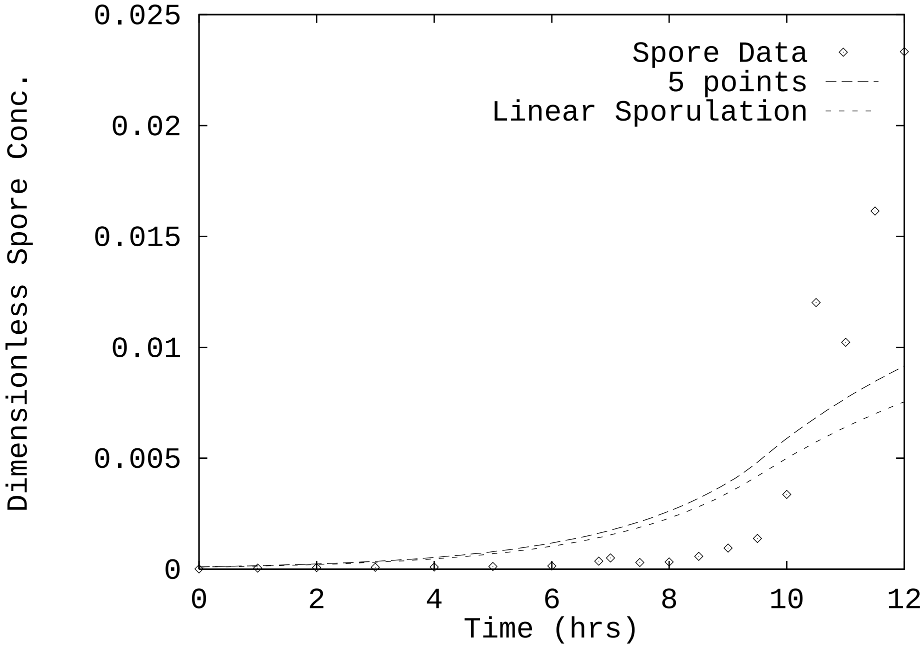

Figure 4.13: Fit of the 5 evenly-spaced, linear-element initiation function to the step-test spore data.

large changes in the growth rate. Since a large change in the sporulation rate occurs for the step-test experiment, but the change in the substrate concentration is relatively small, this indicates the sporulation initiation rate is very sensitive to changes in the substrate for a small range of concentrations near substrate exhaustion. Therefore, to allow for a better fit of the model to the step-test data, it is necessary to provide a concentration of interpolation points at low substrate concentrations, thus allowing for a more accurate description of the sporulation kinetics in the substrate range where sporulation initiation is sensitive to substrate changes.

Redistribution of the interpolation points toward $s_i = 0$ allows for a sig-

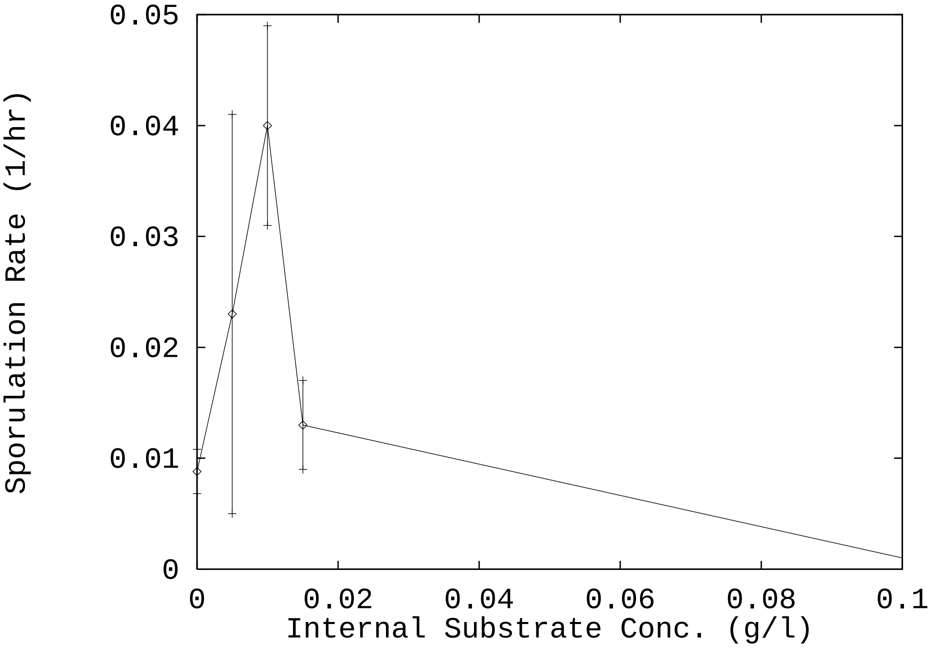

Figure 4.14: Estimated sporulation initiation function for 5 interpolation points concentrated near $s_i = 0$.

nificant improvement in the ability of the model to match the combined step and batch data. For 5 interpolation points, the optimal sporulation initiation function, with the 2σ error bars at the interpolation points, is shown in Figure 4.14. The step-test model fit to the data is shown in Figure 4.15. The confidence limits on the sporulation rate parameters reflect the sensitivity of the batch and step-test fermentations to particular ranges of substrate concentrations. In the batch experiment, substrate is quickly exhausted, and therefore, the data are most sensitive to the rate of sporulation commitment at $s_i = 0$. For this reason, the estimator is relatively confident in the parameter estimate for μ_s at $s_i = 0$. However, the step-test data, using continuous

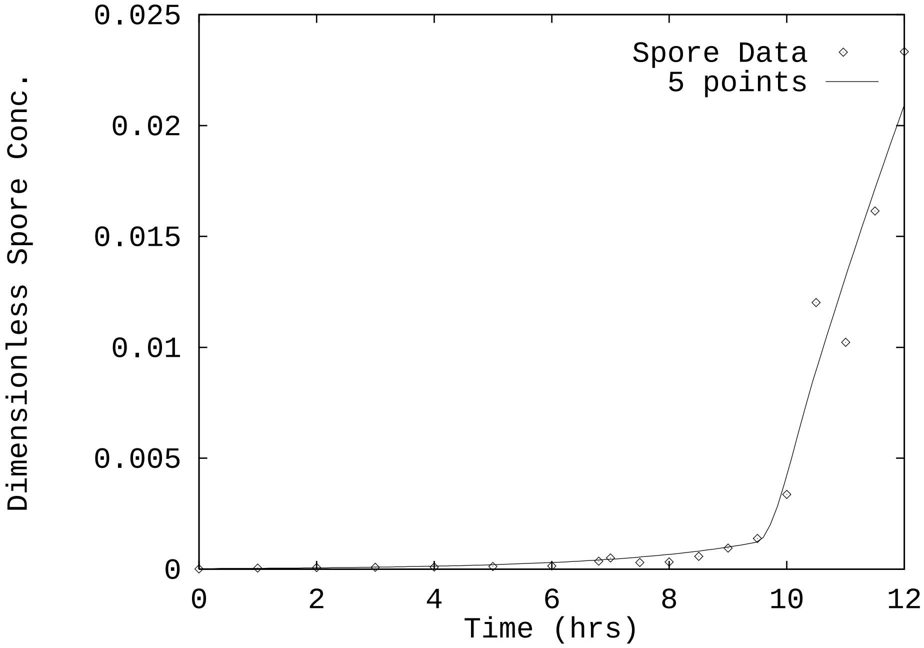

Figure 4.15: Model fit of the 5 point sporulation initiation function to step test S-2-24.

substrate feed, creates an experiment that is sensitive to a narrow range of substrate concentrations around $s_i = 0.01$ (g/l). Therefore, these experiments provide better data for estimating the shape of the sporulation function, in the substrate region around $s_i = 0.01$ (g/l). Both the batch and step-test fermentations are insensitive to substrate concentrations just above exhaustion, and therefore, this region has larger confidence limits.

Based on the fit to the step-test data, and the relatively tight confidence intervals around the sporulation initiation function, it is assumed the piecewise linear approximation is adequate to represent the rate of sporulation.

High-Aeration Steady-State Experiments. A full evaluation of a model's ability to describe system behavior should include an examination of steady-state phenomenon. Running the fermentor under continuous feed conditions allows for confirmation of the existence of stable steady states, and provides an additional check on the ability of the segregated model to predict system behavior under a wide range of operating conditions.

To collect steady-state growth and differentiation data, the fermentor was inoculated in batch mode, and after approximately 12 hours a continuous metered stream of sterile medium was fed to the fermentation vessel. Periodically, samples of fermentation broth were removed from the vessel and biomass and substrate assays were conducted to determine spore, nonspore, and substrate concentration levels. The system was considered at steady state when the biomass and substrate concentration measurements remained constant for a period of approximately 12 hours. For a typical run, steady state was achieved approximately 24 hours after continuous feeding began. After taking several samples for a given steady state, the feed flowrate was adjusted to a new flowrate, and the fermentor was allowed to adjust to a new steady state. Since the kinetics of spore formation are subject to a substantial time delay, the spore concentration consistently lagged the other states in achieving steady state. Steady-state biomass data are provided in Appendix D. Steady-state substrate was not measured due to the fact that the substrate concentration was below measurable values for the glucose assay used in this study.

Accurate predictions of the steady-state biomass data were obtained with only minor adjustments to the model parameters. In particular, slight adjustments of the empirical sporulation initiation function provided good agreement between the predicted and experimental steady-state spore concentrations. The model fit to the steady-state spore concentration for dilution rates

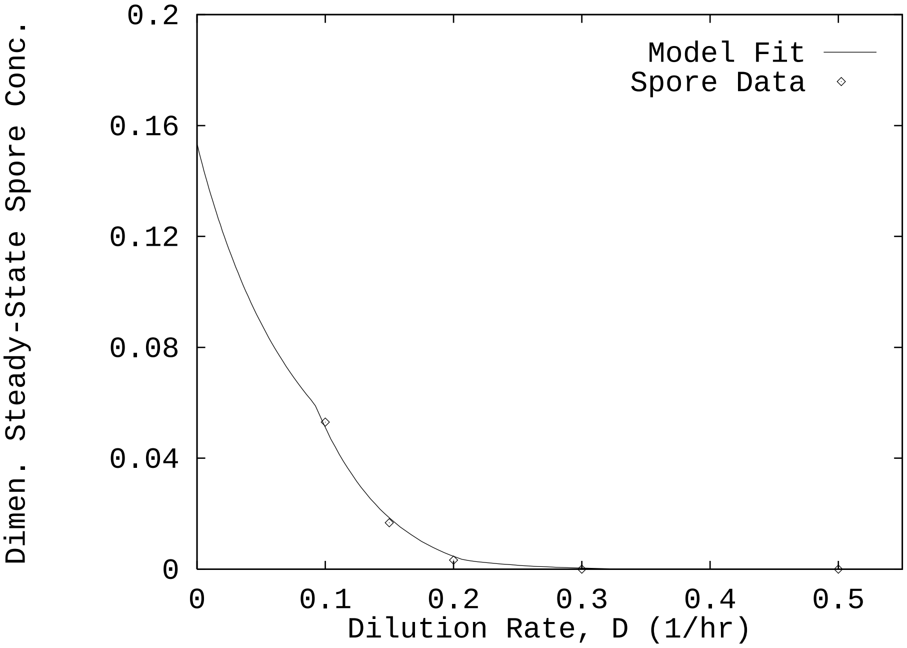

Figure 4.16: Steady-state spore concentration versus dilution rate.

ranging from 0.1–0.5 (1/hr) is shown in Figure 4.16. The model successfully predicts an increase in spore concentration as dilution rate decreases. Dawes and Thornley [22] obtained a similar trend for steady-state spore concentration based dilution rates ranging from 0.05–0.38 (1/hr). An interesting characteristic of the predicted steady-state spore profile is its scalloped appearance at $D = 0.1$ (1/hr). This phenomenon is an artifact of the linear elemental description of the sporulation initiation function. As shown in Figure 4.14, the strong shift in slope of the sporulation initiation function causes this discontinuous slope of the steady-state spore concentration. Without data at lower dilution rates, the validity of this effect remains questionable.

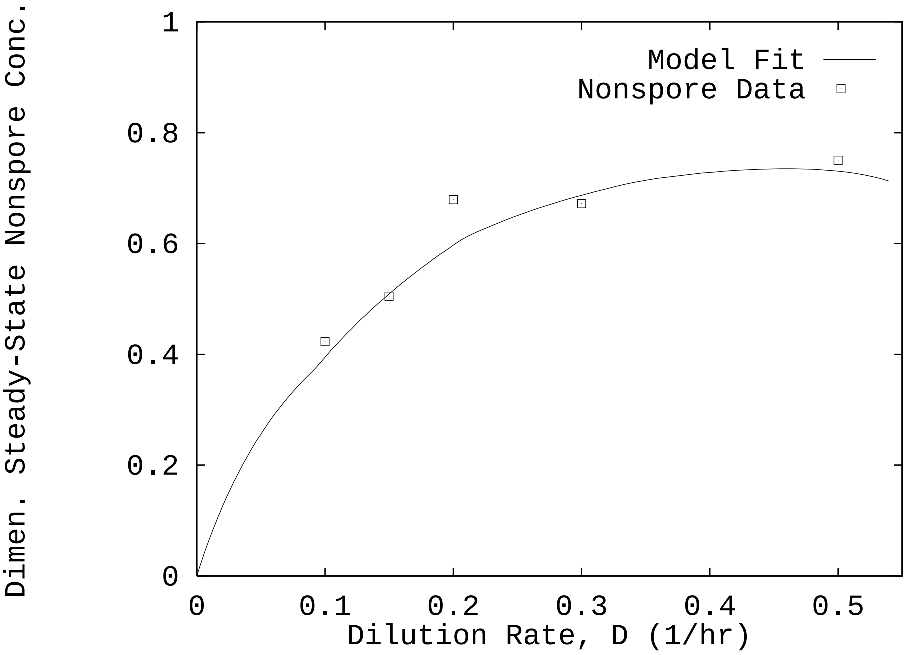

Figure 4.17: Steady-state nonspore concentration versus dilution rate.

The steady-state nonspore concentration data plotted against dilution rate are shown in Figure 4.17. Again, the segregated model does a good job of predicting steady-state biomass behavior. At low dilution rates, it appears that cell death and sporulation initiation are important processes, reducing levels of nonspore biomass at the low substrate conditions. As dilution rate increases, the availability of high substrate concentrations allows for increased vegetative populations.

As an interesting aside, it was discovered that alterations in the sporulation initiation function can lead to non-trivial steady-state multiplicity for the *Bacillus* fermentation. Steady-state multiplicity describes a situation where

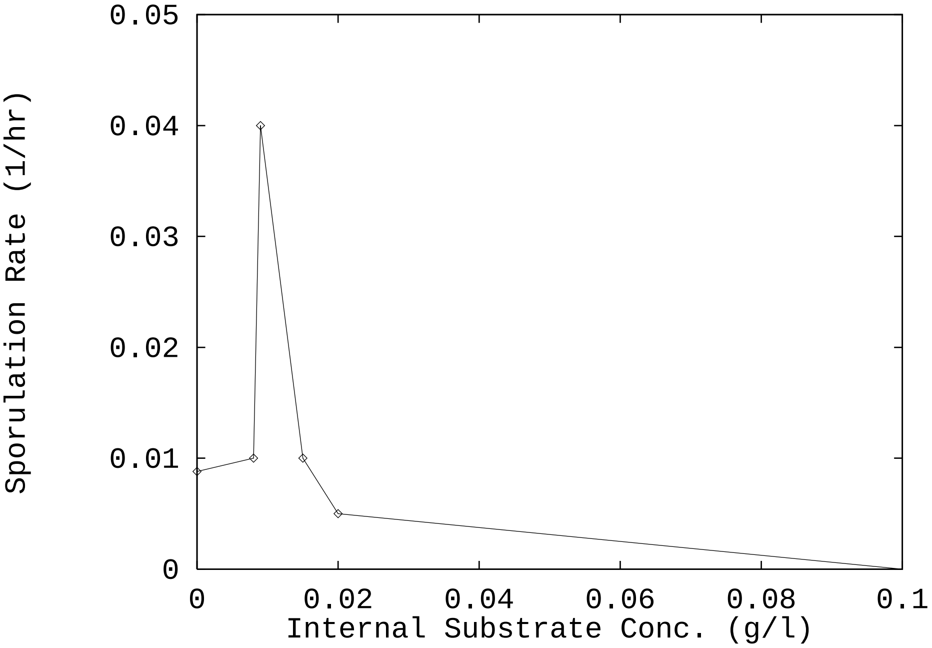

Figure 4.18: Altered sporulation initiation function allowing for non-trivial, steady-state multiplicity.

more than one steady state exists for a given set of operating conditions. In the case of the segregated model, multiple non-trivial fixed-point solutions were discovered when the sporulation initiation function was allowed to decreased rapidly from the maximum initiation rate to a lower sporulation rate between the rate at zero and the maximum rate. An example of this sporulation initiation structure is illustrated in Figure 4.18. For the sporulation initiation function shown, the slowly increasing sporulation rate near zero internal substrate concentration allows for low, stable state-steady spore concentrations at low dilution rates. This phenomenon occurs because the reduced sporulation load at low substrate concentrations allows the effective vegetative cell growth rate to match the dilution rate, thus imparting stability. In the original estimated sporulation initiation function, shown in Figure 4.14, the rate of initiation increases rapidly from zero to the maximum rate, under these initiation conditions the sporulation load on the vegetative cell growth creates a situation in which vegetative growth cannot match the high sporulation rate in tandem with the washout condition imposed by the constant substrate feed. Therefore, low substrate concentration steady-state cannot be obtained, and the low spore steady states do not exist.

During steady-state operation of the fermentor a low-dilution rate steady state was observed that had a substantially reduced spore concentration. Including this seemly anomalous data point in the steady-state data set led to the sporulation initiation function given in Figure 4.18. Using an algebraic continuation algorithm as suggested by Rawlings [89], the steady-state biomass concentrations for the altered sporulation initiation function were obtained. The model fit to the steady-state spore and nonspore biomass data, including the low-spore point, are shown in Figure 4.19. As the fits show, with the altered initiation function, the spore and nonspore biomass concentration show classic bifurcation behavior. Starting at low dilution rate, the lower steady-state branch would be followed until the feed flowrate passed a critical point. Increasing the feed flowrate past the critical point would cause a sudden ignition in the steady-state spore concentration as the fermentor moved to a new steady-state on the upper stable branch. In contrast to the large significant jump in the spore concentration, the model predicts that the change in nonspore biomass concentration would be unnoticeable due to the relatively small effect of the sporulation change on the nonspore biomass concentration.

The possibility of steady-state multiplicity poses an interesting explanation for the observed low-spore steady-state, it must be stated that the lack of data

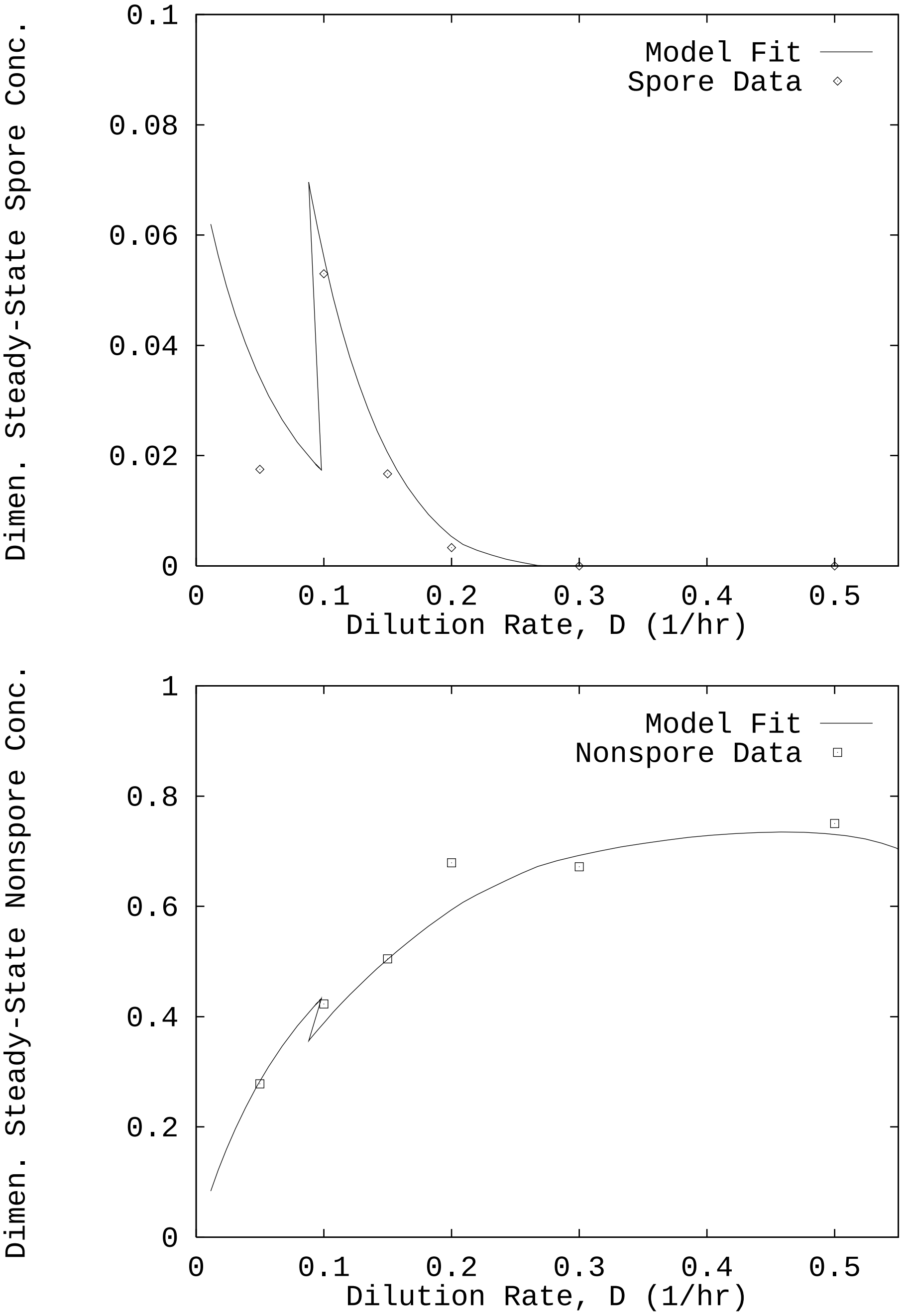

Figure 4.19: Steady-state model fits to the spore and nonspore biomass data including the anomalous low-spore point.

in the low dilution rate region make it impossible to make solid conclusions concerning this phenomenon. It is also important to note that the dilution rate steady state was obtained only once and was not duplicated. This brings into question the possibility that experimental error, or unknown alterations in experimental conditions caused an erroneous reading. It is also possible that asporogenous mutants could have arisen due to the long fermentation times. This would have resulted in low spore counts due to the ability of the mutants to take over the culture. However, it is important to recognize that the segregated model admits the possibility of steady-state multiplicity.

Low Aeration Fermentations. As mentioned previously, fermentations carried out under high airflow and with vigorous mixing conditions did not yield measurable levels of bacitracin. Reducing the inlet airflow, and the rate of mixing yielded bacitracin production under batch operating conditions. In its current form, the segregated model does not account for the effects of dissolved oxygen concentration in the growth, differentiation, and antibiotic production kinetics. For this reason, the growth and differentiation parameters were reestimated to account for the shift in unmodelled operating conditions.

Growth and differentiation data for low-aeration batch fermentation L-10-6 are shown in Figure 4.20. Batch biomass and substrate profiles from high-aeration batch fermentation B-6-14 are included for comparison purposes. Low aeration batch fermentation data are listed in Appendix E.

Qualitatively the spore, nonspore and substrate profiles look similar to the high-aeration batch fermentation. However, the vegetative cell growth rate is noticeably lower under low-aeration, with delayed onset of exponential growth and substrate consumption. It is also obvious that there is a lower biomass yield under low aeration, with significantly lower nonspore biomass number

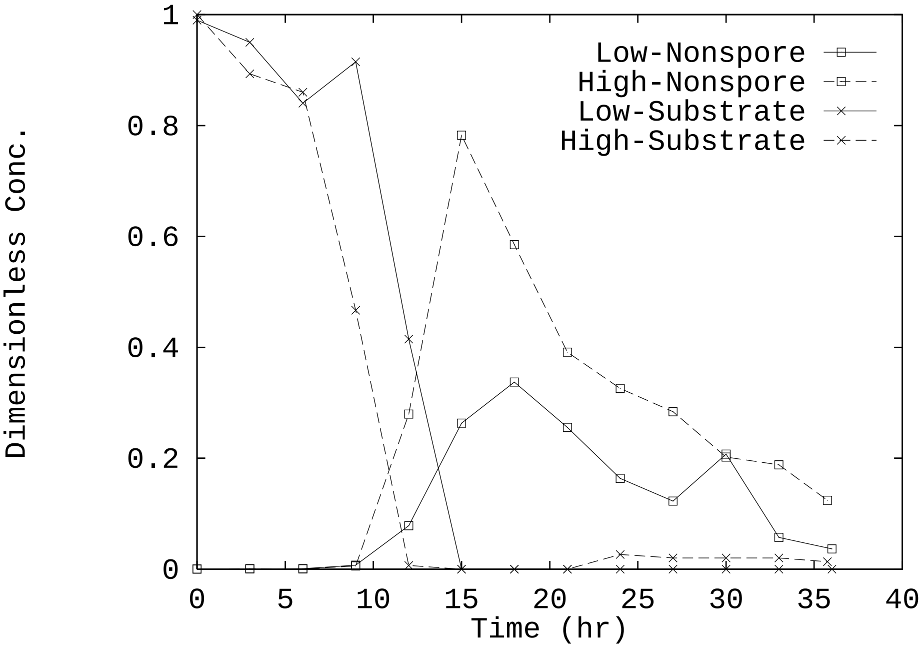

Figure 4.20: Dynamic biomass and substrate concentration profiles for low-aeration batch fermentation L-10-6 compared to high-aeration B-6-14.

concentrations in the low-aeration case compared to high aeration.

Figure 4.21 shows a comparison of the sporulation characteristics between low and high aeration. It is notable that although nonspore biomass production is lower under low-aeration conditions, it appears the level of spore production is higher in a relative sense compared to the high-aeration batch experiment. Also, it appears that the delay between maximum nonspore biomass concentration and the appearance of spores is longer under low aeration. Presumably, reduced aeration affects the *Bacillus* growth and sporulation dynamics by altering the dissolved oxygen concentration in the fermentation broth. However, since neither the segregated or comparison models account

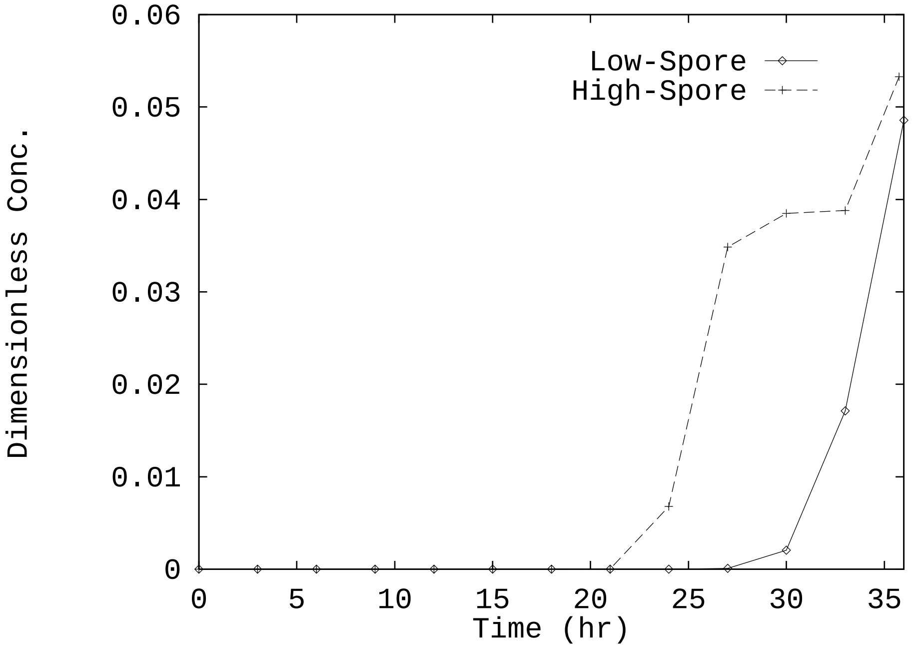

Figure 4.21: Comparison of batch spore and nonspore biomass dynamics for low and high aeration rates.

for dissolved oxygen, the model parameters must be reestimated under the new operating conditions due to the unmodelled effects of aeration changes. However, the basic segregated model structure, utilizing the two-compartment vegetative growth model and the 5-point sporulation initiation function, have been preserved in identifying the segregated model under low aeration.

Using the same estimation methodology for the low-aeration experiments as for the high-aeration, the growth and differentiation parameters have been reestimated for low aeration. The maximum likelihood estimates of the adjustable parameters were obtained using the replicate low aeration batch fermentations L-10-6 and L-10-11. Estimates were obtained by estimation based

Run	Adjustable Parameters			
	α_v	m_v	y_v	τ_m
L-10-6	0.623 ± 0.085	0.128 ± 0.015	0.600 ± 2.13	13.51 ± 2.55
L-10-11	0.604 ± 0.033	0.112 ± 0.014	0.586 ± 0.097	$13.91 \pm .679$
Combined	0.607 ± 0.010	0.114 ± 0.016	0.579 ± 0.097	14.01 ± 0.37

Batch Run	Measurement Error Variances †		
	ν_{spo}	ν_{nspo}	ν_{sub}
L-10-6	4.41×10^{-5}	3.29×10^{-3}	1.86×10^{-3}
L-10-11	8.92×10^{-5}	2.13×10^{-3}	4.18×10^{-3}
Combined	1.20×10^{-4}	3.86×10^{-3}	2.86×10^{-3}

Table 4.6: Low aeration parameter estimates for the adjustable segregated model parameters based on replicate batch experiments L-10-6 and L-10-11.

on the individual runs, and using the combined data. The resulting model parameter values are shown in Table 4.6. The model fit to biomass and substrate data from low-aeration batch fermentation L-10-6 is shown in Figure 4.22.

As expected, the parameter estimates for the low-aeration conditions reflect the reduction in growth rate, and substrate yield, indicated by the contrast in the biomass and substrate profiles for high and low aeration shown in Figure 4.20. The maximum vegetative growth rate, α_v, decreases approximately 20% due to the reduced aeration. Similarly, the substrate yield, y_v, is reduced by almost 40%. Also, the spore maturation time increases under

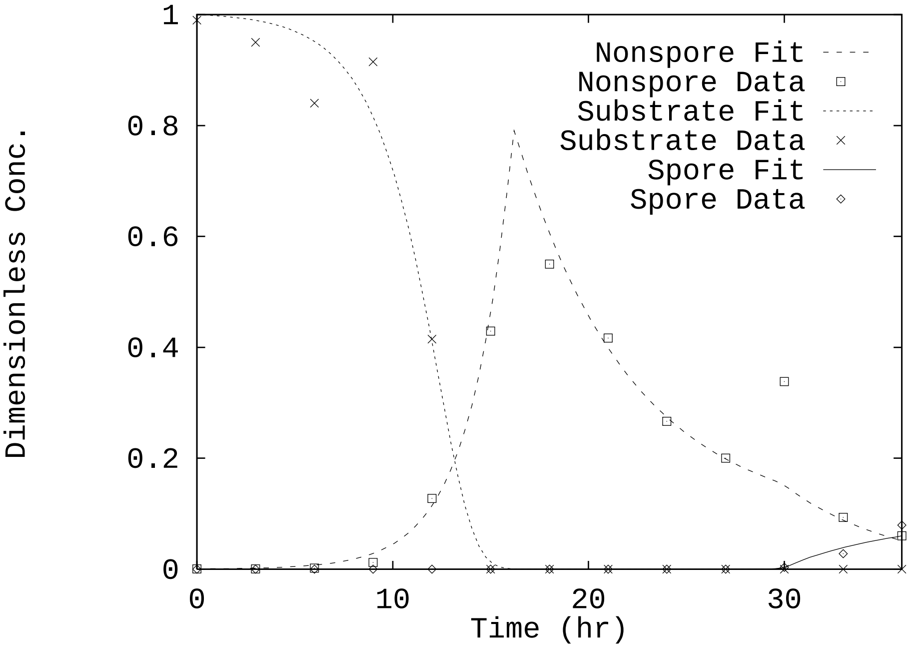

Figure 4.22: Segregated model fit to the low-aeration biomass and substrate profiles from fermentation L-10-6.

low-aeration conditions from about 9 hours to 14 hours.

The shift in growth and differentiation behavior resulting from the decrease in aeration probably reflects an adjustment of the *Bacillus* metabolism from partial oxidation pathway, utilized in oxygen-rich environments, to a mixed-acid fermentative pathway used during oxygen depletion. The oxidative metabolic pathways are energetically more efficient than pure fermentative pathways. The increased efficiency attained in the presence of oxygen provides an explanation for the increased growth rate and substrate yield observed during high aeration fermentations [42, 59].

Low-Aeration Steady State. In an attempt to produce bacitracin under steady-state conditions, the fermentor was run with constant feed at low aeration. Unfortunately, at low-aeration, the manually-controlled air flowrate varied substantially, due to pressure surges in the bench air supply. This prevented successful attainment of steady-state at low aeration. The inability to achieve steady-state was typified by substantial variations in the spore and nonspore biomass measurements even after long periods of continuous feeding. To rectify this problem, a suitable air flow and agitation control system is needed for the fermentation apparatus.

4.3.3 Segregated Model Antibiotic Parameter Identification

As discussed previously, the parameter estimation strategy has been treated as a two-phase process, first the biomass growth and differentiation model was to be identified, then the parameters for the age-dependent antibiotic production function were to be estimated. With good fits to the biomass and substrate data, and reasonable confidence in the growth and differentiation parameters, it is now appropriate to discuss the identification of the bacitracin production parameters.

Similar to the sporulation initiation function, the bacitracin production function has been parameterized as a linear combination of polynomial basis functions in sporangium age. Again, for convenience, the function is cast in terms of Lagrange interpolating polynomials, such that the production parameters have a clear physical meaning, that being the value of the bacitracin production function at the interpolation points.

$$\mu_a(\tau) = \sum_{j=0}^{m} \mu_{a_j} \phi_j(\tau) \tag{4.50}$$

By defining the production function in this fashion, the task is to estimate the antibiotic production rate at each collocation point, thereby constructing the age-dependent antibiotic production expression. The degree, m, needs to be chosen large enough to accurately represent the true production function, but not so large that the function is overparameterized.

Assuming the initial bacitracin concentration is negligible, integration of the bacitracin material balance leads to the following expression for antibiotic concentration during batch fermentation:

$$A(t) = \int_0^t \left[\int_0^{\tau_m} \mu_a(\tau') X_s(t', \tau') \, d\tau' \right] dt' \tag{4.51}$$

Switching the order of integration, and removing the antibiotic production function from the integral in time gives:

$$A(t) = \int_0^{\tau_m} \mu_a(\tau') \left[\int_0^t X_s(t', \tau') \, dt' \right] d\tau' \tag{4.52}$$

Now, remembering that the integration in cell age is approximated using a Gaussian quadrature rule, antibiotic concentration can be approximated using:

$$A(t) \approx \sum_{i=1}^{n} \left[\mu_a(\tau_i) \left(\int_0^t X_s(t', \tau_i) \, dt' \right) \right] w_i \tag{4.53}$$

where τ_i represents a collocation point in the antibiotic production function, and w_i is a Gaussian quadrature weight. The estimation problem is to determine the values of the production function at the age-collocation points, $\mu_a(\tau_i)$, based on bacitracin concentration measurements in time. Utilizing Equation 4.53 with discrete antibiotic concentration data allows for the definition of a matrix operator relating the antibiotic production parameters to the antibiotic concentration profile during batch fermentation:

$$\begin{pmatrix} \left[\int_0^{t_1} X_s(t', \tau_1)\, dt'\right] w_1 & \cdots & \left[\int_0^{t_1} X_s(t', \tau_n)\, dt'\right] w_n \\ \vdots & \ddots & \vdots \\ \left[\int_0^{t_m} X_s(t', \tau_1)\, dt'\right] w_1 & \cdots & \left[\int_0^{t_m} X_s(t', \tau_n)\, dt'\right] w_n \end{pmatrix} \begin{pmatrix} \mu_a(\tau_1) \\ \vdots \\ \mu_a(\tau_n) \end{pmatrix} = \begin{pmatrix} A(t_1) \\ \vdots \\ A(t_m) \end{pmatrix}$$

Defining the $m \times n$ matrix $\mathbf{S}$ to represent the batch antibiotic production model, the $n \times 1$ vector $\boldsymbol{\mu_a}$ to be the vector of production function values at the collocation points, and the $m \times 1$ vector $\mathbf{a}$ to be the antibiotic concentration measurements from times t_1 to t_m, the estimation problem is conveniently presented in matrix notation:

$$\mathbf{S}\boldsymbol{\mu_a} = \mathbf{a} \tag{4.54}$$

In this form it is obvious the production parameters appear linearly in the segregated model. If antibiotic concentration data are collected at many time points, such that the number of measurements exceeds the number of bacitracin production parameters, the system of equations in 4.54 is overdetermined, and this is considered to be a linear least squares problem. The optimal production parameter estimates are obtained by solving the normal equation:

$$\boldsymbol{\mu}_{\mathbf{a}} = \left(\mathbf{S}^T\mathbf{S}\right)^{-1}\mathbf{S}^T\mathbf{a} \tag{4.55}$$

This solution minimizes the two-norm of the bacitracin residual.

Numerical Model Identification Experiments. To test the feasibility of identifying $\mu_a(\tau)$ from batch data, numerical model identification experiments have been conducted. Simulated antibiotic concentration data have been generated using the segregated model with the previously determined growth and sporulation parameters, and an assumed form for the antibiotic production function. To incorporate noise, a random number generator was used to produce normally distributed errors that were added to the simulated antibiotic concentration data.

For the simulated experiments, a third degree polynomial expression in sporangium age was considered to be the "true" production function. As an initial test, the simulated data were left noise free and the model structure

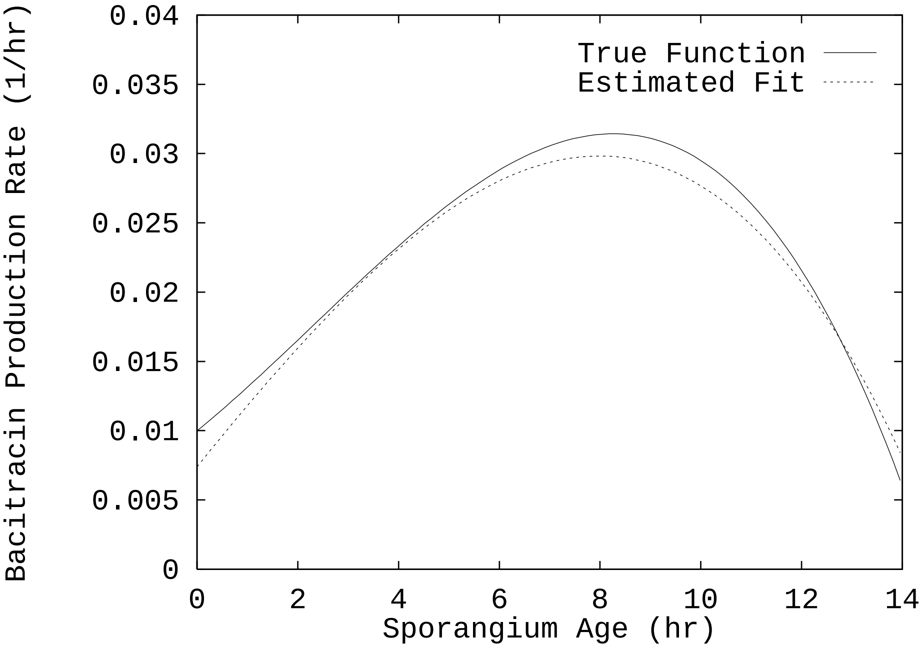

Figure 4.23: Estimate of the age-dependent bacitracin production function using noise-free data and correct model structure.

was assumed to be known. The resulting estimate of the "true" third degree polynomial is shown in Figure 4.23. As Figure 4.23 shows, the estimated production closely resembles the nominal production function, with only slight differences between the "true" and estimated age-dependent functions. This indicates that the antibiotic concentration measurement provides enough sensitivity to reconstruct the production function in the absence of noise.

To examine the effect of measurement error on the estimation process, Gaussian noise of zero mean and 15% standard deviation was added to the simulated data, and the production function was reestimated. The resulting function estimate and model fit to the noisy data are shown in Figures 4.24

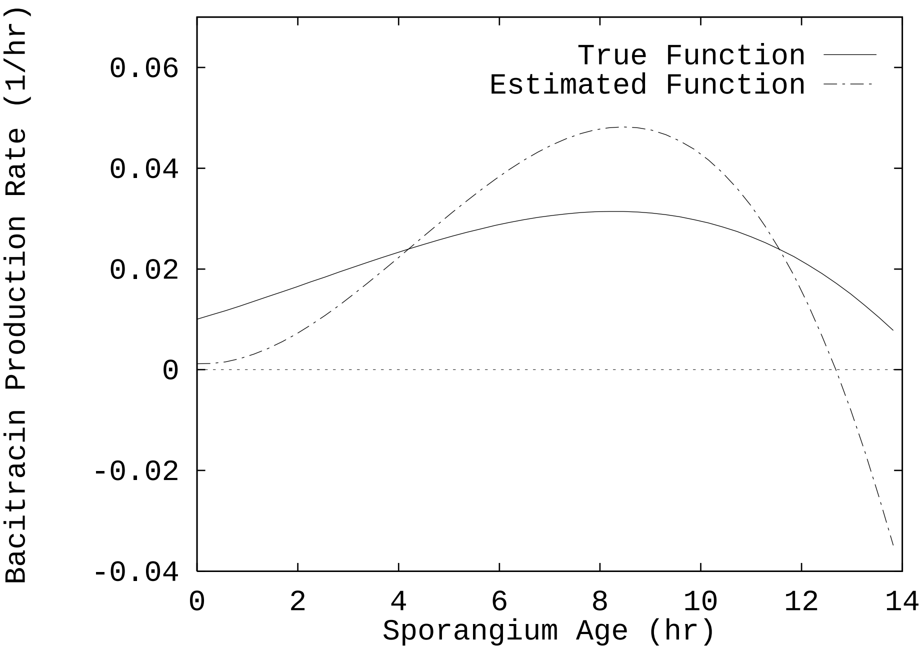

Figure 4.24: Estimate of the age-dependent bacitracin production function based on simulated data with 15% Gaussian noise and the correct model structure.

and 4.25. The estimate of the production function based on noisy data is significantly different then the nominal function, with the estimator over-predicting the maximum rate, and suggesting that negative production rates occur toward the end of sporulation. Based on the estimated production function, it is apparent that the introduction of noise creates problems when trying to determine the production function. This indicates that perturbations in the data lead to significant alterations in the parameter estimates.

Since the estimation problem can be cast as a linear least-squares problem, the effects of noise in the data on the parameter estimates can be analyzed by examining the singular value decomposition (SVD) of the batch production

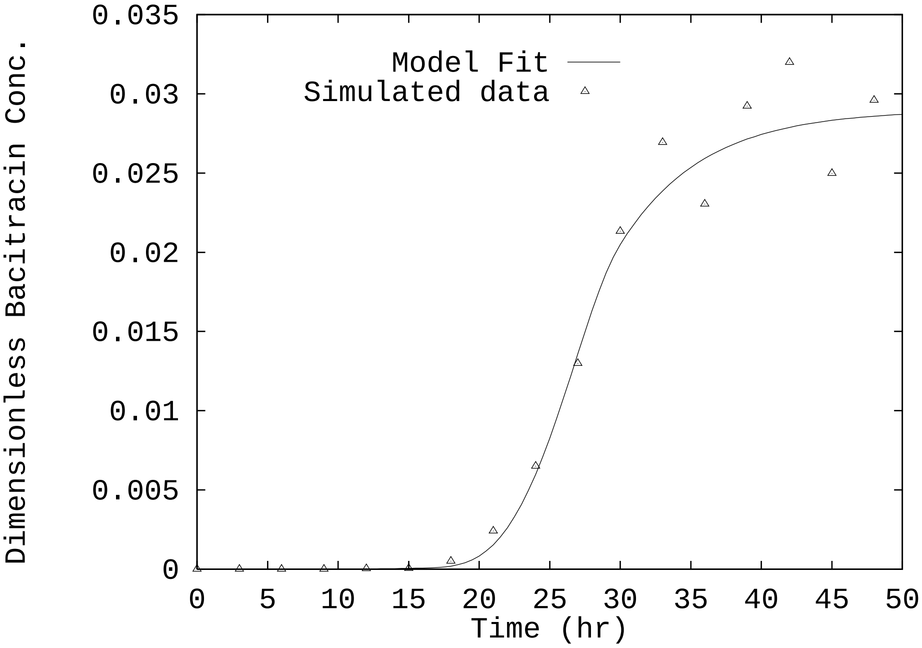

Figure 4.25: Model fit to the simulated data based on the bacitracin production function given shown in Figure 4.24.

matrix, **S**. The SVD of the $m \times n$ matrix **S** is given by:

$$\mathbf{S} = \mathbf{U}\mathbf{\Sigma}\mathbf{V}^T \tag{4.56}$$

The $m \times m$ orthogonal matrix **U** is formed by the normalized eigenvectors of $\mathbf{S}\mathbf{S}^T$, and the $n \times n$ orthogonal matrix **V** is formed by the normalized eigenvectors of $\mathbf{S}^T\mathbf{S}$. The $m \times n$ diagonal matrix $\mathbf{\Sigma}$ contains the n singular values, σ_i, of **S** on the diagonal. The singular values are the square roots of the nonzero eigenvalues of $\mathbf{S}\mathbf{S}^T$ [105].

The singular values indicate the degree to which perturbations in the data are magnified through the model and into the parameter estimates. The columns of the **U** and **V** matrices indicate which independent noise perturbation directions have the most significant impact on the independent parameter directions. To simplify the analysis, $\bar{\mathbf{\Sigma}}$ is chosen to be the $n \times n$ upper submatrix of $\mathbf{\Sigma}$, and further, it is assumed that the singular values are ordered from largest to smallest on the diagonal of $\bar{\mathbf{\Sigma}}$. Also, let $\bar{\mathbf{U}}$ represent the first n columns of the left singular vector matrix $\mathbf{U}$. Using these simplifications the solution to the least square estimation problem is given by:

$$\boldsymbol{\mu}_{\mathbf{a}} = \mathbf{V}\bar{\mathbf{\Sigma}}^{-1}\bar{\mathbf{U}}^{T}\mathbf{a} \tag{4.57}$$

If $\boldsymbol{\delta}\mathbf{a}$ and $\boldsymbol{\delta\mu_a}$ are defined to represent perturbations in the data and the parameters, respectively, and $\mathbf{V}$ and $\mathbf{U}$ are partitioned by columns, then by Equation 4.57 the effect of data perturbations on the estimates is given by:

$$\boldsymbol{\delta\mu}_{\mathbf{a}} = \left[\begin{array}{c|c|c} \mathbf{v}_1 & \cdots & \mathbf{v}_n \end{array}\right] \begin{bmatrix} \frac{1}{\sigma_{max}} & & \mathbf{0} \\ & \ddots & \\ \mathbf{0} & & \frac{1}{\sigma_{min}} \end{bmatrix} \begin{bmatrix} \mathbf{u}_1^T \\ \vdots \\ \mathbf{u}_n^T \end{bmatrix} \boldsymbol{\delta}\mathbf{a} \tag{4.58}$$

In the form presented in Equation 4.58, the SVD provides a clear picture of the effects of noise on the production parameter estimates. The columns of $\bar{\mathbf{U}}$ represent the fundamental directions, by which data noise affect $\boldsymbol{\mu_a}$. The projection of $\boldsymbol{\delta}\mathbf{a}$ onto the fundamental direction, $\mathbf{u}_i$, is scaled by the inverse of the ith singular value $1/\sigma_i$. Therefore, due to the deliberate ordering of the singular values, a perturbation, $\boldsymbol{\delta}\mathbf{a}$, in the direction of u_1 is the most tolerable noise direction because it is scaled by $1/\sigma_{max}$. Using the same logic, noise perturbations in the independent directions of the successive columns become progressively worse because of the increased magnification caused by the corresponding inverse singular values. This indicates the worst perturbation direction is given by $\mathbf{u}_n$, which will be scaled by $1/\sigma_{min}$ Similar analysis shows that the role of the $\mathbf{V}$ matrix is to project the scaled noise perturbations from the fundamental directions onto the physical parameter directions. Therefore, the columns of $\mathbf{V}$ indicate the sensitivity of the parameter directions, with $\mathbf{v}_1$ representing the least sensitive parameter combination, down to the most sensitive combination, $\mathbf{v}_n$.

For the simulated antibiotic production experiments shown in Figures 4.24–4.25, the SVD of the batch model matrix $\mathbf{S}$ yields the following singular values:

$$\bar{\boldsymbol{\Sigma}} = \text{diag}\begin{bmatrix} 2.029 \\ 0.316 \\ 0.048 \\ 0.036 \end{bmatrix} \tag{4.59}$$

At the most basic level, the singular values allow for computation of the condition number, c of the estimation problem:

$$c = \frac{\sigma_{max}}{\sigma_{min}} \tag{4.60}$$

The condition number bounds the relative change in $\boldsymbol{\delta\mu}_{\mathbf{a}}$ due to a data perturbation, $\boldsymbol{\delta}\mathbf{a}$:

$$\frac{||\boldsymbol{\delta\mu}_{\mathbf{a}}||}{||\boldsymbol{\mu}_{\mathbf{a}}||} \leq c\frac{||\boldsymbol{\delta}\mathbf{a}||}{||\mathbf{a}||} \tag{4.61}$$

For the simulated batch experiment, the condition number is found to be: $c \approx 56$. While this is a relatively good condition number from a computational standpoint, in the context of the estimation problem, this condition number indicates that in the worst case perturbations in the data will be magnified over 50 times in estimating $\boldsymbol{\mu}_{\mathbf{a}}$. If the data are relatively noise free, then the age-production function would be easily estimated as is indicated by the noise-free experiment. For the simulated experiment with added noise, the standard deviation of the noise was set at 15% based on experimental experience. At this noise level, the relative error of the estimated production function could be magnified as much as 750%. As indicated by Figure 4.24, the noise has a significant effect on the ability of the estimator to ascertain the true production function.

The SVD analysis of the production parameter estimation problem indicates that the noise level expected in the antibiotic concentration data will likely cause problems in elucidating the age-dependent production function. However, the SVD also indicates how the estimation problem can be altered such that data perturbations which are particularly troublesome can be suppressed, thus allowing estimation of the production parameters with reduced influence of noise. The influence of the poorly conditioned data perturbations can be filtered out by setting the small singular values of $\mathbf{S}$ to 0. In effect, this throws away any information provided by the data in the direction of $\mathbf{u}_i$ corresponding to the singular value σ_i that was set to 0. While it might seem counterproductive to "throw away" information, by using the SVD the data can be selectively cleaned by eliminating information that is particularly corrupting to the estimates.

To analyze the effectiveness of noise suppression for the bacitracin production parameters, the nominal age-dependent production curve has been reconstructed using the selective suppression of the singular values. The production function was reestimated using the noisy simulated data, while suppressing increasing numbers of singular values. The estimated production function based on suppression of the 2 smallest singular values is shown in Figure 4.26. Reestimation of the simulated production function shows that the worst perturbation directions, corresponding to the singular values $\sigma_3 = 0.048$ and $\sigma_4 = 0.036$, have a significant impact on the ability of the estimator to reconstruct the "true" function. By suppressing these 2 singular values, a

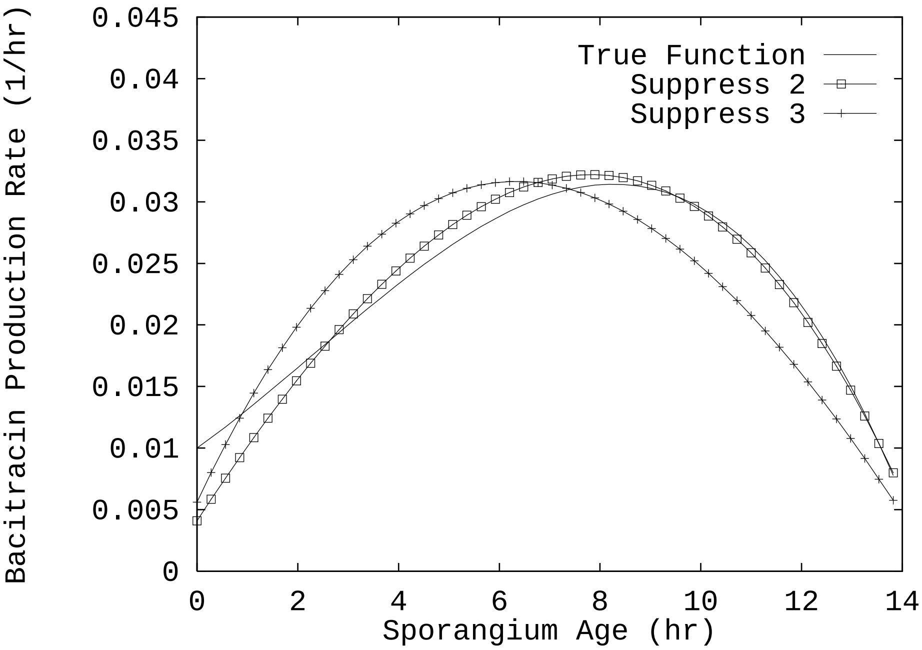

Figure 4.26: Improvement of the estimated bacitracin production function based on suppression of first 2, then 3 of the smallest singular values.

substantial improvement in the estimation production function is realized. A further increase in the suppression level begins to degrade the estimate as is shown in Figure 4.26. This results because there is a limit to the amount of information that can be eliminated and still successfully capture the production function. However, it is interesting to note that even while suppressing the 3 worst directions, there is enough information for the estimator to capture the basic shape of the nominal production function. For the batch production model, suppression of the two smallest singular values gives the best result. Since the two smallest singular values are of approximately the same magnitude, elimination of both helps filter out the majority of the noise. Therefore, by eliminating the two worst noise directions the effect of noise in the estimation problem is controlled, allowing an accurate reconstruction of the nominal production function.

Antibiotic Production Parameter Estimates. To attempt to estimate the actual age-dependent bacitracin production function, the noise suppression technique has been utilized to construct a production function based on the low-aeration batch fermentation experiments. Initially, a third-degree parameterization of the production function was assumed and the bacitracin production parameters were estimated from the data. For batch fermentation L-10-6, the production function estimate based on the the least squares solution without noise suppression, and suppression of the 2 smallest singular values are compared in Figure 4.27. The corresponding model fit to the data for the unsuppressed and suppressed production functions are shown in Figure 4.28. Obviously, the production function obtained without data suppression is physically unrealistic. The presence of large fluctuations in the production rate, along with negative bacitracin production late in the sporulation process, leads to the conclusion that the unsuppressed production function is probably significantly influenced by noise in the data. Suppression of the two smallest singular values leads to a substantial difference in the function estimate. The suppressed function suggests the production rate starts out relatively low, climbs toward a maximum at approximately 5 hours, and finally steadily declines toward zero production at spore maturation. The model fit to the antibiotic concentration data, given in Figure 4.28, shows that the model is able to effectively describe the data using both the suppressed and unsuppressed production functions.

Since the actual age-dependent bacitracin production function is unknown,

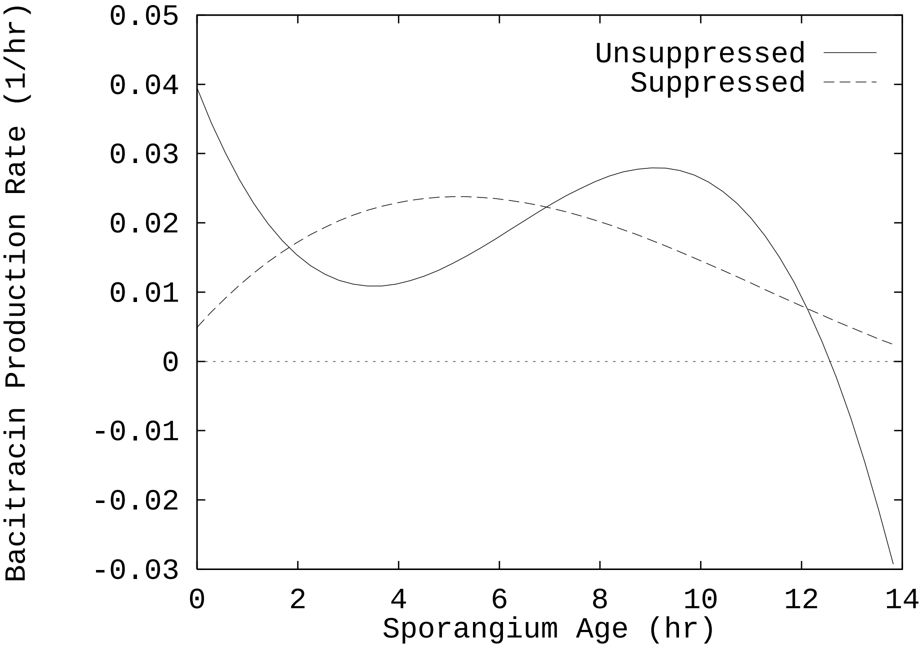

Figure 4.27: Comparison of the estimated bacitracin production function for batch L-10-6, based on no data suppression and suppression of the two smallest singular values.

it is interesting to examine the effects of varying the production function parameterization on the production function estimate and the model fit to the batch data. If the production function parameterization is increased from a cubic polynomial to a quartic, the resulting production parameter estimates using both unsuppressed and suppressed noise are shown in Figure 4.29. The model fits to the batch data based on both the suppressed and unsuppressed production curves are given in Figure 4.30. The estimated quartic production function shows similar behavior to the cubic approximation, in that the estimate based on the unsuppressed data yields a production function with large fluctuations and negative production rates. Noise suppression yields a

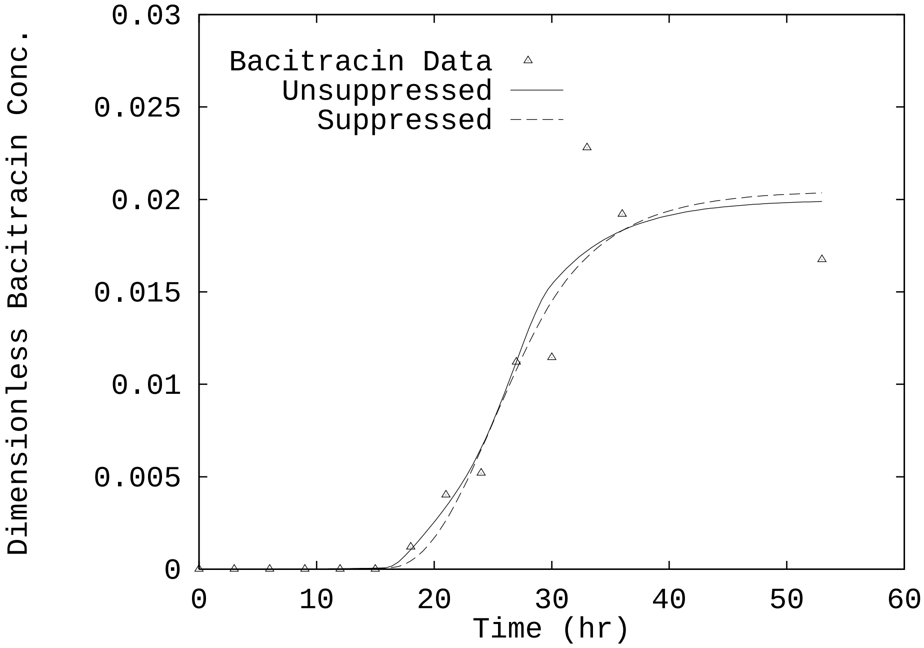

Figure 4.28: Model fit to bacitracin concentration data L-10-6 using the estimated production function without suppression and suppression of the two smallest singular values.

close match to the production function estimate that was found using the suppressed cubic fit. The reappearance of the nearly cubic estimate based on the quartic approximation gives a strong indication that a quartic approximation to the bacitracin production function is overparameterized. Further, examination of the model fit to the batch bacitracin data, shown in Figure 4.30, shows that the unsuppressed quartic model is developing an oscillatory fit to the data. The wavy model prediction implies that the quartic production function is beginning to fit noise, as opposed to the underlying noise-free bacitracin concentration. This oscillatory fit gives additional evidence that a quartic approximation provides too much flexibility in the model, and sug-

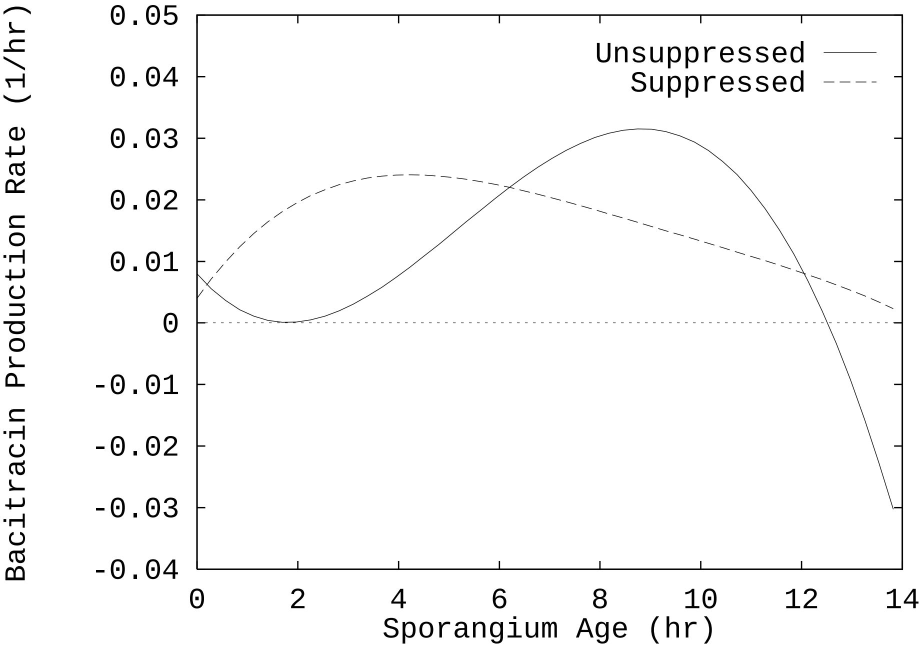

Figure 4.29: Estimated bacitracin production function based on a fourth-degree fit using suppressed and unsuppressed noise for batch fermentation L-10-6.

gests that the production function parameterization should be reduced from the quartic approximation.

Reduction of the antibiotic production function parameterization to a quadratic approximation again shows a large difference between the function estimate based on suppressed and unsuppressed data noise. The quadratic function estimates based on batch fermentation L-10-6 are given in Figure 4.31. The comparison of the suppressed and unsuppressed estimates shows that the ability of the model to exhibit large age-dependent production fluctuations has been eliminated because a quadratic model has constant curvature, and is therefore limited to a single maximum or minimum on the age domain.

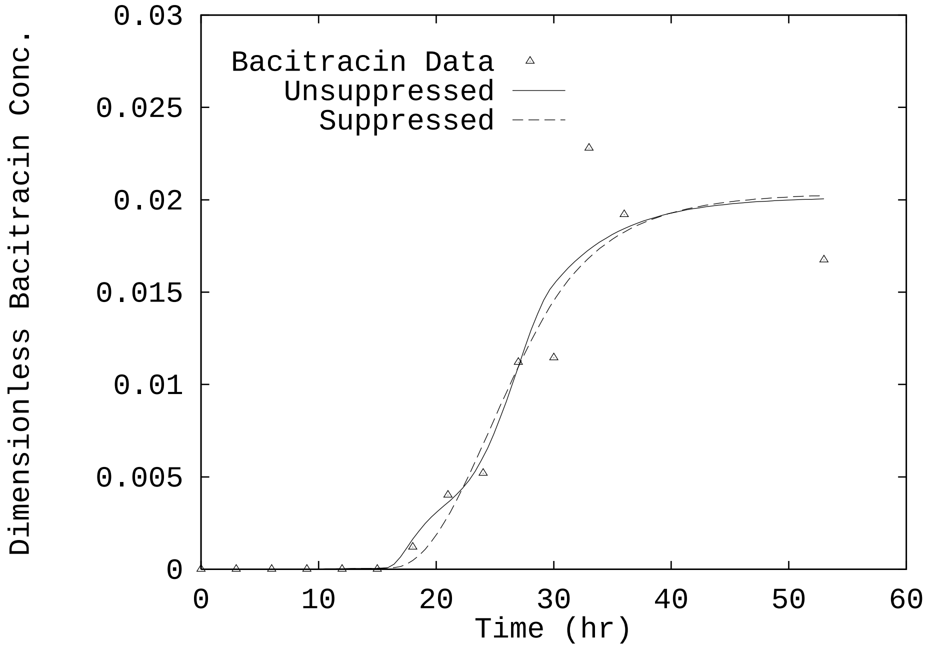

Figure 4.30: Model fit to bacitracin concentration data L-10-6 using the estimated quartic antibiotic production functions from Figure 4.29.

However, the unsuppressed estimate indicates the maximum production rate is achieved immediately upon entering sporulation and decreases steadily toward zero as the sporangia mature. While this estimate does not suffer from the large fluctuations and negative production rates that were evident with the higher order approximations, it seems unrealistic that maximal production rates would be achieved immediately upon entering the differentiation cycle. When singular values suppression is utilized, the quadratic production function approximation is similar to the suppressed cubic and quartic approximations. This production function shape seems more realistic, allowing for a build up in production, achieving a maximum approximately half-way through

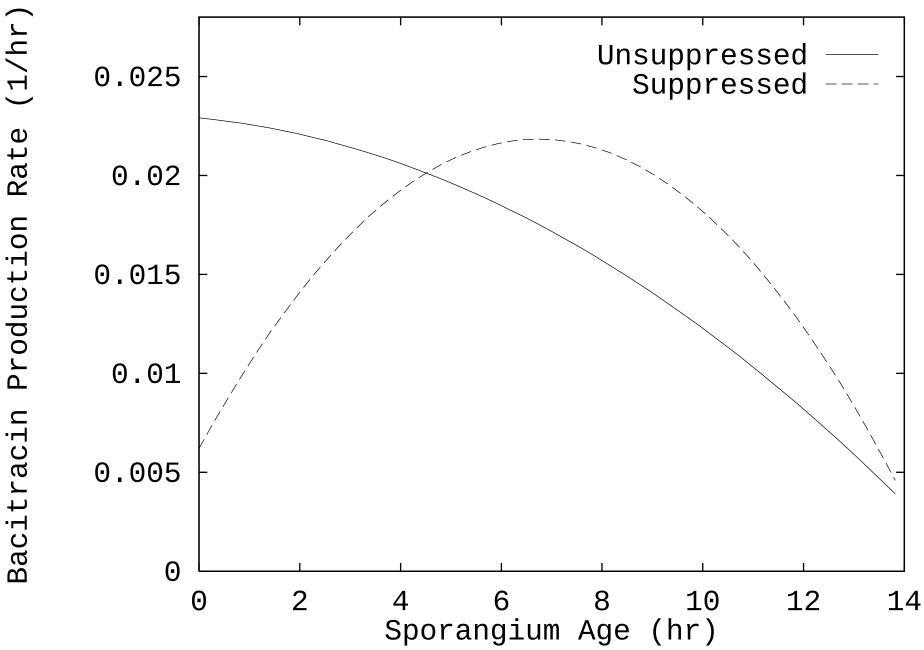

Figure 4.31: Comparison of the suppressed and unsuppressed quadratic estimates of the bacitracin production function based on batch fermentation L-10-6.

the differentiation cycle.

Utilization of the quadratic production function to fit the antibiotic concentration data, as shown in Figure 4.32, gives a similar fit when compared to the higher order parameterizations. This exemplifies the fact that with noise in the antibiotic data it is difficult to ascertain the true relationship between sporangium age and antibiotic production. In fact, due to the measurement noise, it is not possible to conclude that bacitracin production is an age-dependent phenomenon, leaving in question the theory that bacitracin production is an age-dependent function of differentiation. It is clear from the model fits to the batch data using various production function parameterizations that rel-

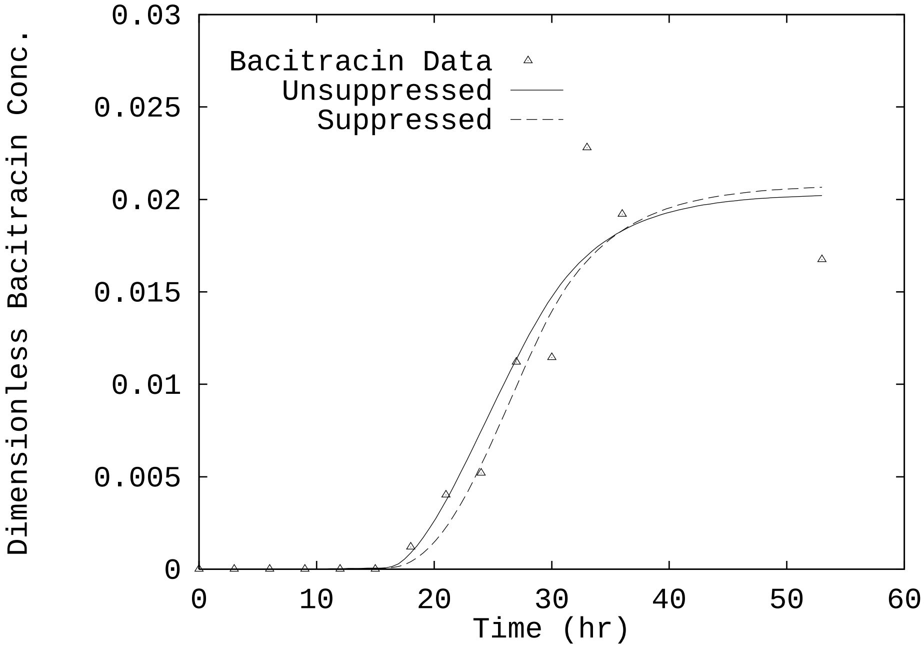

Figure 4.32: Model fit to the bacitracin concentration data L-10-6 using the estimated quadratic antibiotic production functions from Figure 4.31.

atively large differences in the bacitracin production function are lost in the noisy antibiotic concentration data. The corrupting effects of the noise are further exemplified by the large confidence intervals on the production rate parameters for various order parameterizations, shown in Table 4.7. The large confidence intervals on the production parameters reflects the fact that many different curves will do an adequate job of describing the noisy bacitracin data. Therefore, without an accurate measurement of the bacitracin concentration is difficult to make conclusive statements concerning the age dependence of bacitracin production.

Although the age-dependent parameterization of the bacitracin production

	Quadratic	Cubic	Quartic
μ_{a_1}	0.012 ± 0.036	0.005 ± 0.160	0.004 ± 0.040
μ_{a_2}	0.044 ± 0.015	0.023 ± 0.044	0.021 ± 0.105
μ_{a_3}	0.006 ± 0.046	0.014 ± 0.044	0.200 ± 0.062
μ_{a_4}		0.008 ± 0.160	0.009 ± 0.092
μ_{a_5}			0.001 ± 0.370

Table 4.7: Estimates of the production function parameters for quadratic, cubic, an quartic parameterizations based on low aeration batch fermentation L-10-6.

function was not considered well-determined for batch fermentation L-10-6, an interesting question concerning the SVD analysis is whether the basic shape of the estimated production function can be replicated using a similar analysis on additional data. With this in mind, a cubic polynomial approximation for the bacitracin production function has been determined using bacitracin data from the low-aeration replicate batch fermentation, L-10-11. Utilizing unsuppressed noisy data the estimated function exhibits large fluctuations in the bacitracin production rate. Selective conditioning through suppression of the two smallest singular values gives a production function that is very similar to the function observed with the original batch data. A comparison between the replicated cubic production function is shown in Figure 4.33. Although the age functions cannot be determined with a high degree of confidence for either of the fermentations, the similarity between the the two function estimates is striking. Based on this similarity, it seems likely that the SVD analysis is able

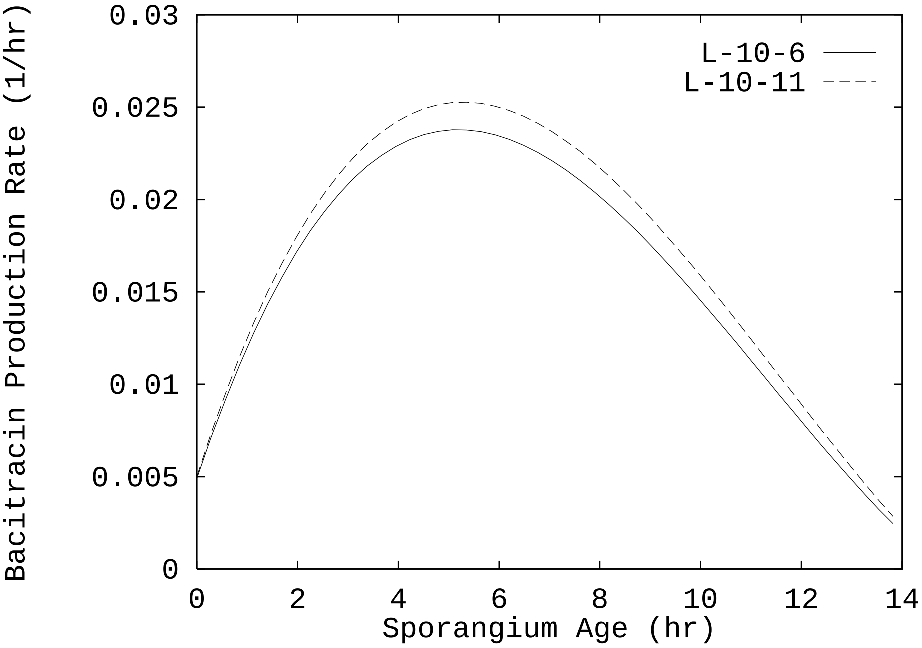

Figure 4.33: Comparison of the cubic polynomial estimates of the age-dependent bacitracin production functions for the replicate batch fermentations L-10-6 and L-10-11.

to uncover some underlying characteristic of the bacitracin production data that is obscured by measurement noise.

Since it is recognized that the noisy data are inadequate to confidently identify any age-dependence of the bacitracin production rate, it is useful to evaluate the ability of a constant production function in modelling the antibiotic production data. For batch L-10-6, the model fit to the bacitracin data using a constant function is given in Figure 4.34. The fit using a constant production rate is equally effective in describing the data as the higher order parameterizations, and suggests that because of the noise, a constant production function could be effectively utilized in modelling the antibiotic

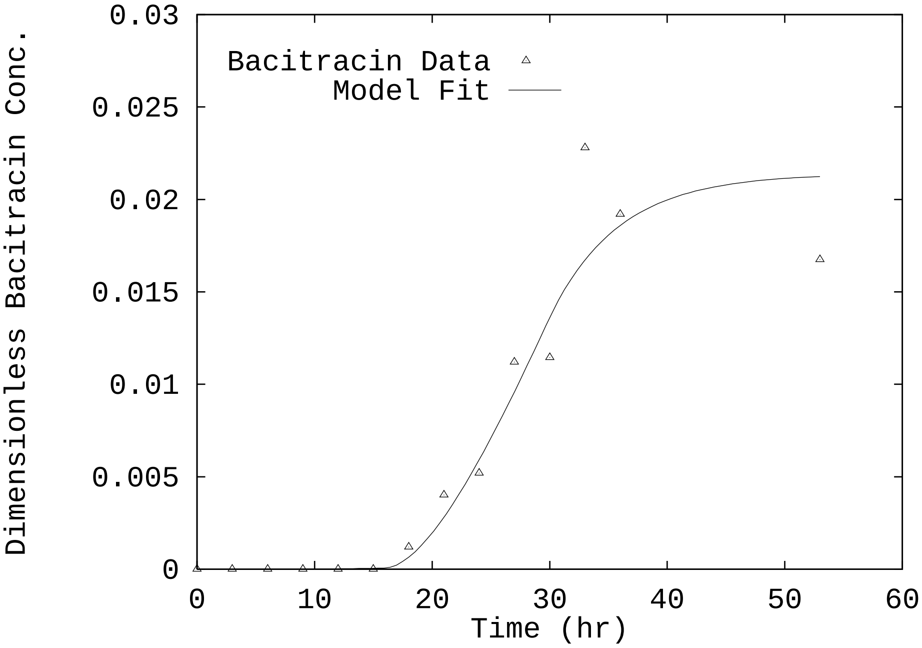

Figure 4.34: Model fit to bacitracin concentration data from L-10-6 using a constant production function.

production rate.

Similar to the age-dependent production function, the repeatability of the constant bacitracin production coefficient has been evaluated by examining the replicate batch data L-10-11. For comparison purposes the constant production coefficient has been estimated using fermentation L-10-11 alone, and in combination with batch L-10-6. Table 4.8 shows a comparison of the constant production function obtained for both individual batch fermentations and using the combined replicate experiments. Figure 4.35 illustrates the corresponding model fit to both data sets utilizing the production estimate obtained from the combined data. The relatively good fit of the segregated

Batch Run	μ_a(1/hr)
L-10-6	0.0166 ± 0.003
L-10-11	0.0177 ± 0.002
Combined	0.0174 ± 0.003

Table 4.8: Constant bacitracin production function based on replicate low-aeration batch data.

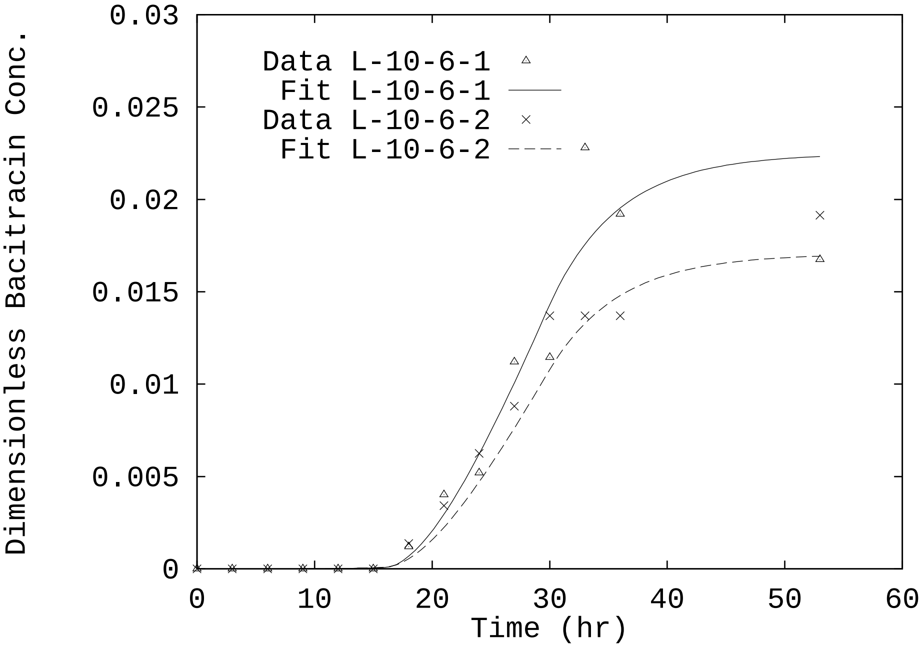

Figure 4.35: Model fit to the replicate batch bacitracin data using the combined constant bacitracin production function.

model to the replicated batch antibiotic data, along with the confident determination of the constant antibiotic production coefficient, gives a good indication that the segregated model is able to capture the underlying mechanism of the bacitracin production for the *B. licheniformis* fermentation.

An important consequence of the model's ability to capture the dynamic bacitracin data using a constant production coefficient, is that the segregated model can be reduced to a delay-differential equation model. This is because the constant bacitracin production rate implies that distinguishability based on sporangium age is not important for predicting antibiotic production. Although this means that the sporangium age distribution is not of primary concern for modelling the instantaneous rate of antibiotic production, it is important for tracking the accumulation of sporangium biomass as cells pass through the differentiation cycle. In fact, a natural implementation of the delay differential equation model would be to model the age distribution using the population balance. Since this is the basis of the segregated model developed in this study, the segregated model formulation is a logical choice for modelling bacitracin production.

4.4 Comparison Model Identification

Like the segregated model, the parameters contained in the comparison model must be estimated using experimental data. A detailed description of the comparison model is given in Section 2.3, and the set of comparison model parameters are listed in Table 2.5.

In the same fashion as the segregated model, a maximum likelihood estimator has been utilized to identify the modified Blanch and Rogers model using the fermentation data. In this section, the identification process for the

MBR model using *B. licheniformis* fermentation data is documented.

To identify the comparison model from experimental data, the relationship between the system measurements and the model states must be made clear. In the segregated model formulation, the biomass is structured into the three physically recognizable *Bacillus* cell morphologies. For this reason, the connection between the segregated model biomass states and the available measurements is obvious. However, the MBR model formulation is based on conceptualized age states that have limited physical basis. For this reason, the connection between the available fermentor outputs and the MBR model states is more subtle. In the comparison model, the biomass is structured into two groups, the immature and mature cells, with antibiotic production being proportional to the rate of cell maturation. Considering the true structure of *Bacillus licheniformis* biomass, use of the terms "immature" and "mature" to describe the different types of cells can only be applied loosely. In the original Blanch and Rogers formulation, growth is localized in one of the two cell groups. To preserve the basic structure of the original model, the modified model retains the localized growth characteristic. In the MBR model, the immature cells are intended to represent the growing biomass, therefore it is logical to equate the vegetative cells with the immature cells. This implies the remaining cells, including sporangia in various stages of development and spores comprise the "mature" biophase. Unfortunately, the techniques utilized to measure the biomass composition do not yield independent information concerning quantity of vegetative and nonvegetative cells. Rather, the plate counting measurements, based on spore heat resistance, are only able to differentiate between spore and nonspore biomass. Unfortunately, the spore biomass comprises only a portion of the "mature" biomass, and therefore is not a useful measurement in the comparison model context. Due to this fact, the biomass measurement for the MBR model is taken to be total biomass concentration.

The remaining outputs are represented in a straightforward manner with an external substrate and antibiotic corresponding directly to the glucose, and bacitracin measurements. Based on the total biomass, substrate, and antibiotic measurements, comparison model outputs are given by:

$$\begin{aligned} \text{Total biomass:} \quad y_{bio} &= N_i + N_m \\ \text{Substrate Conc.:} \quad y_{sub} &= s_e \\ \text{Bacitracin Conc.:} \quad y_{anti} &= A \end{aligned}$$

The three applicable fermentor outputs have been utilized to identify the comparison model parameters. However, in contrast to the segregated model, parameter estimation for the comparison model has not been divided into two tasks. This is because of the lack of information contained in the total biomass and substrate measurements concerning maturation. The only measurement with significant sensitivity to maturation is the antibiotic concentration output. For this reason, all adjustable parameters have been estimated simultaneously utilizing all measurements from a given run.

In the same fashion as the segregated model, the estimation problem is minimized by determining the parameters for which the comparison model is sensitive. These parameters are considered the adjustable parameters, and the insensitive parameters are fixed at their nominal estimated values. Again, the sensitivities must be checked as operating conditions change. The sensitivity of the comparison model under batch operating conditions to the parameters has been determined by perturbing each parameter by ±10% and evaluating the change in the batch model solution. This analysis indicates that the model

Adjustable Parameter	Description
α_{11}	Maximum rate of immature cell reproduction (1/hr)
m_{i1}	Maximum rate of immature cell death (1/hr)
y_i	Immature cell number yield coefficient (1/g)
α_{12}	Maximum rate of maturation (1/hr)
k	Bacitracin production coefficient (g)
s_{i0}	Initial internal substrate concentration (g/l)

Table 4.9: Adjustable comparison model parameters.

is insensitive to several of the parameters. The perturbed solution for the substrate internalization parameters, α_{1i} and K_{1i}, are virtually identical to the unperturbed solution for all three fermentor outputs. The same insensitivity exists for the maturation inhibition coefficient, β_{12}.

For the remaining comparison model parameters, sensitivity analysis shows that relatively small changes in the parameter values leads to observable deviation of the comparison model solution from nominal profiles. For this reason, these parameters are considered significant due to their ability to affect the model solution, and they are treated as adjustable parameters. Based on a batch sensitivity analysis, consisting of 10% parameter perturbations, the sensitive parameters, tabulated in Table 4.9, are considered to be the comparison model adjustable parameters.

In this study, the role of the MBR model is to serve as a comparison of the effectiveness of the segregated and structured modelling approaches in predict-

Fixed Parameters		
Immature growth Michaelis constant	K_{1i}	0.008 (g/l)
Maximum substrate internalization	α_{1i}	8.71(1/hr)
Internalization Michaelis constant	K_{1i}	2.40(g/l)
Maturation inhibition coefficient	β_{12}	0.007

Table 4.10: Fixed parameter values for the modified Blanch and Rogers model based on low-aeration fermentation L-10-6.

ing antibiotic production. For this reason, the parameters of the MBR model have been identified only for the low-aeration fermentation experiments, where bacitracin production was significant. Using the batch fermentation data from experiment L-10-6, the maximum likelihood estimates for the fixed parameters were determined, and are shown in Table 4.10. Since batch fermentations were insensitive to these parameters, they were set to their nominal values and considered fixed. The maximum likelihood parameter estimates for the adjustable parameters were determined using replicated low-aeration fermentations. Estimates were determined using each batch data set individually, and grouped as replicates. The resulting parameters are shown in Table 4.11. The model fit to the low-aeration batch fermentation L-10-6 is shown in Figure 4.36. The comparison model does a reasonable job tracking the batch fermentation. The structured growth law allows the model to effectively capture the substrate and biomass profiles. However, an obvious problem is the inability of the structured model to predict a delay between peak biomass level and the onset of antibiotic production. Using the optimal parameters, the model prediction

Batch Run	Growth Parameter Estimates		
	α_{11}	m_{1i}	y_i
L-10-6	0.602 ± 0.108	0.076 ± 0.034	0.475 ± 0.292
L-10-11	0.606 ± 0.106	0.081 ± 0.026	0.559 ± 0.320
Combined	0.598 ± 0.054	0.091 ± 0.020	0.518 ± 0.211

Batch Run	Maturation Parameter Estimates	
	α_{12}	k
L-10-6	0.010 ± 0.044	$0.039 \pm \infty$
L-10-11	0.007 ± 0.020	$0.036 \pm \infty$
Combined	0.008 ± 0.019	$0.054 \pm \infty$

Table 4.11: Maximum likelihood parameter estimates for the structured comparison model based on low-aeration fermentations, L-10-6 and L-10-11.

precedes the appearance of bacitracin by approximately 5 hours.

Evaluation of the parameter confidence intervals for the comparison model reveals that the batch fermentation data do not allow for confident estimation of most of the adjustable model parameters. The most obvious shortcoming is the inability to estimate the antibiotic production parameter, k, with any level of confidence. The lack of confidence in k points to a major problem in the MBR model. Analysis of the model structure indicates that a single measure of the biomass, in this case total biomass, does not provide enough information to independently estimate all parameters of interest. The problem

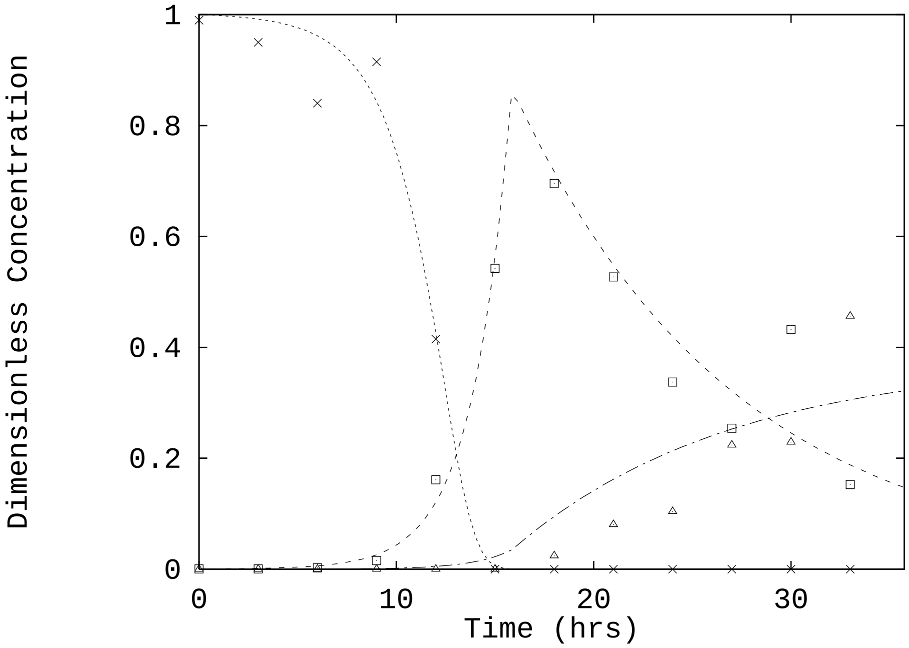

Figure 4.36: Fit of the MBR model to batch fermentation L-10-6. The total biomass counts substrate concentration and bacitracin concentration are represented by □, x, and △, respectively. The model fit to the data are represented by the corresponding lines.

is made clear by considering a batch fermentation. The total biomass is the sum of mature and immature cell numbers:

$$N_T = N_i + N_m \tag{4.62}$$

If the initial mature cell and antibiotic concentrations are negligible then integration of the batch antibiotic production equation gives:

$$A = \int_0^t k \frac{dN_m}{dt}\, dt \tag{4.63}$$

$$A = kN_m \tag{4.64}$$

Manipulation of Equation 4.64 and substitution into Equation 4.62 relates the antibiotic concentration and the immature cell concentration to total biomass measurement:

$$N_T = N_i + \frac{1}{k}A \tag{4.65}$$

However, since the biomass measurement consists only of N_T, then the relationship used to estimate k is underdetermined because the immature cell concentration is unmeasured. This indicates that continuous combinations of the parameter k and the immature cell maturation parameters can satisfy Equation 4.65, and there is no unique solution to the equation based on the available information. Unfortunately, this indicates that the available measurements are insufficient for identifying the relationship between antibiotic production and biomass maturation.

Formally, the MBR model can be classified as a compartmental model. Compartmental systems have been characterized by Jacquez [55] as collections of homogeneous, well-mixed subsystems, known as compartments, that interact by exchanging material between compartments and the surrounding environment. Using this definition, the comparison model is considered to be a two compartment model, with substrate uptake and antibiotic production representing interaction of the biomass compartments with the environment. Commonly in biological compartmental models, not all compartments can be measured, as is the case with the comparison model, where only the total biomass concentration is measured. In situations where complete process measurements are not available, it may not be possible to separately identify all the model parameters even with error free data. The *a priori* determination of identifiability is well established for linear models, with proofs of identifiability based on the uniqueness of the experimental transfer function [94, 2]. However, as a simple test to ascertain the identifiability of a model, Bates and Watts [7] suggest evaluating the rank of the parameter sensitivity matrix at a variety of design points. If the matrix does not achieve full rank at any of the design points, then it is assumed that the parameters are not locally identifiable. With the comparison model, singularity of the sensitivity coefficient matrix leads to a singular parameter covariance matrix. This signals that there exists continuous combinations of parameters that result in the same output profiles, and therefore independent estimation of the bacitracin production coefficient, k, and the maturation parameter, α_{12} was not possible using the available measurements.

4.5 Chapter Summary

The main topic of this chapter has identification and validation of both the segregated and structured comparison fermentation models, which were developed in Chapter 2. Steady-state and dynamic experimental fermentation data at high aeration conditions and batch data for low aeration conditions have been utilized in a maximum likelihood estimation scheme to obtain optimal parameter estimates for both models.

In the segregated model it is assumed that the coupling of growth and differentiation to antibiotic production is one way, with antibiotic having no effect on the latter processes. For this reason, estimation of the segregated model parameters is carried out in two phases. In the first phase, the growth and differentiation parameters were estimated using the biomass and substrate measurements. It was found that the segregated model was insensitive to the substrate internalization kinetic parameters, along with the vegetative growth Michaelis constant. These parameters were considered fixed, and the remaining vegetative growth and differentiation parameters considered adjustable. Adequate confidence was obtained for the adjustable growth and differentiation parameters, except for the sporulation initiation kinetics at low substrate concentration.

Examination of batch fermentations in combination with step-test and steady-state fermentation experiments indicate that a simple inverse relationship between sporulation initiation and growth rate is inadequate to characterize spore production data from a wide variety of operating conditions. To remedy this problem an empirical sporulation initiation function based on piecewise linear basis functions was used to relate sporulation to internal substrate concentration. Estimates indicate that a peak in the sporulation rate occurs at low but nonzero substrate level. A consequence of this sporulation function parameterization is the possiblity of steady-state multiplicity due to stabilizing low-spore production rates at low substrate conditions.

Significant differences in the growth and differentiation kinetics existed between high and low aeration experiments. At high aeration the vegetative growth rate and biomass yield were higher than at low aeration. It was also observed that the spore maturation time increased substantially at low aeration. A second significant difference between the aeration conditions was the expression of bacitracin only under low-aeration conditions.

After the growth and differentiation parameters were identified, the antibiotic concentration measurement was utilized to estimate the age-dependent bacitracin production function. Using singular value decomposition analysis, it was found that a consistent age-dependent antibiotic production function could be obtained from replicated batch data by suppressing the high noise directions in the bacitracin data. However, even with noise suppression, confident estimates of an age-dependent function could not be obtained. By parameterizing the production function as a constant, good fits to the batch data were obtained, with confident replicatable parameter estimates based on the batch antibiotic production data. This implies that the age-segregated model could be reduced to a delay-differential equation model, and still adequately track bacitracin production dynamics.

Utilizing the same fermentation data, the structured comparison model parameters were estimated. It was discovered that the comparison model structure did not allow for incorporation of the spore biomass measurement in the parameter estimation scheme. This resulted in unidentifiable antibiotic production and cell maturation parameters. It was also shown that the two-age compartmental model could not adequately describe delayed onset of antibiotic production in batch culture.

Chapter 5

Model Comparison and Optimal Control

Now that the age-dependent segregated model and the modified Blanch and Rogers (MBR) model have been developed and identified, it is appropriate to compare the advantages and disadvantages of each approach. In choosing comparisons, it must be remembered that the underlying motivation for the development of these models is to provide a mathematical characterization of the antibiotic fermentation suitable for incorporation into a model-based control scheme. With the control-based motivation in mind, the following issues have been considered suitable for comparison: model identifiability, ability to describe experimental observation, and suggested open-loop optimal control strategies.

5.1 Model Identification Issues

Model identification of both the segregated and MBR models was the main subject of Chapter 4. However, model identification also serves as a means by which the two modelling approaches can be compared. As has been explained, the goal of model identification is to estimate the adjustable model parameters based on the available data. The most desirable situation is to identify a model such that it fits the data well, and at the same time obtain parameter estimates that have a high degree of confidence. This indicates that the model structure is adequate, and the data contain sufficient information to estimate the model parameters with confidence. Although this is the ideal situation, a more realistic goal is to obtain confident estimates of the parameters to which the model is sensitive, and to accept poorly determined estimates of the insensitive parameters. Incomplete parameter estimation is tolerable as long as the parameters that have a significant impact on the important model states are well determined.

Because bacitracin production is the goal of the fermentations in this study, the model state of primary importance is bacitracin concentration. Therefore, an important aspect of model identification for this system is the ability to identify the model parameters that describe bacitracin production. Since bacitracin production is related to differentiation, both the differentiation and antibiotic production parameters are needed to predict antibiotic production. Identifiability of the parameters relating to antibiotic production provides a major contrast between the segregated and comparison models. As was discussed in Chapter 4, the inability to measure any aspect of cell maturation in the comparison model made it impossible to identify the dependence of maturation on substrate concentration, or to describe the proposed connection between maturation and bacitracin production. The ill-determined nature of the antibiotic production parameter was reflected by a singular parameter covariance matrix. It is also reflected by the fact that the estimates for the antibiotic production parameter, k, and the maximum rate of maturation, α_{12}, can vary in a continuous fashion and still fit the bacitracin data. Bates and Watts [7] term this situation as an unidentifiable model. The continuous relationship between k and α_{12} is illustrated by the dependence of the parameter estimates on the starting point of the estimation optimization. For a variety of initial guesses, a plot of the estimated bacitracin production parameter, k, versus the inverse of the maximum rate of cell maturation, $1/\alpha_{12}$, is shown in Figure 5.1. The apparent linear dependence indicates that the model predictions for the data depend on the product of the two parameters, such that parameter combinations satisfying $k\alpha_{12} = c$ do an equally good job describing the antibiotic concentration data. This situation results because of the lack of a measurement concerning the concentration of mature cells. Without any information concerning cell maturation, the estimation routine is free to specify the maturation and production parameter, as long as the product of the two results in an antibiotic production rate consistent with the antibiotic concentration data.

Without a measure of mature cell concentration, confident identification of the cell maturation model is not possible. This is a problem for two different reasons. First, the unclear relationship between cell maturation and cultural conditions makes it impossible to predict how cell maturation kinetics change under different operating conditions. This suggests the parameters for cell maturation will change depending on the experimental conditions used for their estimation. Second, the problems associated with unidentifiability of the antibiotic production and cell maturation parameters suggests that even

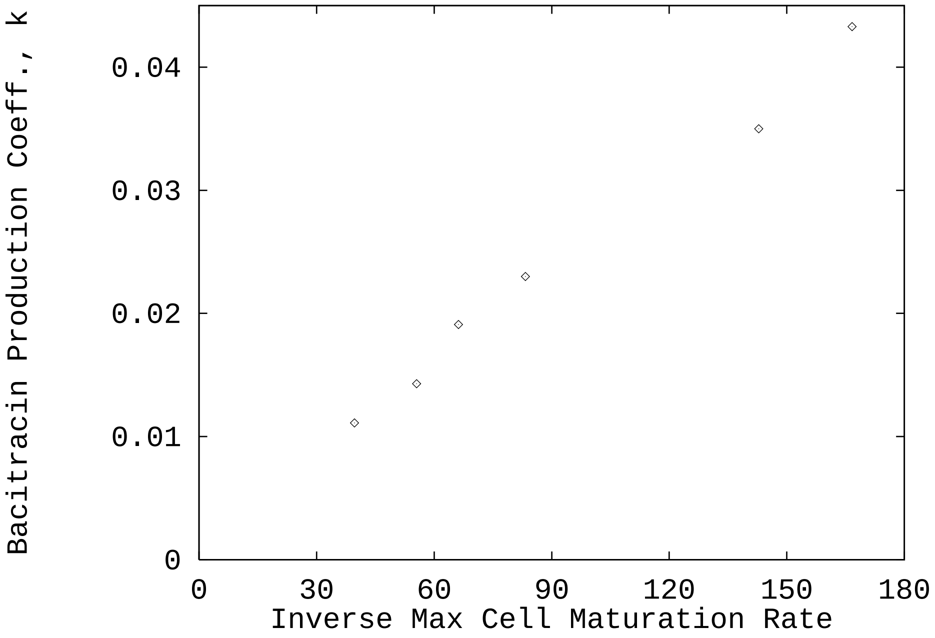

Figure 5.1: A plot of the estimated bacitracin production coefficient, k, versus the inverse of the estimated maximum cell maturation parameter, $1/\alpha_{12}$, for a variety of initial parameter guesses.

under consistent operating conditions, these parameters cannot be estimated confidently, and furthermore their estimates depend on the initial guess. The root of these problems is the lack of a measurement of the mature cell concentration. Although these problems result from insufficient measurement, the fact that the comparison model does not recognize the three cell morphologies forces the loss of the independent biomass information contained in the spore concentration measurement. Therefore, the non-physical basis of the comparison model structure creates problems in terms of model identification.

To rectify the problems associated with model identification, a logical adjustment to the comparison model would be to reconsider the model structure

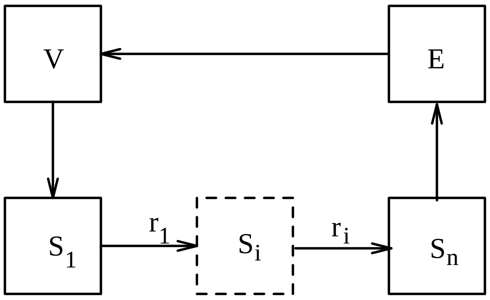

Figure 5.2: A compartmental model including sporangium age states representing intermediate stages of sporangium maturation. V - vegetative cells, E - endospores, S_1–S_n - sporangium age compartments.

and add individual compartments for each phase of the *Bacillus* life cycle. This would allow for a direct correspondence between the spore and nonspore biomass measurements, and would serve to provide independent information for the identification of the sporulation and antibiotic production kinetics. However, the delayed appearance of spores is difficult to model using a single state for the sporangium phase. Ollis [79] treated the delayed appearance of spores by introducing a lag term between biomass production and appearance of spores. However, assuming that spore production is simply proportional to delayed vegetative cell concentration fails to acknowledge any dependence of sporulation initiation on cultural conditions. Therefore, it would be expected that model parameters would vary substantially depending on operating conditions.

An alternative to the time-delay approach used by Ollis is the creation of sporangium age compartments representing intermediate stages of spore formation. The addition of age compartments is illustrated in Figure 5.2. This approach was used by Schulz et al. [93] with four age-states to model endotoxin formation in *B. thuringiensis.* However, the artificial representation of the continuous sporangium maturation process by distinct age bins introduces new parameters to describe the rate of transfer of cells from one stage to the next. This would again cause problems in the model identification due to a condition known as parameter exchangeability. Bates and Watts [7] define exchangeability as the condition where exchange of parameters results in identical model predictions for the measured states. This condition is exemplified by the multi-age structured model diagrammed in Figure 5.2. If the intermediate age compartments are unmeasured then switching the rate expressions describing the transfer of sporangia from one age bin to the next is undetectable in the data. Therefore, from Figure 5.2, exchange of the rate parameters r_1 and r_i would give the same model predictions for the measured states, and therefore individual identification of the parameters is not possible.

In contrast to the MBR model, the segregated model explicitly recognizes the existence of the three distinct *B. licheniformis* cell morphologies, and further, allows for the time delay between sporulation initiation and production of a mature spore. Because the segregated model formulation has a physical basis, it is possible to incorporate the spore biomass measurement data into the parameter estimation scheme. This independent information concerning the differentiation process is critical for confident estimation of the sporulation initiation parameters. Establishment of sporulation kinetics allows for estimation of the the dependence of antibiotic production on the differentiation. Although it was not possible to make definite statements concerning the age-dependence of antibiotic production, it was possible to confidently estimate the bacitracin production coefficient based on the zeroth moment of the sporangium age distribution. The combination of the antibiotic concentration data and the spore biomass measurement provide enough information to prevent the problems of parameter unidentifiability in the segregated model.

Regarding model identification of the segregated model compared to the multi-compartment sporangium model suggested by Schulz et al. [93], the natural incorporation of sporangium aging in the segregated model avoids the problems involved with estimation of parameters needed to describe the interchange of cells between age groups. This is because the population balance provides a continuous description of the sporangium age distribution, and therefore, explicitly accounts for continuous aging of cells. In contrast, the multi-compartment aging model is a lumping technique which reduces the order of the infinite dimensional age-distribution to a finite dimensional representation. The continuous description of the sporangium age distribution prevents the problem of parameter exchangeability, and allows for confident estimation of the model parameters using the available measurements.

5.2 Analysis and Comparison of Model Fits

From a control standpoint, a primary reason for developing a nonlinear process model is for the implementation of a model-based control scheme. Generally, this approach is taken when process nonlinearities are severe enough to threaten the stability of a linear controller, or when a wide range of operating conditions are anticipated, such that a single linear model is inadequate to describe the process in the operating region of interest. For the bacitracin system, the models developed in this work are intended to serve as tools for the development of open-loop optimal control strategies. The control strategies suggested by each model will be discussed in detail later in this chapter. However, since the accuracy of the process model has a significant effect on the ability of the controller to predict meaningful optimal control profiles, an important comparison tool is the relative ability of the models to describe the data.

The MBR model has difficulty accurately describing antibiotic production. This is probably due to inadequate age structure that does not allow for a delay between substrate exhaustion and maturation. As a result the predicted bacitracin production precedes observed production by several hours. Even though this result suggests problems with the model structure, a more rigorous analysis can be obtained by examining the model residuals. As mentioned in Section 4.1, the residual is defined as the difference between the model prediction and the measured value of the variable. If the model structure is correct, and the model parameters are close to their true value, then the residuals should reflect measurement error. In this case, normally distributed measurement error of zero mean has been assumed. A plot of the bacitracin concentration residuals versus time for the comparison model fits to fermentations L-10-6 and L-10-11 are shown in Figure 5.3. The residual plots show similar trends between the two fermentations, with the model recognizing the initial delay in the bacitracin production, followed by overprediction of production mid-way through the run and finishing by underpredicting bacitracin concentration. The presence of an obvious trend for both fits indicates that the residuals are not randomly distributed, but rather, they result from inadequacy of the comparison model structure. A simple analysis of the randomness of the residuals is obtained by examining the number of runs in the residual time series. A run consists of an uninterrupted sequence of residuals of the same sign. If the residuals are random then a certain number of runs would be expected for a given number of observations. A table of the cumulative distribution of the number of runs expected for a given number of observations is provided by Draper and Smith [26]. Ignoring the zero residuals, an analysis of the run distributions for the comparison model fits to fermentations

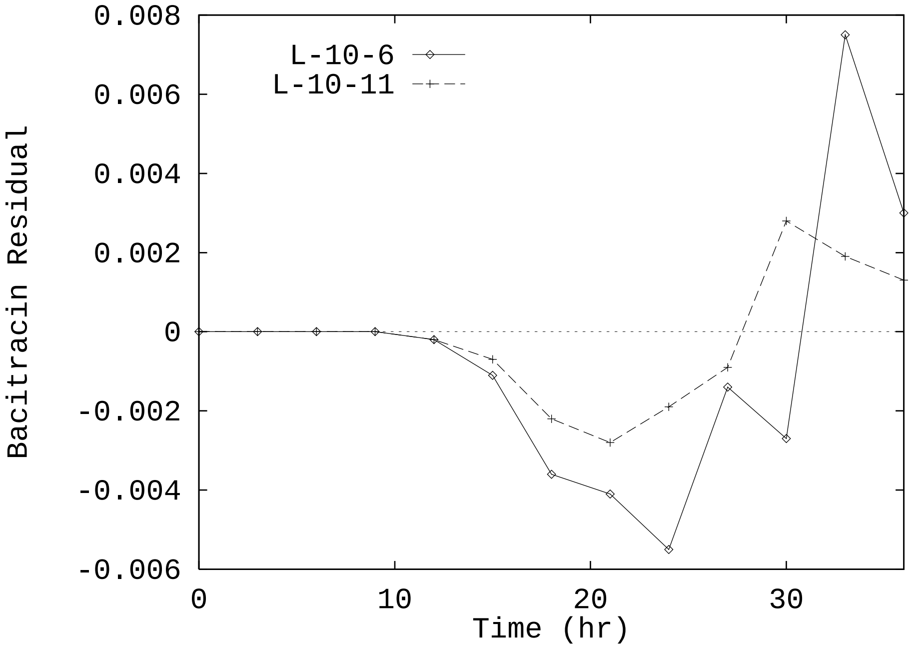

Figure 5.3: Residuals of the comparison model fit to bacitracin concentration data versus time.

L-10-6 and L-10-11 are summarized in Table 5.1. Analysis of the run distributions confirms the suspicion that the residuals are most likely not randomly distributed. Both fits have an unusually low number of runs, with the probability that random measurement error would result in 2 runs being about 5.6% for L-10-6 and approximately 2.5% for L-10-11. Based on this analysis it seems unlikely that randomly distributed errors could account for the residuals, and the most obvious explanation for the residual distribution is structural model error.

A similar analysis for the segregated model fit to the antibiotic concentration data has been carried out. The residual plots for fermentations L-10-6

Fermentation	L-10-6	L-10-11
+ Residuals	2	3
− Residuals	7	6
Runs	2	2
Probability	0.056	0.024

Table 5.1: The summarized statistical data for the comparison model residual runs.

Fermentation	L-10-6	L-10-11
+ Residuals	5	5
− Residuals	4	4
Runs	6	3
Probability	0.786	0.071

Table 5.2: The summarized statistical data for the segregated model residual runs.

and L-10-11 are shown in Figure 5.4. In contrast to the residuals obtained from the comparison model fits to the bacitracin data, the segregated model residuals are lower in magnitude and do not show the obvious trends that were apparent in with the comparison model. Analysis of the residual runs for the segregated model are given in Table 5.2. These results indicate that the residuals from both fits of the segregated model to the low-aeration fermentations have a reasonable number of runs, suggesting that the resulting residuals could

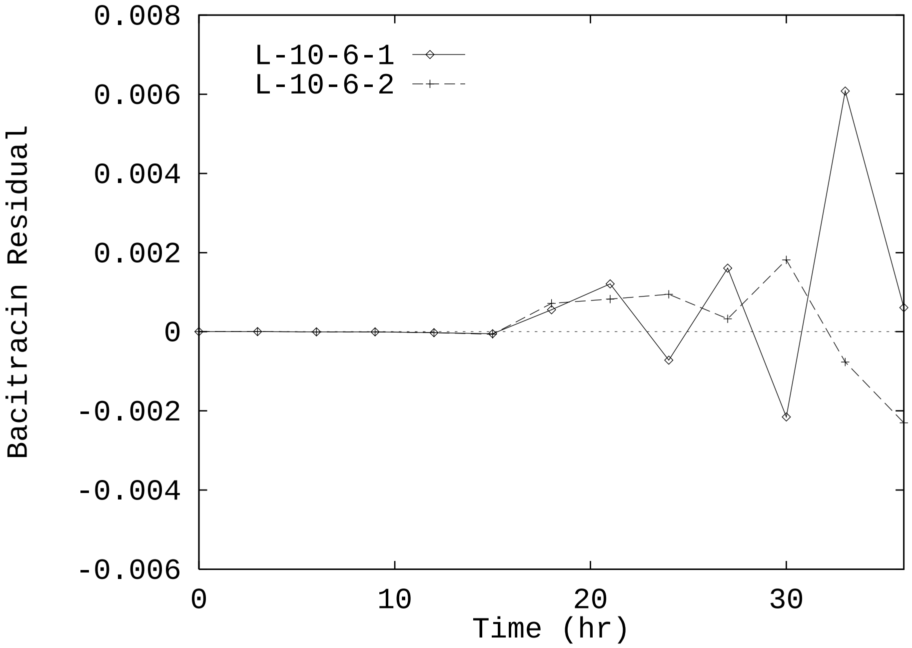

Figure 5.4: Residuals of the segregated model fit to bacitracin concentration data from fermentations L-10-6 and L-10-11 versus time.

be explained by random measurement errors. This is particularly true with L-10-6 where 6 runs were observed. For the fit to L-10-6, 6 runs or less would be expected 78% of the time if random measurement errors were responsible for the residuals. The results are less convincing for L-10-11, where 3 runs where observed. In the second case 3 runs or less would be expected about 7% of the time. Based on this analysis, it is not possible to reject the segregated model based on structural model error arguments. This is in contrast to the comparison model, which is a likely candidate for rejection based on analysis of the bacitracin concentration residuals.

5.3 Optimal Control Strategies

Analysis of the control strategies suggested by each model provides a means by which the advantages of the two modelling approaches can be effectively compared. If both models suggest similar control strategies, realizing nearly identical benefits, then the higher level of complexity and sophistication present in the segregated model is of little utility. However, if the inability of the more simple MBR model to completely capture the dynamics of the bacitracin system significantly affects the suggested control policy, then the additional work associated with development and identification of the segregated model may prove worthwhile.

Since the techniques utilized to obtain biomass and antibiotic concentration measurements require substantial processing time, the ability to feedback process information to an on-line fermentation control scheme is limited. Therefore, open-loop control is the focus of this discussion. The term open-loop suggests that a control law is determined off line, and is then applied to the process without allowing for alteration of the control strategy due to unmodelled processes disturbances or plant/model mismatch. In the presence of major process disturbances, or significant plant/model mismatch, the ability of an open-loop controller to achieve the desired goal can be significantly reduced. However, lacking the ability to feedback process information in a timely fashion, open-loop control studies can provide insight into effective control policies, and as measurement capabilities improve, controllers can be redesigned to take advantage of feedback.

The application of open-loop optimal control to secondary metabolite systems is common in the fermentation literature. A review of recent publications dealing with application of optimal control to secondary metabolite fermentations is provided by Fordyce et al. [33]. For a more general discussion concerning optimal control the reader is directed to Ray [90] and Bryson and Ho [3].

5.3.1 Bacitracin Optimal Control Problem

Both the age-structured and the age-segregated models attempt to describe the dependence of antibiotic production on cultural conditions. In particular, both models describe the relationship between limiting substrate concentration and cultural differentiation resulting in antibiotic production. Therefore, a logical application of control theory is the determination of optimal substrate feeding strategy resulting in attainment of some process goal. As a comparison between the two models, the process goal has been selected as maximization of bacitracin concentration at a predetermined final time. Therefore, the objective is to determined the time dependent feed flowrate, $F(t)$, of constant substrate concentration, s_f, such that maximum bacitracin concentration is achieved.

Objective Function. The objective function for the control problem of interest is defined as the bacitracin concentration, $A(t)$, at the final time $t = t_f$. and the optimal control problem is maximization of the objective function subject to bounds on the input flowrate and model equation constraints:

$$\max_{F(t)} \Phi = A(t_f) \tag{5.1}$$

$$\dot{\mathbf{x}} = \mathbf{f}(\mathbf{x}, \mathbf{x}', F, \theta) \tag{5.2}$$

$$F_{\min} \leq F(t) \leq F_{\max} \tag{5.3}$$

where $\mathbf{x}$ and $\mathbf{f}$ represent the model states and equations respectively, and $\boldsymbol{\theta}$ represent model parameters. By substituting the modelling equations from the segregated model or the MBR model into Equation 5.2 the optimal open-loop control problem is defined for each model. Ray [90] outlines several techniques for solving problems of this nature by explicitly satisfying the necessary conditions for optimality. These include control-vector iteration or formulation of a two-point boundary-value problem. As an alternative, Ray suggests a direct search optimization technique, termed control-vector parameterization. In this approach, a functional form of the optimal input profile is chosen in advance by parameterizing the manipulated variables as a linear combination of time-dependent basis functions. The open-loop control profile is determined using an optimization routine to find the set of basis-function coefficients such that the objective function is optimized. For analysis of the bacitracin maximization problem, the feed flowrate has been parameterized as a sequence of piecewise constants, and the magnitude of the flow steps have been treated as decision variables in the nonlinear optimization routine NPSOL [39]. Using piecewise constant flowrate profiles, the sensitivity of the optimal profile to the input parameterization can be examined by increasing or decreasing the number of steps in the optimization. Further, bounds on the input flowrate are easily implemented as simple bounds on the piecewise constants.

Sensitivity Issues. An important consideration when determining the optimal feeding strategy is the sensitivity of the optimum to the predicted profile. The sensitivity is important because it gives an indication of the accuracy needed while implementing the input profile, and helps to determine the time spans where control has a significant impact on the optimization goal. A detailed discussion of sensitivity is given by Fiacco [29], and an applications-oriented summary is provided by Eaton and Rawlings [28].

If the vector of piecewise constant flowrates are defined as $\mathbf{u}$, and the active model constraints are given by $\mathbf{h}$, then the optimal control problem can be stated in a general manner as:

$$\max_{\mathbf{u}} \Phi(\mathbf{x}, \mathbf{u}) \tag{5.4}$$

$$\text{s.t. } \mathbf{h}(\mathbf{x}, \mathbf{u}) = \mathbf{0} \tag{5.5}$$

However, using a sequential solution technique to solve the optimal control problem results in elimination of model equality constraints because the modelling equations are satisfied explicitly at each iteration of the optimizer. In the absence of model equality constraints and recognizing that the gradient of the objective function is zero at an optimum, then a quadratic approximation to the objective function results in the following relationship between a change in the input profile and a change in the objective function:

$$\delta\Phi \approx \delta\mathbf{u}^T \mathbf{H} \delta\mathbf{u} \tag{5.6}$$

where $\mathbf{H}$ represents the Hessian matrix containing the second derivatives of the objective function with respect to the input flowrates. If it is assumed that the input variables are independent, implying that alteration of the feed flowrate at a given step has little effect on the optimal feed flowrate at a later time, then Equation 5.6 can be used to compute the approximate deviation of the optimal flowrates that will result in a predetermined deviation of the objective function. Using Equation 5.6, it is possible to compute an approximate bound on the optimal input profile:

$$\delta u_i = \sqrt{\frac{\delta\Phi}{H_{ii}}} \tag{5.7}$$

This bound indicates the sensitivity of the objective function to input flowrates, and provides a basis for determining the inputs that need tight control.

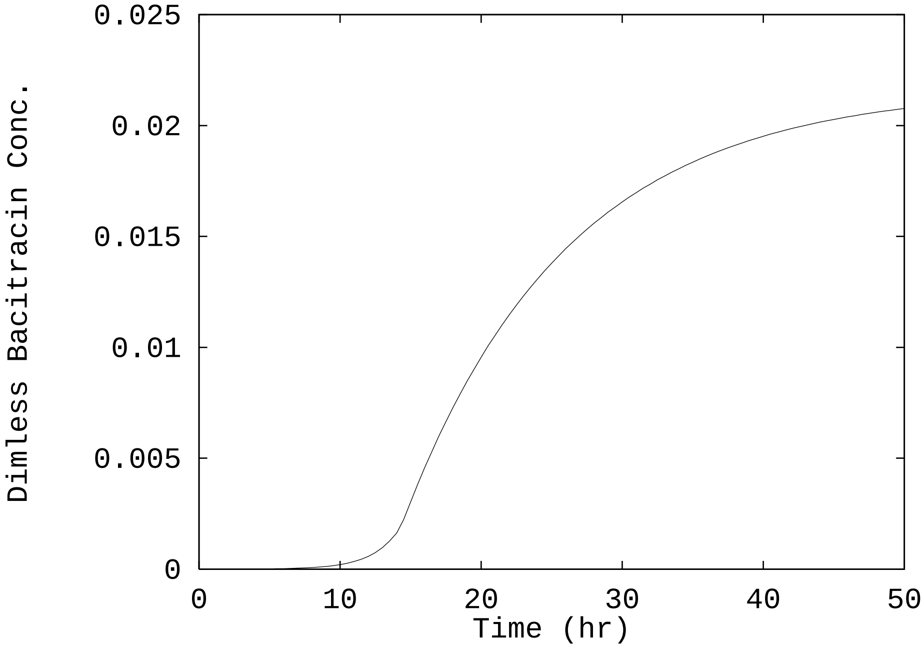

Figure 5.5: The predicted bacitracin concentration profile based on batch fermentation determined as optimal based on the MBR model.

5.3.2 Comparison Model Optimal Control Strategy

Computation of the optimal open-loop feeding strategy for a 50 hour fermentation, based on the MBR model, suggests that batch fermentation is the most effective operating policy for maximization of bacitracin at the final time. The predicted batch antibiotic profile is shown in Figure 5.5. Under batch operating conditions, the model routine predicts a final bacitracin concentration of 0.027 dimensionless bacitracin units, corresponding to 0.054 g/l.

Convergence to a batch operating strategy for the optimal control problem was achieved from a variety of initial profile guesses and also for 5 and 10 step input parameterizations. Based on these results it appears the suggested strategy is to allow rapid vegetative growth until limiting substrate is exhausted. At the point of substrate exhaustion, the Dawes and Thornley [22] cell maturation model exhibits a maximum, and therefore, the culture exhibits a maximal rate of cell maturation. Since bacitracin production is considered proportional to cell maturation, in batch fermentation the cells are induced to maximal bacitracin production. At any point during the fermentation, initiation of substrate feeding suppresses cell maturation, and therefore lowers the rate of bacitracin production. Also, addition of the bacitracin-free feed stream dilutes the current bacitracin level, reducing the antibiotic concentration at the final time.

The sensitivity of the bacitracin concentration at the final time to the batch operating policy has been examined by determining bounds on the flowrate inputs. Using Equation 5.7 with the assumption of independent inputs, bounds on the input flowrate steps that would induce a change of 1% in the final bacitracin concentration are shown in Figure 5.6. The bounds on the batch input profile indicate that the final bacitracin concentration is highly sensitive to the batch operating policy. Small inlet flowrates lead to a 1% reduction in the final bacitracin concentration. This analysis indicates that the final concentration is more sensitive to deviations later in the fermentation than at the beginning. This is because the antibiotic concentration is particularly susceptible to washout at the end of the fermentation when production levels are low.

5.3.3 Segregated Model Optimal Feeding Strategy

In the same manner as the comparison model, the optimal substrate feed profile for maximization of bacitracin concentration in a 50 hour fermentation

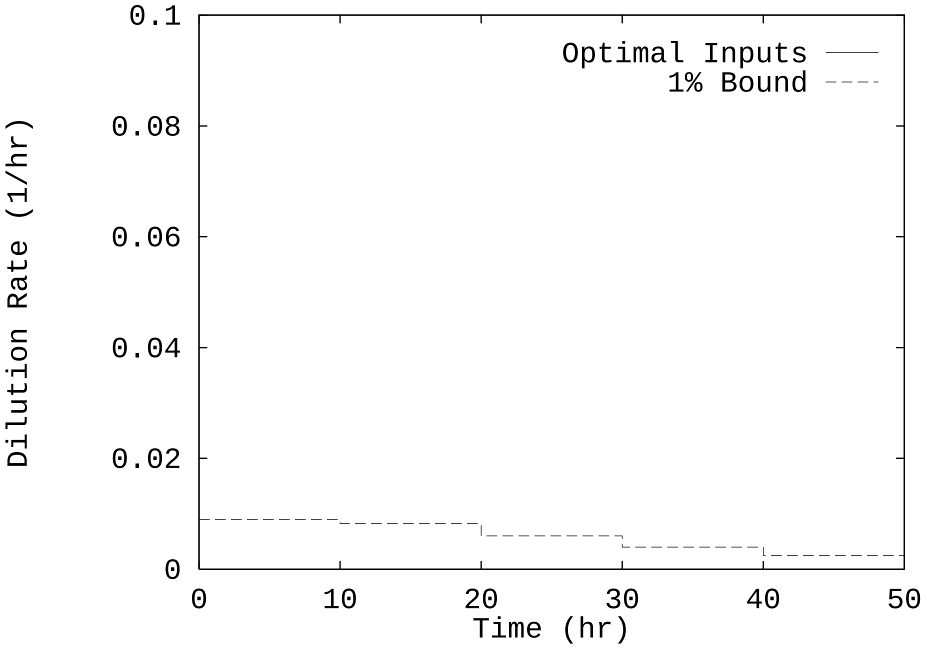

Figure 5.6: Bounds on the feed flowrate around the optimal batch operating policy that would induce a 1% reduction in final bacitracin concentration.

has been determined based on the segregated model. For 5 and 10 step piecewise constant inputs, the optimal open-loop feeding strategies are shown in Figure 5.7. In contrast to the comparison model, the segregated model suggests a non-batch operating policy for maximization of final bacitracin concentration. While the input policies for 5 and 10 flowrate steps differ slightly, the resulting model predictions for bacitracin concentration indicate that approximately 30% higher bacitracin concentration over batch levels could be realized using either of the optimal input profiles. The differences in the 5 and 10 step input profiles result from the different levels of parameterization, with a slightly higher antibiotic concentration realized using more inputs. However,

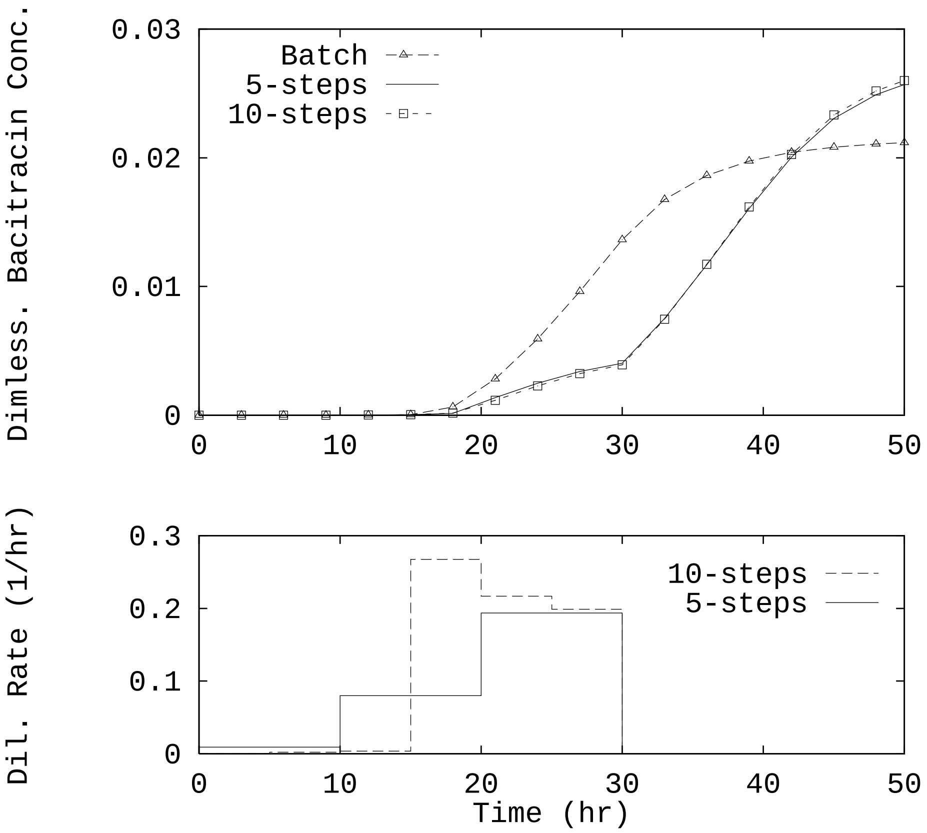

Figure 5.7: Optimal feeding policy for maximization of bacitracin using 5 and 10 step piecewise constant inputs based on the segregated model. For comparison purposes, the batch bacitracin profile is also shown.

the slight increase obtained with 10 steps over 5 is insignificant according to model simulations.

Even though the exact feeding policies computed for 5 and 10 steps differ, the basic strategy is similar in both cases. The advantages of feeding over batch operation are illustrated by a comparison of the vegetative cell and external limiting substrate concentration between batch fermentation and the

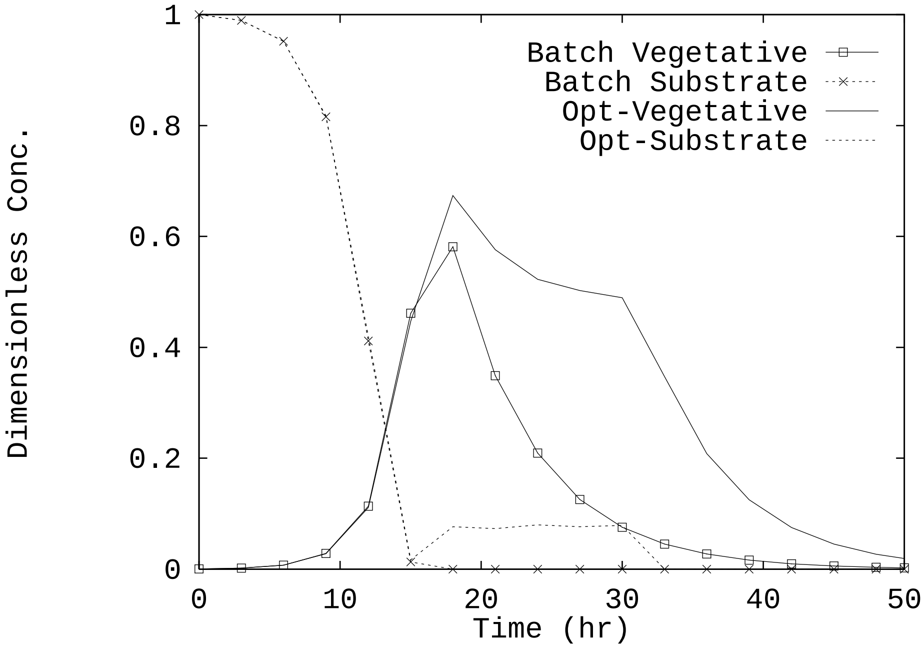

Figure 5.8: Comparison of batch and optimal vegetative and substrate concentration profiles for the optimal 10-step inlet feed policy.

optimal 10-step feed policy shown in Figure 5.8. The optimal feeding strategy is to start the fermentation in or close to batch mode. Therefore, the batch and optimally-fed fermentations show similar rapid cell growth and substrate consumption at the beginning of the fermentation. Batch operation is continued until substrate is nearly exhausted, at which point the optimal strategy varies from batch fermentation. When substrate exhaustion approaches, the feed rate is stepped up to a moderate level, thus maintaining limiting substrate concentration at a high enough level to promote sporulation, while preventing the rapid rate of cell death typical of batch mode. The difference in the optimal feeding policy and the batch fermentation becomes evident at about 15 hours,

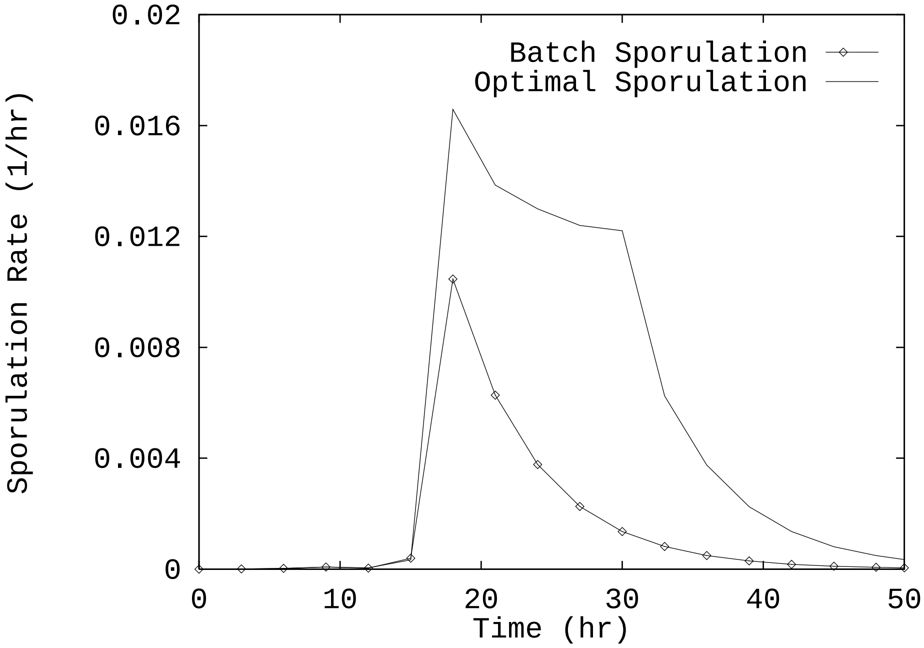

Figure 5.9: A comparison between the optimal sporulation rate and the predicted batch sporulation rate based on the segregated model.

when the vegetative cell concentration of the fed fermentation sustains a high level, and the associated substrate concentration climbs to a low, but non-zero level, avoiding rapid cell death exhibited by the batch culture. The moderate feed rate continues until a majority of the cells have sporulated, and antibiotic production is maximized. A comparison between the fed-fermentation sporulation rate, and that predicted for batch operation is given in Figure 5.9. This figure shows that by starting substrate feeding at the point of substrate exhaustion, the rate of sporulation can be substantially increased. This is because substrate levels can be controlled so that sporulation is favored over cell death. This is the primary advantage of the feeding strategy in maximizing bacitracin concentration. By avoiding massive cell death more cells begin the differentiation process and contribute to bacitracin production. Moderate feeding continues until the competing processes of bacitracin washout, caused by feeding of an antibiotic free stream, and increased bacitracin production from sustained sporulation begin to cancel. At that point, feeding is stopped and bacitracin concentration is allowed to buildup from production of the sporangium population.

In the same manner as the MBR-based optimal feeding strategy, the sensitivity of the control objective to the computed input profile for the segregated model has been evaluated. Bounds on the 5 step input profile indicating the change in each flow step that would result in a 1% change in the final bacitracin concentration are shown in Figure 5.10. The sensitivity analysis indicates that the final bacitracin concentration is fairly sensitive to the input profile, with tight bounds on optimal feed flowrates. Similar to the comparison model, the bounds on the flowrate are tighter at the end of the fermentation than at the beginning. As with the MBR model, this is due to the dominance of washout phenomenon as sporangium production rate declines at the end of the fermentation.

Comparison of the optimal feeding strategies suggested by the modified Blanch and Rogers model and the segregated model highlight a major difference in the two approaches. The ability of the segregated model to recognize a non-monotonic dependence of sporulation initiation on substrate concentration yields a optimal feed strategy that forces limiting substrate concentration to a level that favors sporulation over cell death, and therefore takes advantage of the maximum in sporulation initiation to produce more antibiotic. In contrast to this, the structure of the comparison model does not allow for adequate identification of the cell maturation model, and thus the model sug-

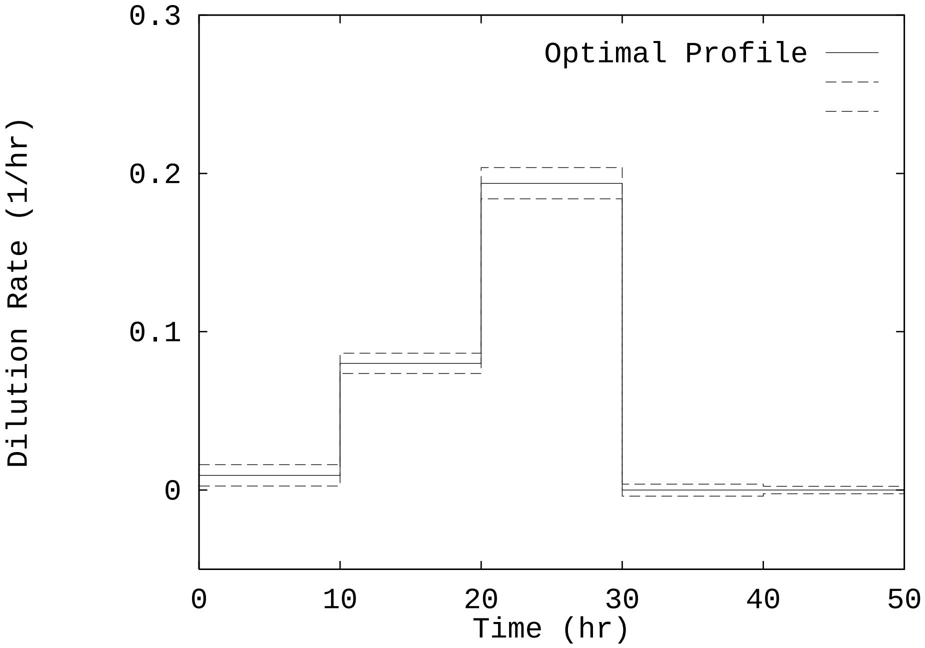

Figure 5.10: Bounds on the input feeding profile that would result in a 1% change in the final bacitracin concentration profile.

gests maximum maturation occurs at substrate exhaustion. This leads to the prediction that bacitracin is maximized during batch operation.

5.4 Chapter Summary

Comparisons of the modified Blanch and Rogers model and the age-segregated model with respect to identifiability, accuracy of model fit, and open-loop optimal control strategies have been the subject of this chapter.

Concerning model identification, a basic conclusion is that the model structure has a significant impact on model identification. In the case of the MBR model, the lack of sufficient morphological structure prevents utilization of the spore biomass measurement resulting in inadequate identification of the connection between cell maturation and bacitracin production. Because of this, the antibiotic production and cell maturation parameters are unidentifiable, with parameter estimates depending on the initial guess for the parameters.

In contrast, the segregated model accounts for the morphological changes in the *Bacillus* life cycle, allowing for adequate identification of sporulation initiation kinetics and antibiotic production parameters.

Further, analysis of the effectiveness of the two models in fitting bacitracin production data suggest that the simplistic two-age-group structure of the comparison model is insufficient for describing the delayed appearance of bacitracin in batch culture. This is indicated by the lack of runs in the batch bacitracin residuals, suggesting nonrandom residuals symptomatic of structural model error. A similar analysis of the segregated model shows smaller bacitracin residuals than observed with the MBR model, and also the presence of a significantly larger number of residual runs indicative of residuals representing measurement error.

Finally, the open-loop optimal feeding strategies for maximization of bacitracin at the final time were computed for both modelling approaches. Based on the comparison model, a batch operating strategy was determined to be optimal for bacitracin maximization. In contrast, a non-batch feeding profile was suggested by the segregated model. The different control strategies hinge on the respective model's description of the connection between substrate concentration and cell differentiation. For the comparison model, the ill-conceived model structure prevents adequate model identification. This leads to acceptance of the monotonic decreasing relationship between substrate concentration and cell maturation, which implies that the maximum rate of bacitracin production is achieved after total substrate exhaustion. The ability of the segregated model to better identify the connection between substrate and differentiation allowed for prediction of non-batch optimal feeding strategies for improved fermentor performance. The segregated model suggests an optimal substrate feeding such that feed is utilized to avoid substrate exhaustion and promote sporulation over cell death. This policy predicts a 30% increase in bacitracin concentration at termination of the fermentation.

Chapter 6

Conclusions and Recommendations

The goal of this work has been to develop and explore the utility of a segregated population model for bacterial secondary metabolite production. The motivation for this goal has been the desire to evaluate the ability of segregated models to characterize observed growth and production behavior associated with bacterial secondary metabolite systems. As a part of the evaluation process, the advantages and disadvantages of the segregated modelling approach compared to the more common, but less sophisticated structured secondary metabolite models have been examined.

As a model system the production of the peptide antibiotic bacitracin by *Bacillus licheniformis* was chosen as a means of comparison between the two modelling approaches. The *B. licheniformis* system was considered a good choice for comparison purposes for several reasons. The product of interest, bacitracin, has industrial relevance, with both medical and veterinary applications. Further, bacitracin production is associated with sporulation, leading to a possible connection between the findings of this study and other sporulation-related systems. This connection of bacitracin production to the *Bacillus* differentiation cycle also presents a clear motivation for application of the population balance to model the purported age-dependent product production kinetics. Finally, an existing structured model, found in the fermentation literature, for production of an antibiotic closely related to the bacitracin fermentation was considered adaptable to serve as a comparison model for examination of the relative advantages and disadvantages of the structured models and segregated models.

The basis of the segregated model developed in this study was the explicit representation of the three distinct cell morphologies found during the *Bacillus* life cycle. A simple two-compartment, structured model was conceived to represent the vegetative biomass, along with an unstructured state for characterization of the spore biomass fraction. The sporangium cells were considered distinguishable based on progress through the differentiation pathway. Therefore, the sporangium biomass was characterized using an age-dependent number density state, with sporangium age reflecting time since commitment to sporulation. In addition to the 3-state representation of the biomass, model states representing the external and internal limiting substrate concentrations, and bacitracin concentration were also included in the segregated model.

To describe the interrelationships between the different phases of biomass and the cell environment, constitutive equations were proposed. Based on a single limiting-substrate assumption, Monod saturation kinetics were used to describe substrate internalization and vegetative cell growth, and an endogenous metabolism term was added to the growth law to represent cell death. To characterize commitment of vegetative cells to sporulation, an empirical piecewise linear sporulation initiation function was proposed. Finally, the age-dependent bacitracin production rate was modelled using a linear combination of polynomial basis functions with experimentally determined coefficients.

With states representing the three biomass morphologies, substrate concentration, and antibiotic, the dynamic segregated fermentation model was developed for a continuous stirred-tank fermentation vessel. This was achieved by forming material balances on the unstructured biomass states, the bacitracin concentration, and the limiting substrate states. A population balance on the sporangium age distribution, accounting for birth of new sporangium through initiation, and removal of cells through spore maturation, was performed to describe the rate of change of the sporangium age density. The fermentation model was completed by integration of the microscopic material and population balance over the volume of a stirred-tank fermentation vessel.

By using orthogonal collocation on finite elements to discretize the sporangium age distribution, the bacitracin production integral was approximated. This was incorporated into a numerical integration scheme, using a semi-analytical solution to the sporangium population balance equation to obtain dynamic descriptions of the segregated fermentation system. Steady-state solutions were obtained by incorporating the discretized model into an algebraic equation solver.

A structured comparison model was developed by modifying a two-age compartmental model for production of gramicidin S from *Bacillus subtilis* developed by Blanch and Rogers [11]. Modifications included a structured growth law concentrated in the immature biophase, and utilization of a maturation function based on a linear dependence between growth and maturation. Bacitracin production was assumed to be proportional to the rate of cell maturation. Both dynamic and steady-state comparison model solutions were obtained using straightforward numerical solutions techniques.

To obtain data for identification of both models a laboratory-scale fermentation apparatus was constructed. The fermentation apparatus consisted of a 2 liter, aseptic vessel with associated temperature and pH control hardware. The fermentor was equipped to run in batch or continuous mode. Sterile nutrient medium and air were fed to the fermentor in manual control modes. To access bacterial growth and differentiation, the differential heat sensitivity of vegetative and spore biomass was utilized in a plate count assay procedure. Bacitracin concentration was assayed using the agar-plate diffusion method, and limiting substrate concentration was obtained using an off-line glucose analyzer.

A two-phase approach was used for identification of the segregated model parameters. Assuming that bacitracin has an insignificant effect on growth and differentiation kinetics, the biomass and substrate concentration measurements were utilized to estimate growth and differentiation parameters. Following identification of the growth and differentiation models, bacitracin production kinetics were estimated using bacitracin concentration measurements alone. Initially, batch fermentation experiments were utilized to obtain primary parameter estimates for model identification. Initial experiments were done under high aeration conditions, for which little or no bacitracin was produced. Based on these results only growth and differentiation were accessed under high-aeration conditions. Sensitivity analysis of the segregated model parameters indicated a primary dependence of the model solution on the maximum vegetative growth rate, maximum cell death rate, growth yield coefficient, and the spore maturation time. The maximum likelihood estimates of the sensitive and insensitive model parameters were obtained from the batch data. After the initial estimation, the insensitive model parameters were considered fixed, and any model adjustments due additional fermentation data were seen only in the sensitive model parameters. Replicated high-aeration batch fermentations showed close resemblance between runs, and the segregated model was able to effectively track the dynamic biomass, and substrate concentration measurements.

To improve confidence in the model parameters, fermentation data from a variety of operating conditions was incorporated in the estimation scheme. Through the inclusion of dilution step-test experiments, and steady-state biomass data for a variety of dilution rates confident estimates of the adjustable model parameters was obtained. The data also indicate that there exists a apparent maximum in sporulation initiation rate at a low, but non-zero substrate concentration.

Switching to low-aeration conditions, batch fermentations show reduced growth rates and cell yields, but measurable levels of bacitracin were produced. Unfortunately, steady-state conditions for constant nutrient were not established under low aeration. This most likely resulted from the inability to maintain constant low air flowrates using manual air flow control. In light of this, batch experiments alone were used to access the age-dependent bacitracin production kinetics. The relative insensitivity of the bacitracin concentration state to the shape of the production function, in combination with noise in the bacitracin concentration data, prevented confident determination of the age-dependent antibiotic production function. However, using singular value decomposition (SVD) to detect and remove the ill-conditioned noise directions from the bacitracin data, a consistent shape for the production function was estimated. Although the SVD analysis yielded interesting results concerning the possible shape of an age-dependent production function, it does nothing to improve parameter confidence. Therefore, considering the general insensitivity of the bacitracin concentration to the shape of the production function, it was possible to adequately model the dynamic antibiotic data assuming bacitracin production was proportional to the total sporangium concentration. Since this represents a constant age-production function, the data from this study do not allow for confirmation of the theory that bacitracin production kinetics are dependent on the stage of development in the differentiation cycle.

In contrast to the segregated model, the comparison model parameters could not be adequately identified from the available measurements. This resulted from the lack of a mature cell biomass measurement, resulting in unidentifiable cell maturation and bacitracin production parameters. Therefore, parameter estimates depended on the initial guess used in the estimation algorithm, with the measurements only being sensitive to a combination of the model parameters. Furthermore, it was determined that the two age-compartment model structure was inadequate to represent the delay between fermentor inoculation and the appearance of antibiotic.

As a comparison between the two models, the open-loop optimal feeding strategies for maximization of bacitracin concentration at a predetermined final time was determined for both models. The time-dependent feeding profile was parameterized as a sequence of piecewise constants, and the optimal piecewise constant flowrates were found using a successive quadratic programming optimization algorithm. The optimal profiles computed for the two models differed substantially, with the structured comparison model predicting a batch fermentation strategy for maximization of bacitracin. In contrast, the segregated model open-loop feeding policy suggested batch operation until limiting substrate was nearly exhausted, then moderate feeding to maintain a low substrate concentration thus favoring sporulation over cell death. Using this policy the segregated model indicates the potential for a 30% increase in bacitracin concentration for the given final time.

Based on this work, many interesting questions for further study have arisen. First, the proposed maximum in sporulation initiation could be studied with low-dilution rate steady-state runs. As part of this examination, experimental verification of steady-state multiplicity suggested by the segregated model, would prove interesting. Currently, steady-state multiplicity has not been reported for *Bacillus* systems, and the confirmation of such phenomenon would pose interesting questions concerning the regulation of sporulation.

Further, the dependence of bacitracin production on aeration conditions raises the question of the role of dissolved oxygen in the processes cell growth, differentiation, and antibiotic production. Although aeration was shown to have a significant effect on the bacitracin fermentations, the examination of only two aeration rates leaves these effects relatively uncharacterized. Adaption of the fermentation apparatus to measure and control dissolved oxygen concentration would provide the opportunity to gain insight into the role of oxygen in the bacitracin fermentation kinetics. With this information, the segregated model could be modified to include oxygen effects, allowing for a more complete description of the fermentation characteristics over the operating space.

The improved productivity predicted by the segregated model through open-loop optimal control provides a logical experimental path for further study. However, prior to testing feeding strategies it would be appropriate to develop improved antibiotic production media to achieve industrially observed bacitracin titers. Then, based on the model identified for the improved medium, optimal control strategies could be experimentally examined to determine whether increased productivity was truly realizable. Concerning additional improvement in control, a second manipulated variable for control purposes could be obtained by the addition of aeration measurement and control capabilities. Inclusion of oxygen effects in the model could provide a significant improvement in productivity due to the apparently counteractive effects of dissolved oxygen on growth and antibiotic production kinetics.

In conclusion, although incorporation of age-dependent antibiotic production phenomenon was relatively unimportant for the prediction of antibiotic concentration, the segregated model structure did allow for for the description of sporangia and spore concentration dynamics over a range of operating conditions. This characterization proved important in terms of model identification, and predicted optimal control strategies. Therefore, it is felt that this study shows that the extra effort needed to develop and identify a segregated model can prove worthwhile.

Nomenclature

A bacitracin concentration (g/l)

$\mathbf{a}$ batch antibiotic production measurements

a_{11} specific rate of immature cell reproduction (1/hr)

a_{12} specific rate of cell maturation (1/hr)

a_{21} specific rate of mature cell to immature cell division (1/hr)

$\mathbf{B}$ semidefinite weighting matrix

B birth mechanisms in the population balance ($1/(\mathrm{l} \cdot \mathrm{hr})$)

b bacitracin zone inhibition proportionality factor (I.U.bacitracin/ml)

$\mathbf{c}$ vector of parameter constraint equations

D death mechanisms in the population balance ($1/(\mathrm{l} \cdot \mathrm{hr})$)

D fermentor dilution rate (inverse residence time) (1/hr)

d inhibition zone diameter (mm)

$\mathbf{e}$ vector of model residuals

$\mathbf{f}$ vector of model equations

F_i inlet fermentor feed flowrate (l/hr)

F_o outlet fermentor feed flowrate (l/hr)

$\mathbf{H}$ hessian matrix

$\mathbf{h}$ model equations posed as optimization constraints

$\mathbf{i}$ unit parameter coordinate vector

k bacitracin production coefficient g

K_g spore germination Michaelis constant (g/l)

K_i substrate internalization Michaelis constant (g/l)

K_v vegetative growth Michaelis constant (g/l)

K_{1i} substrate internalization Michaelis constant (g/l)

K_{11} immature reproduction Michaelis constant (g/l)

L likelihood function

L_i polynomial basis function

m number of measurements per experiment

m bacitracin standard curve exponent parameter (1/mm)

m_v specific rate of endogenous metabolism (1/hr)

m_{i1} specific rate of immature cell death (1/hr)

n number of experiments in a given run

N normal probability distribution

N_i number concentration of immature cells (1/l)

N_m number concentration of mature cells (1/l)

N_T total cell number concentration (1/l)

p probability distribution

s_c critical substrate concentration needed to sustain growth (g/l)

s_e external substrate concentration (g/l)

s_f substrate feed concentration (g/l)

s_i internal substrate concentration (g/l)

$\mathbf{S}$ batch antibiotic production model

S parameter confidence region

t time (hr)

$\mathbf{U}$ singular value decomposition left singular vectors

$\mathbf{u}$ vector of manipulated variables

$\mathbf{v}$ eigenvector

$\mathbf{V}$ singular value decomposition right singular vectors

$\tilde{\mathbf{V}}$ measurement error covariance matrix

$\mathbf{V}_\theta$ parameter covariance matrix

V_r fermentor volume (l)

w_i Guassian quadrature weight

W close data subset

$\mathbf{W}$ parameter sensitivity matrix

X_e spore number concentration (1/l)

X_s sporangium number density $(1/(\mathrm{l}\cdot\mathrm{hr}))$

X_v vegetative cell number concentration (1/l)

$\mathbf{x}$ vector of external population coordinates

$\mathbf{x}$ vector of model states

$\mathbf{y}$ vector of model outputs

$\mathbf{y}$ vector of internal population coordinates

y_a antibiotic yield coefficient (1/g)

y_g germination yield coefficient (1/g)

y_i immature cell yield coefficient (1/g)

y_s sporulation yield coefficient (1/g)

y_v vegetative cell number yield coefficient (1/g)

y_{anti} antibiotic concentration measurement (I.U.bacitracin/ml)

$\mathbf{z}$ vector of independent coordinates in the population balance

Greek/Script Symbols

α_g maximum specific rate of spore germination (1/hr)

α_i maximum specific rate of substrate internalization (1/hr)

α_j coefficient of the jth age-dependent bacitracin production basis function

α_s maxium specific rate of sporulation initiation (1/hr)

α_v maximum specific rate of vegetative cell growth (1/hr)

α_{1i} maximum rate of substrate internalization (1/hr)

α_{11} maximum rate of immature cell reproduction (1/hr)

α_{12} maximum rate of immature cell maturation (1/hr)

β_s sporulation inhibition coefficient

β_{12} maturation inhibition coefficient

γ parameter confidence probability

γ_j coefficient of jth sporulation initiation basis function

$\boldsymbol{\epsilon}$ vector of measurement errors

$\boldsymbol{\theta}$ vector of model parameters

$\mathcal{L}$ concentrated likelihood function

λ eigenvalue

$\boldsymbol{\mu_a}$ vector of antibiotic production coefficient

μ_a specific rate of bacitracin production (1/hr)

μ_g specific rate of spore germination (1/hr)

μ_i specific rate of substrate internalization (1/hr)

μ_s specific rate of sporulation initiaiton (1/hr)

μ_v specific rate of vegetative cell growth (1/hr)

ν measurement error variance

$\boldsymbol{\Sigma}$ singular value matrix

τ sporangium age (hr)

τ_m sporangium maturation age (hr)

ϕ_j jth sporulation initiation basis function

Φ optimization objective function

$\boldsymbol{\psi}$ measurement error distribution parameters

Subscripts/Superscripts

0 initial condition

$\hat{}$ dimensionless quantity

$'$ derivative with respect to the sporangium age

$\tilde{}$ observed value of measurement including measurement error

* optimal value

Appendix A

Spore Germination Data

The spore germination data for germination experiments B-Spo-1 and B-Spo-2 are presented in this appendix.

A.1 Spore Germination Fermentation B-Spo-1

Spore germination experiment B-Spo-1 was performed under the following conditions:

- temperature: 37° C
- medium: 0.15% glucose minimal medium
- pH: maintained at 7.0 using 1.0 molar NaOH
- aeration: high
- inoculum: 50; ml spore suspension

Time (hr)	Spore Count (1/ml)
0.0	1.56×10^6
1.0	1.79×10^6
2.0	1.62×10^6
4.0	1.71×10^6
6.0	1.68×10^6
8.0	1.49×10^6

Table A.1: Data from spore germination experiment B-Spo-1.

A.2 Spore Germination Fermentation B-Spo-2

Spore germination experiment B-Spo-2 was performed under the following conditions:

- temperature: 37° C
- medium: 0.15% glucose minimal medium
- pH: maintained at 7.0 using 1.0 molar NaOH
- aeration: high
- inoculum: 50; ml spore suspension

Time (hr)	Spore Count (1/ml)
0.0	1.80×10^6
10.0	1.45×10^6
11.0	1.40×10^6
12.0	1.53×10^6
13.0	1.23×10^6
14.0	1.40×10^6
15.0	1.42×10^6

Table A.2: Data from spore germination experiment B-Spo-2.

Appendix B

High Aeration Batch Fermentation Data

The batch fermentation data for the high aeration fermentation experiment B-6-14 are presented in this appendix.

B.1 Batch Fermentation B-6-14

Batch fermentation B-6-14 was performed under the following conditions:

- temperature: 37° C
- medium: 0.15% glucose minimal medium
- pH: maintained at 7.0 using 1.0 molar NaOH
- aeration: high
- inoculum: 5 ml vegetative inoculum

Time (hr)	Spore Count (1/ml)	Nonspore Count (1/ml)	Glucose (g/l)
0.0	1.50×10^1	4.49×10^5	1.50
3.0	9.50×10^1	1.07×10^6	1.34
6.0	2.37×10^2	4.49×10^5	1.29
9.0	2.05×10^2	8.07×10^6	0.69
12.0	2.01×10^2	3.81×10^8	0.01
15.0	3.58×10^2	1.07×10^9	0.00
18.0	7.17×10^2	7.98×10^8	0.00
21.0	4.04×10^4	5.32×10^8	0.00
24.0	9.24×10^6	4.44×10^8	0.04
27.0	4.76×10^7	3.87×10^8	0.03
30.0	5.25×10^7	2.74×10^8	0.03
33.0	5.30×10^7	2.56×10^8	0.03
35.8	7.26×10^7	1.69×10^8	0.02

Table B.1: Data for high aeration batch fermentation B-6-14.

Appendix C

Sporulation Step-Test Fermentation Data

The step-test fermentation spore maturation data are presented in this appendix.

C.1 Step Test S-2-24

Step-test fermentation S-2-24 was performed under the following conditions:

- temperature: 37° C
- medium: 0.27% glucose minimal medium
- pH: maintained at 7.0 using 1.0 molar NaOH
- aeration: high
- initial steady-state dilution rate: 0.5 (1/hr)

- dilution rate at $t = 0$: 0.1 (1/hr)

Time (hr)	Spore Count (1/ml)
0.0	4.50×10^4
1.0	1.25×10^5
2.0	2.05×10^5
3.0	2.19×10^5
4.0	2.79×10^5
5.0	3.39×10^5
6.0	4.00×10^5
6.8	9.99×10^5
7.0	1.60×10^6
7.5	8.50×10^5
8.0	9.00×10^5
8.5	1.60×10^6
9.0	2.65×10^6
9.5	3.85×10^6
10.0	9.40×10^6
10.5	3.35×10^7
11.0	2.85×10^7
11.5	4.50×10^7
12.0	6.50×10^7

Table C.1: Data for sporulation step-test S-2-24.

Appendix D

Steady-State Biomass Data

The steady-state biomass data are presented in this appendix.

Steady-state fermentations were performed under the following conditions:

- temperature: 37° C
- medium: 0.15% glucose minimal medium
- pH: maintained at 7.0 using 1.0 molar NaOH
- aeration: high

Dilution Rate (1/hr)	Spore Count (1/ml)	Nonspore Count (1/ml)
0.10	7.95×10^7	6.35×10^8
0.15	2.51×10^7	7.58×10^8
0.20	4.95×10^6	1.02×10^9
0.30	7.00×10^4	1.01×10^9
0.50	2.00×10^4	1.13×10^9

Table D.1: Data for high aeration steady-state biomass data.

Appendix E

Low Aeration Batch Fermentation Data

The batch fermentation data for the low-aeration fermentation experiment L-10-6.

E.1 Batch Fermentation L-10-6

Batch fermentation L-10-6 was performed under the following conditions:

- temperature: 37° C
- medium: 0.20% glucose minimal medium
- pH: maintained at 7.0 using 1.0 molar NaOH
- aeration: low
- inoculum: 5 ml vegetative inoculum

Time (hr)	Spore Count (1/ml)	Nonspore Count (1/ml)	Glucose (g/l)	Bacitracin (g/l)
0.0	0.00×10^1	4.49×10^5	1.98	0.00×10^1
3.0	0.00×10^1	6.54×10^5	1.90	0.00×10^1
6.0	0.00×10^1	2.30×10^6	1.68	0.00×10^1
9.0	0.00×10^1	1.48×10^7	1.83	0.00×10^1
12.0	0.00×10^1	1.56×10^8	0.83	0.00×10^1
15.0	0.00×10^1	5.26×10^8	0.00	0.00×10^1
18.0	0.00×10^1	6.75×10^8	0.00	2.39×10^{-3}
21.0	0.00×10^1	5.10×10^8	0.00	8.03×10^{-3}
24.0	0.00×10^1	3.27×10^8	0.00	1.04×10^{-2}
27.0	1.79×10^5	2.45×10^8	0.00	2.24×10^{-2}
30.0	4.08×10^6	4.14×10^8	0.00	2.92×10^{-2}
33.0	3.42×10^7	1.14×10^8	0.00	4.56×10^{-2}
36.0	9.72×10^7	7.20×10^7	0.00	3.84×10^{-2}
53.0				3.35×10^{-2}

Table E.1: Data for low-aeration batch fermentation L-10-6.

Bibliography

[1] S. Aiba and M. Hara. Studies on continuous fermentation part 1. The concept of the mean cumulative-age of microbes. *J. Gen. Appl. Microbiol.*, 11(1):25–49, 1965.

[2] D. H. Anderson. *Compartmental Modelling and Tracer Kinetics.* Lecture Notes in Biomathematics. Springer-Verlag, New York, 1983.

[3] Jr. Arthur E. Bryson and Yu-Chi Ho. *Applied Optimal Control.* Hemisphere Publishing Corp., New York, 1975.

[4] James E. Bailey and David F. Ollis. *Biochemical Engineering Fundamentals.* McGraw-Hill Book Company, New York, second edition, 1986.

[5] R. K. Bajpai and M. Reuß. A mechanistic model for penicillin production. *J. Chem. Tech. Biotechnol.*, 30:332–344, 1980.

[6] Y. Bard. *Nonlinear Parameter Estimation.* Academic Press, New York, 1974.

[7] Douglas M. Bates and Donald G. Watts. *Nonlinear Regression Analysis and its Applications.* John Wiley and Sons, New York, 1988.

[8] Eric B. Becker, Graham F. Carey, and J. Tinsley Oden. *Finite Elements: An Introduction*, volume 1. Prentice-Hall, Inc., Englewood Cliffs, New Jersey, 1981.

[9] Robert W. Bernlohr and G. D. Novelli. Some characteristics of bacitracin production by *bacillus licheniformis.* *Arch. Biochem. Biophys.*, 87:232–238, 1960.

[10] Robert W. Bernlohr and G. D. Novelli. Bacitracin biosynthesis and spore formation: The physiological role of an antibiotic. *Arch. Biochem. Biophys.*, 103:94–104, 1963.

[11] H. W. Blanch and P. L. Rogers. Production of gramicidin s in batch and continuous culture. *Biotech. Bioeng.*, 13:843–864, 1971.

[12] K. E. Brenan, S. L. Campbell, and L. R. Petzold. *Numerical Soluton of Initial-Value Problems in Differential-Algebraic Equations.* North-Holland, New York, 1989.

[13] D. E. Brown and R. C. Vass. Maturity and product formation in cultures of microorganisms. *Biotech. Bioeng.*, 15:321–330, 1973.

[14] V. Běhal, V. Erban, and J. Votruba. Modelling of physiology and kinetics of the overproduction of tetracyclines. In G. Szabó, S. Biró, and M. Goodfellow, editors, *Sixth Int. Symp. on Actinomycetes Biology*, pages 271–273, 1985.

[15] C. T. Calam, S. H. Ellis, and M. C. McCann. *J. Appl. Chem. Biotechnol.*, 21:181, 1971.

[16] C. T. Calam and D. W. Russel. Microbial aspects of fermentation process development. *J. Appl. Chem. Biotechnol.*, 23:225, 1973.

[17] Makis Caracotsios and Warren E. Stewart. Sensitivity analysis of initial value problems with mixed odes and algebraic equations. *Comput. Chem. Eng.*, 9(4):359–365, 1985.

[18] Jr. Charles P. Moran. Sigma factors and the regulation of transcription. In Issar Smith, Ralph A. Selpecky, and Peter Setlow, editors, *Regulation*

of Procaryotic Development, chapter 8, pages 167–184. American Society for Microbiology, Washington, D. C., 1989.

[19] A. Constantinides, J. L. Spencer, and E. L. Gaden. Optimization of batch fermentation processes. i. Development of mathematical models for batch penicillin fermentations. *Biotech. Bioeng.*, 12:803, 1970.

[20] Grant D. Darker, Helen B. Brown, Alfred H. Free, Barbara Biro, and John T. Goorley. The assay of bacitracin. *J. Amer. Pharm. Assoc.*, pages 156–160, 1957.

[21] I. W. Dawes and J. Mandelstam. Sporulation of *bacillus subtilis* in continuous culture. *J. Bacteriol.*, 103(3):529–535, Sept. 1970.

[22] I. W. Dawes and J. H. M. Thornley. Sporulation in *bacillus subtilis.* theoretical and experimental studies in continuous culture systems. *J. Gen. Microbiol.*, 62:49–66, 1970.

[23] V. G. Debabov. The industrial use of *bacilli.* In David A. Dubnau, editor, *The Molecular Biology of the* Bacilli, chapter 11, pages 331–371. Academic Press, New York, 1982.

[24] G. Van Dedem and M. Moo-Young. Cell growth and extracellular enzyme synthesis in fermentations. *Biotech. Bioeng.*, 15:419–439, 1973.

[25] T. J. Donohue and R. W. Bernlohr. Effect of culture conditions on the concentrations of metabolic intermediates during growth and sporulation of *bacillus licheniformis* . *J. Bacteriol.*, 135(2):363–372, 1978.

[26] N. R. Draper and H. Smith. *Applied Regression Analysis.* John Wiley and Sons, Inc., New York, 1966.

[27] Kevin H. Dykstra, Xiang-Ming Li, and H. Y. Wang. Computer modeling of antibiotic fermentation with on-line product removal. *Biotech. Bioeng.*, 32:356–362, 1988.

[28] J. W. Eaton and J. B. Rawlings. Feedback control of chemical processes using on-line optimization techniques. *Comput. Chem. Eng.*, 14(4/5):469–479, 1990.

[29] Anthony V. Fiacco. *Introduction to Sensitivity and Stability Analysis in Nonlinear Programming*, volume 165 of *Mathematics in Sicence and Engineering*. Academic Press, New York, 1983.

[30] Bruce A. Finlayson. *The Method of Weighted Residuals and Variational Principles.* Academic Press, New York, 1972.

[31] V. M. Fishman and V. V. Biryukov. Kinetic model of secondary metabolite production and its use in computation of optimal controls. In *Biotechnology and Bioengineering Symposium No. 4*, page 647, 1974.

[32] M. C. Flickinger and D. Perlman. Application of oxygen-enriched aeration in the production of bacitracin by *bacillus licheniformis*. *Antimicrobial Agents and Chemotherapy*, 15(2):282–293, February 1979.

[33] A. P. Fordyce, J. B. Rawlings, and T. F. Edgar. Control strategies for fermentation processes. In D. R. Omstead, editor, *Computer Control of Fermentation Processes*, Boca Raton, 1990. CRC Press.

[34] A. G. Fredrickson, D. Ramkrishna, and H. M. Tsuchiya. Statistics and dynamics of microbial cell populations. *Math. Biosci.*, 1:327–374, 1967.

[35] Ø. Frøyshov. The bacitracins: Properties, biosynthesis, and fermentation. In E. J. Vandamme, editor, *Biotechnology of Industrial Antibiotics*,

chapter 24, pages 665–694. Marcel Dekker, Inc., New York, 1984.

[36] A. Ronald Gallant. *Nonlinear Statistical Models.* John Wiley and Sons, New York, 1987.

[37] Christie J. Geankoplis. *Transport Processes and Unit Operations.* Allyn and Bacon, Inc., Boston, 2nd edition, 1983.

[38] Philipp Gerhardt and Robert E. Marquis. Spore thermoresistance mechanisms. In Issar Smith, Ralph A. Slepecky, and Peter Setlow, editors, *Regulation of Procaryotic Development: Structural and Functional Analysis of Bacterial Sporulation and Germination*, chapter 2, pages 43–64. American Society for Microbiology, Washington, D. C., 1989.

[39] Philip E. Gill, Walter Murray, and Margaret H. Wright. User's guide for npsol (version 4.0): A fortran package for nonlinear programming. Technical report, Systems Optimization Laboratory-Department of Operations Research. Stanford University, Stanford, California 94305, January 1986.

[40] A. R. Giona, L. Marrelli, L. Toro, and R. De Santis. Kinetic analysis of penicillin production by semi-continuous fermentors. *Biotech. Bioeng.*, 18:473, 1976.

[41] Ruth E. Gordon, William C. Haynes, and C. Hor-Nay Pang. *The Genus* Bacillus, volume 427. Agricultural Research Service: United States Department of Agriculture, Washington, D. C., 1973.

[42] Gerhard Gottschalk. *Bacterial Metabolism.* Springer-Verlag, New York, 1979.

[43] H. I. Haavik. Studies on the formation of bacitracin by *bacillus licheniformis*: Effect of glucose. *J. Gen. Microbiol.*, 81:383–390, 1974.

[44] H. I. Haavik. Studies on the formation of bacitracin by *bacillus licheniformis*: Role of catabolite repression and organic acids. *J. Gen. Microbiol.*, 84:321–326, 1974.

[45] H. I. Haavik. Possible functions of peptide antibiotics during growth of producer organisms: Bacitracin and metal (ii) ion transport. *Acta Pathol. Microbiol. Scand. Sect. B*, 84:117–124, 1976.

[46] H. I. Haavik and S. Thomassen. A bacitracin-negative mutant of Bacillus licheniformis which is able to sporulate. *J. Gen. Microbiol.*, 76:451–454, 1973.

[47] Geoffrey W. Hanlon and Norman A. Hodges. Bacitracin and protease production in relation to sporulation during exponential growth of *bacillus licheniformis* on poorly utilized carbon and nitrogen sources. *J. Bacteriol.*, 147(2):427–431, 1981.

[48] A. Harder and J. A. Roels. Application of simple structured models in bioengineering. *Adv. Biochem. Eng.*, 21:55–107, 1982.

[49] E. Hegewald and I. Rückbeil. Model of growth and product formation of *streptomyces hygorscopicus* in batch culture and prediction for continuous culture. In *7th International Symposium on Continuous Culture of Microorganisms*, Prague, Czechoslovakia, July 1978.

[50] David Hendlin. The nutritional req;uirements of a bacitracin-producing strain of *bacillus subtilis*. *Archives of Biochemistry*, 24:435–446, 1949.

[51] R. J. Hickey. Bacitracin, its manufacture and uses. *Progress in Industrial Microbiology*, 5:93–150, 1964.

[52] B. Hodgson. Possible roles for antibiotics and other biologically active peptides at specific stages during sporulation of *bacillaceae*. *J. Theo. Bio.*, 30:111–119, 1970.

[53] Andrea Holmberg, Risto Sievänen, and Gunnel Carlberg. Fermentation of *bacillus thuringiensis* for exotoxin production: Process analysis study. *Biotech. Bioeng.*, 22:1707–1724, 1980.

[54] H. M. Hulburt and S. Katz. Some problems in particle technology: A statistical mechanical formulation. *Chem. Eng. Sci.*, 19:555–574, 1964.

[55] J. A. Jacquez. *Compartmental Analysis in Biology and Medicine*. Elsevier, New York, 1972.

[56] J. W. Jeong, J. Snay, and M. M. Ataai. A mathematical model for examining growth and sporulation processes of *bacillus subtilis*. *Biotech. Bioeng.*, 35:160–184, 1990.

[57] Edward Katz and Arnold L. Demain. The peptide antibiotics of *bacillus*: Chemistry, biogenesis, and possible functions. *Microbiol. Rev.*, 41(2):449–474, June 1977.

[58] T. C. Koopmans and W. C. Hood. The estimation of simultaneous linear economic relationships. In W. C. Hood and T. C. Koopmans, editors, *Studies in Econometric Method*. Wiley, New York, 1953.

[59] Peter J. Kramer. An analysis of the major metabolic products of *bacillus licheniformis* jf–2. Honors Thesis, May 1990. The University of Texas at Austin.

[60] Leon Lapidus and George F. Pinder. *Numerical Solution of Partial Differential Equations in Science and Engineering.* John Wiley and Sons, 1982.

[61] R. Losick, P. Youngman, and P. J. Piggot. Genetics of endospore formation. *Annual Review of Genetics*, 20:625–669, 1986.

[62] Richard Losick and Lee Kroos. Dependence pathways for the expression of genes involved in endospore formation in *bacillus subtilis.* In Issar Smith, Ralph A. Slepecky, and Peter Setlow, editors, *Regulation of Procaryotic Development. Structural and Functional Analysis of Bacterial Sporulation and Germination*, chapter 11, pages 223–241. American Society of Microbiology, Washington, D. C., 1989.

[63] Richard Losick and Philip Youngman. Endospore formation in *bacillus.* In Richard Losick and L. Shapiro, editors, *Microbial Development*, pages 63–88. Cold Spring Harbor Laboratories, Cold Spring Harbor, New York, 1984.

[64] R. Luedeking and E. L. Piret. A kinetic study of the lactic acid fermentation, batch process at controlled pH. *J. Biochem. Microbial Technol. Engng.*, 3:393, 1974.

[65] S. Majumdar, S. Basu, S. K. Das, and S. K. Bose. Relationship between sporulation and synthesis of mycobacillin and dipicolinic acid under condition of glucose repression in *bacillus subtilis. Folia Microbiologica*, 31:196, 1986.

[66] S. Majumdar and S. K. Bose. Derepression of sporulation and synthesis of muycobacillin and dipicolinic acid by guanosine 3–5 cyclic monophos-

phate under conditions of glucose repression in *bacillus subtilis*. *J. Gen. Microbiol.*, 131:2783, 1985.

[67] S. Majumdar, S. K. Ghosh, N. K. Mukhopadhyay, and S. K. Bose. Accumulation of peptides by mycobacillin-negative mutants of *bacillus subtilis* b_3. *J. Gen. Microbiol.*, 131:119, 1985.

[68] M. A. Marahiel, W. Danders, M. Krause, and H. Kleinkauf. Biological role of gramicidin s in spore functions. *Eur. J. Biochem.*, 99:49, 1979.

[69] J. F. Martin and L. E. McDaniel. Kinetics of biosynthesis of polyene macrolide antibiotics in batch cultures: Cell maturation time. *Biotech. Bioeng.*, 15:925–938, 1975.

[70] Juan F. Martin and Arnold L. Demain. Control of antibiotic biosynthesis. *Microbiol. Rev.*, 44(2):230–251, June 1980.

[71] M. Matsumura, T. Imanaka, T. Yoshida, and H. Taguchi. Modeling of cephalosporin c production and its application to fed-batch culture. *J. Ferm. Technol.*, 59:115, 1981.

[72] R. D. Megee, S. Kinoshita, A. G. Fredrickson, and H. M. Tsuchiya. Differentiation and product formation in molds. *Biotech. Bioeng.*, 12:771–801, 1970.

[73] Alexander M. Mood, Franklin A. Graybill, and Duane C. Boes. *Introduction to the Theory of Statistics.* McGraw-Hill Book Company, New York, 3rd edition, 1963.

[74] Jorge J. More, Burton S. Garbow, and Kenneth E. Hillstrom. User guide for minpack-1. Technical Report ANL–80–74, Argonne National Laboratory, March 1980.

[75] Michiko M. Nakano and Peter Zuber. Molecular biology of antibiotic production in *bacillus*. *Crit. Rev. Biotechnol.*, 10(3):223–240, 1990.

[76] Wayne L. Nicholson and Peter Setlow. Sporulation, germination and outgrowth. In C. R. Harwood and S. M. Cutting, editors, *Molecular Biology Methods for* Bacillus, chapter 9, pages 391–450. John Wiley and Sons Ltd., New York, 1990.

[77] K. Ochi, J. C. Kandala, and E. Freese. Evidence that *bacillus subtilis* sporulation induced by the stringent response is caused by a decrease in gtp or gdp. *J. Bacteriol.*, 151:1062–1065, 1982.

[78] James Y. Oldshue. *Fluid Mixing Technology.* McGraw-Hill Co., New York, 1983.

[79] David F. Ollis. A simple batch fermentation model: Theme and variations. *Ann. N. Y. Acad. Sci.*, 413:144–156, 1983.

[80] S. Pažoutova, J. Vortruba, and Z. Řeháček. A mathematical model of growth and alkaloid production in the submerged culture of *claviceps purpurea*. *Biotech. Bioeng.*, 23:2837, 1981.

[81] M. Perego and J. A. Hoch. Isolation and sequence of the spo0e gene: its role in initiation of sporulation in *bacillus subtilis*. *Mol. Microbiol.*, 1:125–132, 1987.

[82] Linda R. Petzold. A description of DASSL: A differential/algebraic system solver. In R. Stepleman, editor, *Scientific Computing*, pages 65–68, Amsterdam, 1983. North-Holland Company.

[83] P. J. Piggot and J. G. Coote. Genetic aspects of bacterial endospore formation. *Bacteriological Reviews*, 40(4):908–962, 1976.

[84] J. M. Piret and A. L. Demain. Sporulation and spore properties of *bacillus brevis* and it gramicidin s negative mutant. *J. Gen. Microbiol.*, 129:1309, 1983.

[85] D. Ramkrishna. Statistical models of cell populations. *Adv. Biochem. Eng.*, 11(1):1–47, 1979.

[86] D. Ramkrishna. The status of population balances. *Rev. Chem. Eng.*, 3(1):49–95, 1985.

[87] D. Ramkrishna, A. G. Fredrickson, and H. M. Tsuchiya. Dynamics of microbial propagation: Models considering inhibitors and variable cell composition. *Biotech. Bioeng.*, 9:129, 1967.

[88] Alan D. Randolph and Maurice A. Larson. *Theory of Particulate Processes.* Academic Press, New York, 2nd edition, 1988.

[89] James B. Rawlings. *Simulation and Stability of Continuous Emulsion Polymerization Reactors.* PhD thesis, University of Wisconsin, 1985.

[90] W. Harmon Ray. *Advanced Process Control.* Butterworths, Boston, 1989.

[91] P. Schaeffer. Sporulation and the production of antibiotics, exoenzymes, and exotoxins. *Bacteriological Reviews*, 33(1):48–71, March 1969.

[92] P. Schaeffer, J. Millet, and J. P. Aubert. Catabolic repression of bacterial sporulation. *Proc. Nat. Acad. Sci.*, 54:704–711, 1965.

[93] V. Schulz, R. Schorcht, Yu. N. Ignatenko, Z. V. Sakharova, and M. P. Khovrychev. Modellgestotzte optimierung der kontinuierlichen fermentation von δ-endotoxin. *Stud. Biophys.*, 107(1):43–51, 1985.

[94] G. A. F. Seber and C. J. Wild. *Nonlinear Regression.* John Wiley and Sons, New York, 1989.

[95] L. E. Shnaider and V. V. Biryukov. Modelling and optimization of oxytetracycline biosynthesis process. In A. Johnson, editor, *Modelling and Control of Biotechnological Processes*, pages 217–222, Oxford, 1985. IFAC, Pergamon Press.

[96] Ping Shu. Mathematical models for the product accumulation in microbiological processes. *J. Biochem. Microbiol. Tech. Eng.*, 3(1):95–109, 1961.

[97] M. L. Shuler. Dynamic modelling of fermentation systems. In M. Moo-Young, editor, *Comprehensive Biotechnology Volume 2. The Principles of Biotechnology: Engineering Considerations*, chapter 6, pages 119–131. Pergamon Press, Ltd., New York, 1985.

[98] M. L. Shuler. On the use of chemically structured models for bioreactors. *Chem. Eng. Commun.*, 36:161–189, 1985.

[99] M. L. Shuler, S. Leung, and C. C. Dick. A mathematical model for the growth of a single bacterial cell. *Annals N.Y. Acad. Sci.*, 326(35), 1979.

[100] Issar Smith. Initiation of sporulation. In Issar Smith, Ralph A. Slepecky, and Peter Setlow, editors, *Regulation of Procaryotic Development. Structural and functional Analysis of Bacterial Sporulation and Germination*, chapter 9, pages 185–210. American Society of Microbiology, Washington, D. C., 1989.

[101] J. Snay, J. W. Jeong, and M. M. Ataai. Effects of growth conditions on carbon utilization and organic by-product formation in *b. subtilis. Biotechnology Progress*, 5(2):63–69, 1989.

[102] Abraham L. Sonenshein. Metabolic regulation of sporulation and other stationary-phase phenomena. In Issar Smith, Ralph A. Slepecky, and Peter Setlow, editors, *Regulation of Procaryotic Development. Structural and Functional Analysis of Bacterial Sporulation and Germination*, chapter 5, pages 109–130. American Society for Microbiology, Washington, D. C., 1989.

[103] R. Y. Stanier, E. A. Adelberg, and J. Ingraham. *The Microbial World.* Prentice-Hall Inc., Englewood Cliffs, New Jersey, fourth edition, 1976.

[104] Maciej Starzak and Rakesh K. Bajpai. A structured model for vegetative growth and sporulation in *bacillus thuringiensis*. *Appl. Biochem. Biotechnol.*, 28/29:699–718, 1991.

[105] Gilbert Strang. *Linear Algebra and its Applications.* Harcourt Brace Jovanovich, Publishers, San Diego, 3rd edition, 1988.

[106] H. M. Tsuchiya, A. G. Fredrickson, and R. Aris. Dynamics of microbial cell populations. *Advances in Chemical Engineering*, 6:125–205, 1966.

[107] The United States Pharmacopeial Convention, Rockville, Maryland. *The United States Pharmacopeial Convention Monograph*, 22 edition, 1990.

[108] E. J. Vandamme, D. Leyman, D. De Buyser, P. De Visscher, J. Spriet, G. C. Vansteenkiste, O. Nimi, A. Poirier, and A. L. Demain. Environmental influences on the dynammics of the gramicidin s fermentation. In Horst Kleinkauf and Hans von Döhren, editors, *Peptide Antibiotics: Biosynthesis and Functions*, pages 117–136. Walter de Gruyter, New York, 1982.

[109] J. Villadsen and W. Stewart. Solution of boundary-value problems by orthogonal collocation. *Chem. Eng. Sci.*, 22:1483, 1967.

[110] E. D. Weinberg. Bacitracins, gramicidin, and tyrocidine. In David Gottlieb and Paul D. Shaw, editors, *Antibiotics: Biosynthesis*, pages 240–253. Springer-Verlag, New York, 1967.

[111] F. M. Williams. A model of cell growth dynamics. *J. Theo. Bio.*, 15:190–207, 1967.

[112] M. K. Woolford. Studies on the significance of three *bacillus* species to the ensiling process. *Journal of Applied Bacteriology*, 43:447–452, 1977.

[113] Young J. Yoo, Theodore W. Cadman, Juan Hong, and Randolf T. Hatch. Fed-batch fermentation for the production of α-amylase by *bacillus amyloliquefaciens*. *Biotech. Bioeng.*, 31:357, 1988.

[114] M. Young and J. Mandelstam. Early events during bacterial endospore formation. *Advances in Microbial Physiology*, 20:103–162, 1979.

[115] P. Zuber and R. Losick. Role of *abrb* in *spo0a*- and *spo0b*- dependent utilization of a sporulation promoter in *bacillus subtilis*. *J. Bacteriol.*, 169:2223–2230, 1987.

Vita

Andrew Fordyce was born in Wheatridge, Colorado on June 11, 1963 to James M. and Alice L. Fordyce. After an uneventful childhood, Andrew attended Arapahoe High School in Littleton, Colorado, where he developed an interest in chemistry and mathematics. Upon graduation from high school, Andrew enrolled in Colorado State University and majored in chemical engineering. After a period of two years, Andrew transferred to The University of Colorado at Boulder, where he obtained a bachelor's of science in chemical engineering in May, 1985.

After a brief tour of Europe, Andrew returned to the United States and entered the graduate program in chemical engineering at The University of Texas at Austin.

Permanent address: 4737B White Rock Circle
Boulder, Colorado 80301

This dissertation was typeset by the author using the LaTeX document preparation system.